



Norwegian University
of Life Sciences

Master's Thesis 2021 30 + 30 ECTS

Faculty of Science and Technology

Analytical and experimental assessment of the connection in a CLT-Steel dissipating system

Viktoria Amble Larsen
Isak Anfinsen Lunde

Structural Engineering and Architecture

Abstract

To achieve the long-term climate and energy goals set by the EU, the housing stock in Europe is in need of renovation. This thesis is part of a four-year long European project called e-SAFE: energy and Seismic AFFordable rEnovation solutions. The project aims to renovate existing buildings by considering different aspects, in particular the seismic retrofitting system called e-CLT. A CLT panel is attached to the exterior buildings and connected with an innovative friction connection, in order to provide energy dissipation and limit the damage to the building.

Throughout this thesis, the focus will be on the friction connection. Five different designs of the friction connection were provided to be tested and analyzed. Each design has two versions with different bolt size. The goal of the design was to provide a stable and repeatable behavior with a predetermined slip friction force. The connections were analyzed using FEM-analysis software as well as tested experimentally in a press.

A model was created for each of the specimen with the goal of simulating the behavior in the press. This would give an initial impression of the ability of each specimen to be used in the system. Due to limitations in the Ansys software a 5 mm displacement was applied to the specimen to simulate the friction force. In the physical experiments the specimens were tested in a press, where a displacement up to 50 mm was applied. The setup in the press was made to be as stiff as possible, so that the friction connection could be isolated and investigated. To collect the data from the testing, several sensors were attached to the specimens and the press.

The results from the FE model indicated that the design of the specimens and the different bolt sizes influenced the resulting stresses, deformations, and forces. Large bolt size gave lower stress concentrations around the bolt holes, while deformations and forces were related to the shape of the specimens. The collected data and observations from the experiments showed variation in the behavior of the different specimens. The size of the bolts caused twisting in several specimens and led to unstable behavior. This was not observed in the FEM-analysis due to simplifications.

There was a correlation between the FE model and the experiments performed. Specimens with small deformations in the FE model gave the most stable and reliable behavior during the experimental activity. The thesis concludes with a recommendation for which specimen to include in full-scale testing.

Sammendrag

For å oppnå de langsiktige klima- og energimålene satt av EU, må bygningsmassen i Europa renoveres. Denne masteroppgaven er del av et fireårig europeisk prosjekt kalt e-SAFE: *energy and Seismic AFfordable rEnovation solutions*. Prosjektets mål er å rehabilitere eksisterende bygninger med fokus på forskjellige aspekter. Et viktig aspekt er rehabilitering av bygningers evne til å tåle jordskjelv med et system kalt e-CLT. Systemet består av en massivtreplate som monteres på utsiden av eksisterende bygninger med en innovativ friksjonsforbindelse. Dette systemet vil kunne dempe kreftene og begrense skadeomfanget på bygninger i et jordskjelv. Gjennom denne oppgaven er fokuset på friksjonsforbindelsen. Fem forskjellige design av friksjonsforbindelsen ble testet og analysert. Hvert design hadde to forskjellige versjoner med forskjellig boltestørrelse. Målet med forbindelsen var å oppnå en stabil og repetitiv oppførsel med en forhåndsbestemt glidekraft. Forbindelsen ble analysert med bruk av FEM-analyse og testet eksperimentelt i en presse.

En modell ble laget for hver av eksemplarene med et mål om å simulere hvordan oppførselen ville bli i pressen. Dette skulle gi et inntrykk av om de forskjellige eksemplarene kunne brukes i systemet. På grunn av begrensninger i Ansys programvaren ble det påført 5 mm forskyvning på testeksemplarene for å simulere friksjonskraften. I de fysiske eksperimentene ble testeksemplarene undersøkt i en presse der 50 mm forskyvning ble påført. Oppsettet i pressen ble laget slik at det ville bli så stivt som mulig. På denne måten ble friksjonsforbindelsen isolert og kunne bli undersøkt. Flere sensorer ble brukt på testeksemplaret og pressen for å samle inn data under testene.

Resultatene fra FE modellen viste at utformingen av testeksemplarene og størrelsen på boltene påvirket de resulterende spenningene, deformasjonene og kreftene. Stor boltestørrelse ga lavere spenningskonsentrasjoner rundt bolthullene, mens deformasjonene og kreftene ble knyttet til utformingen av testeksemplarene. Innsamlet data og observasjoner fra eksperimentene viste variabel oppførsel ved forskjellig utforming. Boltestørrelsen førte til vridning og ustabil oppførsel i flere av testeksemplarene. Dette ble ikke observert i FEM-analysen på grunn av forenklinger i modellen.

Det var en sammenheng mellom resultatene i FE modellen og eksperimentene.

Testeksemplarene med minst deformasjoner i FE modellen ga den mest stabile og pålitelige oppførselen i eksperimentene. Denne masteroppgaven konkluderer med en anbefaling av hvilket testeksemplar som burde inkluderes i en fullskalatest.

Acknowledgement

This thesis was written as a collaboration between Viktoria Amble Larsen and Isak Anfinsen Lunde in the spring of 2021.

Firstly, we are deeply grateful to our supervisor, Roberto Tomasi, for including us in this rewarding project. It was motivating to be part of the e-SAFE research project. He has provided us with advice, guidance, and support during the semester. Due to the Covid-19 situation, we encountered several problems related to the physical tests. Roberto Tomasi made an invaluable effort to enable us to carry out testing.

We would also like to express our sincere gratitude to Francesco Boggian for helping us with the testing and preparations in the lab. Your deep knowledge to the project has been invaluable to us in this period. Thank you for all the time and effort you have put into helping us with this thesis.

Our gratitude also extends to Øyvind Hansen for always providing us with mechanical solutions.

Lastly, we would like to thank our families and friends for supporting us.

Ås, May 2021,

Viktoria Amble Larsen and Isak Anfinsen Lunde

Contents

Abstract.....	i
Sammendrag	ii
Acknowledgement	iii
1 Introduction	1
2 Theory.....	4
2.1 Earthquake.....	4
2.2 Structural damping	6
2.3 Friction	8
2.4 Slotted bolted connections	9
2.5 Shim materials.....	11
2.6 Preloaded bolts	15
2.7 Ansys structural analysis software	17
3 Profiles.....	20
3.1 Previous research.....	23
4 Method: Experimental activity	25
4.1 Setup.....	25
4.1.1 Test preparation	26
4.2 Sensors	27
4.3 Software	29
4.4 Experimental tests	31
4.4.1 Preload	31
4.4.2 Preliminary testing with old specimen.....	34
4.4.3 Monotonic testing in Instron100.....	35
4.4.4 New testing campaign with Instron300	37
4.5 Limitations	39
5 Method: FEM-analysis	40

5.1	Materials.....	40
5.2	Contacts.....	40
5.3	Analysis settings.....	41
5.4	Restraints.....	41
5.5	Output.....	42
5.6	Verification of preloaded bolts.....	43
5.7	Verification of the friction connection	45
5.7.1	Simple model	45
5.7.2	Real model	46
5.8	Remote displacement	46
5.9	Simulation cases.....	48
5.10	Limitations	52
6	Results and discussion: FEM-analysis	53
6.1	Verification of the preloaded bolts.....	53
6.2	Verification of the friction connection	55
6.2.1	Simple model	55
6.2.2	Real model	57
6.3	Remote displacement	59
6.4	Simulation cases.....	60
6.5	Ansys analysis.....	64
6.5.1	ALT.....	64
6.5.2	ALT-AS	70
6.5.3	STD-1H.....	78
6.5.4	STD-2H.....	85
6.5.5	Hybrid	88
6.5.6	Comparison	94
7	Results and discussion: Experimental activity	101

7.1	Preliminary testing	101
7.2	Monotonic testing.....	106
7.3	New testing campaign	112
7.3.1	ALT specimen.....	112
7.3.2	ALT-AS specimen	114
7.3.3	STD Specimen	116
7.3.4	Hybrid Specimen	118
7.4	Shim layer	118
7.5	Bolt size.....	121
7.6	Temperature development.....	123
8	Comparison: FEM-analysis and experimental activity	125
9	Conclusion.....	130
10	Further work.....	131
11	List of figures.....	132
12	List of tables.....	137
13	References.....	138
Appendix.....		140
Appendix A: Nominal Torque		
Appendix B: Measurements and drawings of the specimens		
Appendix C: Results from experimental testing		
Appendix D: Sensor characteristics		

1 Introduction

To achieve the long-term climate and energy goals set by the EU, the housing stock in Europe is in need of renovation. e-SAFE, energy and Seismic AFFordable rEnovation solutions, is a four-year European project that intends to develop a system for renovating multistory buildings combining energy and seismic upgrading. This project aims to meet the long-term climate goals and will ensure earthquake-proof safety objectives, as well as greater aesthetic and functional attractiveness, internal comfort, reduced construction time and costs, less inconvenience for occupants, accessible financing solutions and innovative business models as seen in Figure 1-1 [1].

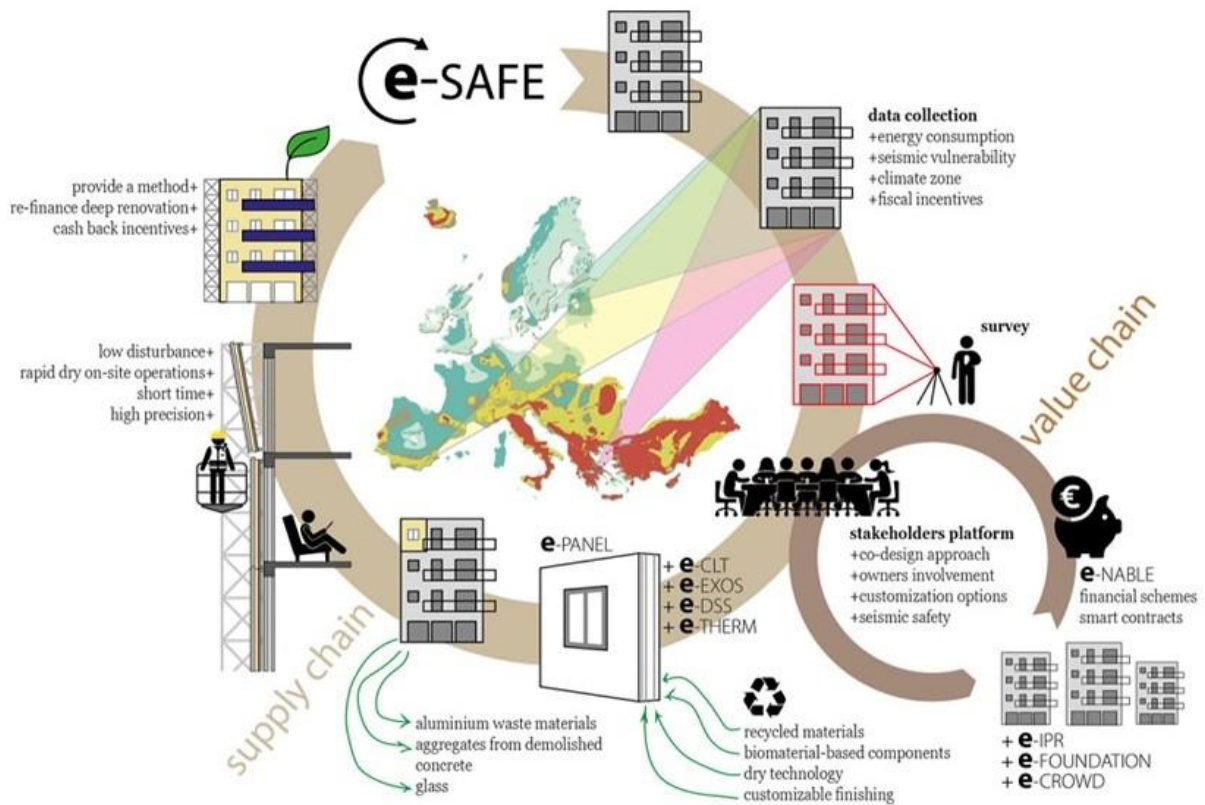


Figure 1-1 e-SAFE [1]

e-SAFE is based on a multidisciplinary methodology, as seen in Figure 1-1 above, and thereby benefits from both technological innovation and process innovation. The technologically innovative idea is to cover the outer shell of buildings with thermal-acoustic insulation (e-PANEL) and a structural system with prefabricated CLT-panels combined with friction connection dampers that increases seismic performants (e-CLT and e-EXOS) [2]. The seismic retrofitting system is called e-CLT. This thesis is part of the e-CLT project which are researching the system combining the CLT-panel and the innovative friction connection dampers.

The system is illustrated in Figure 1-2 were (b) shows the existing multistory building with the prefabricated and customized CLT-panel. The CLT-panel is connected to the concrete frame with four steel friction dampers, as seen in Figure 1-2 (a). The purpose of these friction connection dampers is to dissipate some of the energy caused by the ground motion. When an earthquake forces the ground into motion, the connections will stay rigid until a certain level of force is applied, then start to slide. The connections will dissipate energy during the sliding and prevent the building from being damaged [1].

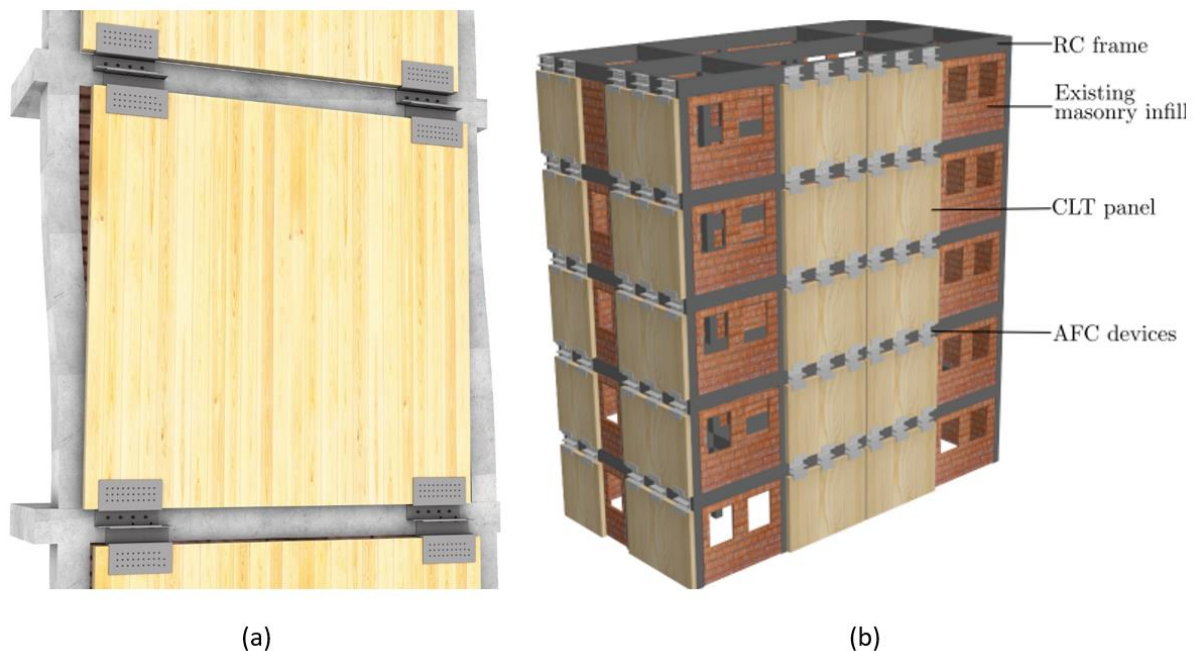


Figure 1-2 Illustration of the CLT panel system

Through this thesis the friction connection will be investigated and tested. The friction connections are proposed and designed to have a connection part to the CLT-panel, a part connected to the RC frame and a sliding part to dissipate energy. To understand the behavior of this type of connections, unique designs were made. They were modelled in a program called Ansys and produced so they could be tested physically in a press. Due to the situation in the society with COVID-19 the physical testing of the connections were limited.

The connections were analyzed by observing the behavior of the specimens in form of the friction surfaces, friction coefficient, slip friction force, shim layers and preload of the bolts. The goal for the specimens is to behave stable when a force is applied, and that the behavior is repeatable as well as the specimens maintain the strength and reduce the amount of damage.

This thesis is a continuation of two previous master thesis, Magnus Rød Hatletveit's, *Mechanical assessment of a steel dissipation system for RC buildings retrofitting with CLT panels* [3], and Mathilde Birch-Aune Marthinsen's, *Experimental assessment of a steel dissipating system* [4]. Each thesis was part of the same project, e-SAFE. The results and findings from their thesis were used to develop the innovative design of the specimens.

2 Theory

2.1 Earthquake

Earthquake is a sudden, violent movement or fracture of the earth's crust that causes ground vibration. The energy that is released when the crust fractures and slips is called seismic waves and travels through the interior of the earth or cross the surface. The largest damage is caused by the seismic waves. Earthquakes have taken millions of lives and cost many billions through the history [5].

The crust is the outermost layer of the earth and is divided into tectonic plates. The tectonic plates are the reason some countries are more disposed to earthquakes than others. These plates are floating on a dense, liquid layer beneath them. Areas where the plates bump into each other, pull away from each other or pass each other is where earthquakes usually happen [6].

To analyze the entity of an earthquake some parameters need to be introduced. Magnitude is the most common measure that indicates the released energy from the seismic source regardless of the location of the event and how it feels [7]. Most people know this as the Richter Scale, developed by U.S seismologist Charles Richter in 1935. The intensity is not based on accurate measurements, it is based on observations of earthquake effects on buildings and a description of people's experience of the tremors. With enough observations from different places and people, you will be able to extract a lot of information about the earthquake [8].

Another important parameter is the peak ground acceleration which is the largest increase in velocity recorded by a particular station during an earthquake [9]. Acceleration Response Spectrum is a plot of the peak acceleration value of a series of oscillators of varying natural frequency, which are forced into motion by the same ground movement. This can be considered as the main tool to evaluate seismic load and the most interesting is the maximum response of the system [10].

Earthquake engineering's main goal is to prevent building collapse during earthquakes, thereby minimizing the risk of death or injury to people in or around those buildings. A good earthquake design is where the designer controls the building by dictating how the building is to respond. EN 1998:2004 *Eurocode 8: Design of structures for earthquake resistance* is a standard produced to meet these conditions and gives two requirements for structures in seismic regions [11]:

- No-collapse requirement
- Damage limitation requirement

Figure 2-1 below shows the seismic hazard map of Europe and is created by an international team of European specialists. They achieved a unified methodology for seismic hazard mapping across Europe. The map shows the peak ground acceleration level that has a 10% exceedance in 50 years with a 475-year return period [12].

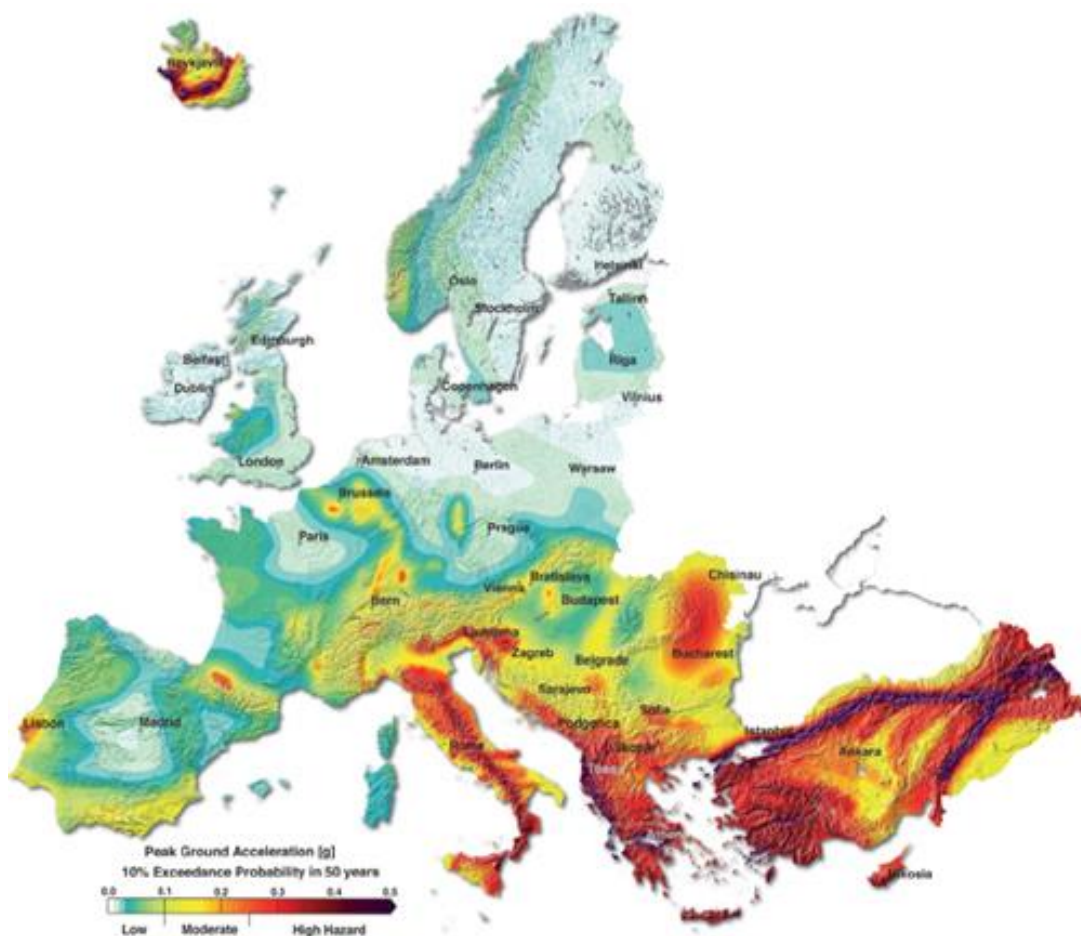


Figure 2-1 European seismic hazard map [12]

2.2 Structural damping

A building exposed to an earthquake will potentially endure large forces and deformations. Deformation of the building can lead to permanent distortion of the structural elements or in worst case, collapse of the building. Structural dampers are used to avoid these critical deformations. The dampers dissipate energy from the earthquake and reduce the amplitude of which the building is exposed to [13]. There are three different types of damping used in structures: viscous-, solid- and coulomb damping.

Viscous damping is one of the most used types of damping. The damping force produced in this damper is proportional to the velocity. Examples of viscous dampers is forcing your hand through water, or shock absorbers in cars. In these cases, the damping force increases with increased velocity. In structural buildings dampers often consist of a cylinder and a piston filled with a fluid as illustrated in Figure 2-2. When a force is applied, fluid is forced through holes in the piston. How much damping is provided can be altered by changing the velocity of the fluid, number and size of the holes or the dimension of the piston [14].



Figure 2-2 Example of a viscous damper [14]

Structural damping is a type of damping which occurs internally in the material of a vibrating object. It occurs due to the friction inside the element leading to energy dissipation [14]. The book *Mechanical vibrations* describes this using a modified elastic modulus [15, pp. 47]:

$$E_s = E(1 + i\eta)$$

Where;

$\eta =$ the solid damping factor which depends on type of material (2-1)

$E =$ Young's modulus

Coulomb damping is most relevant for this thesis. Coulomb damping occurs due to friction between two surfaces. The friction creates a force which always oppose the applied force, leading to damping. The *Mechanical vibrations* describe the force like this [15, pp. 47]:

$$f = \mu N$$

Where;

$N =$ the normal force acting on the connection (2-2)

$\mu =$ the friction coefficient depending on the material

2.3 Friction

Friction is a force between two surfaces that oppose the direction of movement [16]. It is a nonconservative force where the applied energy dissipates into heat, wear on the elements and deformation of the elements. There are two types of friction: static- and dynamic. Also called static and kinetic. Static friction is the force required to set a stationary object into motion. Dynamic friction occurs when the object is in motion [17]. The static friction is always larger than the dynamic friction [16]. Friction coefficient is a dimensionless ratio between the applied normal force and the friction force. The Greek letter μ is used for the friction coefficient [18]. It is also divided into static- and kinetic friction coefficient. Figure 2-3 shows the static- and kinetic friction coefficient. The static friction coefficient decreases gradually down to the kinetic friction coefficient with a slip length D_c as seen in Figure 2-3 [19]. There are many non-structural factors that affect the size of the friction coefficient. Temperature is a factor that make the friction coefficient depend on the surroundings [17]. That also means that the friction coefficient might change depending on location. Therefore, tabulated values of the friction coefficient are highly uncertain and laboratory testing should be conducted to fully understand how the friction behaves.

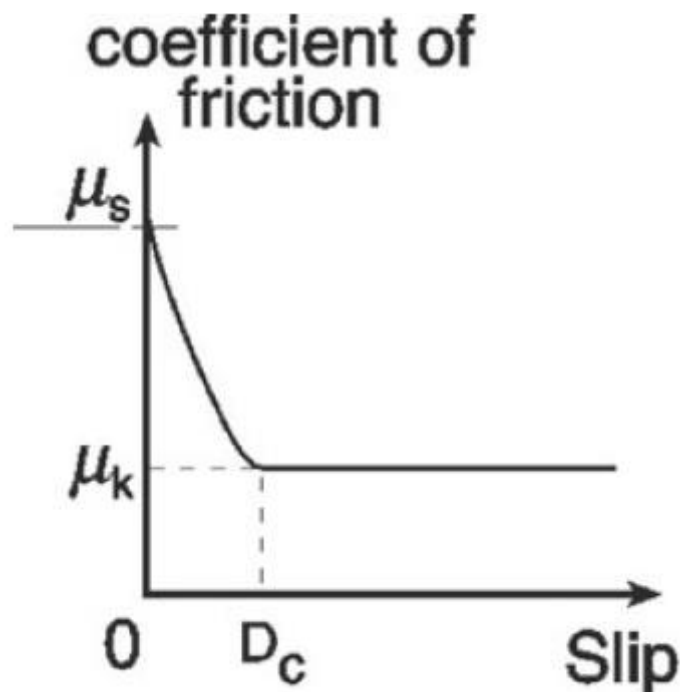


Figure 2-3 Static- and kinetic friction coefficient [19]

2.4 Slotted bolted connections

A slotted bolted connection system aims to dissipate energy through friction, create inelastic deformation, and develop non-linear behavior. This type of connection can be classified as a symmetrical friction connection (Figure 2-4) or an asymmetrical friction connection (Figure 2-5 (a)). Seen in Figure 2-4 and Figure 2-5 (a), the slotted bolted connection includes a plate with slotted holes placed between two shim layers and two outer plates, clamped together with bolts [20]. This is a type of coulomb damper introduced in chapter 2.2.

The difference between a symmetric and asymmetric friction connection is the distribution of force. In a symmetric friction connection, the force (V_{ss}) acting on the slotted bolted plate is equally distributed to the two outer plates ($V_{ss}/2$) working opposed of the slotted bolted plate. In the asymmetrical friction connection, the force (V_{ss}) acting on the slotted bolted plate is distributed to one of the outer plates working opposed of the slotted bolted plate. This gives a more complex stress in the bolts which lead to a more gradual force development in the beginning before it stabilizes, as seen in Figure 2-5 (b) [20].

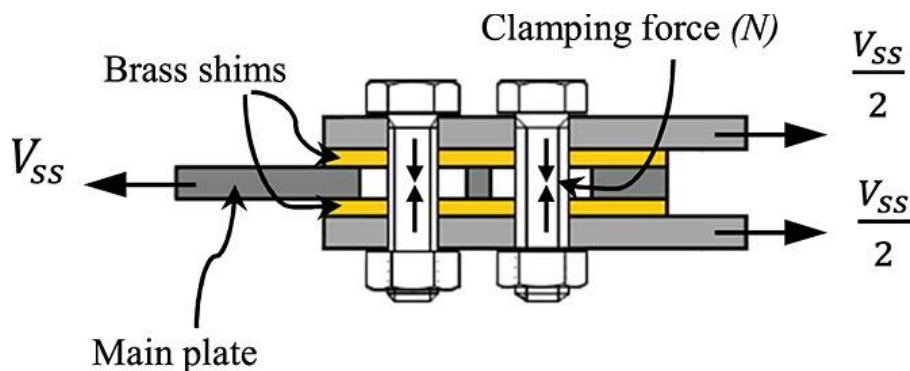


Figure 2-4 Symmetric friction connection [20]

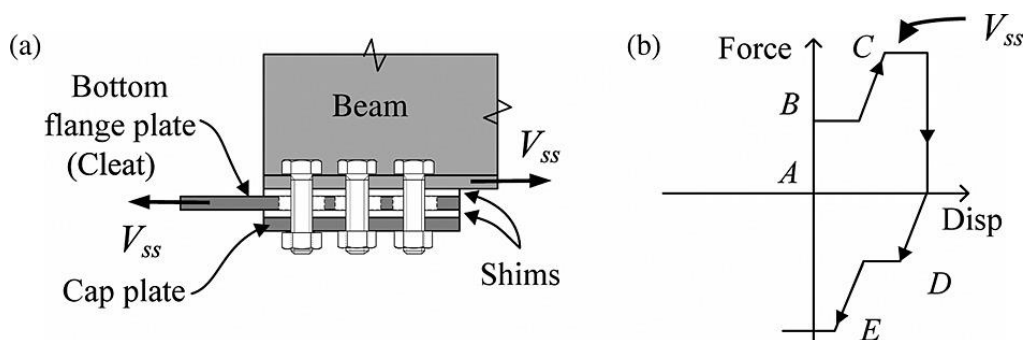


Figure 2-5 Asymmetric friction connection [20]

For a slip friction connection, the goal is to be stationary up to a predetermined slip force ($F_{s,R}$). When the slip friction force is achieved the connection will slip and then slide. This enables the connection to dissipate energy, where normal connections would go into plastic zone and possibly become damaged [21]. Friction is made by prestressed bolts that press the elements together explained in chapter 2.6. The slip force depends on the number of bolts, friction surfaces, tension force in the bolts and the friction coefficient. The nominal slip resistance of a connection is given in formula:

$$F_{s,R} = n_s n_b \mu F_{p,C}$$

Where;

(2-3)

n_s = number of friction surfaces

n_b = number of bolts

μ = friction coefficient

$F_{p,C}$ = preload force

2.5 Shim materials

A shim layer is a thin plate placed in the middle of two friction surfaces. The purpose of the shim layer is to dissipate energy and make a more stable and reliable connection. Which material the shim layer is made of affects the behavior and wear. The paper *Behavior of Asymmetrical Friction Connections using different shim materials* of Golondrino et.al. performed tests on asymmetrical friction connections using shim layers of different types of materials. The hardness of the materials was defined with Brinell hardness (HB) and ranged from aluminum with 75 HB to Bisalloy 500 with 500 HB. Figure 2-6 show the resulting hysteresis loop shapes of the testing performed on the different materials: (a) aluminum 75 HB, (b) brass 82 HB, (c) steel 130 HB, (d) Bisalloy 80 HB, (e) Bisalloy 400 HB, (f) Bisalloy 500 HB [22]. Figure 2-6 (a) and (b) show a moderate stability in the hysteresis loop due to small amount of wear between the layers. Figure 2-6 (c) and d show an unstable hysteresis loop due to large amount of wear between the layers. Figure 2-6 (e) and f show the most stable hysteresis loops. This is due to low wear due to the hardness of the shim layer. The test concluded that the stability of the hysteresis loop was dependent on the hardness of the shim materials.

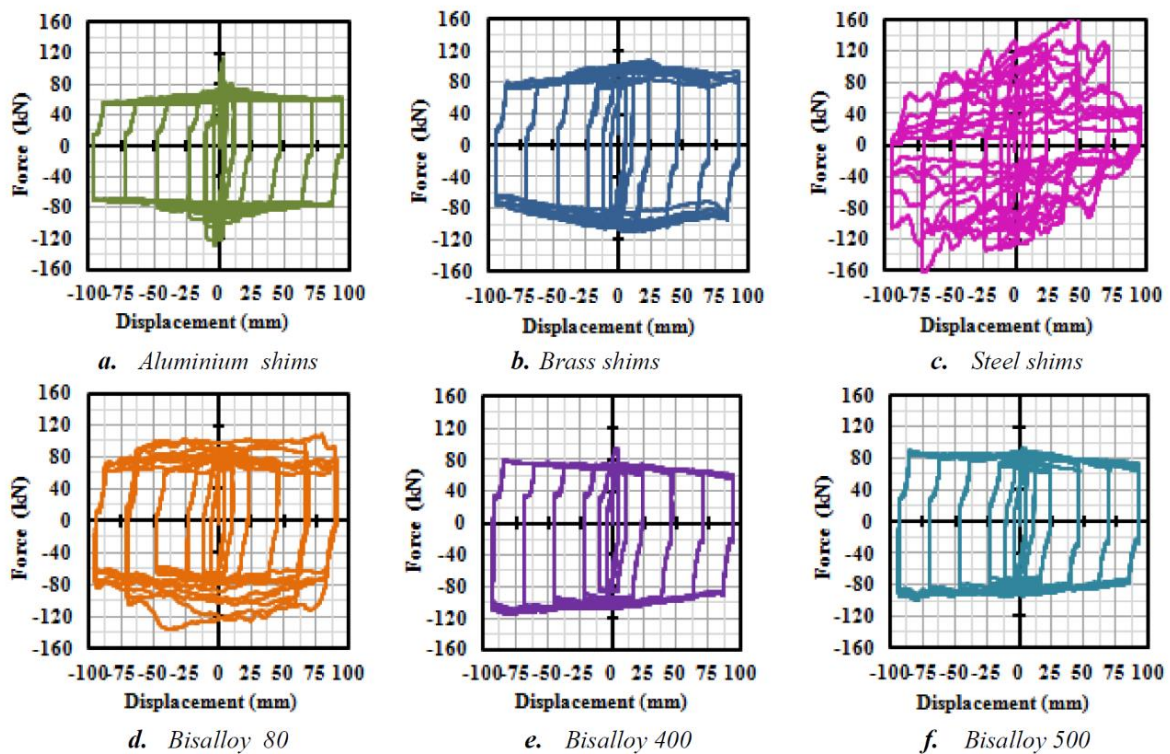


Figure 2-6 Hysteresis loop shape for different materials [22]

Khoo et.al. conducted several tests on the use of shim layers in the paper *Influence of steel shim hardness on the Sliding Hinge Joint performance* [23]. The test is from an asymmetrical friction connection in a sliding hinge joint made of G300 mild steel. There were placed shims between the layers with materials G300 mild steel, G80 high strength quenched and tempered steel and G400 abrasion resistant steel as seen in Figure 2-7. The materials had a Brinell hardness of 168 HB, 266 HB and 382 HB [23].

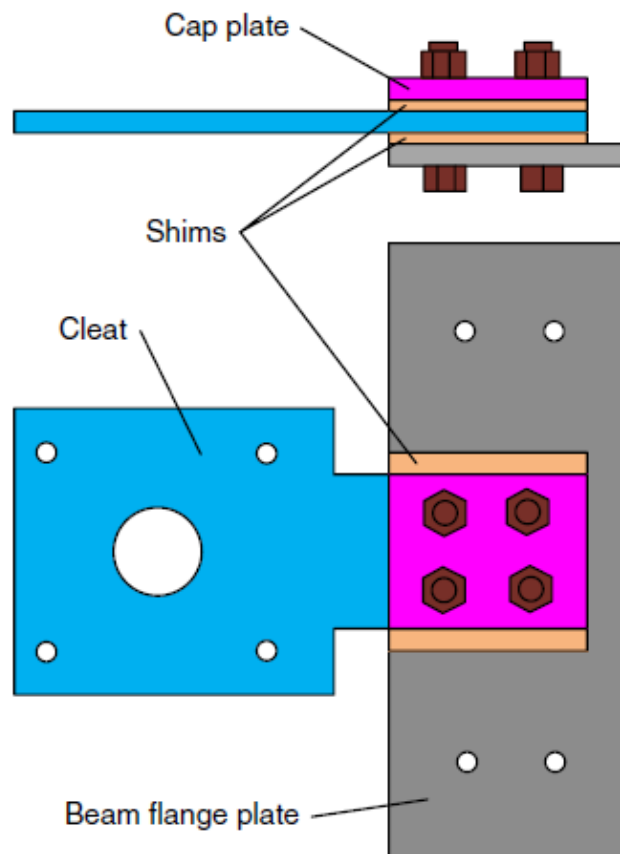


Figure 2-7 Set up of the sliding bolt component [23]

Each connection with the different shim materials was tested two different times each, with the following displacement being applied:

- 3 cycles of 3,5 mm (1 Hz)
- 3 cycles of 6,9 mm (1 Hz)
- 3 cycles of 10,5 mm (1,5 Hz)
- 5 cycles of 13,8 mm (1,5 Hz)

Figure 2-8 shows the hysteresis loops for the different hardness in the shim layers. Figure 2-8 (a) show that the softest material yields the worst hysteresis curve and (e), the hardest material has the best hysteresis curve. This test shows similar results as Golondrino et.al [22], that the hysteresis loops become more stable with increased hardness. In addition, the test performed indicates that the behavior of the connection becomes more similar in the first and second run with increased hardness, and thereby accomplish a more stable and reliable connection [23].

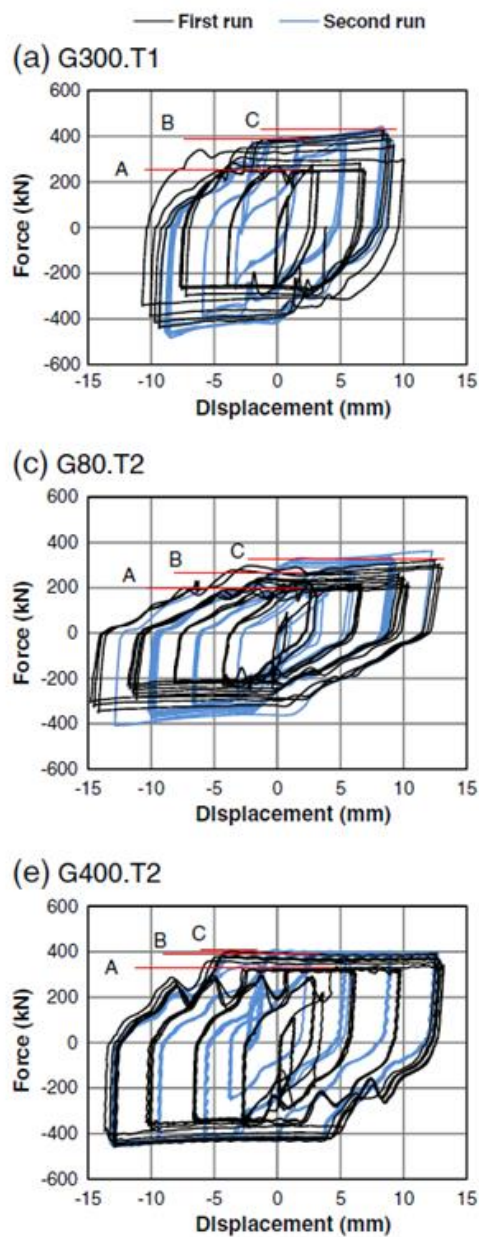


Figure 2-8 Hysteresis curves for G300, G80 and G400 shims [23]

As introduced in 2.3, there are several factors that make the friction coefficient vary. Golondrino et.al. examined which effect hardness of the shim layer would have on the friction coefficient. The result from the test is shown in Figure 2-9 and it is observed that the medium hardness materials had the largest friction coefficient in both static and dynamic state. The hardest materials, Bissalloy 400 and Bissalloy 500 have a more similar friction coefficient than the softer materials. This result corresponds with the more stable hysteresis loop for the hard materials [22].

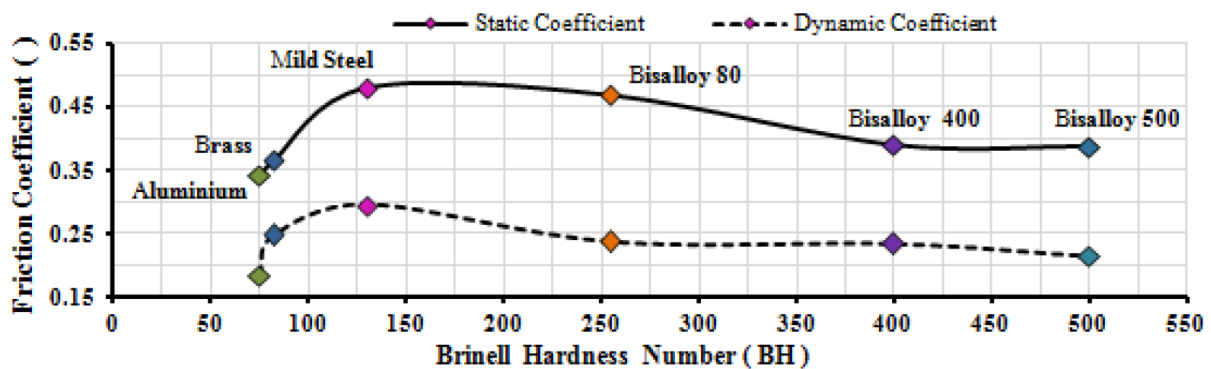


Figure 2-9 Variation of the friction coefficient with increased hardness [22]

The work of both Golondrino et.al. [22] and Khoo et.al. [23] show bilinear hysteresis loops. Golondrino et.al. investigated what effect the sliding length had on the hysteresis loop (Figure 2-10), and found that less sliding length had a more defined bilinear shape (a), and longer sliding length had a more defined square shape (c) [22]. From Figure 2-10 it can also be observed that the force stabilizes after a displacement of 3-5 mm.

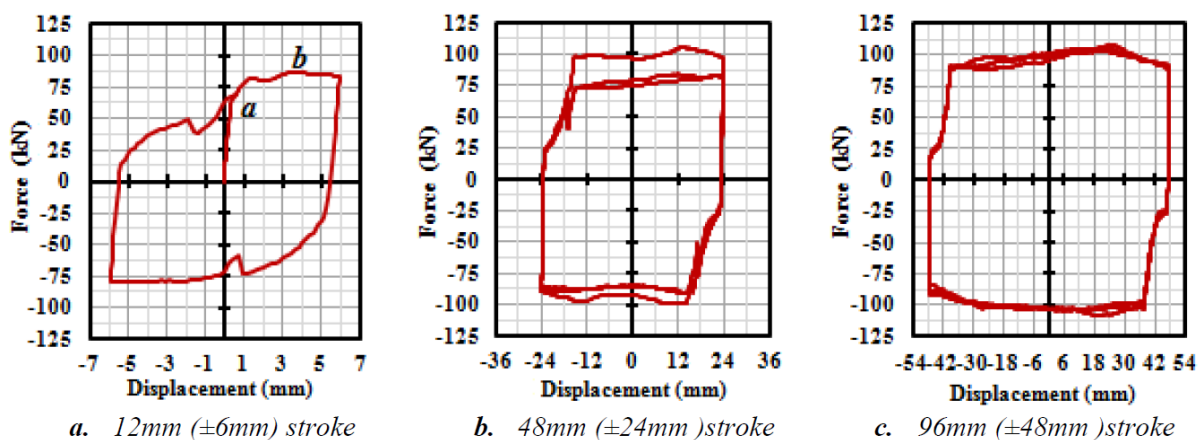


Figure 2-10 Hysteresis loop of AFC specimen with different sliding lengths [22]

2.6 Preloaded bolts

Preload is applied to a bolt to tighten and prevent a gap in a joint. When the bolt is tightened there will become tension in the bolt. Due to this tension, there will become compression in the plates. This compressive force will press the parts of the joints together. If an external load is applied on the joint creating more tension in the bolt, the compression on the plate will reduce due to the preload. This will make the connection become loose and is often unwanted [24].

To define the amount of preload for each bolt, the Eurocode recommend a preload of 70 % of the tensile capacity of the bolt. The equation is given by EN 1090-2 [25] and EN 1993-1-8 [26] and equation (2-4) is used unless otherwise specified:

$$F_{p,C} = 0.7 \cdot f_{ub} \cdot A_s$$

Where;

$F_{p,C}$ = nominal minimum preloading force

f_{ub} = nominal ultimate strength of the bolt material as defined in EN 1993-1-8

A_s = stress area of the bolt

(2-4)

Procedure of tightening a preloaded bolt is explained in EN-1090 chapter 8.5 [25]. Two relevant methods of tightening are presented: the torque method and the combined method. Which method to use is determined by the bolts K-class defined in EN-14399 chapter 5.4 [27]. The K-class is mainly decided by the delivery conditions of the bolt assemblies: bolts, washers, and nuts:

- K1 – supplied as a set from one manufacturer. The component may be packed in separate packages.
- K2 – supplied as a set from one manufacturer. The component shall be packed in the same package.

The combined method is used for both class K1 and K2, and the torque method is used for class K2. The preloading torque is calculated according to EN1090-2 chapter 8.5.2 [25]:

$$M_r = k_m \cdot d \cdot F_{p,C}$$

Where;

M_r = bolt installation torque (2-5)

k_m = torque coefficient

d = the nominal bolt diameter

$F_{p,C}$ = nominal minimum preloading force (2-4)

Torque method explained in EN1090-2 chapter 8.5.4 could only be used for K2 class and consist of the following two steps [25]:

Step 1 – apply a torque of 0,75M_r

Step 2 – apply a torque of 1,10M_r

Combined method explained in EN1090-2 chapter 8.5.4 could be used for both K1 and K2 class and consist of the following two steps [25]:

Step 1 – apply a torque defined from table 20 in EN 1090-2 chapter 8.5.4.

Step 2 – a specified part turn in applied in accordance to table 21 in EN1090-2 chapter 8.5.4 [25]

2.7 Ansys structural analysis software

Ansys® Academic Research Mechanical, 2020 R2, is a program that helps solving complex structural engineering problems [28]. Ansys uses finite element method (FEM) to solve the static analysis by using a numerical method solving differential equations. This method divides a bigger element or component into smaller pieces, called finite elements and are connected to each other by nodes. Knowing the characteristics of all finite elements, the characteristic of the entire system can be solved. The finite element analysis is a way to simulate loading conditions on a design and determine the designs response to those conditions [29].

The result will get more accurate the finer the finite elements are but will also result in more data. To achieve the best result without generating too much data and using too much time, the program uses different types of mesh. Meshing is when a complex geometry is divided into smaller pieces so that they can be used as local approximations of larger domains [30]. If a coarser mesh is used, the result will be more imprecise than if a fine mesh is used. On the other hand, the analysis itself will spend much more time and the amount of data will be considerably larger when a very fine mesh is used. It can therefore be profitable to use a mesh that gives reliable results at the same time as the analysis is carried out relatively quickly without excessive amounts of data.

In Ansys, you can choose to use an automatic meshing where you can choose between several scales in coarseness and fineness. When using the automatic variant, Ansys chooses which shapes are used in the various places in the model. The most common shapes in the structural analysis are tetrahedron and hexahedron, see Figure 2-11.

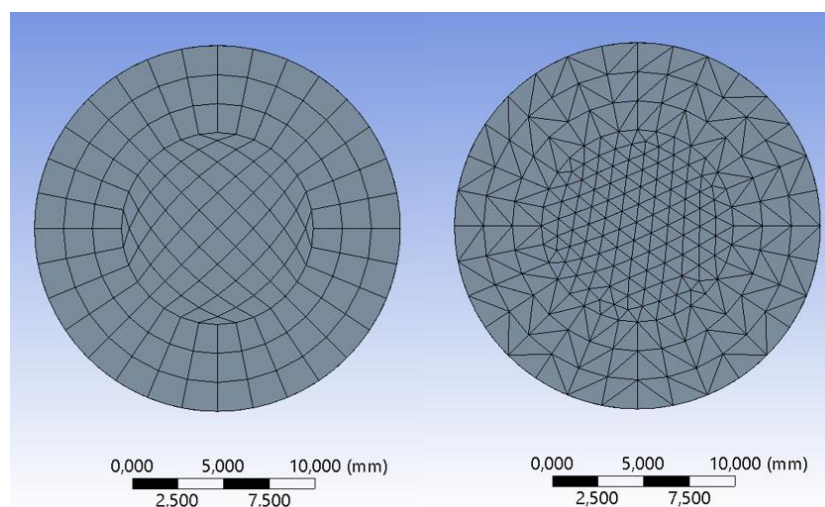


Figure 2-11 Hexa and tetra meshing shape

The hexa shape is used when the model “allows” it since it will give better results. This is because the hexa shape has fewer elements and nodes compared to the tetrahedron shape. In areas where the model can be complex, tetrahedra are used as a shape since it is easier to adapt.

Ansys is a simulation program that is well suited for engineering use, with a modern graphical user interface that can connect different CAD programs and be transferred directly for analysis. The workbench and modelling in Ansys can be done directly in ANSYS SpaceClaim. Ansys space claim is a user-friendly modelling program [31].

According to Ansys’s user guide, a static structural analysis “determines the displacements, stresses, strains, and forces in structures or components caused by loads that do not induce significant inertia and damping effects” [32].

The analysis should be performed with a simple loading that varies slowly with time. Types of loading that can be applied are external forces or pressures, steady-state inertial forces, imposed displacements and temperatures. The static analysis can be linear or nonlinear. Different types of nonlinearities can be enabled to meet the needs of the model. Large deflection is a nonlinear effect that is typically used for slender structures or when you expect large deformations. With large deflections enabled, Ansys considers the effect that deformation has on the stiffness. This nonlinearity demands that the analysis needs to converge on a result. To be able to converge, the load might need to be applied in several sub steps. This is by default *program controlled* and happens automatically in Ansys, but could lead to a more demanding calculation and that the result table changes with the convergence of the model.

Contact between elements in Ansys is automatically created when two different bodies touch each other. These contacts can be defined as *bonded*, *no separation*, *frictionless*, *rough*, or *frictional*. The two relevant definitions are *bonded* and *frictional*. *Bonded* is the default setting and prevent all types of separation and sliding. *Frictional* is used when two bodies resist sliding relative to each other up to a point that is defined by a fraction of the contact pressure, the friction coefficient. The state before the relative sliding starts is called *sticking* and after sliding starts is called *sliding*. This status can be visualized with the *contact tool* function [32].

The *fixed* support boundary condition in Ansys constraints the object from moving and rotating in all directions. A *remote displacement* boundary condition makes it possible to

apply displacement and rotations at a location. It can also prevent rotation and displacement by defining the value as zero. All boundary conditions make it possible to use the *force reaction* function to retrieve the moment- and force reactions. This function can also retrieve forces from contact regions between bodies, for example in the friction connection.

Bolt pretension is a function in Ansys used to apply pretension to bolts. It can be applied to a cylindrical face, edge, body, or several bodies. This function compresses the body in the middle indicated with two arrows. The pretension could be applied as a load or as an adjustment defined by a length. To fix the pretension, a lock step should be applied.

3 Profiles

There are five different designs of the specimens, made with M10 and M20 bolts. In Figure 3-1 one of the designs is shown and is called the STD specimen. How the specimen looks like in reality, with the middle part connected to the RC frame and the top and bottom part connected to the CLT-panel, is shown in the left of the figure. The right side of the figure illustrates the specimen modelled in Ansys and is the produced specimens used in the upcoming tests. The top part of the specimen is called the anchor profile and the bottom part is called the fixed profile. In the STD specimen, the slotted hole is in the fixed profile. The additional plate, shown in the figure, are used to create a more stable friction surface and reduce damage around the slotted hole. The red plates in the figure are the shim layers and one is placed between the anchor profile and the fixed profile, and the other between the fixed profile and the additional plate.

STD

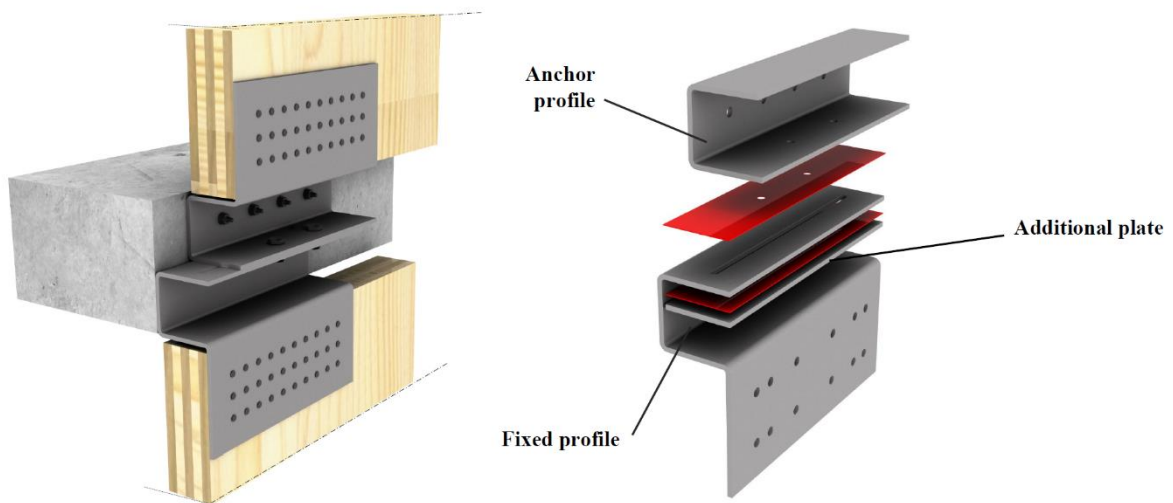


Figure 3-1 STD specimen

In Figure 3-2, specimen ALT and ALT-AS is illustrated. These specimens have a different shape than the STD, with the fixed profile straight and not bent. The anchor profile is also here connected to the RC frame but in these specimens the slotted hole is in the anchor profile and the additional plate is therefore moved to the inside of the anchor profile. The shim layers are not shown in this figure but in the ALT specimen one shim layer is placed between the additional plate and the anchor profile, and the other one is placed between the anchor profile and the fixed profile. For the ALT-AS specimen there is an extra profile called the alignment component. This is designed so that the specimen is easier to mount on the RC frame and the CLT-panel, as the fixed profile is facing the existing building. One of the shim layers in this specimen is placed between the additional plate and the anchor profile, and the other is placed between the anchor profile and the alignment component.

ALT

ALT-AS

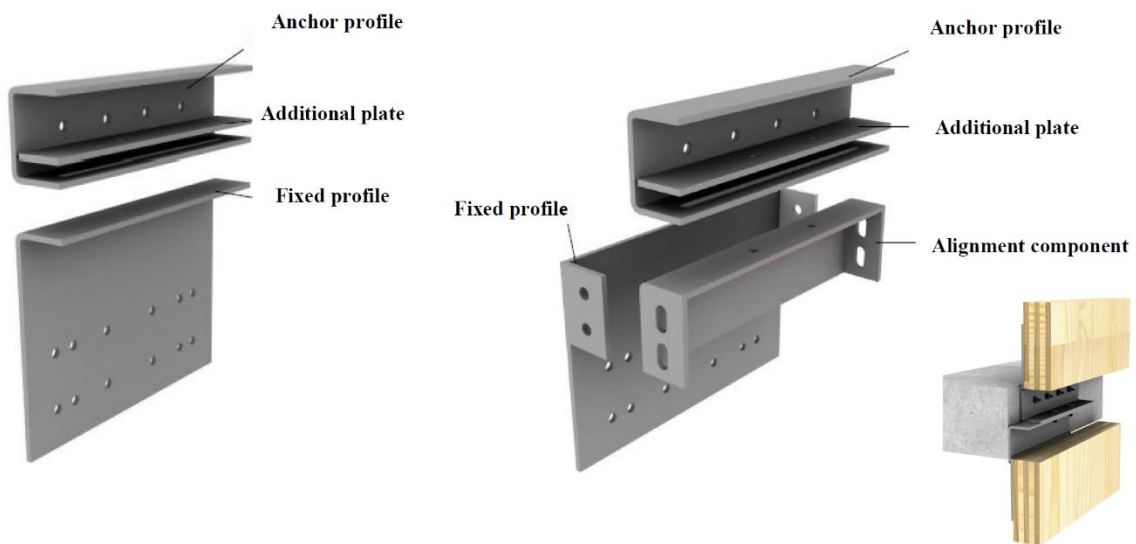


Figure 3-2 ALT and ALT-AS specimen

Figure 3-3 shows the fourth specimen called Hybrid. Similar to ALT and ALT-AS, the fixed profile is straight, but the connection is facing outwards and is mirrored by the fixed profile in ALT specimen. The anchor profile for the Hybrid specimen is the same as the one in the STD specimen when it is connected to the CLT-panel. In the produced specimen for testing, Hybrid do not include this bent part, only a simpler anchor profile like the other specimens. The slotted hole is placed in the fixed profile and the additional plate is placed under this slotted hole. For this specimen, the shim layers are illustrated in red in the figure.

HYBRID

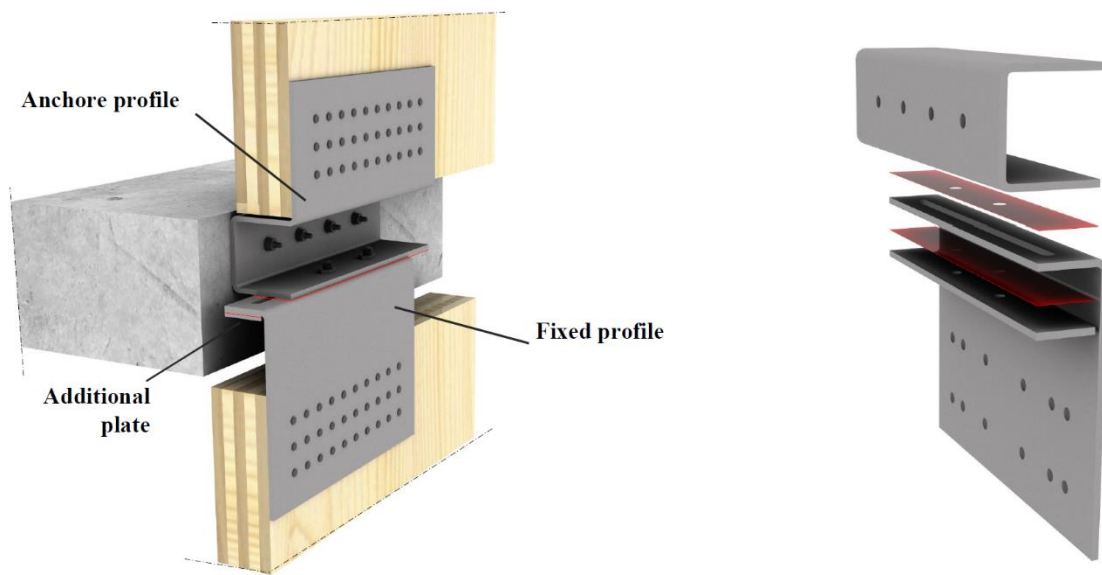


Figure 3-3 Hybrid specimen

The thickness of all the steel in the specimens are 8 mm and the shim layers are 2 mm. In all the specimens two shim layers are used. Table 3-1 shows the name of all the specimens, where the slotted hole is placed, what type of bolts they are designed with and type of material. All the specimens are made of steel with a yielding strength of 355 MPa (S355). The shim layers are designed with both M10 and M20 bolts and made with a hard material called Hardox with a hardness of 450 HB. There are three sets of each specimen, and the specimens are marked with the name of the specimen then underscore and which number of specimens it is when they are tested.

Table 3-1 Description of specimens

Specimen	Slotted hole	Bolts	Material
ALT	Anchor profile	M10/M20	S355
ALT-AS	Anchor profile	M10/M20	S355
Hybrid	Fixed profile	M10/M20	S355
STD-1H	Fixed profile	M10/M20	S355
STD-2H	Fixed profile	M10	S355
Shim layer	-	M10/M20	Hardox 450

3.1 Previous research

Hatletveit addressed a friction connection by modeling and analyzing in Ansys. He analyzed connections like the STD and ALT specimens. Through his simulation and investigation, he looked at all the aspects of the friction connection dampers with both seismic loads and gravity loads. From his numerical analysis he concluded that the ALT specimen had the best results of all the specimens he analyzed. He therefore developed an updated version of the ALT called the ALT-AS, which is one of the specimens analyzed in this thesis. This specimen is optimized for easier mounting [3].

In Marthinsen's thesis several physical tests were performed on specimens developed from Hatletveit's results. The tests were done in a press at NMBU, where a force was applied on the anchor profile in all the specimens that were tested. The press went up and down in a certain cycle in relation to displacements given in millimeters. Marthinsen introduced the use of shim layers during her tests to achieve a more stable behavior in the friction connections. These shim layers were made of aluminum, a softer material than the rest of the specimen made of steel, and led to a more stable behavior [4]. For this thesis, the shim layer material is changed to Hardox 450 steel, a harder material than the rest of the specimen.

In Marthinsen's tests, M14 bolts were used in the friction connection part of the specimens. The conclusion of her thesis was that to have two asymmetric slotted holes led to more twisting and was directly related to more bending moment in the fixed profile. It was discovered that the preload that was used for the first tests was too high to achieve the intended slip friction force. Therefore, the method in finding the preload was changed and

this method was a deviation from the standard but gave better results. During the tests, some preload was lost but it was not measured.

In this thesis the bolt size was changed from M14 to M10 and M20, no asymmetric slotted holes were used, and the material of shim layers were changed to Hardox 450. The specimen with the best behavior in the analysis and experimental tests will be recommended for full-scale testing.

4 Method: Experimental activity

Through this chapter the setup and testing procedure are described. The testing was divided into monotonic and cyclic tests. Two different presses were used for the testing, Instron100 and Instron300. Instron100 is an electric actuator press with a dynamic load capacity of 100 kN. Instron300 is a hydraulic press with a dynamic load capacity of 300 kN.

4.1 Setup

In Figure 4-1 and Figure 4-2 the setup is shown and was the same in Instron100 and Instron300. The setup was made so that the specimens would be held in the same position as in reality. For the setup, two columns were connected by a rail (C and D) and a T-shaped element (E) was used to move the anchor profile up and down. All the elements used in the setup was as stiff as possible so the friction connection (G) could be isolated and investigated. F and H in the figure is the fixed profile (F) and the anchor profile (H). Connection A and B are fixed.

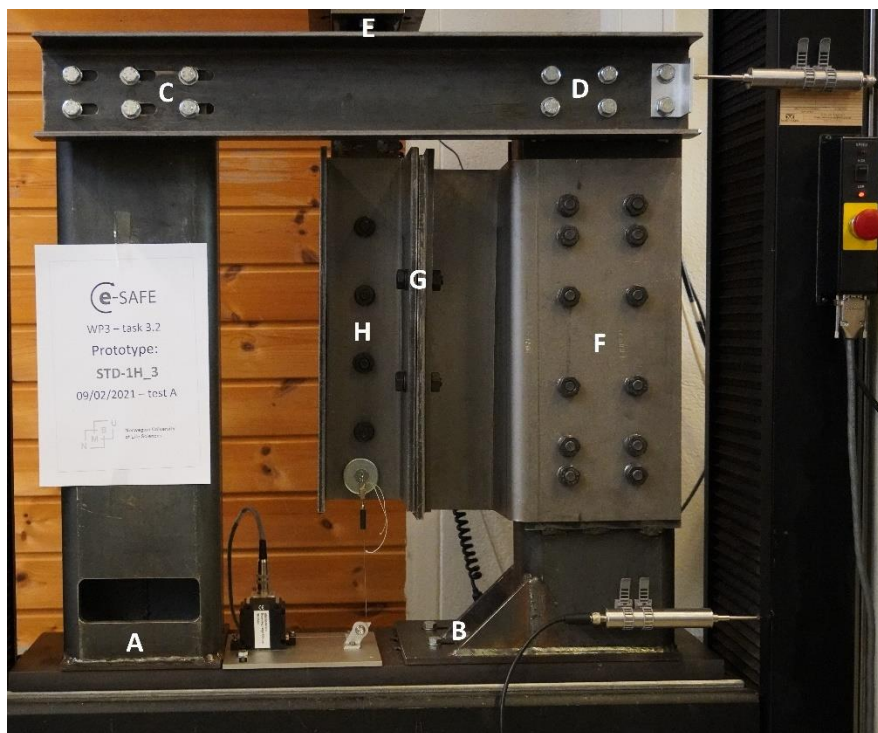


Figure 4-1 Set up in Instron100

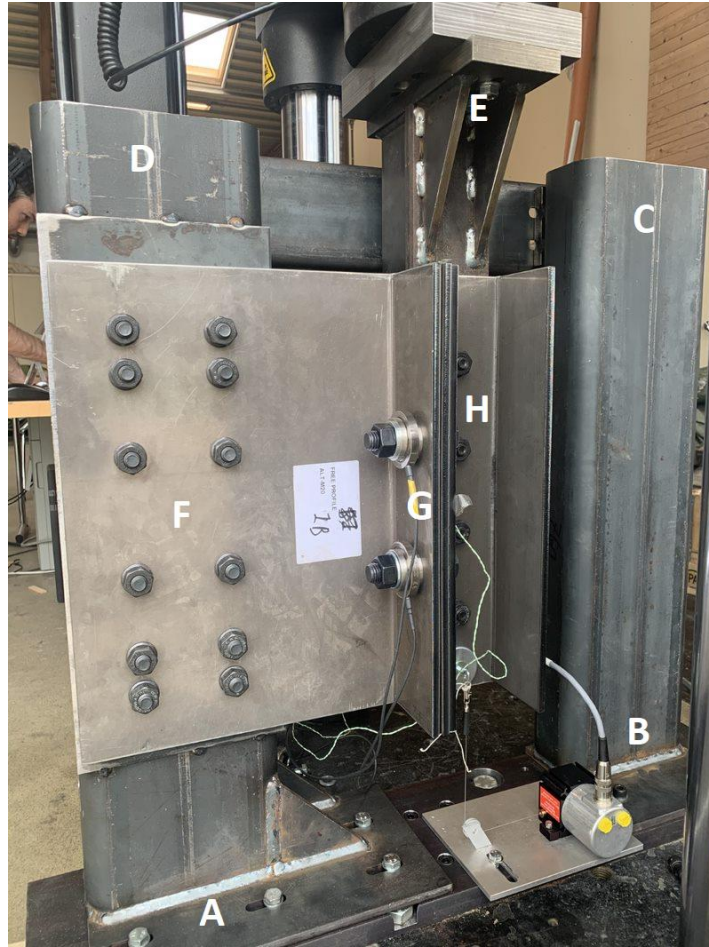


Figure 4-2 Set up in Instron300

4.1.1 Test preparation

Before performing the tests, all specimens were measured and is found in Appendix B. A wire brush on an electrical drill was used to brush the shim layers and achieve a clean mill scale condition without rust or other residues before mounting it [33]. When mounting the specimens to the press, the first step was to tighten the friction connection part with the steps described in chapter 4.4.1.

In the friction connection part, the shim layer and additional plate was placed and tightened. Then the fixed profile and anchor profile (F) were tightened with 110 Nm with a torque wrench and then the anchor profile was tightened again with 160 Nm with a torque wrench. These bolts were tighten following the procedure according to the torque method explained in chapter 2.6. After that the columns and the rail holding the columns together (A, B, C and D) were tightened. Finally, the T-profile was tightened (E), and all the instruments were mounted. This order was used so that the friction connection part in the specimens would be as aligned as possible.

4.2 Sensors

The press has internal sensors logging displacement and load. In addition, several types of sensors to collect data from the tests were used. To measure the displacement of the moving element, the anchor profile, a wire sensor was used. This was mounted with a magnet as seen in Figure 4-3 and used in all the tests.

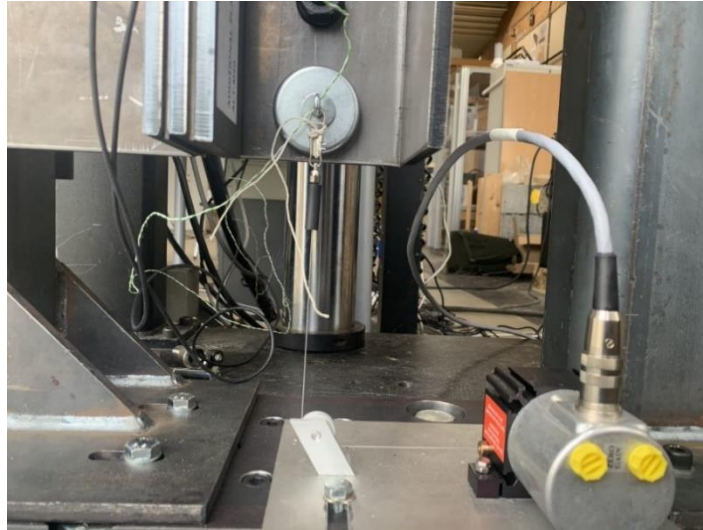


Figure 4-3: Wire sensor

Two washer sensors were used to measure the preload of the bolts. They were placed between the anchor profile and the washers to the bolts as seen in Figure 4-4. The top sensor was marked with a yellow tape. These sensors were only used with the bolt sizes M10 and M20.



Figure 4-4: Washer sensor

To record any rotation in the T-shaped element an inclinometer was used. This was attached to the back of the T-shaped element as shown in Figure 4-5. The inclinometer sensor was used in the monotonic testing and in the new testing campaign.



Figure 4-5: Inclinometer sensor

The last sensor that was used was a thermocouple and was placed in the friction area to measure the temperature development during the tests, as shown in Figure 4-6. This sensor was used in the new testing campaign.



Figure 4-6 Thermocouple

To control that the frame remained stiff during the tests, two LDT sensors were used. One was placed at the top of the column and one at the bottom in the Instron100. The LDT sensors are shown in Figure 4-7 and used in tests 1 to 10, shown in chapter 4.4.2 and 4.4.3.

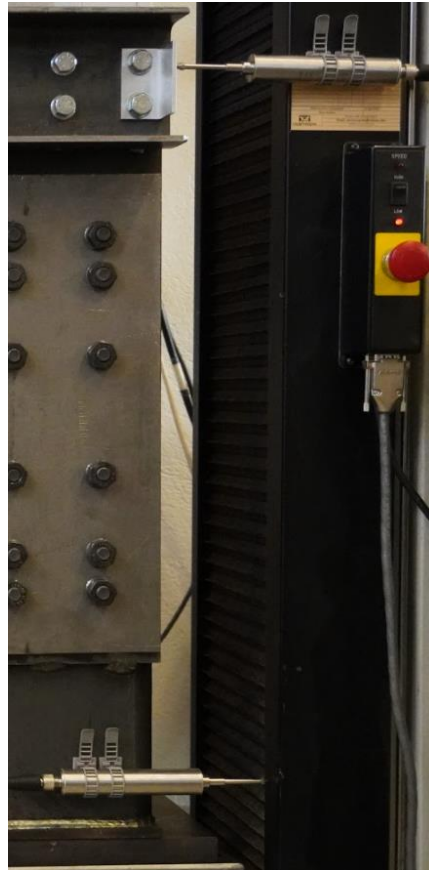


Figure 4-7 LDT sensor

4.3 Software

Instron100 is controlled by Bluehill software and Instron300 is controlled by Labview software. The two softwares are quite similar in use and Labview is described in detail in this chapter. Bluehill is described in detail by Marthinsen [4, Appendix B]. Figure 4-8 shows the interface of the Labview software. To the left in the figure, the manual speed is set. This is the speed of the press when operated manually. In the middle of the figure there is a section where a test procedure can be made. Here the speed, number of blocks, number of cycles and the displacement must be defined. When the test starts it goes through the program until it is finished, or the stop button is pressed. To the right in the figure, a graph of the ongoing test is

visualized. It shows the amplitude of the press in millimeter as the program runs. The real time position of the press in millimeter is shown at the top of the figure.

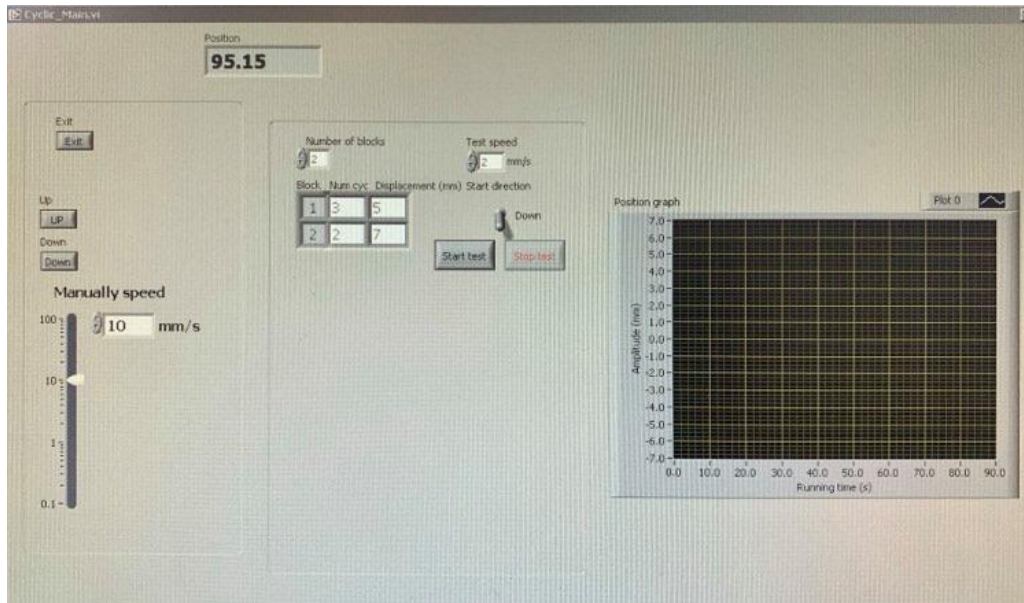


Figure 4-8 Interface of the Labview software

Two different types of tests were performed on the specimen in Instron300, a monotonic and a cyclic test. Both tests had different tests setup in Labview. The monotonic test had a simple procedure with only 1 block as seen in Table 4-1. The speed for the tests was 2 mm/s.

Table 4-1 Procedure of the monotonic test

Block	Number of cycles	Displacement [mm]	Speed [mm/s]
1	1	100	2

The cyclic test had a procedure with 6 blocks as seen in Table 4-2. The speed for these tests was also 2 mm/s.

Table 4-2 Procedure of the cyclic test

Block	Number of cycles	Displacement [mm]	Speed [mm/s]
1	1	5	2
2	3	10	2
3	3	20	2
4	3	30	2
5	3	40	2
6	3	50	2

In both Instron100 and Instron300, all data from the sensors, load cell and position of the press, was collected using Catman data acquisition software. Catman was used in combination with two Quantum X data acquisition systems, HBM MX440B and HBM MX840. The two Quantum X were connected to all sensors. Figure 4-9 shows the interface of Catman with the connected sensors. All the sensors except for the washer sensors and the thermocouple were reset to zero before starting the test. The settings for each sensor can be seen in appendix D.

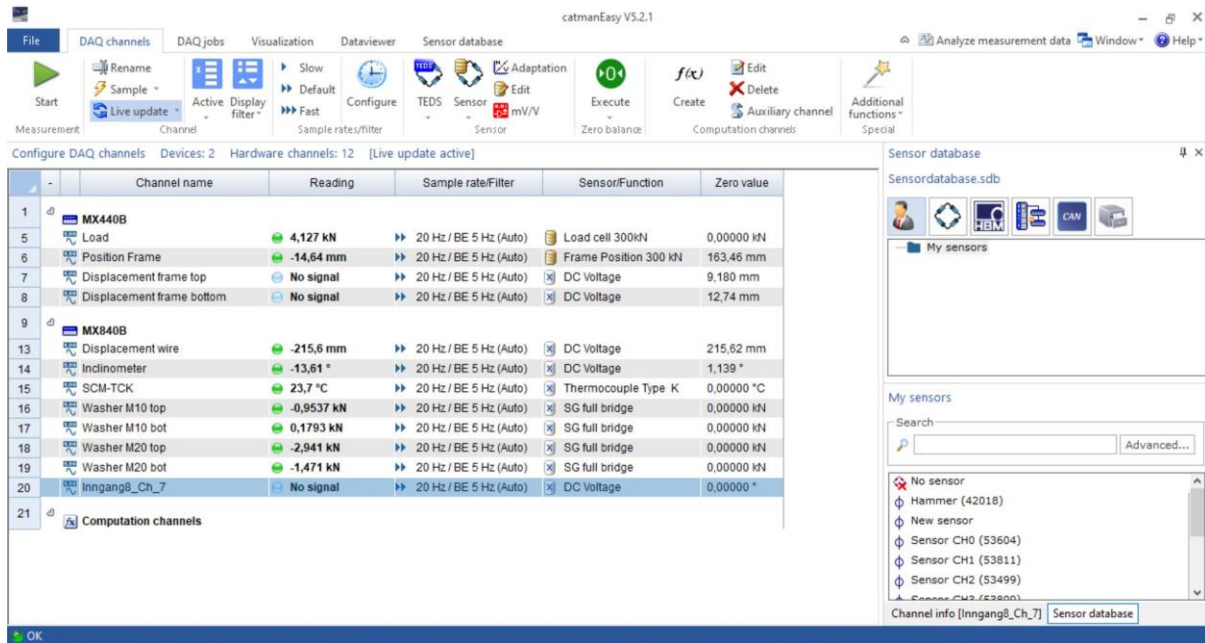


Figure 4-9 Interface of the Catman software

4.4 Experimental tests

In the work of this thesis there were constant uncertainties with the function of the press and the COVID-19 regulations. As a result, fewer tests were performed. This chapter describes the three rounds of testing that were possible to perform during this period and the procedure of the tests.

4.4.1 Preload

The tests of the specimens were performed with different preload. For the calculation of the preload equation (2-4) was used. When applying the preload to the bolts a torque wrench was used. There were two types of torque wrench used to tighten the bolts. One had a span reaching from 14 Nm to 115 Nm and the other had a span from 60 Nm to 350 Nm. For the smaller bolts the torque wrench with the lower values were used and for the larger bolts the

one with the higher values were used. In this chapter the calculation of preload and torque value for the different tests are shown.

Tests 1 to 3 and 8 (chapter 4.4.2) were with the M14 bolts and had a preload of 30 %, calculated from eq. (2-4):

$$F_{p,C} = 0,3 \cdot (0,7 \cdot f_{ub} \cdot A_s) = 24,1 kN$$

Where:

F_{ub} is 1000 MPa, ultimate tensile strength for 10.9 steel bolts

A_s is 115 mm², area of section of one M14 bolt

For the M14 bolts the k_m value is 0,129 and was provided by the producer. Tests 1 to 3 and 8 were done in Instron100 and the applied torque value was:

$$M_r = k_m \cdot d \cdot F_{p,C} = 0,129 \cdot 14 \text{ mm} \cdot 24,1 \text{ kN} = 43,5 \text{ Nm}$$

First tightening step: $0,75M_r = 32,7 \text{ Nm}$

Second tightening step: $1,1M_r = 48 \text{ Nm}$

In tests 4 to 7 (4.4.2) a preload of 25 %, instead of 30 %, was used with M14 bolts. This gave a preload of 20 kN and the torque values was:

$$M_r = k_m \cdot d \cdot F_{p,C} = 0,129 \cdot 14 \text{ mm} \cdot 20 \text{ kN} = 36,1 \text{ Nm}$$

First tightening step: $0,75M_r = 27 \text{ Nm}$

Second tightening step: $1,1M_r = 39,7 \text{ Nm}$

For both monotonic and cyclic tests, described in chapter 4.4.3 and 4.4.4, the friction coefficient of 0,22 was assumed and is the dynamic friction coefficient used in the Ansys modelling. The goal was to reach a slip friction force of 30 kN and that gave a preload with two frictions surfaces and two bolts of:

$$F_{p,C} = \frac{F_{s,R}}{n_s n_b \mu} = \frac{30\,000 \text{ N}}{2 \cdot 2 \cdot 0,22} = 34,1 \text{ kN}$$

For the 8.8 M10 and M20 bolts the k_m value was not declared by the producer, but from the table with standardized torques values (M_r) given in the product catalog shown in Appendix A, the k_m value is found by a back-calculation. The hypothesis is that the table is referred to 70% of ultimate strength. For M10 bolts that gives:

$$F_{p,C} = 0,7 \cdot f_{ub} \cdot A_s = 0,7 \cdot 800 \text{ N/mm}^2 \cdot 58 \text{ mm}^2 = 32\,480 \text{ N}$$

$$k_m = \frac{M_r}{d \cdot F_{p,C}} = \frac{47 \text{ Nm}}{0,01 \text{ m} \cdot 32\,480 \text{ N}} = 0,145$$

For M20 bolts:

$$F_{p,C} = 0,7 \cdot f_{ub} \cdot A_s = 0,7 \cdot 800 \text{ N/mm}^2 \cdot 245 \text{ mm}^2 = 137\,200 \text{ N}$$

$$k_m = \frac{M_r}{d \cdot F_{p,C}} = \frac{385 \text{ Nm}}{0,01 \text{ m} \cdot 137\,200 \text{ N}} = 0,140$$

The value is $k_m = 0.145$ for M10 and $k_m = 0.140$ for M20.

This preload, 34,1 kN, was used in tests 9.1 to 14 (chapter 4.4.3 and 4.4.4) and the torque values for the M10 bolts were:

$$M_r = k_m \cdot d \cdot F_{p,C} = 0,145 \cdot 10 \text{ mm} \cdot 34,1 \text{ kN} = 49,5 \text{ Nm}$$

First tightening step: $0,75M_r = 37 \text{ Nm}$

Second tightening step: $1,1M_r = 54,3 \text{ Nm}$

For the M20 bolts the applied torque value was:

$$M_r = k_m \cdot d \cdot F_{p,C} = 0,140 \cdot 20 \text{ mm} \cdot 34,1 \text{ kN} = 95,5 \text{ Nm}$$

First tightening step: $0,75M_r = 71,8 \text{ Nm}$

Second tightening step: $1,1M_r = 105,3 \text{ Nm}$

For the M14 bolts the applied torque value was:

$$M_r = k_m \cdot d \cdot F_{p,C} = 0,129 \cdot 14 \text{ mm} \cdot 34,1 \text{ kN} = 61,6 \text{ Nm}$$

First tightening step: $0,75M_r = 46 \text{ Nm}$

Second tightening step: $1,1M_r = 67,5 \text{ Nm}$

For the M16 bolts the applied torque value was:

$$M_r = k_m \cdot d \cdot F_{p,C} = 0,129 \cdot 16 \text{ mm} \cdot 34,1 \text{ kN} = 70,4 \text{ Nm}$$

First tightening step: $0,75M_r = 52,8 \text{ Nm}$

Second tightening step: $1,1M_r = 77,4 \text{ Nm}$

In the last tests (chapter 4.4.4), 15 to 21, the preload was reduced to 50 % of the previous preload. This gave a preload of 17,05 kN and the torque values for the M10 bolts was:

$$M_r = k_m \cdot d \cdot F_{p,C} = 0,145 \cdot 10 \text{ mm} \cdot 17,05 \text{ kN} = 24,7 \text{ Nm}$$

First tightening step: $0,75M_r = 18,5 \text{ Nm}$

Second tightening step: $1,1M_r = 27,1 \text{ Nm}$

For the M20 bolts the applied torque value was:

$$M_r = k_m \cdot d \cdot F_{p,C} = 0,140 \cdot 20 \text{ mm} \cdot 17,05 \text{ kN} = 47,7 \text{ Nm}$$

First tightening step: $0,75M_r = 35,6 \text{ Nm}$

Second tightening step: $1,1M_r = 52,6 \text{ Nm}$

4.4.2 Preliminary testing with old specimen

The new specimens had not arrived at NMBU in early February. It was therefore decided to do some preliminary testing with the old specimen from Marthinsen's work [4, pp. 2-4]. The goal of these tests was to test the equipment, software and the new Hardox 450 shim layers which had already arrived at the University. The tests were performed as cyclic with cycles

1x5 mm + 3x10 mm + 3x20 mm + 3x30 mm + 3x40 mm + 3x50 mm and a speed of 0,5 mm/s. As a safety measure the press was set to stop if it reached 50 kN. Tests 1 to 8 were performed on different specimens with the Instron100 machine and can be seen in Table 4-3.

Table 4-3 Overview of the preliminary testing

N	Date	Specimen	Torque step 1-2 [Nm]	Friction Bolts	Shim Layers	Protocol
1	8-feb	STD_3	32.7-48	M14	Hardox450	Cyclic
2	8-feb	STD-1H_2	32.7-48	M14	Hardox450	Cyclic
3	9-feb	STD-R_2	32.7-48	M14	Hardox450	Cyclic
4	9-feb	STD-1H_3	27-39.7	M14	Hardox450	Cyclic
5	9-feb	ALT_2	27-39.7	M14	Hardox450	Cyclic
6	10-feb	ALT_2	27-39.7	M14	Hardox450	Cyclic
7	11-feb	ALT_2	27-39.7	M14	Hardox450	Cyclic
8	12-feb	ALT_2	32.7-48	M14	Aluminum	Cyclic

4.4.3 Monotonic testing in Instron100

Technical issues with the Instron100 had the testing put on hold because a technician from abroad had to come and repair the press. Due to the covid-19 situation the borders were kept closed and it was therefore not possible to repair the press. It was decided to try monotonic compression testing with the new specimen in the Instron100 as the problems seemed to be linked to the press lifting upwards in the cyclic testing.

As the new washer sensors had not been tried before, they were first tested on a specimen on the floor, see Figure 4-10. It was decided to apply the same torque as planned for the rest of the tests (4.4.1):

M10 bolts:

- Step 1: 37 Nm
- Step 2: 54.3 Nm

M20 bolts:

- Step 1: 71.8 Nm
- Step 2: 105.3 Nm

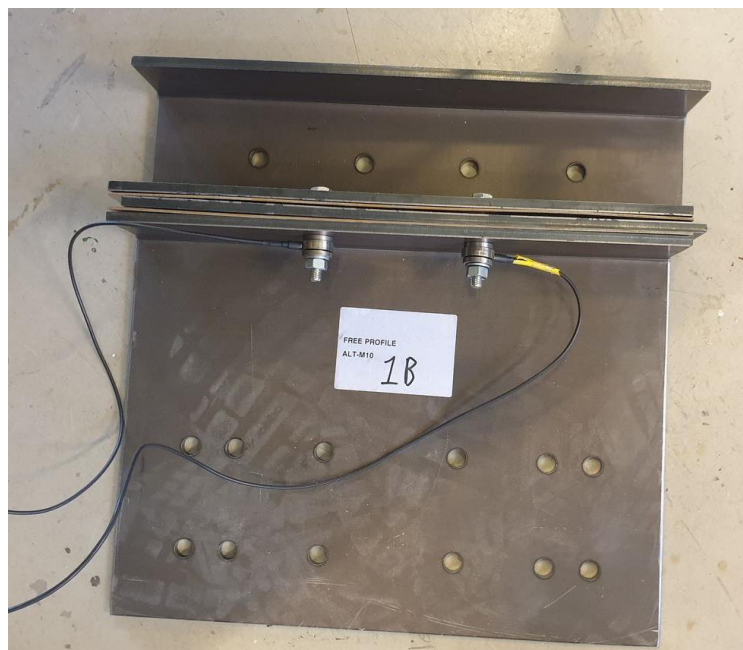


Figure 4-10 Set up of the washer sensor test.

Tests 9 and 10 were performed with a 100 mm compression with 2 mm/s as seen in Table 4-4. These were the first tests with new specimens and washer sensors. The washer sensors gave unexpected readings and test 9 was therefore done 3 times, and test 10 was done 5 times as seen in Table 4-4. Tests 10.4 and 10.5 were done with friction bolts of M16 and M14.

Table 4-4 Overview of the monotonic testing in Instron100

N	Date	Specimen	Torque step 1-2 [Nm]	Friction Bolts	Shim Layers	Protocol
9.1	22-apr	ALT-M10_1	37-54.3	M10	Hardox450	Monotonic
9.2	22-apr	ALT-M10_1	37-60	M10	Hardox450	Monotonic
9.3	22-apr	ALT-M10_1	37-54.3	M10	Hardox450	Monotonic
10.1	23-apr	ALT-M20_1	71.8-105.3	M20	Hardox450	Monotonic
10.2	23-apr	ALT-M20_1	71.8-105.3	M20	Hardox450	Monotonic
10.3	23-apr	ALT-M20_1	71.8-105.3	M20	Hardox450	Monotonic
10.4	23-apr	ALT-M20_1	52.8-77.4	M16	Hardox450	Monotonic
10.5	23-apr	ALT-M20_1	46-67.5	M14	Hardox450	Monotonic

4.4.4 New testing campaign with Instron300

In mid-May, the new Instron300 press was ready to be used for cyclic testing. The tests were performed with all the new specimens. Tests 11 to 14 were performed with a torque that theoretically would give a slip force of 30 kN. For the remaining tests (tests 15 to 21), the torque was reduced by 50 %. All the tests were performed cyclic with cycles 1x5 mm + 3x10 mm + 3x20 mm + 3x30 mm + 3x40 mm + 3x50 mm, except for test 14 which was monotonic with 100 mm compression. An overview of the tests can be seen in Table 4-5. All the tests were performed with a speed of 2 mm/s.

Table 4-5 Overview of the new testing campaign with Instron300

N	Date	Specimen	Torque step 1-2 [Nm]	Friction Bolts	Shim Layers	Protocol
11	14-May	ALT-M20_1	71.8-105.3	M20	Hardox450	Cyclic
12	15-May	ALT-M20_2	71.8-105.3	M20	Hardox450	Cyclic
13	15-May	ALT-M10_1	37-54.3	M10	Hardox450	Cyclic
14	16-May	ALT-M10_1	37-54.3	M10	Hardox450	Monotonic
15	16-May	ALT-AS-M10_1	18.5-27.1	M10	Hardox450	Cyclic
16	16-May	ALT-AS-M20_1	35.6-52.6	M20	Hardox450	Cyclic
17	16-May	STD-1H-M10_1	18.5-27.1	M10	Hardox450	Cyclic
18	16-May	STD-1H-M20_1	35.6-52.6	M20	Hardox450	Cyclic
19	18-May	STD-2H-M10_1	14	M10	Hardox450	Cyclic
20	18-May	HYB-M10_1	18.5-27.1	M10	Hardox450	Cyclic
21	18-May	HYB-M20_1	35.6-52.6	M20	Hardox450	Cyclic

4.5 Limitations

This chapter present observations and factors that could have influenced the results from the experimental activity.

- It was observed a horizontal deformation in the Instron100 press during large loads.
- It was observed swaying in the Instron300 press during large loads.
- The presses only applied a displacement of 50 mm in the cyclic tests, so the full sliding length in the friction connection were not fully tested.
- For both M10 and M20 bolts the k_m -value were unknown and found by a back-calculation. It was therefore uncertain if the applied torque was correct.
- The torque wrench used to tighten the bolts was a manual wrench with an unknown accuracy.
- The washer sensors were not reliable and could not be used to indicate the applied preload.
- The preload was calculated assuming a friction coefficient of 0,22
- Both the tests done in Instron100 and Instron300 made asymmetric graphs from the results. The reason for this is unknown.
- It was limited time for testing due to Covid-19. Instron300 was repaired in the middle of May and cyclic testing were therefore only performed once per specimen.

5 Method: FEM-analysis

The model and settings used in the analysis of the different specimens in Ansys are described in this chapter. These models were made to give an indication of how the behavior of the specimens would be in the press. The specimens were modeled to have the same conditions as in the press, to be able to compare the results with the experimental activities.

5.1 Materials

All the elements in the model are defined with a Young's modulus of 210 000 MPa and a Poisson's ratio of 0,3 (Table 5-1).

Table 5-1 Material Properties in Ansys

Young's Modulus	210 000 MPa
Poisson's Ratio	0,3
Bulk Modulus	175 000 MPa
Shear Modulus	80 769 MPa

5.2 Contacts

Contacts between elements in the model are defined as either bonded or frictional. Bonded is chosen for the contact between the bolt and the nut, and between the anchor profile and the T-shaped element. Frictional is chosen for the rest of the contacts. The friction coefficient is defined as 0,3 for all the contacts except for the sliding surface, which is marked with red in Figure 5-1. The sliding surface has a friction coefficient of 0,39 in the static friction and 0,22 in the dynamic friction.

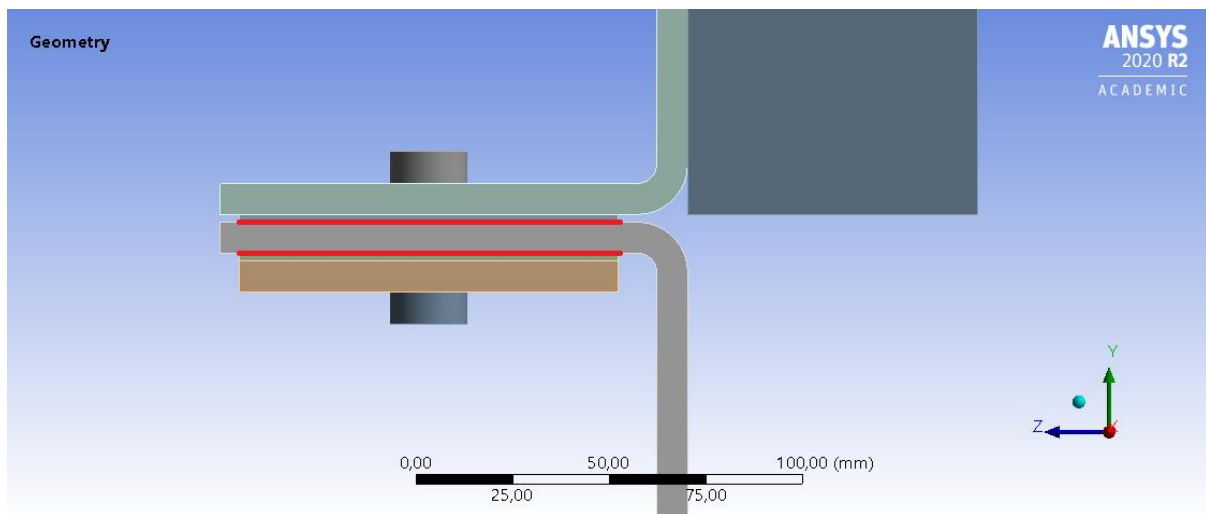


Figure 5-1 Sliding surface indicated with red

5.3 Analysis settings

The analysis settings in Ansys are set to default value, except for the following settings:

- *Large deflection* is set to *on*
- *Nodal forces* are set to *yes*
- *Contact miscellaneous* is set to *yes*

This makes the results converge with large deformation and includes nodal and contact values to the results. The analysis is divided into two steps. Both steps are set to last one second each. Step 1 starts at 0 second, and step 2 starts at 1 second. The amount of substeps, which the step is divided into, is program controlled. Therefore, it varies from model to model how many substeps each step is divided into, but the total step time is always 1 second.

5.4 Restraints

A fixed support is applied to the back surface of the fixed profile illustrated with blue in Figure 5-2. The remote displacement is applied to the top surface of the T-shaped element illustrated in yellow in the Figure 5-2.

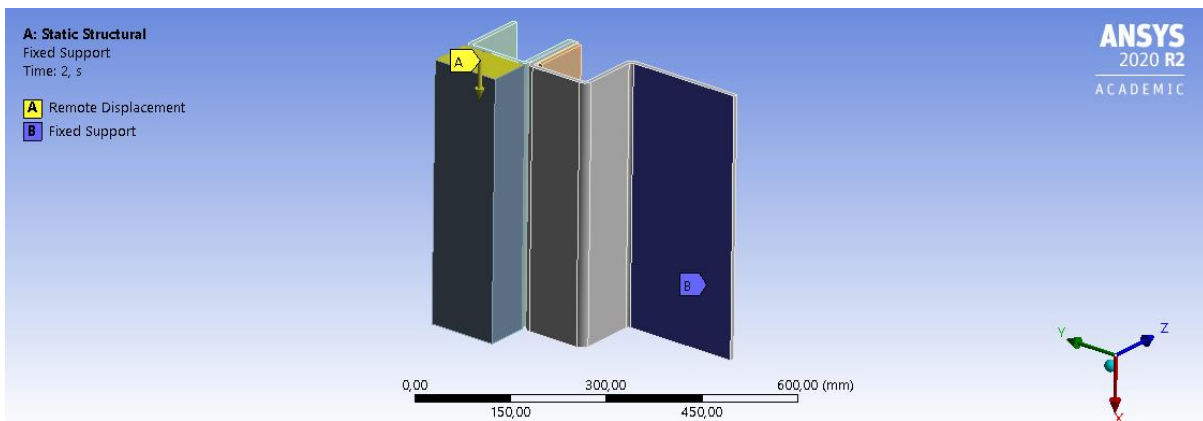


Figure 5-2 Restraints in the model

5.5 Output

Relevant deformations, stresses, forces, and status was retrieved for all the specimens. It was made an evaluation in every simulation which results that would be included. The forces are retrieved from the force reaction in the fixed profile and from force probes in the two sliding surfaces. The force probes are in friction surface 1 and friction surface 2. These two friction surfaces are between the shim layer and either the anchor- or fixed profile as described for the different specimen in Table 5-2 and illustrated in Figure 5-1.

Table 5-2 Definition of friction surface 1 and 2

	Friction surface 1	Friction surface 2
STD-1H	Shim layer/fixed profile	Shim layer/fixed profile
STD-2H	Shim layer/fixed profile	Shim layer/fixed profile
ALT	Shim layer/anchor profile	Shim layer/anchor profile
ALT-AS	Shim layer/anchor profile	Shim layer/anchor profile
Hybrid	Shim layer/fixed profile	Shim layer/fixed profile

5.6 Verification of preloaded bolts

The bolt is divided into two parts: the bolt and the nut. The nut is defined as bonded with the shaft (Figure 5-3). The bolt head and the shaft are defined as one element, but the surface is split at the area where the nut is located. This split is made to enable the function *bolt pretension* to be applied only to the surface of the bolt shaft like illustrated in Figure 5-4. In the verification of the bolts a standard M10 8.8 bolt is used. The M10 bolt has a shaft with diameter 10 mm and a washer with diameter of 20 mm. The bolt head and the washers were simplified as one element with the diameter of a standard washer of 20 mm.

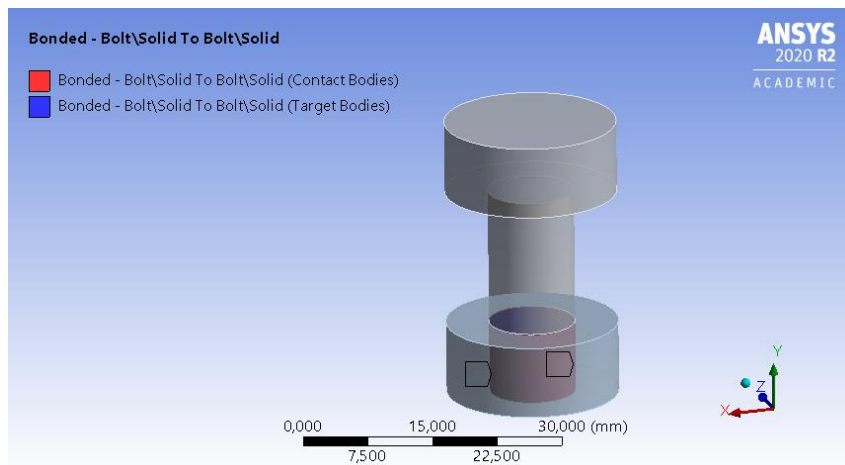


Figure 5-3 Bonded contact between bolt and nut

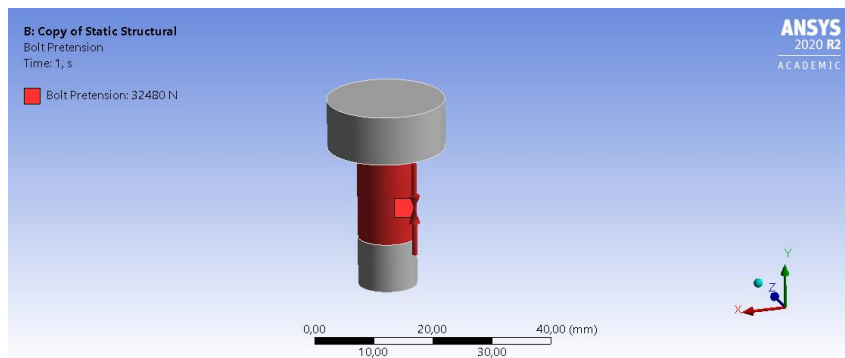


Figure 5-4 Application of the bolt pretension function

To illustrate the results of the bolt more accurately, a multizone mesh with hexa shape was used in this verification, see Figure 5-5.

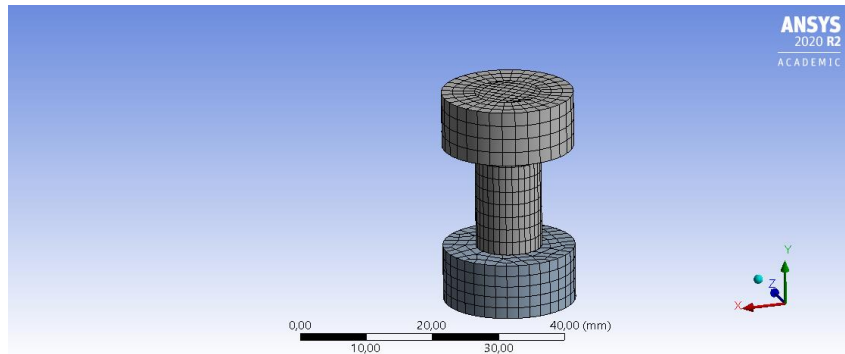


Figure 5-5 Mesh in the bolt

A fixed support was applied, as illustrated in blue in Figure 5-6, at the bottom surface of the bolt head and the top surface of the nut.

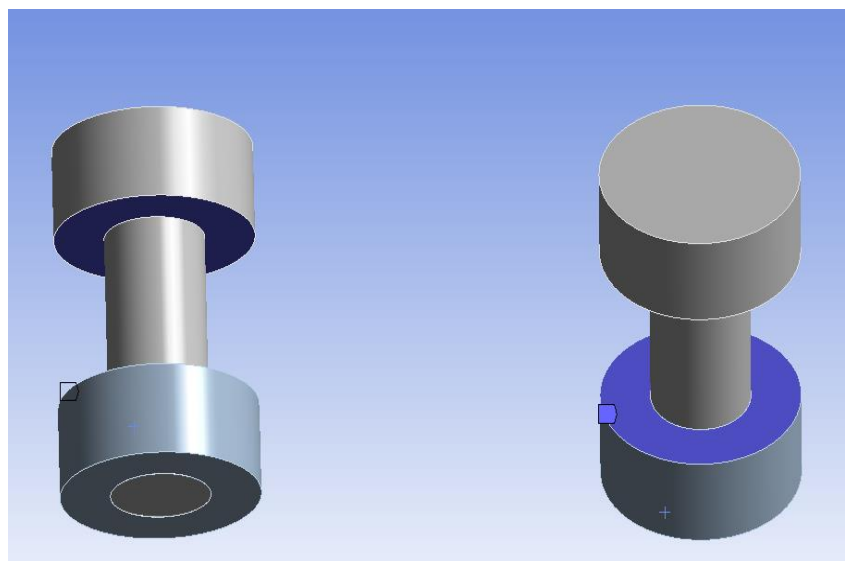


Figure 5-6 Fixed surfaces

The M10 8.8 bolt was applied a preload of 32 480 N which is 70% of the bolt capacity (eq. (2-4)). Stresses and strain were retrieved from the model and compared to hand calculations.

5.7 Verification of the friction connection

Two models were made to verify that the friction connection would behave as expected, a simple- and a real model. The method on how the simulations were performed are described in this chapter.

5.7.1 Simple model

To verify that the behavior of the friction connection would be as expected, a simple model was made. This model consisted of two plates, one with simple holes and one with a slotted hole as shown in Figure 5-7. The model is inspired by the friction surface of the ALT specimen, where the top plate is the anchor profile, and the bottom plate is the fixed profile. Both the plates are 450x60 mm and 8 mm thick. The bolts are standard M10 bolt with the same diameter as in chapter 5.6. The slotted hole is 380 mm long and 10 mm wide. The normal holes in the fixed plate are 10 mm.

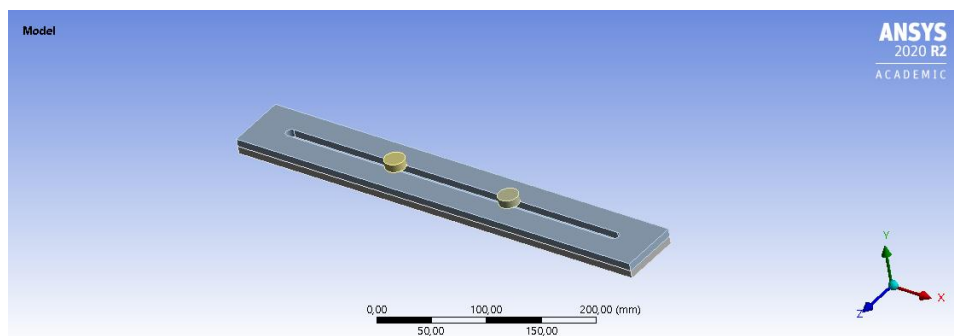


Figure 5-7 Geometry of the simple model

An automatic mesh was used, and a fixed support was applied to the bottom face of the fixed profile. A remote displacement was applied to the top face of the anchor profile. This was to prevent rotation around the Y-axis and to apply a 5 mm displacement in X-direction. The analysis was divided into two steps (Figure 5-8). In the first step, the bolts got loaded with their preload, and then locked. In the second step, the displacement at the top plate was applied. The pretension of the bolts was 32 480 N. Relevant stresses and force reaction from both the fixed support and the friction surface are retrieved.

Steps	Time [s]	<input checked="" type="checkbox"/> X [mm]	<input checked="" type="checkbox"/> RY [°]
1	1	0,	= 0,
2	1	0,	0,
3	2	5,	= 0,
*			

Steps	<input checked="" type="checkbox"/> Define By	<input checked="" type="checkbox"/> Preload [N]	<input checked="" type="checkbox"/> Preadjustment [mm]	<input checked="" type="checkbox"/> Increment [mm]
1	1.	Load	32480	N/A
2	2.	Lock	N/A	N/A
*				

Figure 5-8 Load steps

5.7.2 Real model

This model was made to verify that the connection with the shim layers and additional plate would behave as expected. This model is also inspired by the ALT specimen. It consists of the layers illustrated in Figure 5-9. All the layers have the same size of 450x60 mm. The additional plate, anchor profile and the fixed profile are 8 mm thick, and the shim layers are 2 mm thick. The slotted hole in the anchor profile is 380 mm long and 10 mm wide. The holes in the other layers are 10 mm. Standard M10 bolts with the size in chapter 5.6 is used.

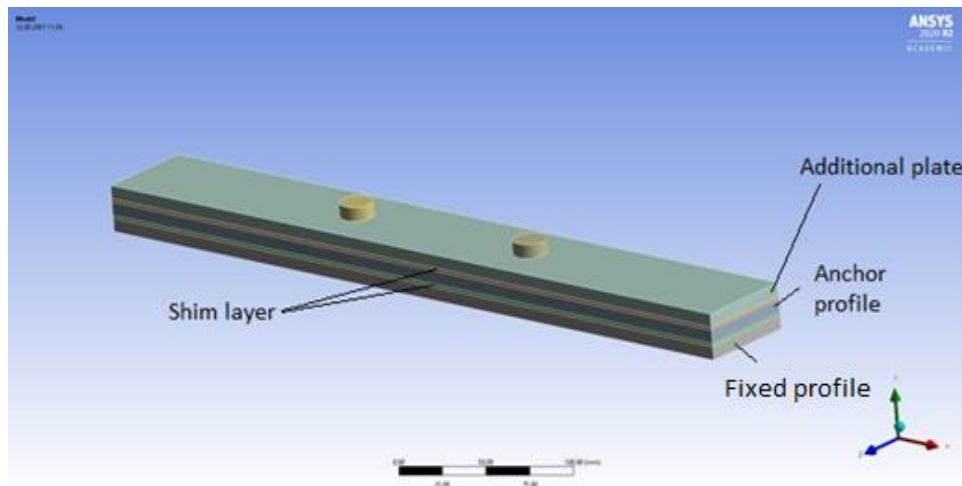


Figure 5-9 Geometry of the real model

A fixed support was applied to the bottom face of the fixed profile to prevent movement and rotation. A remote displacement was applied to the top face of the anchor profile to prevent rotation around the Y-axis and to apply a displacement of 5 mm in X-direction. The preloading procedure was the same as in chapter 5.7.1. The resulting force was extracted from the fixed support and force probe between the two shim layers and the anchor profile. In addition, relevant stresses were retrieved.

5.8 Remote displacement

When applying the remote displacement on a surface, Ansys automatically place it in the middle of the element surface. The remote displacement functions apply displacement and rotations at a given location. At first, the remote displacement was placed on the back surface of the anchor profile (Figure 5-10). This led to a rotation around the mid-point of the anchor profile, which would be unrealistic in the case of the press where the force was applied at the

top and not in the middle of the element. Figure 5-11 illustrates the anchor profile which are connected to the T-shaped element pushing the specimens up and down in the press. This would be the profile connected to the RC frame. When placing the remote displacement in the middle, the rotation of the element would be around this point as shown to the right in the Figure 5-11. A test was conducted to understand the behavior of the profiles with these conditions. Figure 5-10 shows where the remote displacement was applied on the anchor profile.

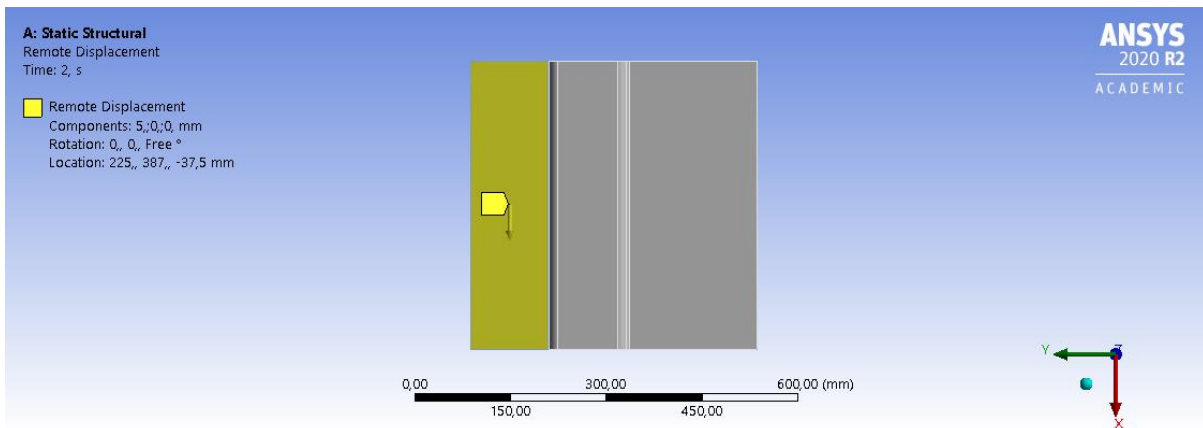


Figure 5-10 Rotation point in the middle of the anchor profile

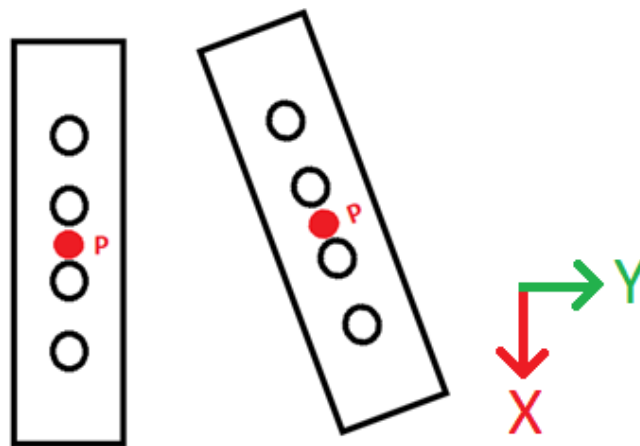


Figure 5-11 Rotation point in the middle

To be able to compare the results from Ansys with the results from the press, the remote displacement was placed on the top of the anchor profile as seen in Figure 5-12 below. In this new model an element was made behind the anchor profile to act as in the press. The connection between the new element, the T-shaped element, and the anchor profile was set to

be bonded. The remote displacement was applied to the top surface of this geometry, as seen in Figure 5-13. This location of the remote displacement was used in case A, B and C.

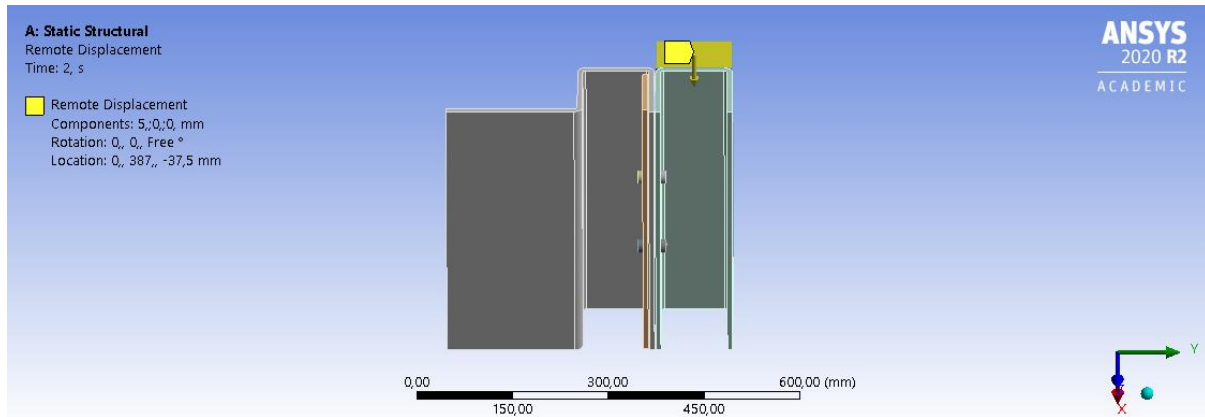


Figure 5-12 Rotation point on the top of the press profile

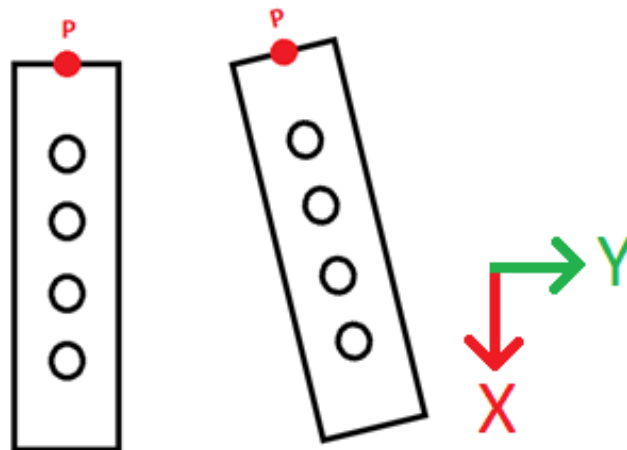


Figure 5-13 Rotation point at the top

5.9 Simulation cases

To define the boundary conditions in Ansys several tests were performed. All the tests were done with the same M10 8.8 bolts with a preload of 70% of the capacity for each bolt found by eq. (2-4).

$$F_{p,C} = 0.7 \cdot 58 \text{ mm}^2 \cdot 800 \text{ MPa} = 32\,480 \text{ N}$$

From theory the slip friction force is found by eq. (2-3).

$$F_{s,R} = 2 \cdot 2 \cdot 0,3 \cdot 32\,480 \text{ N} = 38\,976 \text{ N}$$

This gives a theoretical slip force of 38 976 N with a friction coefficient of 0,3, two friction surfaces and two bolts.

In all the tests a displacement of 5 mm is applied in the X-direction. The slip friction force is found from the force reaction and the force probe in the two friction surfaces, described in chapter 5.5. The deformation in the figures in this chapter is automatically scaled to easier understand how it behaves.

The specimens made in Ansys were modeled like the produced specimens so the results from Ansys could be compared with the physical tests. The restraints were therefore chosen to replicate the behavior of the press. To define these restraints three cases were performed, case A, B and C.

The coordinate system of the model is shown in Figure 5-14 and Figure 5-15.



Figure 5-14 XY-plane in Ansys (STD-1H)

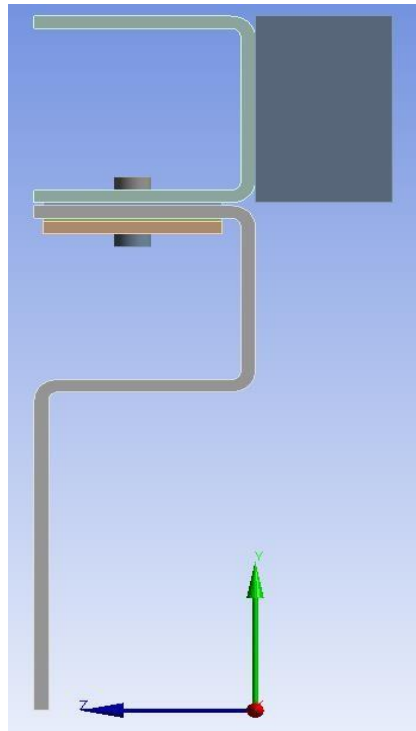


Figure 5-15: YX-plane in Ansys (STD-1H)

The difference between case A, B and C were the restraints in rotation and deformation in X-, Y- and Z-direction. These cases were done to define the most accurate condition of the specimens in Ansys (compared to the conditions in the press). Specimen STD-1H and ALT were chosen because the behavior of the two specimens is outmost different. Case A was defined as the least restricted case with deformation in Y-direction and rotation around Z-axis as free DOF. The free DOF for case A is shown in Figure 5-16 and in Table 5-3.

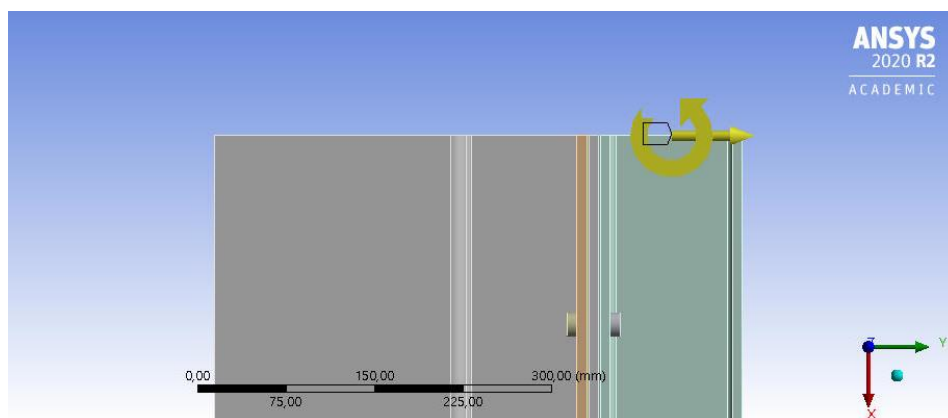


Figure 5-16 Free DOF in case A

Case B was simulated with only rotation around Z-axis as free DOF. The free DOF for case B is shown in Figure 5-17 and Table 5-3.

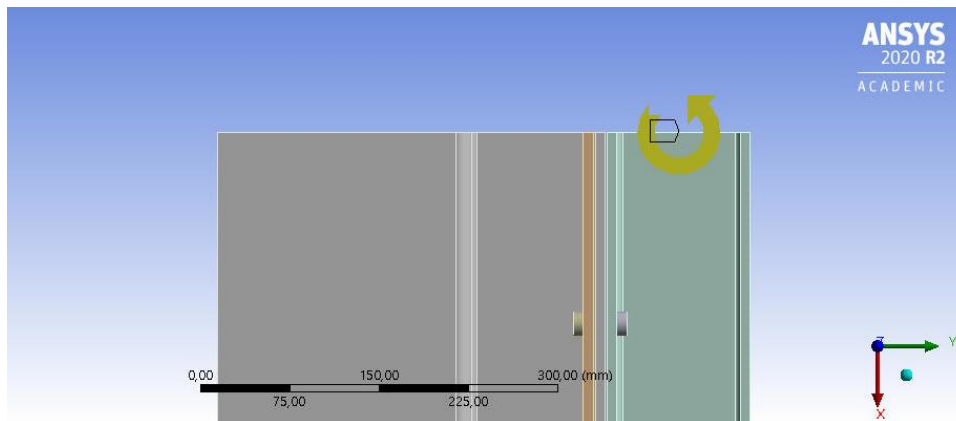


Figure 5-17 Free DOF in case B

Case C is simulated with all DOF fixed as shown in Table 5-3.

Table 5-3 Restraints in case A, B and C

	A	B	C
X	Fixed (5 mm)	Fixed (5 mm)	Fixed (5 mm)
Y	Free	Fixed	Fixed
Z	Fixed	Fixed	Fixed
RX	Fixed	Fixed	Fixed
RY	Fixed	Fixed	Fixed
RZ	Free	Free	Fixed

5.10 Limitations

Several simplifications were made in the Ansys model to make it able to converge and to reduce simulation time.

- The bolt head and the washers were simplified as one element with the diameter of a standard washer.
- The bolt holes and the width of the slotted hole in the model is simplified to be the same as the bolt's diameter. Models with M10 bolts have holes with 10 mm diameter. Models with M20 bolts have 20 mm diameter.
- All friction contacts are simplified with a friction coefficient of 0,3, except the surfaces in the friction connection.
- The connection between the fixed profile and the CLT plate is simplified as a fixed support without bolts.
- The connection between the anchor profile and the concrete is simplified with a remote displacement without bolts.
- The model is defined as a statical analysis with a displacement of 5 mm applied.

6 Results and discussion: FEM-analysis

In this results and discussion chapter the results from the FEM-analysis are presented and discussed. The first part of this chapter shows the results from the verification made in Ansys. After that, all the results from Ansys are presented specimen by specimen. The specimens are then compared with each other in the end of this chapter.

6.1 Verification of the preloaded bolts

From Ansys the normal stress in the Y-direction of the bolt is 422 MPa (Figure 6-1). The normal stress was calculated by hand with a pretension in the bolt of $N = 32\,480\text{ N}$ and a cross section area $A = 78.54\text{ mm}^2$:

$$\sigma = \frac{N}{A} = \frac{32\,480\text{ N}}{78.54\text{ mm}^2} = 414\text{ MPa}$$

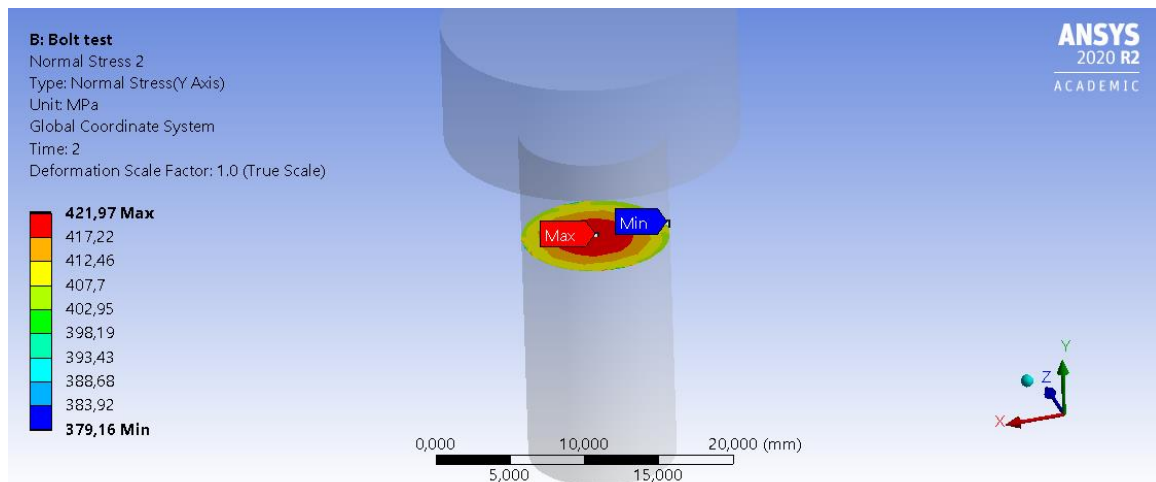


Figure 6-1 Normal stress in the bolt [MPa]

The maximum normal elastic strain from Ansys is 0,002 (Figure 6-2). The normal elastic strain was calculated by hand with the normal force and the Young's modulus of steel $E=210\,000\text{ N/mm}^2$:

$$\varepsilon = \frac{\sigma}{E} = \frac{413.55}{210\,000} = 0.00197$$

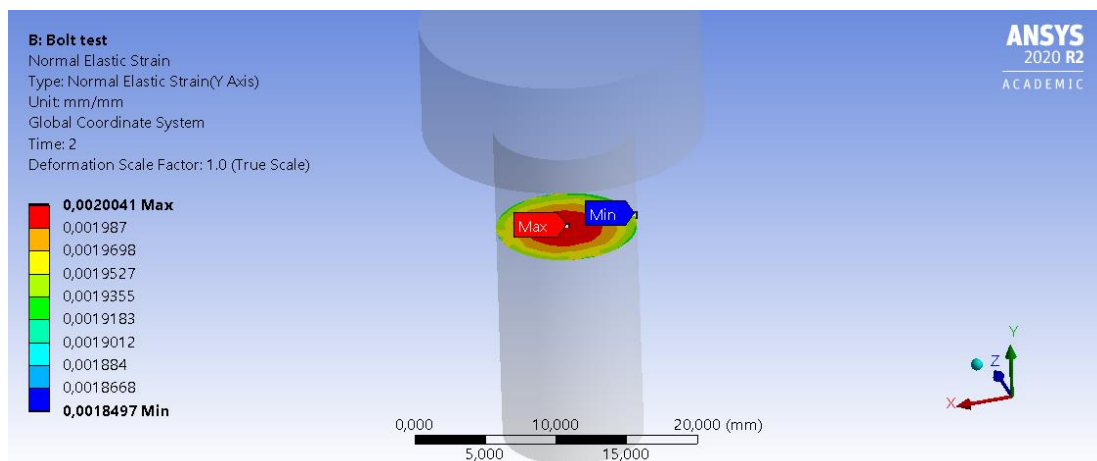


Figure 6-2 Normal elastic strain in the bolt [MPa]

The normal stress and the elastic strain from the applied preload are as expected from the hand calculations. That verifies this method of applying the preload using the *preload* function and the setup of the bolt in two parts. It is also verified that the two-step method of first loading the preload and then lock it works as expected.

6.2 Verification of the friction connection

6.2.1 Simple model

Figure 6-3 shows the deformation in X-direction. The anchor profile deforms as expected 5 mm, and the fixed profile does not deform. It is also observed in Figure 6-3 that the left side of the anchor profile slightly deforms in the Y-direction. The maximum deformation in Y-direction is 1,2 mm. This deformation likely occurs due to the application of the displacement being on the top surface of the plate.

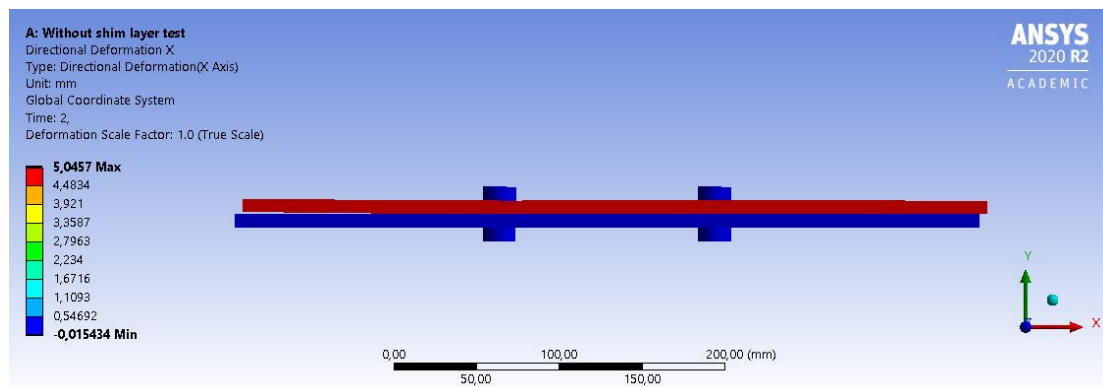


Figure 6-3 Deformation in X-direction [mm]

The maximum stress in the slotted plate is 446 MPa (Figure 6-4). The bolts washers are in direct contact with the slotted hole and makes a concentrated stress. There is only a small area which reach the maximum stress. Yielding will likely not be a problem in this case.

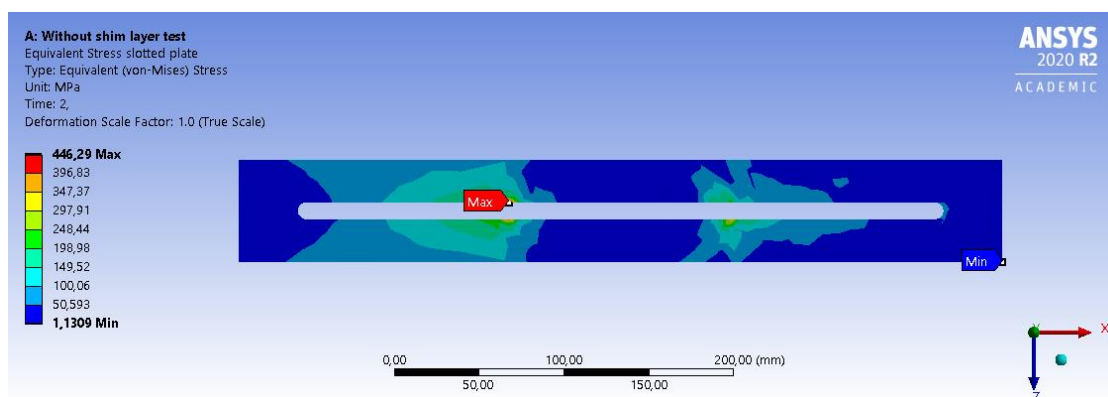


Figure 6-4 Maximum equivalent stress along the slotted hole [MPa]

The maximum stress in the fixed profile is 405 MPa seen in Figure 6-5. It is in the edge of the hole where the bolts are pushed against due to the displacement of the anchor profile. There is only a small area which reach the maximum stress.

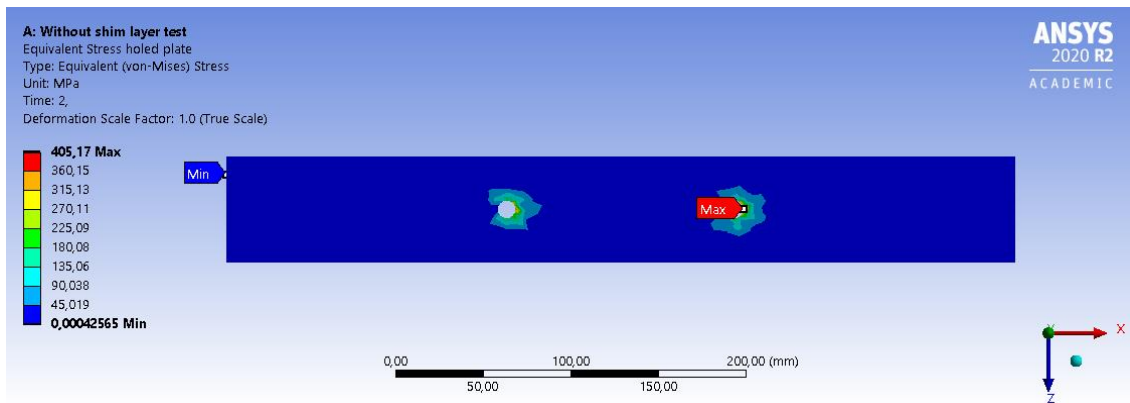


Figure 6-5 Maximum equivalent stress in the fixed profile [MPa]

The slip force was calculated using equation (2-3) with two friction surfaces, two bolts, 0,3 friction coefficient and a preload of 32 480 N:

$$F_{S,R} = 2 * 2 * 0.3 * 32\ 480 = 38\ 976\ N$$

From Ansys the force reaction from the fixed support in the fixed profile is 38 959 N. This result is the same as the hand calculation, which verify that the model behaves as expected. It also confirms that there are two friction surfaces even if the surface between the bolt head and the fixed profile is small. It will work as a friction surface, but due to the small contact area it will give a larger stress around the slotted holes with the risk of damage. The force probes from the friction surfaces were not calculated in Ansys because it was not possible to define it with the two bolts.

6.2.2 Real model

The deformation in X-direction is shown in Figure 6-6. The anchor profile deforms as expected 5 mm and the fixed profile does not deform. It is observed from Figure 6-6 that the additional plate deforms around 0,2 mm in the X-direction.

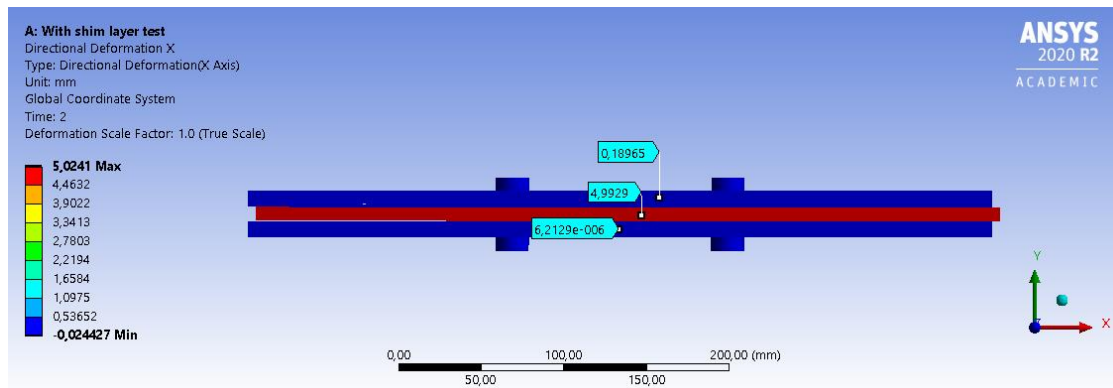


Figure 6-6 Deformation in X-direction [mm]

The maximum equivalent stress in the anchor profile is 112 MPa. As seen in Figure 6-7, the stress is distributed over a large area due to the distribution of forces from the additional plate. Since the stress is well distributed, it does not reach a high concentration.

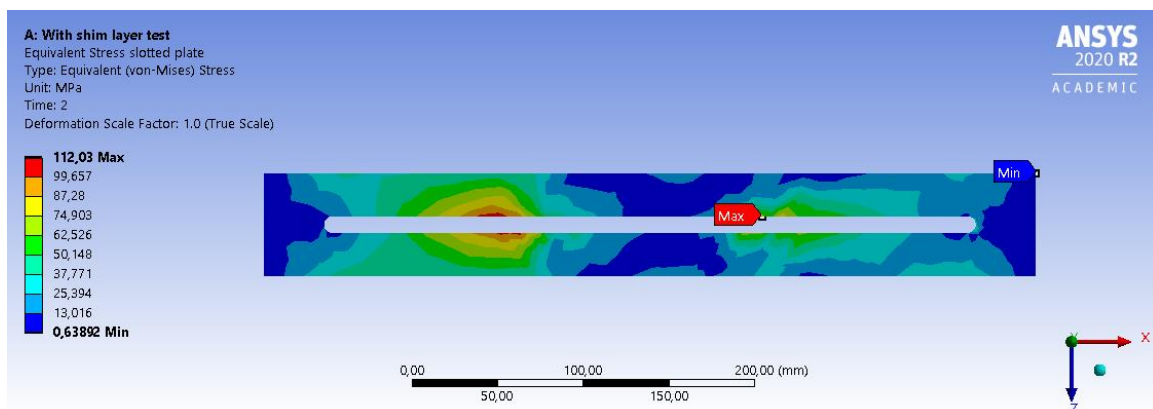


Figure 6-7 Maximum equivalent stress along the slotted hole [MPa]

The fixed profile reaches a higher stress concentration than the additional plate seen in Figure 6-8 and Figure 6-9. Figure 6-8 shows that there is only a small area of concentrated stress around the right side of the holes. This concentration is reaching a maximum of 691 MPa. In the additional plate in Figure 6-9, it is observed that the concentration is lower with a maximum of 467 MPa.

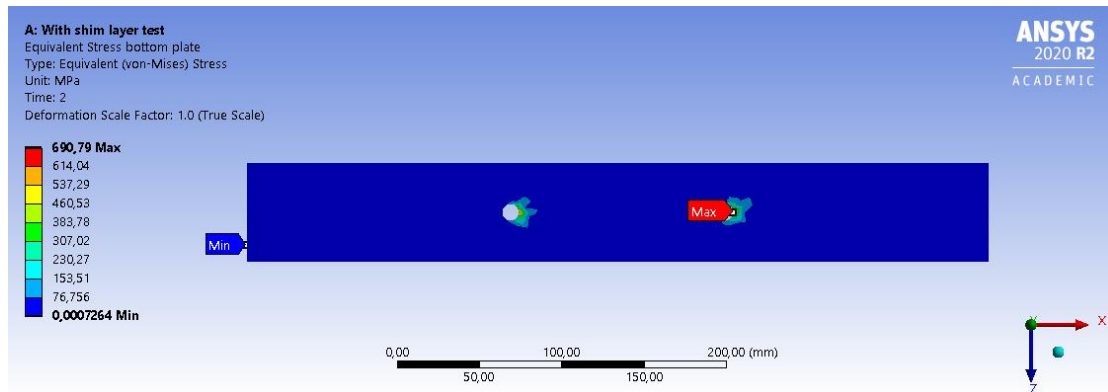


Figure 6-8 Maximum equivalent stress in the fixed profile [MPa]

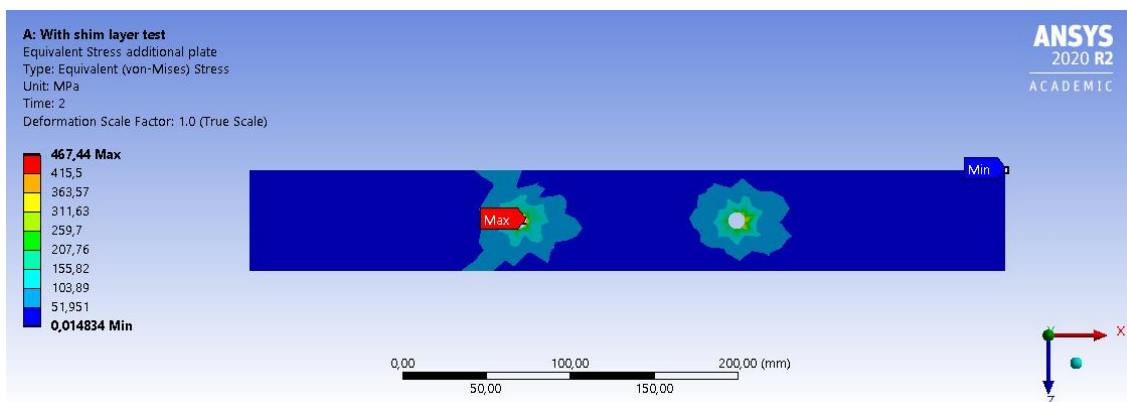


Figure 6-9 Maximum equivalent stress in the additional plate [MPa]

The slip force was calculated in the same way as for the simplified model in chapter 6.2.1. Equation (2-3) was used with two friction surfaces, two bolts, 0,3 as friction coefficient and a preload of 32 480 N:

$$F_{s,R} = 2 \cdot 2 \cdot 0,3 \cdot 32\,480 = 38\,976\,N$$

From Ansys the force reaction from the fixed profile is 37 273 N, which is close to the hand calculation and the simplified model, but a bit lower. The reason for this lower force reaction

may be caused by some variations with the force convergence in Ansys. In this model there were also included results from force probes in the two friction surfaces. The two friction surfaces gave a total friction force of 37 312 N which correlates with the force reaction in the fixed profile.

6.3 Remote displacement

When placing the remote displacement in the middle of the element, the deformation in Y-direction gets zero in the middle of the anchor profile, and the displacement is approximately 5 mm in the top and bottom. This indicates that the specimen is rotating. Figure 6-10 shows the behavior of the element in Y-direction where the green indicates zero.

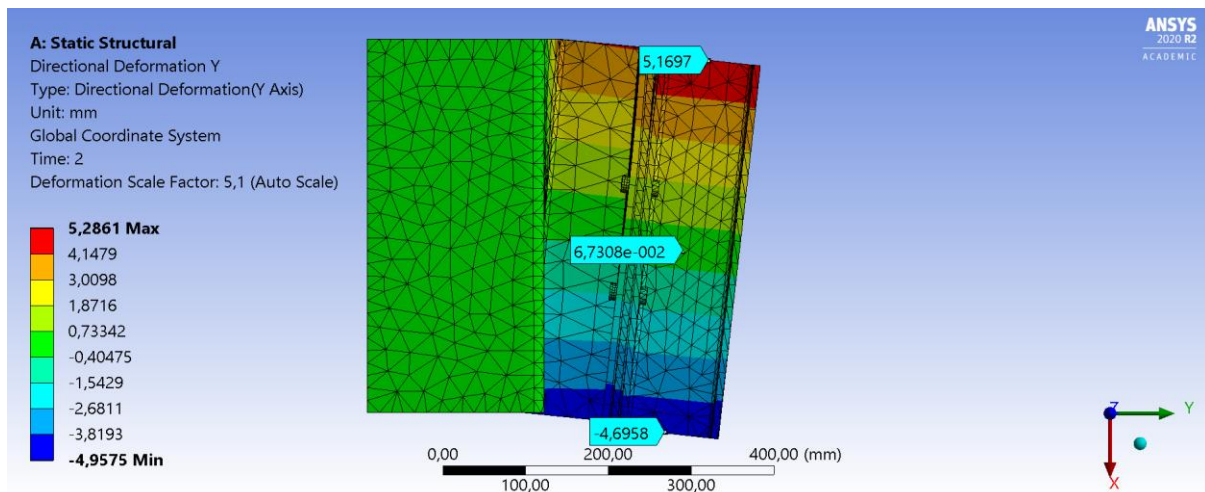


Figure 6-10 Deformation in Y-direction with remote displacement in the middle [mm]

Placing the remote displacement at the top of the element, the deformation in Y-direction is zero at the top and the rotation around Z-axis is free as seen in Figure 6-11. The deformation is approximately zero in the top, but has deformed 4 mm in the bottom. This indicates a more accurate behavior compared to the press. This is the location of the remote displacement used in the following cases A, B and C.

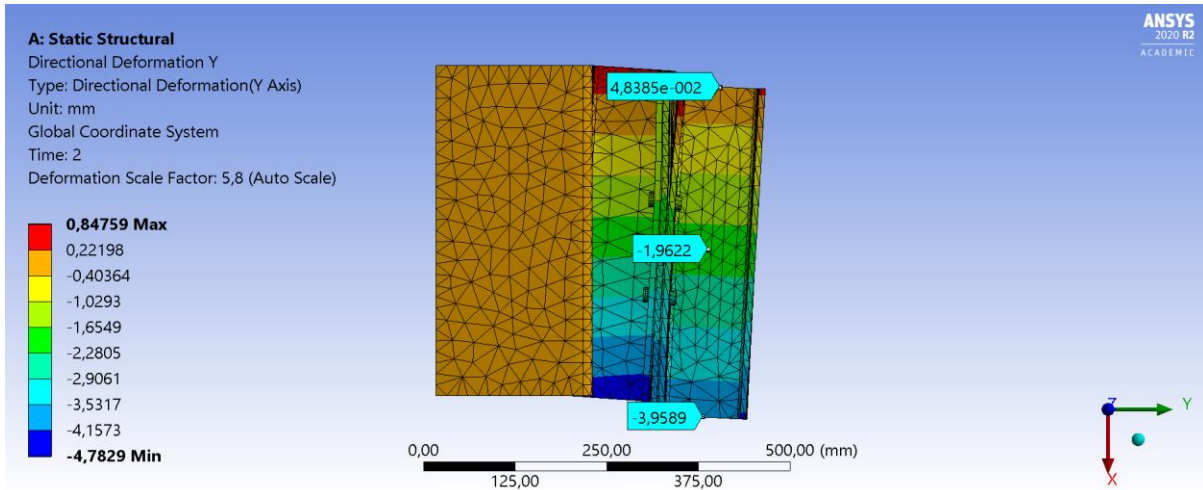


Figure 6-11 Deformation in Y-direction with remote displacement in the top [mm]

6.4 Simulation cases

In this chapter three different cases are presented, where the difference is the restraints in X-, Y- and Z-direction. The cases are shown for specimen STD-1H and ALT.

For case A the deformation in Y-direction is free and rotation around Z-axis is free, as shown in Figure 6-12.

Steps	Time [s]	<input checked="" type="checkbox"/> X [mm]	<input checked="" type="checkbox"/> Z [mm]	<input checked="" type="checkbox"/> RX [°]	<input checked="" type="checkbox"/> RY [°]
1	1	0,	= 0,	= 0,	= 0,
2	1	0,	0,	0,	0,
3	2	5,	= 0,	= 0,	= 0,
*					

Figure 6-12 Restraints in case A

For the STD-1H specimen the result shows a force reaction of 38 495 N with a deformation in the positive Y-direction at top of the element of 5,2 mm and at the bottom a deformation of 4,9 mm in the negative direction seen in Figure 6-13. The force reaction for the ALT specimen is 38 608 N. The deformation in Y-direction is 0,4 in the positive direction at the top and 0,4 at bottom in the negative direction, as seen in Figure 6-14. In this case the STD-1H specimen is rotating around the axis while the ALT specimen is sliding more but also shows a small rotation around the Z-axis.

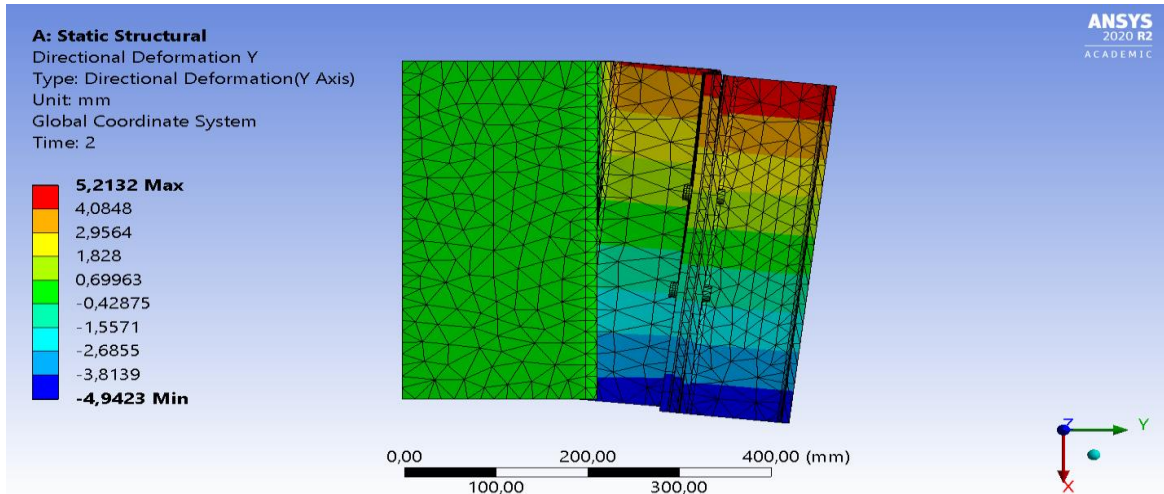


Figure 6-13 STD-1H Case A, deformation in Y-direction [mm]

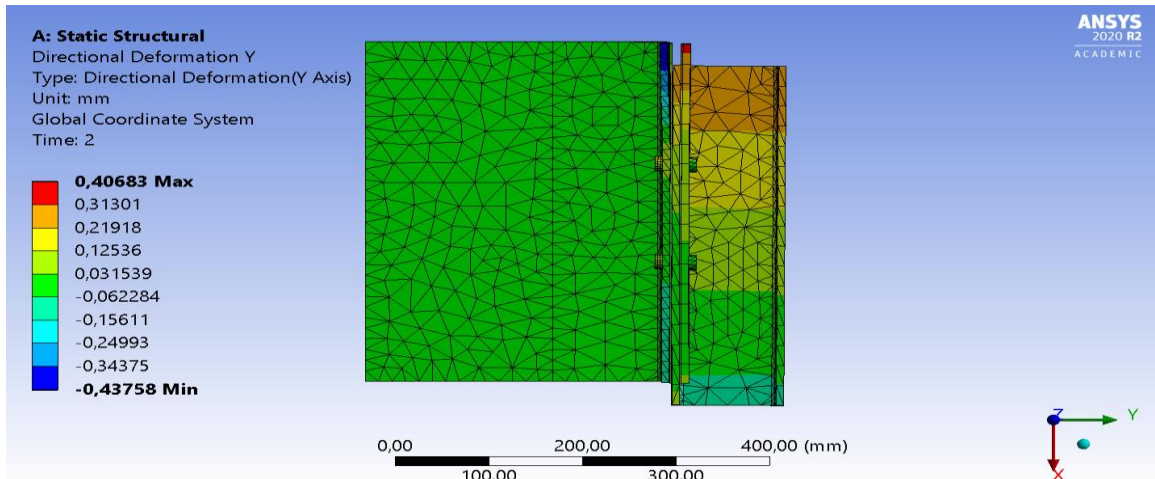


Figure 6-14 ALT Case A, deformation in Y-direction [mm]

In case B rotation around Z-axis is the only free degree of freedom, as shown in Figure 6-15.

Steps	Time [s]	<input checked="" type="checkbox"/> X [mm]	<input checked="" type="checkbox"/> Y [mm]	<input checked="" type="checkbox"/> Z [mm]	<input checked="" type="checkbox"/> RX [°]	<input checked="" type="checkbox"/> RY [°]
1 1	0,	0,	= 0,	= 0,	= 0,	= 0,
2 1	1,	0,	0,	0,	0,	0,
3 2	2,	5,	= 0,	= 0,	= 0,	= 0,
*						

Figure 6-15 Restraints in case B

For the STD-1H specimen the force reaction reaches 59 105 N and the deformation in Y-direction at the top in the positive direction is 0,6 mm and in the negative direction at bottom

4,7 mm, as seen in Figure 6-16. In this case the STD-1H specimen is bending more than in case A, and this leads to the increased force reaction. The ALT specimen has a force reaction of 40 214 N and a deformation in Y-direction of 0,2 mm at the top and - 0,6 mm at the bottom, as seen in Figure 6-17.

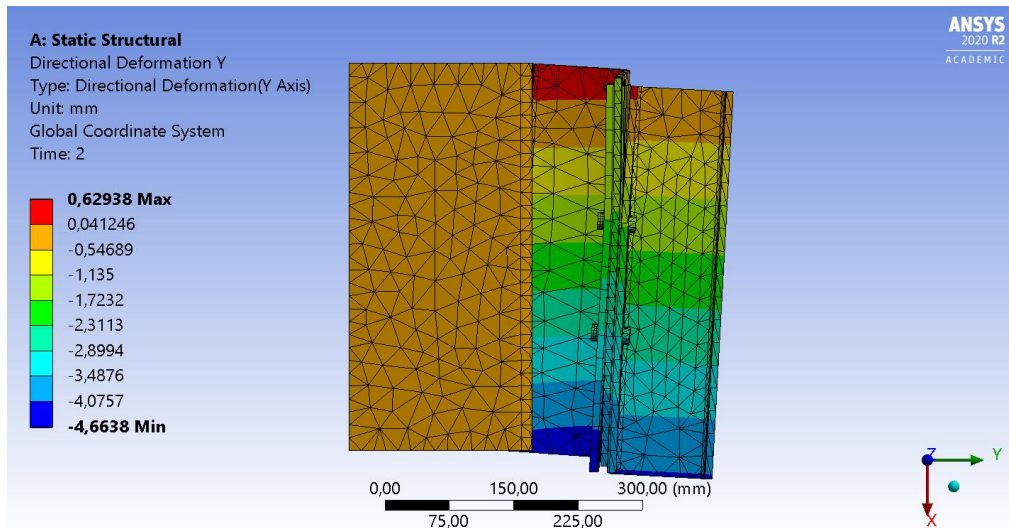


Figure 6-16 STD-1H Case B, deformation in Y-direction [mm]

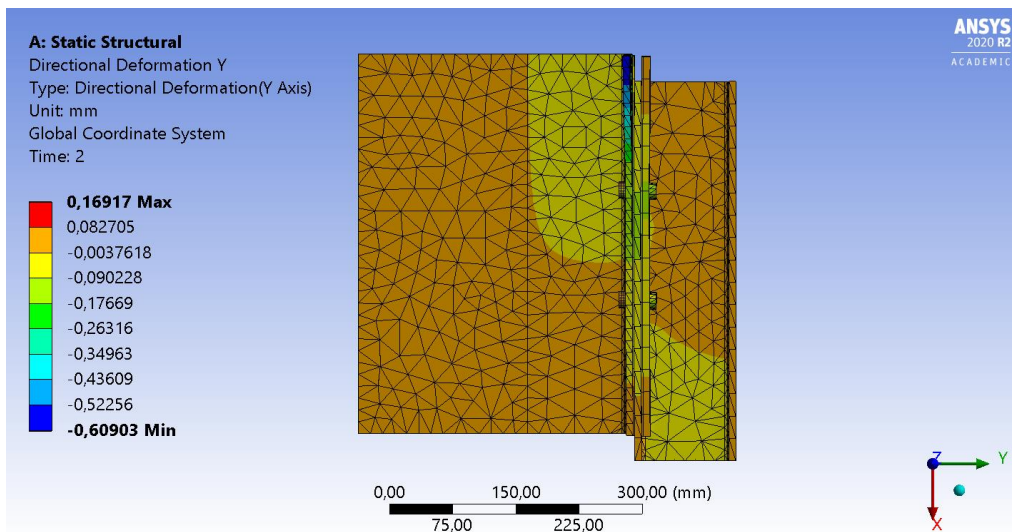


Figure 6-17 ALT Case B, deformation in Y-direction [mm]

For case C all directions and rotations are restrained, as shown in Figure 6-18.

Steps	Time [s]	X [mm]	Y [mm]	Z [mm]	RX [°]	RY [°]	RZ [°]
1	1	0,	= 0,	= 0,	= 0,	= 0,	= 0,
2	1	0,	0,	0,	0,	0,	0,
3	2	5,	= 0,	= 0,	= 0,	= 0,	= 0,
*							

Figure 6-18 Restraints in case C

The STD-1H specimen reaches a force reaction of 51 971 N in case C which is lower than in case B. At the top of the element the deformation in Y-direction is 0,7 mm in the positive direction and at the bottom 2 mm in the negative direction, seen in Figure 6-19. For this case, the deformation in Y-direction is lower than in the previous case A and B for specimen STD-1H. The force reaction for the ALT specimen is 39 349 N and the deformation in Y-direction is 0,2 mm at the top and 0,6 mm at the bottom as in case B, see Figure 6-20.

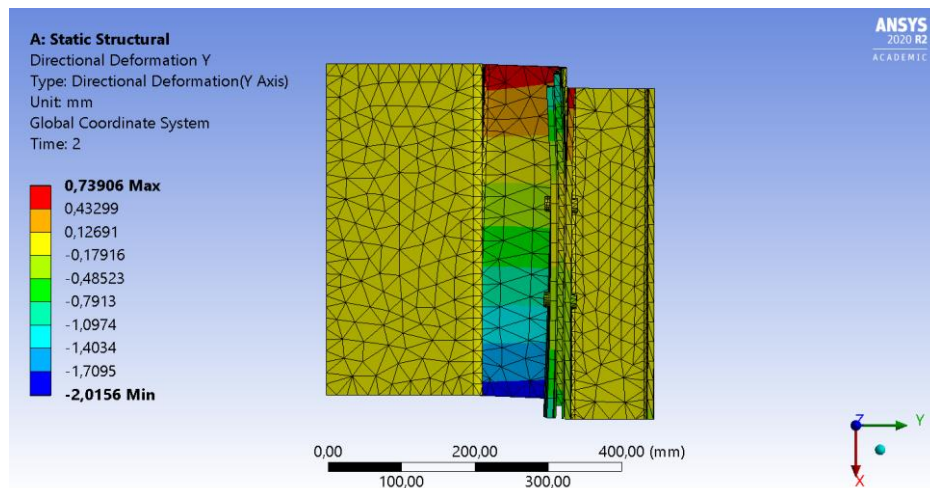


Figure 6-19 STD-1H Case C, deformation in Y-direction [mm]

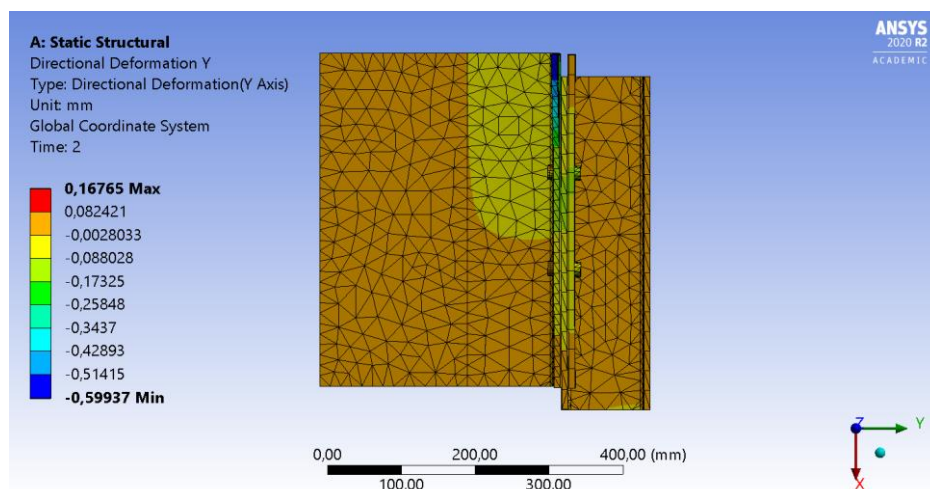


Figure 6-20 ALT Case C, deformation in Y-direction [mm]

In Table 6-1 a summary of the force reaction and deformation in Y-direction in cases A, B and C are shown. In the table the T means top, and B means bottom.

Table 6-1 Summary of the force reaction and deformation in Y-direction in case A, B and C for specimen STD-1H and ALT

	STD-1H		ALT	
	Force reaction [N]	Displacement [mm]	Force reaction [N]	Displacement [mm]
Case A	38 018	T: 5,2 B: -4,9	38 608	T: 0,4 B: -0,4
Case B	59 105	T: 0,6 B: -4,7	40 214	T: 0,2 B: -0,6
Case C	51 971	T: 0,7 B: -2,0	39 349	T: 0,2 B: 0,6

For case A rotation around Z-axis occurs with both specimens. This type of rotation will not take place in the press or in reality with the CLT-panel. For case B and C, the ALT specimen is barely affected by the change of restraints but for the STD-1H specimen the restraints have a bigger impact on the force reaction and deformation. These results show that only the STD-1H specimen is affected by the different restraints in case B and C, so the upcoming results will only include case C. Case C is the case where all restraints are applied and will be the condition closest to the restrains in the press.

6.5 Ansys analysis

Through this chapter the results of all specimens with both M10 and M20 bolts are shown and illustrated. All results are simulated with case C according to chapter 5.9. In chapter 6.5.1 to 6.5.5, the deformations, maximum equivalent stresses, force reactions and contact status in friction surface 2 (Table 5-2) is presented for each specimen with the dynamic friction coefficient of 0,22. In chapter 6.5.6 all results from the specimens are compared, also including results from the analysis made with the static friction coefficient of 0,39.

6.5.1 ALT

The ALT specimen has a straight fixed profile that is connected to the backside of the CLT-panel. There is no bend between the fixed profile and the friction connection, like in the STD specimens. This makes the specimen stiff against bending around the Z-axis. In Y-direction, there is an insignificant amount of deformation, as seen in Figure 6-21. It is only deforming at the edges of the additional plate, and at the tip of the friction surface. This is likely due to the prestressed bolts which applies a pressure on the middle, causing it to bend slightly at the edges. As seen in Figure 6-22 the deformation in Y-direction in ALT M20 is approximately the same as for specimen M10.

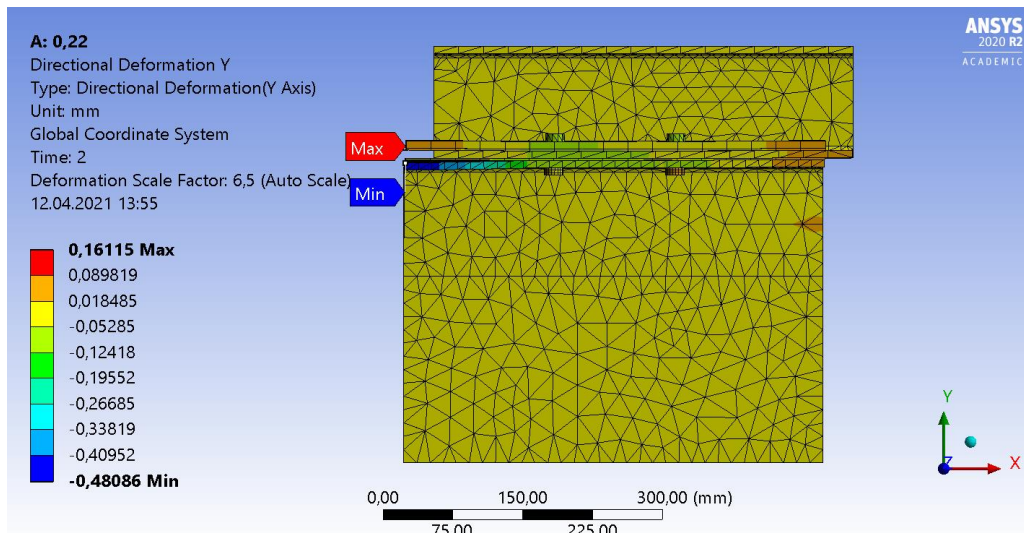


Figure 6-21 Deformation in Y-direction ALT M10 [mm]

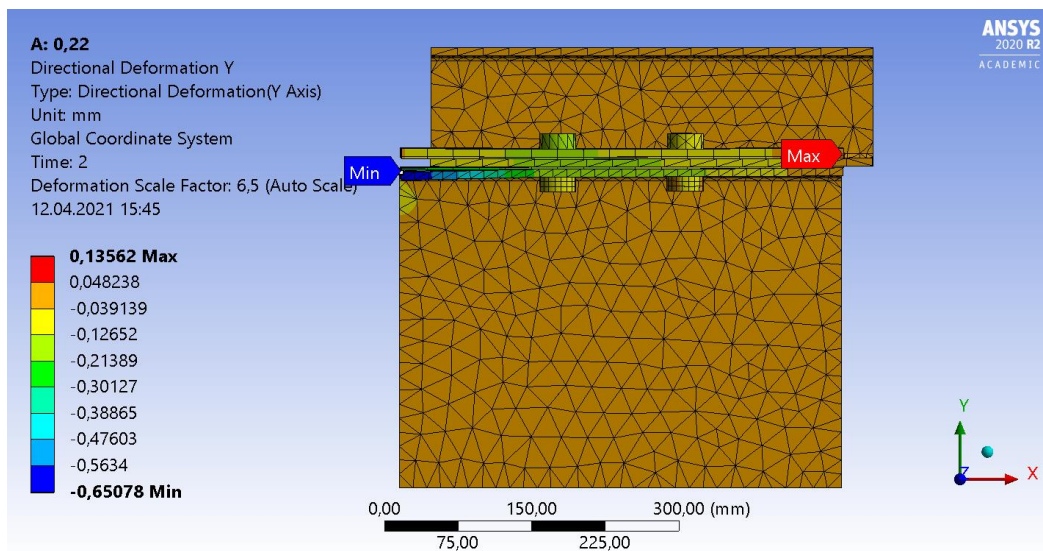


Figure 6-22 Deformation in Y-direction ALT M20 [mm]

The deformation in Z-direction in this specimen is also small, as seen in Figure 6-23 for the M10 specimen and Figure 6-24 for the M20 specimen. This small deformation keeps the slotted hole approximately straight and will enable the specimen to slide without increased resistance. This is confirmed from the forces in Table 6-2 showing that the force reaction from the fixed profile is approximately the same as the sum of the force probes. When the force reaction and the sum of force probes are similar it indicates that the specimen is sliding without the influence of bending.

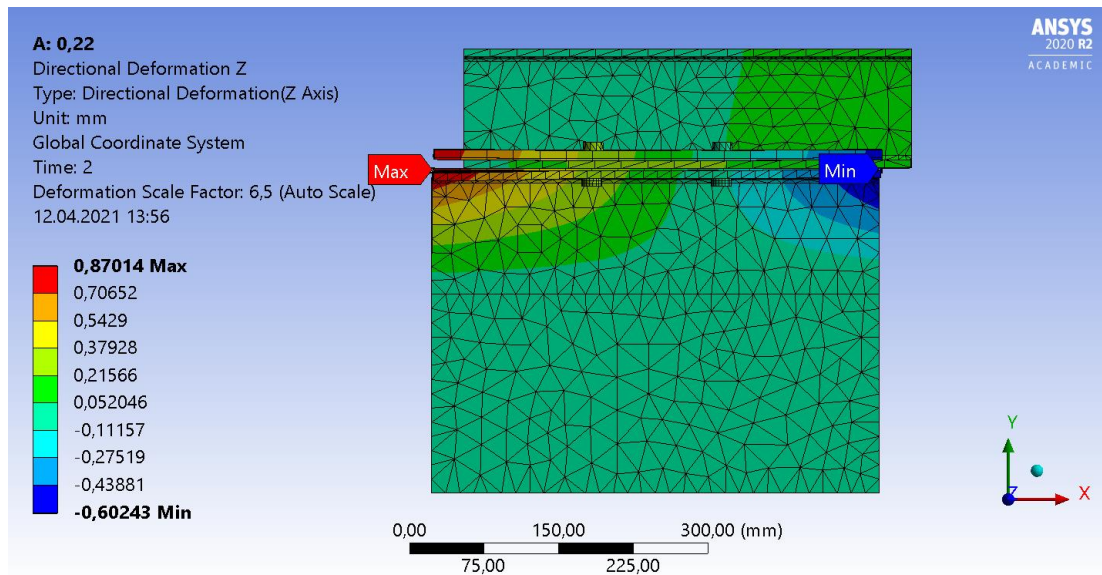


Figure 6-23 Deformation in Z-direction ALT M10 [mm]

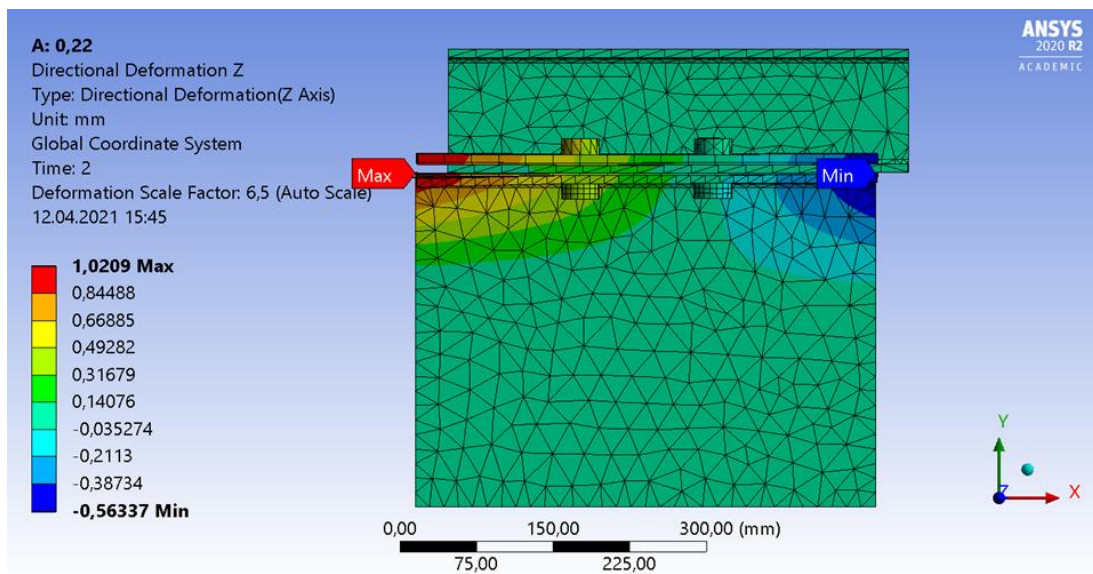


Figure 6-24 Deformation in Z-direction ALT M20 [mm]

Table 6-2 Force reactions in ALT M10 and M20

Bolt size	Friction coefficient	Force reaction [N]	Force probe 1 [N]	Force probe 2 [N]	Sum force probe [N]
M10	0,22	30 862	14 441	16 153	30 594
M20	0,22	30 392	15 000	15 551	30 551

In the fixed profile the equivalent stress is centered around the bolted holes. Figure 6-25 shows the equivalent stress for the fixed profile with M10 and Figure 6-26 for the M20 profile. The maximum equivalent stress is centered around the bolted holes in both the M10 and the M20 profile.

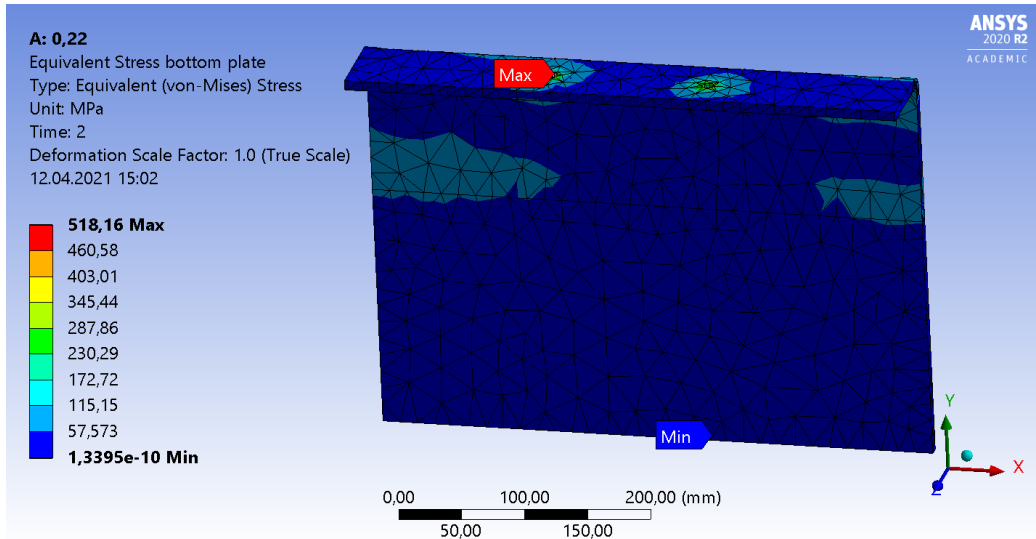


Figure 6-25 Equivalent stress in the fixed profile ALT M10 [MPa]

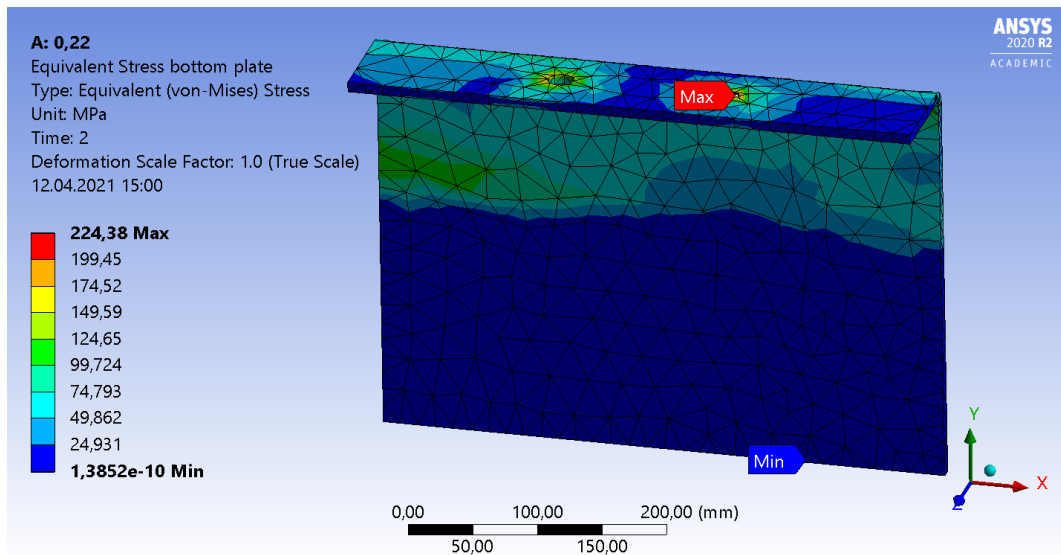


Figure 6-26 Equivalent stress in the fixed profile ALT M20 [MPa]

Pressure in the additional plate is directly applied from the preloaded bolts as seen in Figure 6-27 for the additional plate M10 and Figure 6-28 for the additional plate M20. A concentration of stress is observed in a small area around left hole of 440 MPa in the M10 additional plate and 250 MPa in the M20 additional plate.

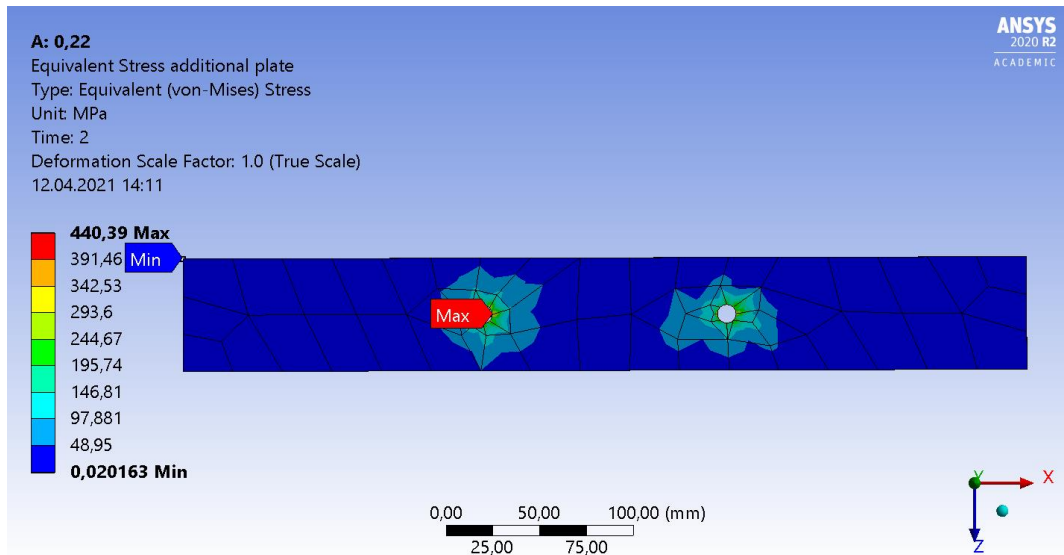


Figure 6-27 Equivalent stress in the additional plate ALT M10 [MPa]

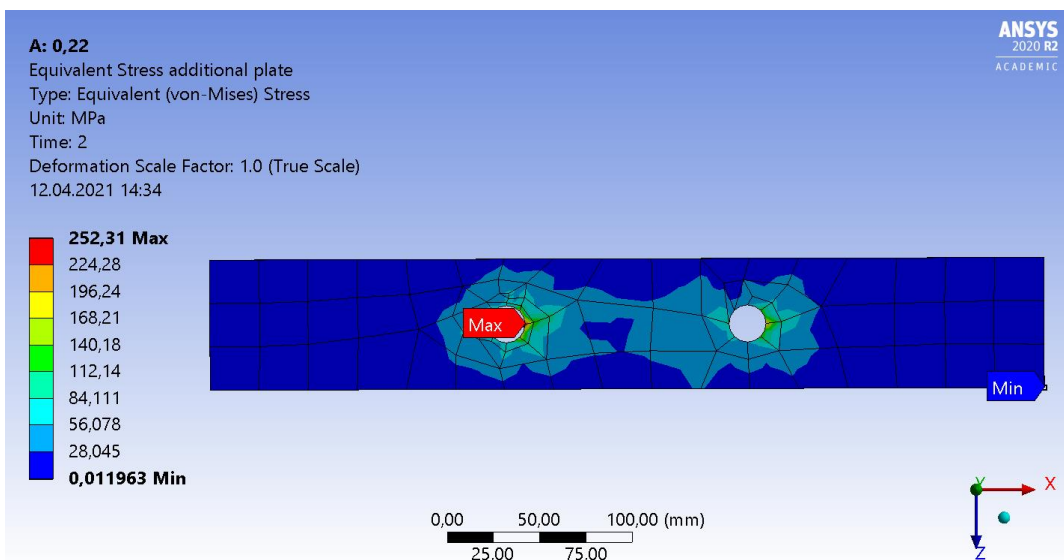


Figure 6-28 Equivalent stress in the additional plate ALT M20 [MPa]

The equivalent stress in the anchor profile is illustrated in Figure 6-29. Equivalent stresses are evenly distributed over nearly all the contact area. This is because the additional plate distributes the forces applied by the preloaded bolts. A stress concentration is observed around the edge of the slotted hole. Since the force is distributed by the fixed profile and the additional plate, the equivalent stress is approximately the same for ALT M10 and ALT M20.

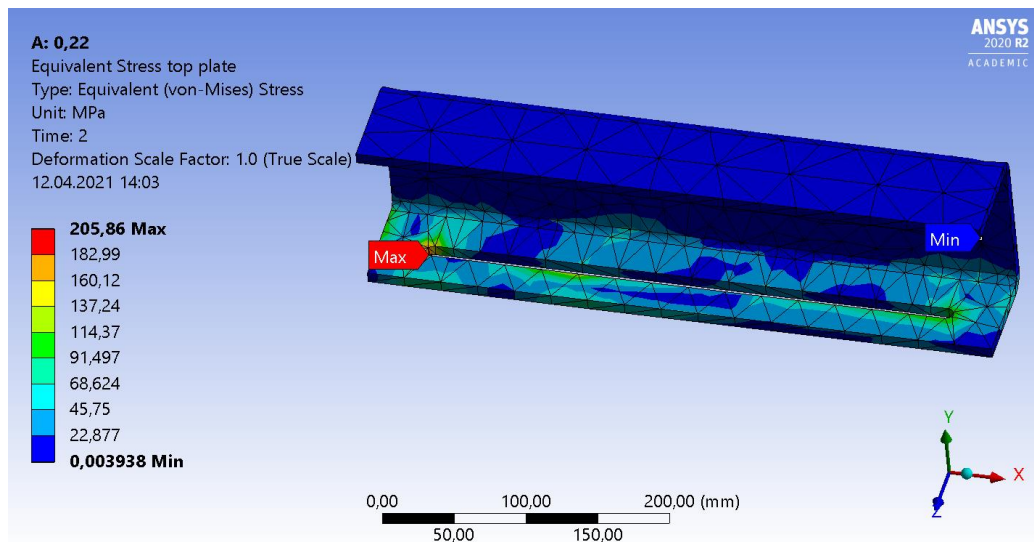


Figure 6-29 Equivalent stress in the anchor profile ALT M10 [MPa]

Contact status in friction surface 2 is shown in ALT M10 and ALT M20 is shown in Figure 6-30 and Figure 6-31. *Sliding* is illustrated with orange in the figure and is where the two plates are pushed so close that the friction is active. *Near* is where the plates are close, but the friction is not activated. As observed in the figures, *sliding* is around the bolts and in the corners of the ALT M10. In the ALT M20 the *sliding* zone is smaller in the left of the figure. The large area of *sliding* indicates that the sliding surface is well utilized.

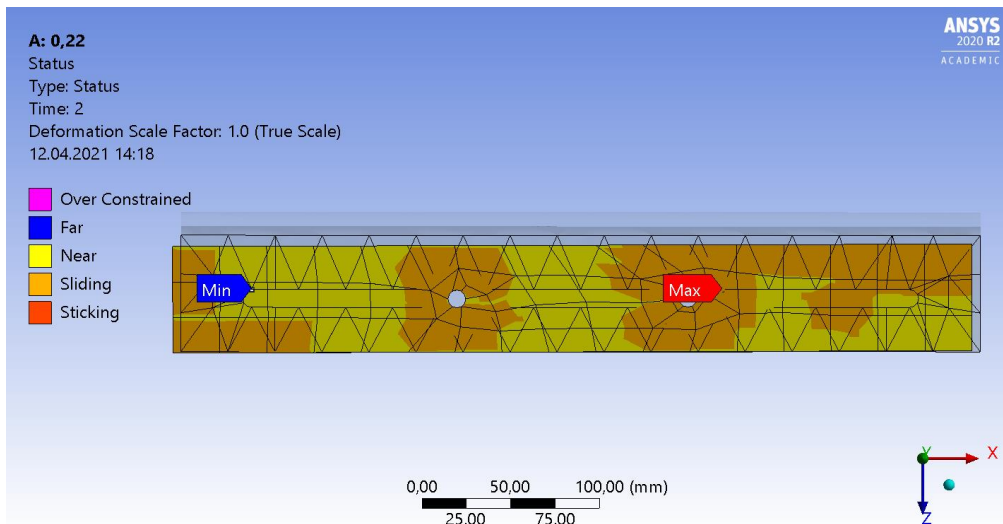


Figure 6-30 Contact status in friction surface 2 ALT M10

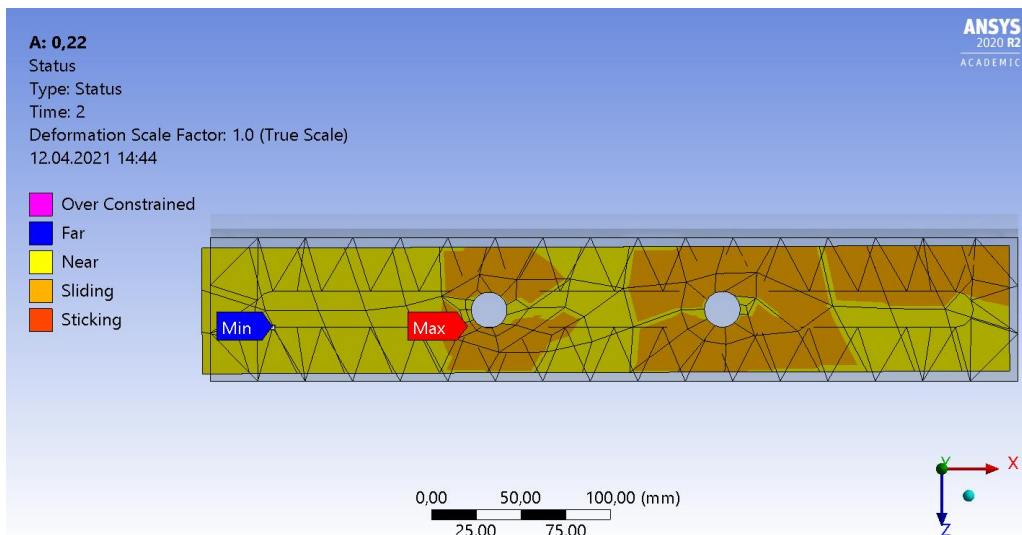


Figure 6-31 Contact status in friction surface 2 ALT M20

6.5.2 ALT-AS

The ALT-AS specimen is like the ALT, but the top is modified with an alignment component. In Y-direction the deformation in ALT-AS specimen is small for both the M10 specimen and the M20 specimen. Figure 6-32 and Figure 6-33 shows the deformation in ALT-AS M10 and M20. It is 0,2 mm with M10 and M20 at the right side of the specimen, and -0,3 mm with M10 and 0,4 mm with M20 at the left side of the specimen. Most of the deformation is centered in the connection between the fixed profile and the alignment profile.

It indicates that the rotation in the element makes the connection slightly deform, which could lead to less stress in the rest of the specimen.

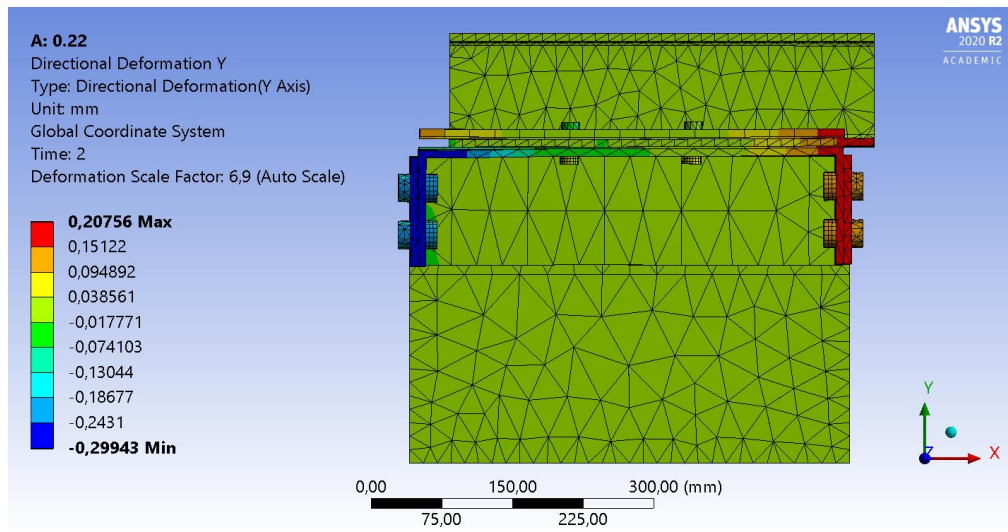


Figure 6-32 Deformation in Y-direction ALT-AS M10 [mm]

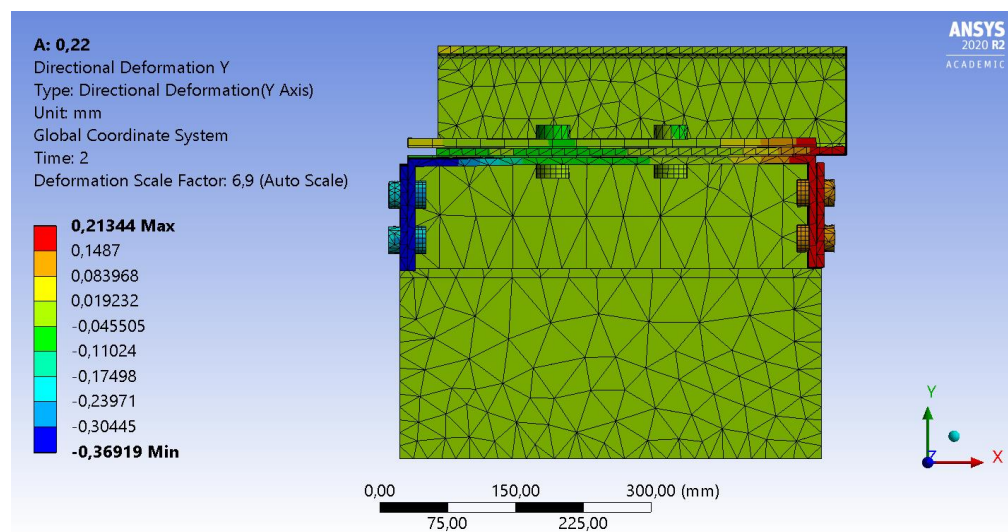


Figure 6-33 Deformation in Y-direction ALT-AS M20 [mm]

The deformation in Z-direction is illustrated in Figure 6-34. A small deformation of approximately 0,6 mm on the left side and around - 0,4 mm on the right is observed. This deformation is approximately the same for both the M10 and the M20 specimens as seen in Figure 6-35. This deformation is lower than in the ALT seen in Figure 6-23 and Figure 6-24. The reason for this is the increased stiffness in the fixed profile with the connection to the alignment profile.

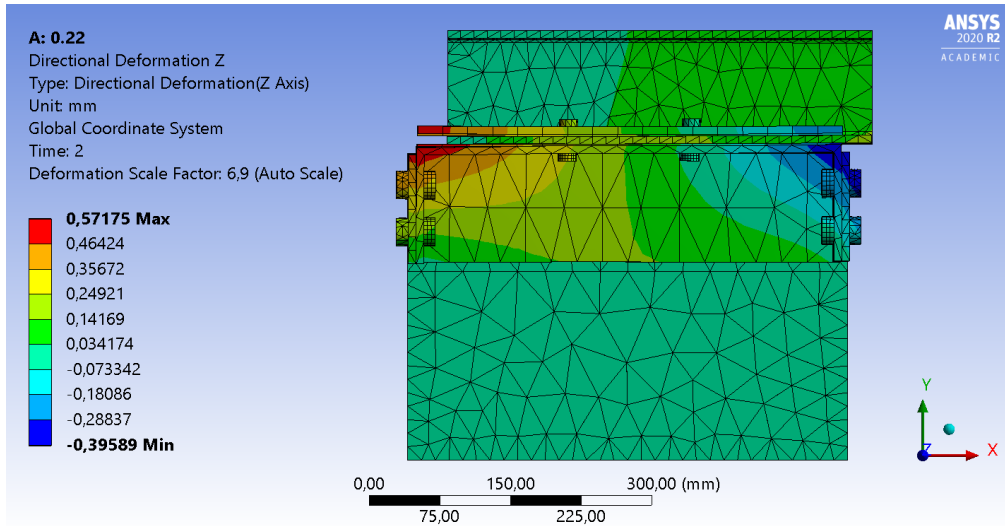


Figure 6-34 Deformation in Z-direction ALT-AS M10 [mm]

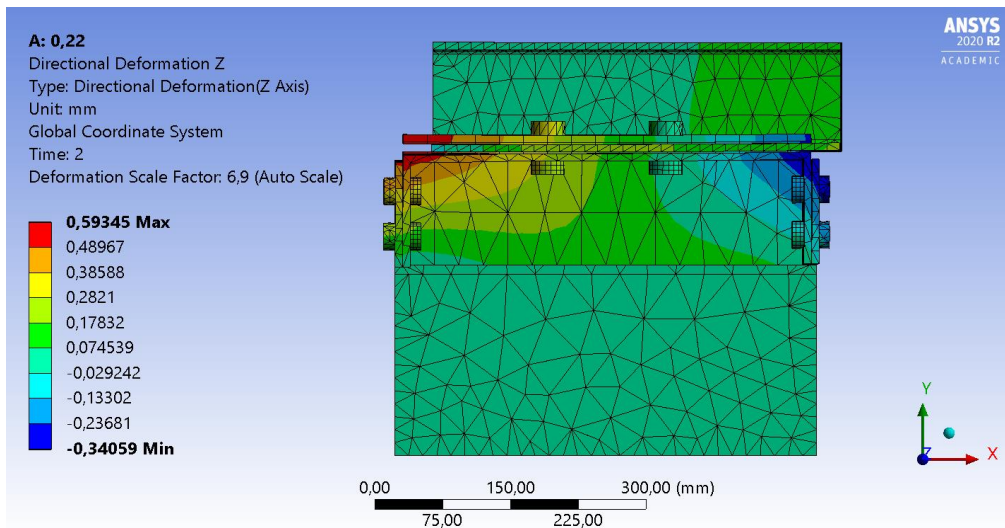


Figure 6-35 Deformation in Z-direction ALT-AS M20 [mm]

In Table 6-3 the force reactions and probe forces with the dynamic friction coefficient for specimen M10 and M20 are shown. The force reaction and sum of force probe is approximately similar for M10 and M20 bolts with a force of around 31,5 kN. This is close to the theoretical slip force of 30 kN and is an indication that the ALT specimen with M10 and M20 bolts has a stable sliding behavior.

Table 6-3 Force reaction and force probe with the dynamic friction coefficient for ALT-AS M10 and M20

Bolt size	Friction coefficient	Force reaction [N]	Force probe 1 [N]	Force probe 2 [N]	Sum force probe [N]
M10	0,22	31 511	15 384	16 187	31 571
M20	0,22	31 993	14 926	16 440	31 366

For the anchor profile the maximum equivalent stress is located on the left side in the slotted hole with M10 and M20, as illustrated in Figure 6-36 and Figure 6-37. These profiles have an area with concentration of stress around the edges of the slotted hole. The maximum value of equivalent stress is reduced by 100 MPa in the M20 specimen.

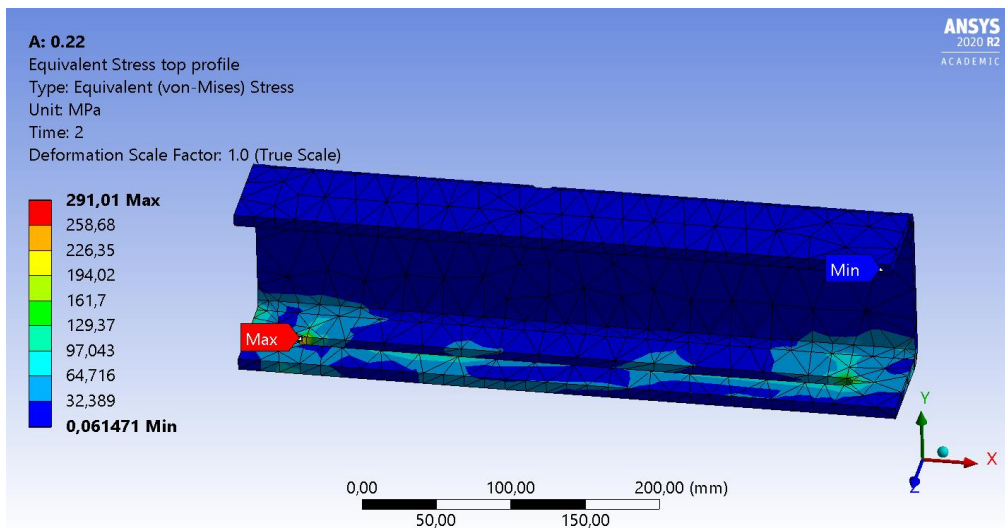


Figure 6-36 Equivalent stress in the anchor profile ALT-AS M10 [MPa]

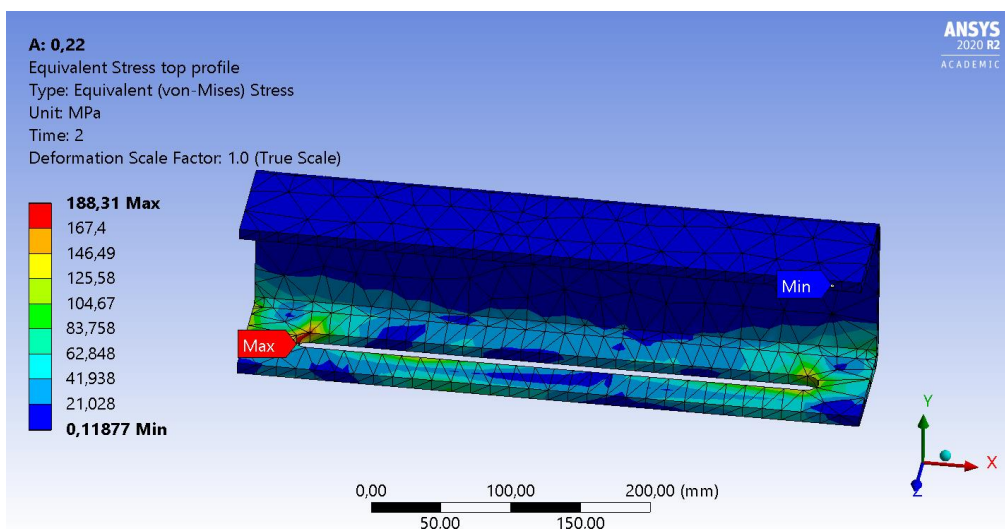


Figure 6-37 Equivalent stress in the anchor profile ALT-AS M20 [MPa]

The additional plate with M10 bolts has a maximum equivalent stress of 542 MPa located around the bolt hole. The stress is shown in Figure 6-38. In the additional plate with M20 bolts the equivalent stress is illustrated in Figure 6-39 and is 260 MPa. The equivalent stress is reduced by half compared with the M10 bolts. The location of the maximum stress is on the left side as with the M10 bolts.

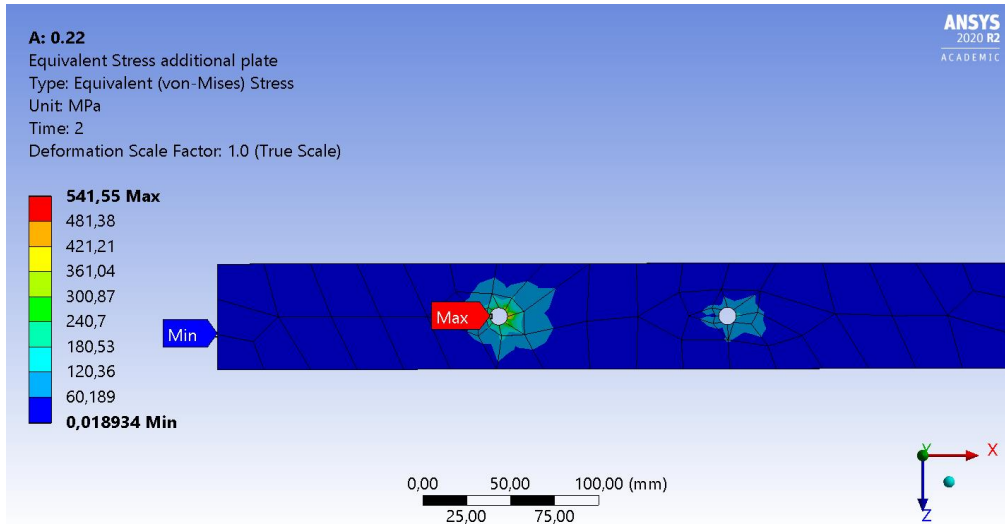


Figure 6-38 Equivalent stress in the additional plate ALT-AS M10 [MPa]

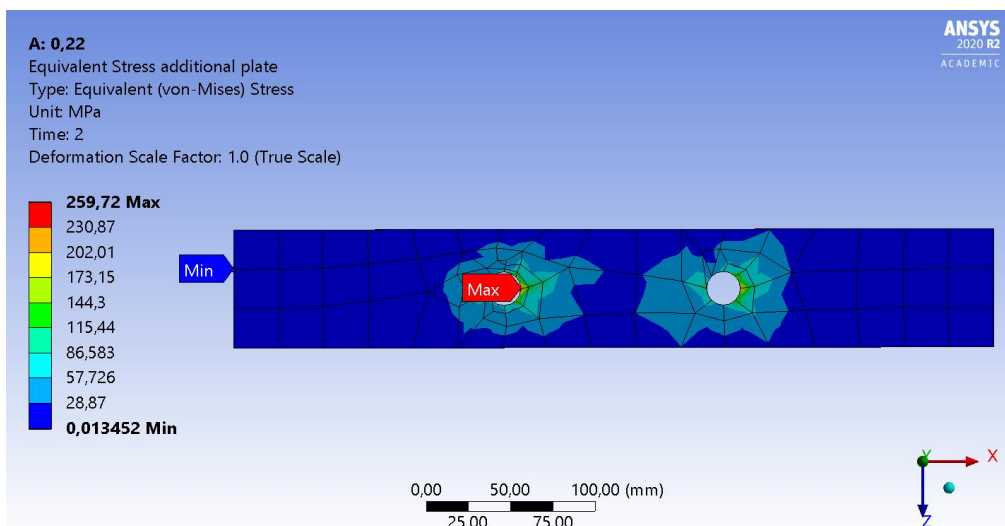


Figure 6-39 Equivalent stress in the additional plate ALT-AS M20 [MPa]

This fixed profile has a different design than all the other specimens, but like the other profiles the highest stress is around the bolted holes. In this profile, as shown in Figure 6-40 and Figure 6-41, the maximum equivalent stress is between 366 MPa and 386 MPa. Both ALT-AS M10 and M20 use M16 bolts to combine the alignment profile with the fixed profile. The equivalent stress in the fixed profile is approximately the same for both M10 and M20 specimens.

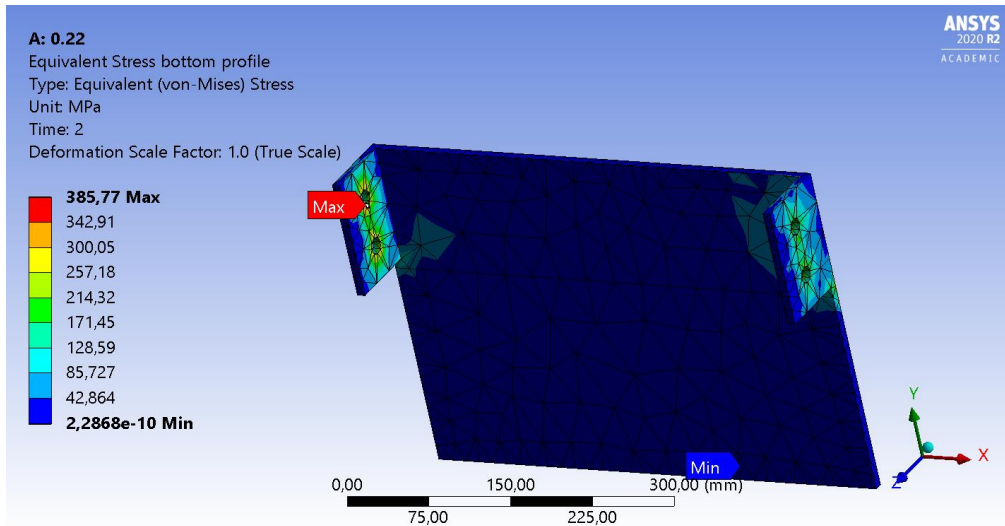


Figure 6-40 Equivalent stress in the fixed profile ALT-AS M10 [MPa]

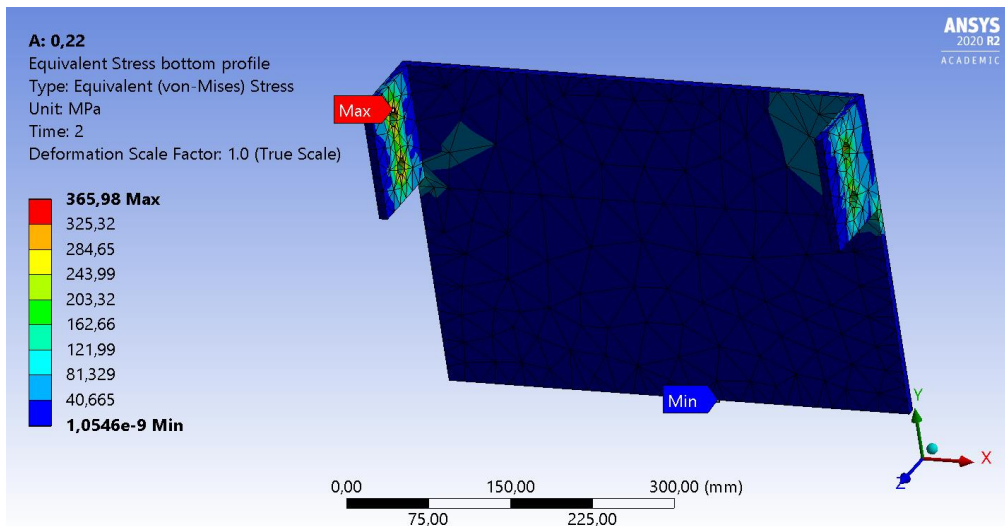


Figure 6-41 Equivalent stress in the fixed profile ALT-AS M20 [MPa]

For the alignment component the maximum equivalent stress is shown in Figure 6-42 and Figure 6-43. Seen from the figures, the maximum equivalent stress is in the holes around the bolts in the friction connection with the M10. With the M20 bolts, the maximum equivalent stress moves to the M16 bolts in the alignment connection.

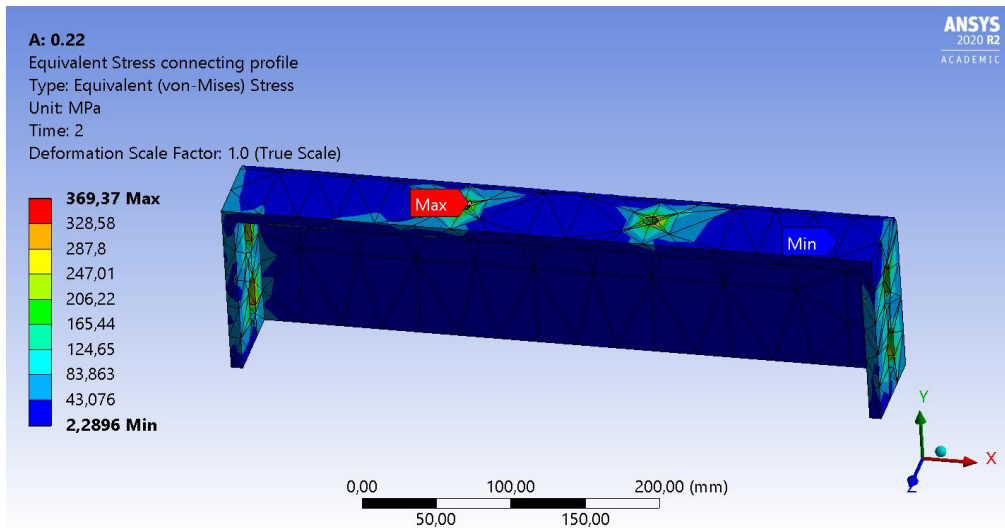


Figure 6-42 Equivalent stress in the alignment component ALT-AS M10 [MPa]

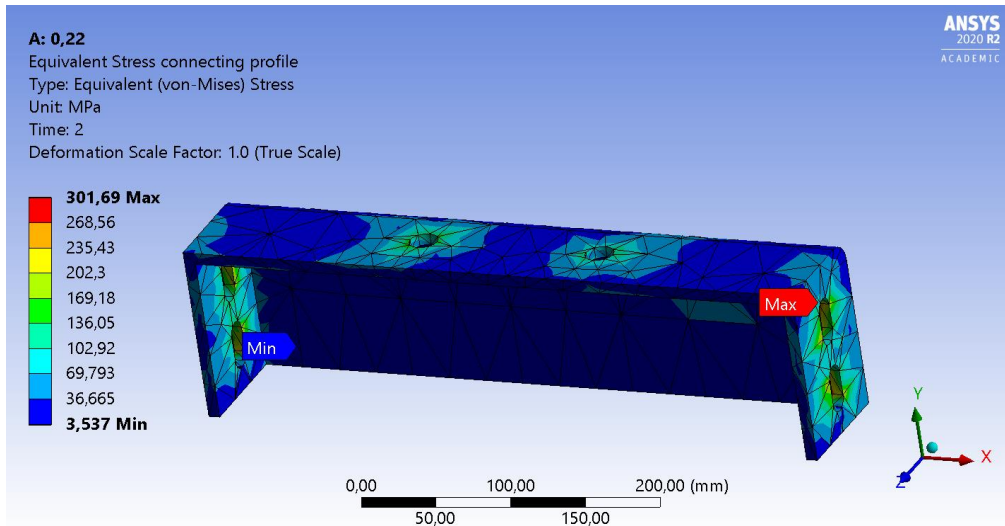


Figure 6-43 Equivalent stress in the alignment component ALT-AS M20 [MPa]

Figure 6-44 and Figure 6-45 shows the contact status for friction surface 2 in ALT-AS M10 and M20. A large area of both the M10 and M20 is *sliding* indicating a well utilized friction surface.

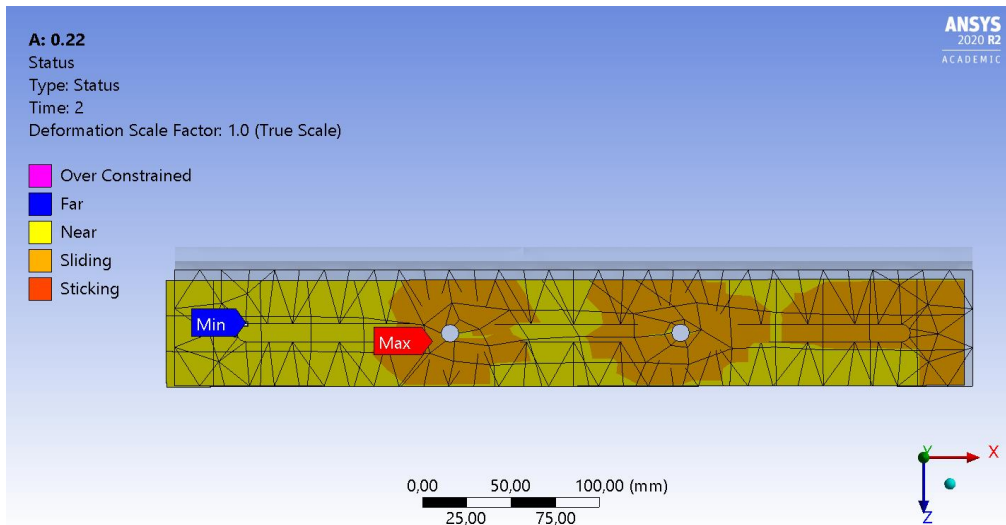


Figure 6-44 Contact status in friction surface 2 ALT-AS M10

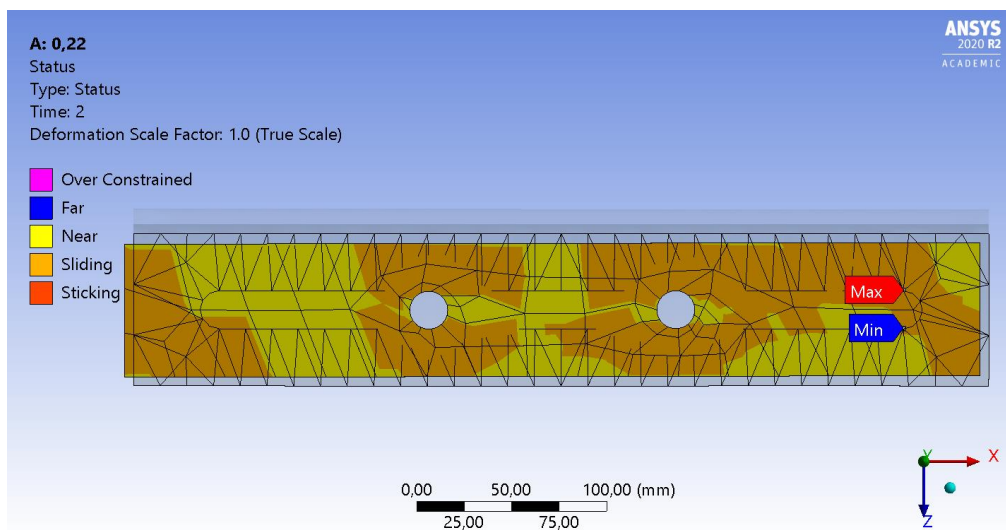


Figure 6-45 Contact status in friction surface 2 ALT-AS M20

Figure 6-46 and Figure 6-47 shows the contact status between the alignment component and the fixed profile. A large area around the M16 bolt has status *sticking* indicating that the connection is approximately stationary with the applied preload.

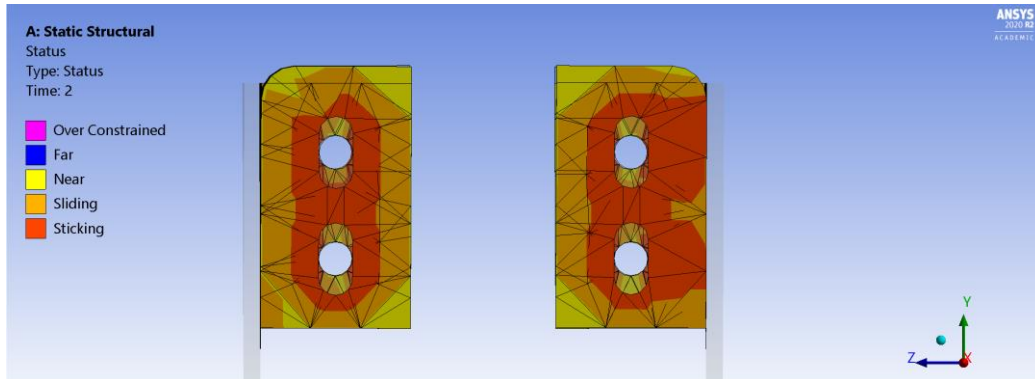


Figure 6-46 Contact status between alignment component and fixed profile, ALT-AS M10

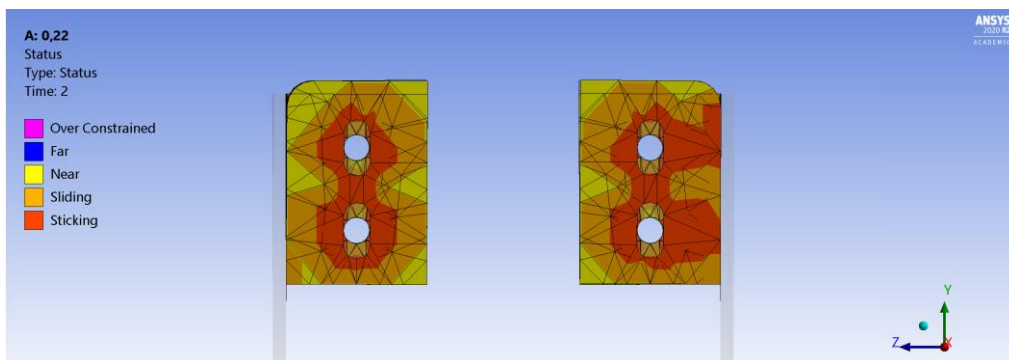


Figure 6-47 Contact status between alignment component and fixed profile, ALT-AS M20

6.5.3 STD-1H

STD-1H specimen has a bend in the fixed profile with one slotted hole. Figure 6-48 shows the deformation in Y-direction. The deformation is 0,6 mm on the left side and -1,6 mm on the right side. This indicates that the specimen is rotating from the applied displacement and reduces the possibility of sliding. Figure 6-49 shows that the size of the bolts does not influence the deformation in Y-direction.

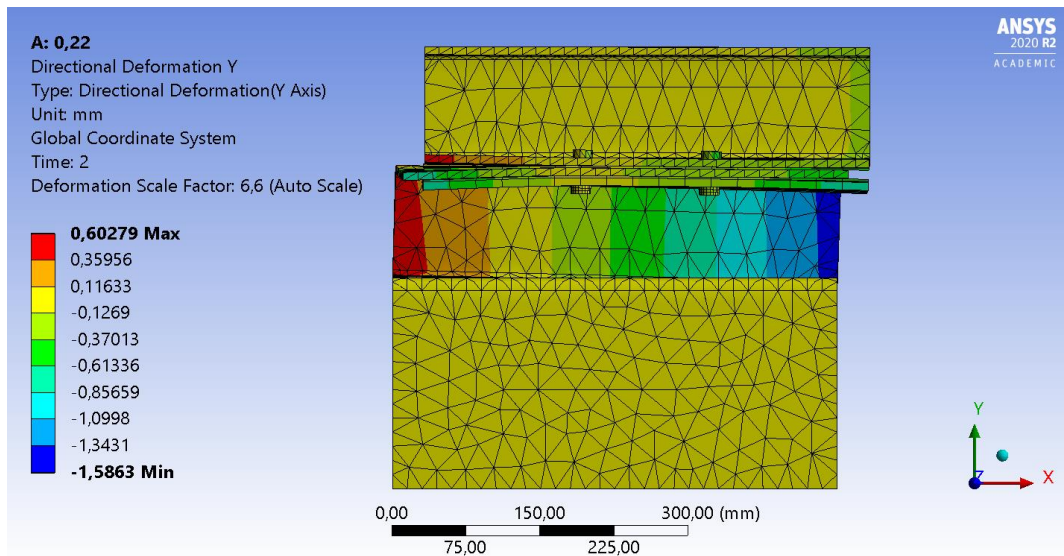


Figure 6-48 Deformation in Y-direction STH 1H M10 [mm]

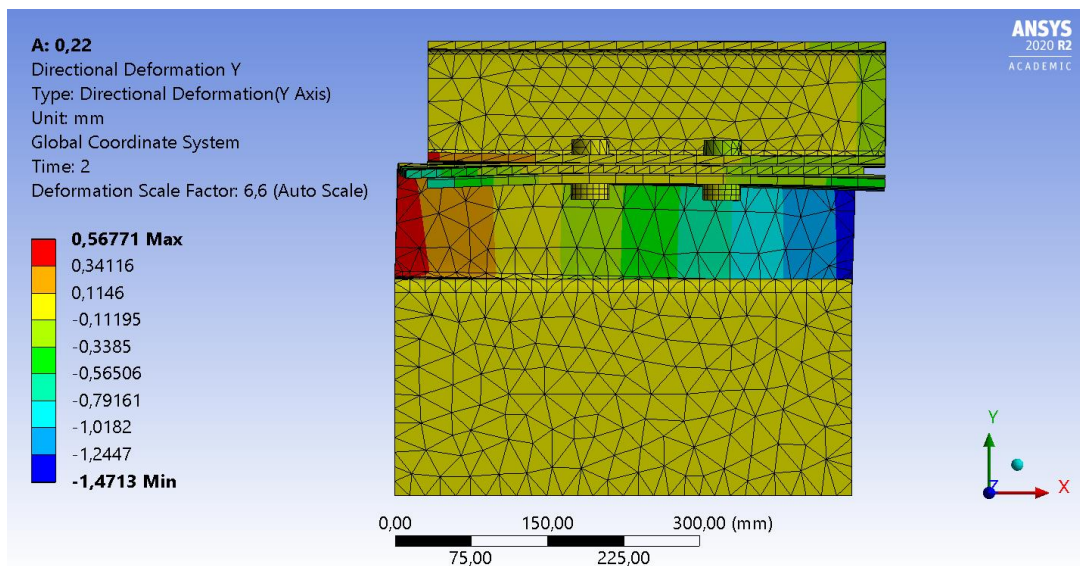


Figure 6-49 Deformation in Y-direction STD-1H M20 [mm]

Deformation in Z-direction with M10 and M20 bolts are shown in Figure 6-50 and Figure 6-51. This result shows that after applying a displacement of 5 mm in X-direction, the specimen will twist around 2 mm. With this deformation, the bolts will hit the sides of the slotted hole and increase the force needed to make the friction surface slide.

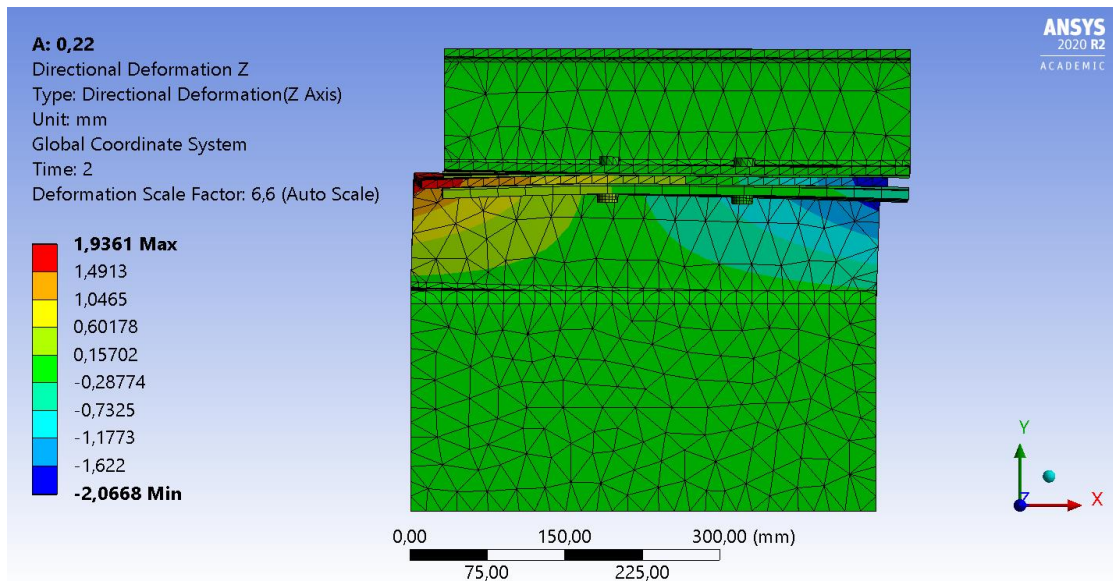


Figure 6-50 Deformation in Z-direction STH 1H M10 [mm]

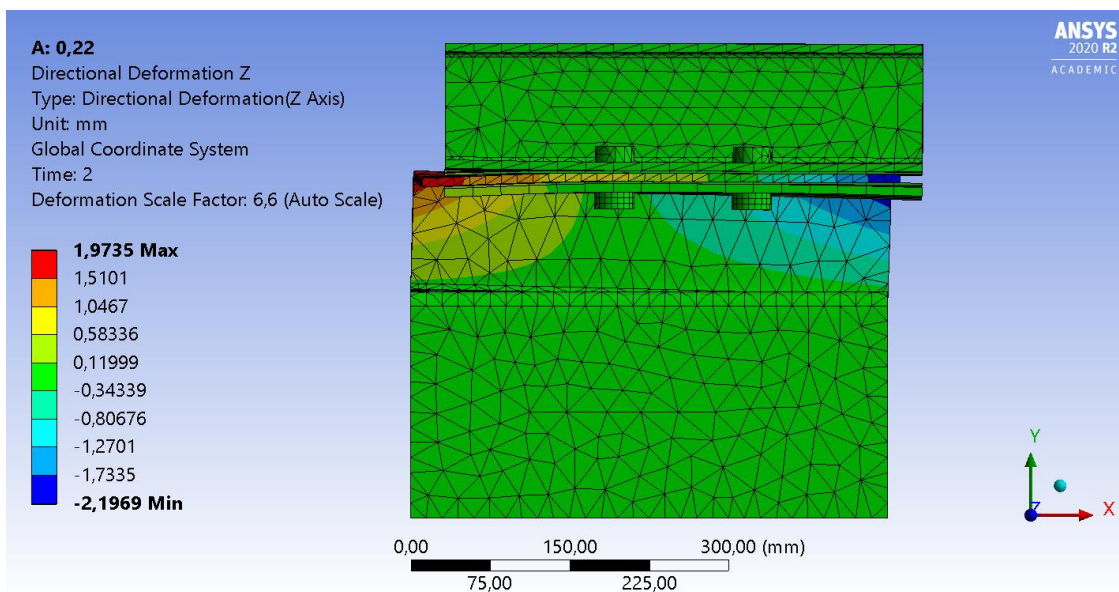


Figure 6-51 Deformation in Z-direction STD-1H M20 [mm]

Table 6-4 shows that the force reaction in the fixed profile is larger than the force generated in the friction surfaces (force probe). This indicated that the bending in the STD-1H specimen and the rotating of the slotted hole makes the specimen deform rather than sliding in the friction surface.

Table 6-4 Force reactions in STD-1H M10 and M20

Bolt size	Friction coefficient	Force reaction [N]	Force probe 1 [N]	Force probe 2 [N]	Sum force probe [N]
M10	0,22	38 782	19 629	14 454	34 083
M20	0,22	37 079	18 613	14 681	33 294

The equivalent stress in the anchor profile with M10 bolts is 657 MPa and is illustrated in Figure 6-52. Figure 6-53 shows that the maximum equivalent stress is reduced by half with the M20 bolts and is located in the bend rather than around the holes. This is because the M20 bolts divides the stress over a larger area.

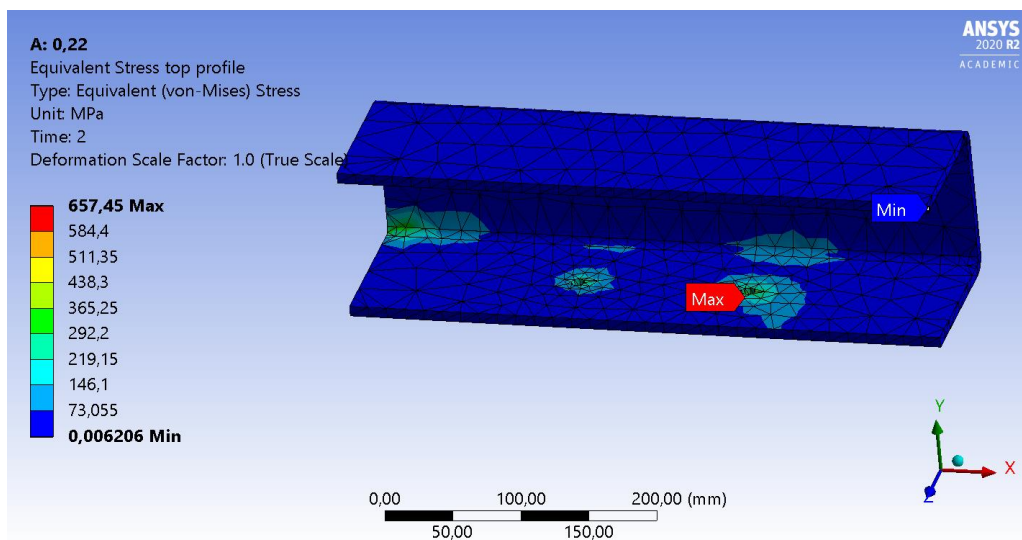


Figure 6-52 Equivalent stress in the anchor profile STD 1H M10 [MPa]

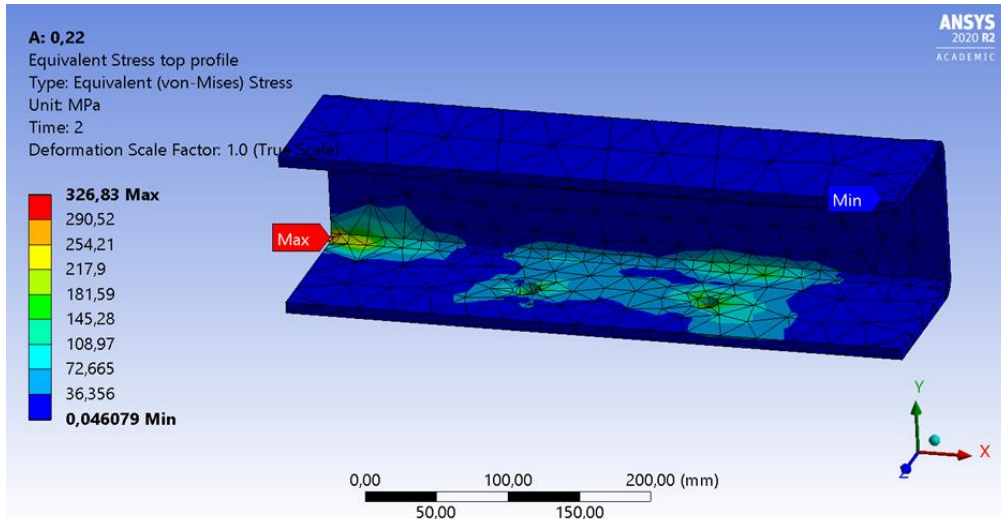


Figure 6-53 Equivalent stress in the anchor profile STD-1H M20 [MPa]

The equivalent stress in the additional plate occurs around the bolted holes and is seen in Figure 6-54 with the M10 bolts and Figure 6-55 with the M20 bolts. With both bolt sizes, the maximum equivalent stress is in the right bolt hole. Maximum equivalent stress is almost double with the M10 bolts compared to the M20 bolts.

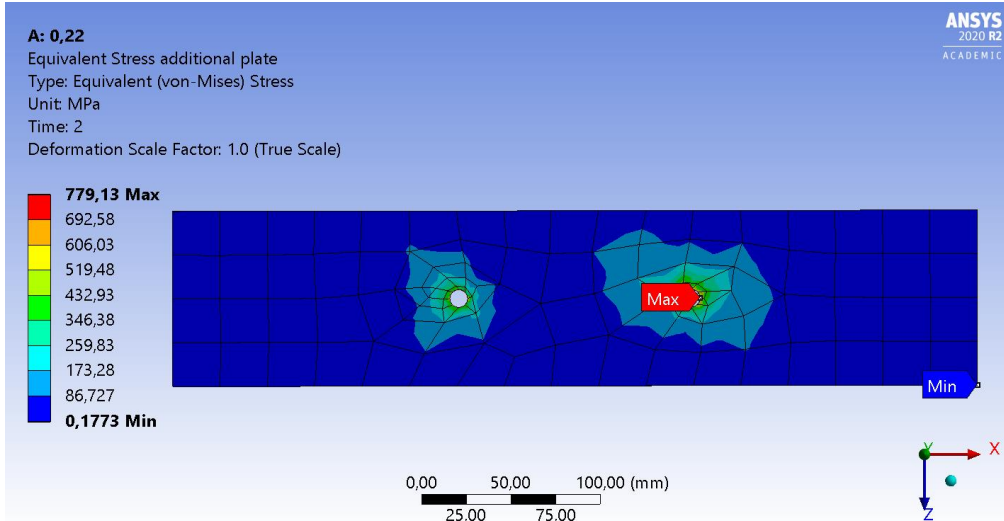


Figure 6-54 Equivalent stress in the additional plate STD-1H M10 [MPa]

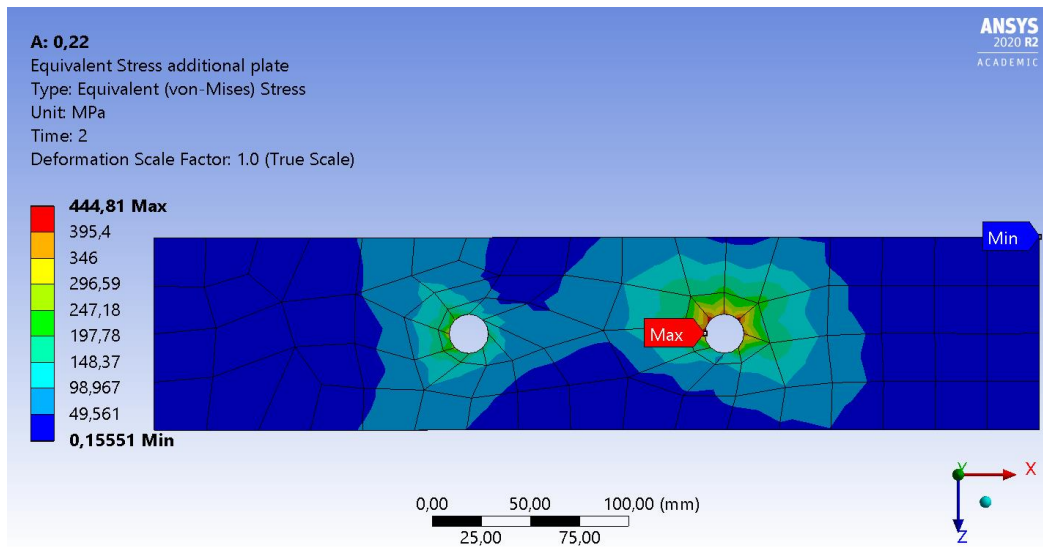


Figure 6-55 Equivalent stress in the additional plate STD-1H [MPa]

In the fixed profile, the equivalent stress is distributed along the surface of the slotted hole, and the maximum stress is located at the end of the slotted hole on the right side, as seen in Figure 6-56. The preload from the bolts is distributed through the anchor profile and the additional plate. This makes the equivalent stress in the fixed profile similar with the M10 and M20 bolts.

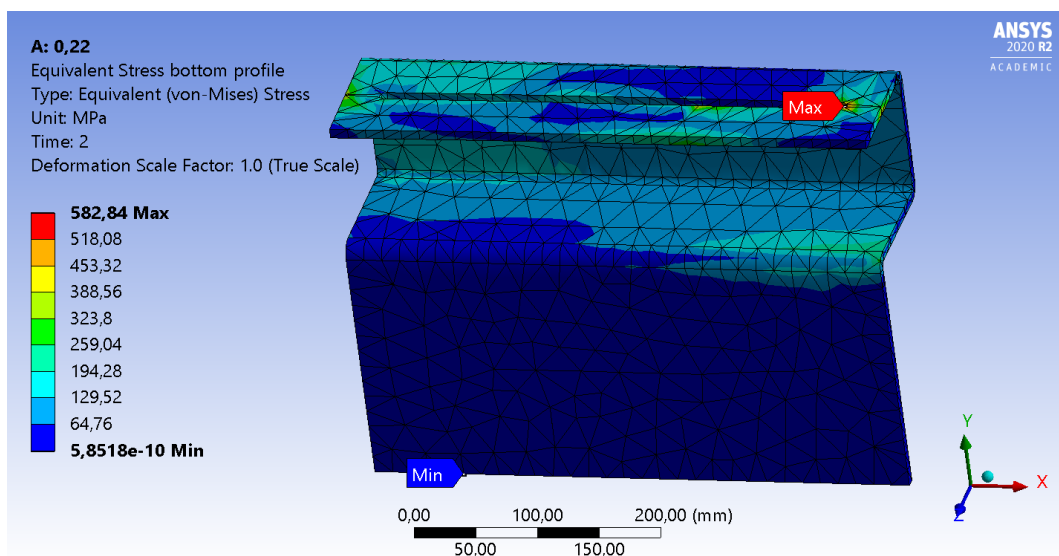


Figure 6-56 Equivalent stress in the fixed profile STH 1H M10 [MPa]

Figure 6-57 and Figure 6-58 show the contact status in friction surface 2 in STD-1H M10 and M20. *Sliding* status is observed around the bolt holes and in the inner part of the surface. The specimen with M20 bolts has less *sliding* status than the M10 specimen.

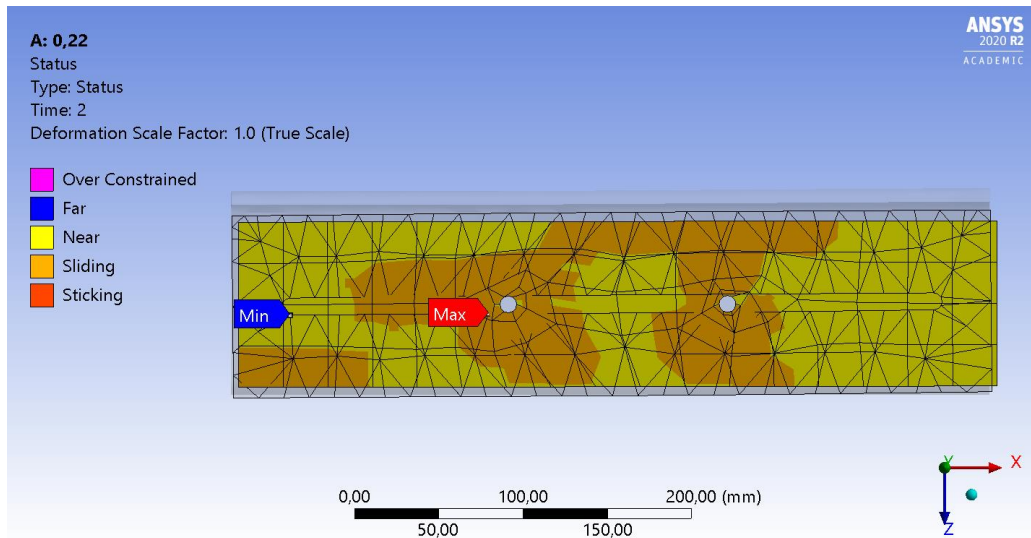


Figure 6-57 Contact status in friction surface 2 STD-1H M10

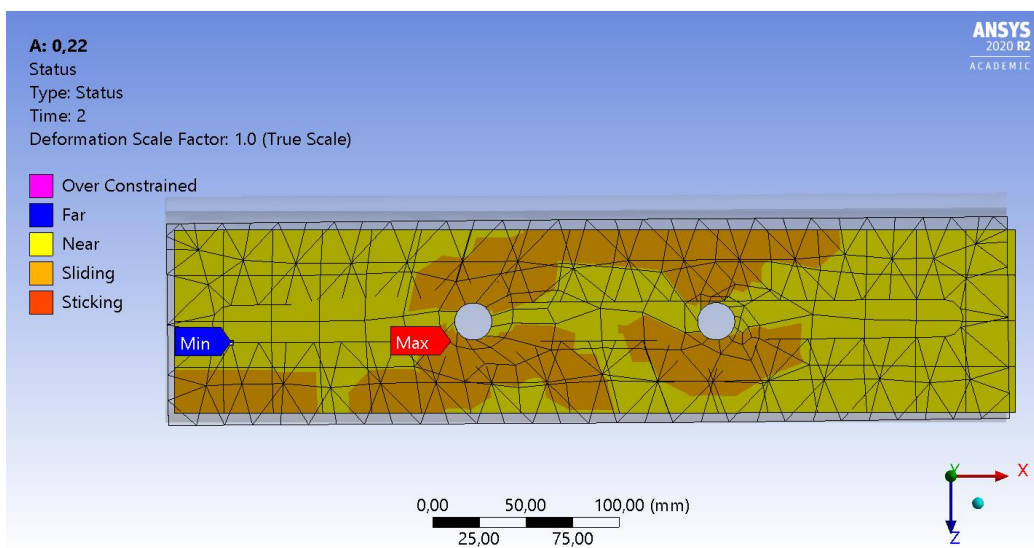


Figure 6-58 Contact status in friction surface 2 STD-1H M20

6.5.4 STD-2H

STD-2H specimen has the same bend as the STD-1H, but with two parallel slotted holes instead of one. This gives a total of four bolts in the friction connection. To achieve the slip force of 30 000 N, the preload per bolts is reduced by half due to the double number of bolts. Figure 6-59 shows that the STD-2H has a similar behavior as the STD-1H with a deformation in the bend.

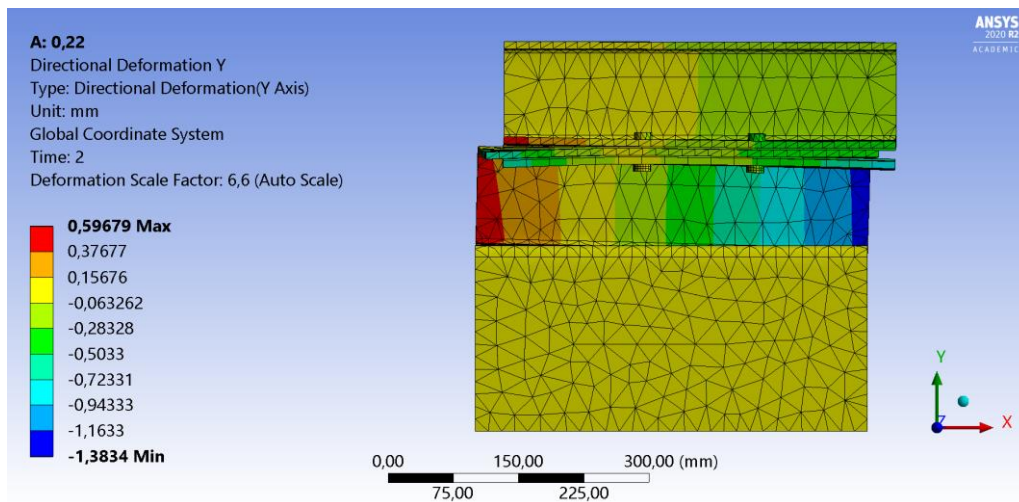


Figure 6-59 Deformation in Y-direction STH 2H M10 [mm]

Figure 6-60 shows the deformation in Z-direction. This behavior is also similar to the STD-1H. However, as seen from Table 6-5, this specimen reaches a higher force reaction than the STD-1H. This indicates that the four bolts being forced into the sides of the slotted hole during the twisting, creates more resistance than with two bolts. This makes an increased force reaction. The sum of the force probes is the same as for STD-1H and is an indication that none of the STD specimens are sliding without the effect of bending and twisting.

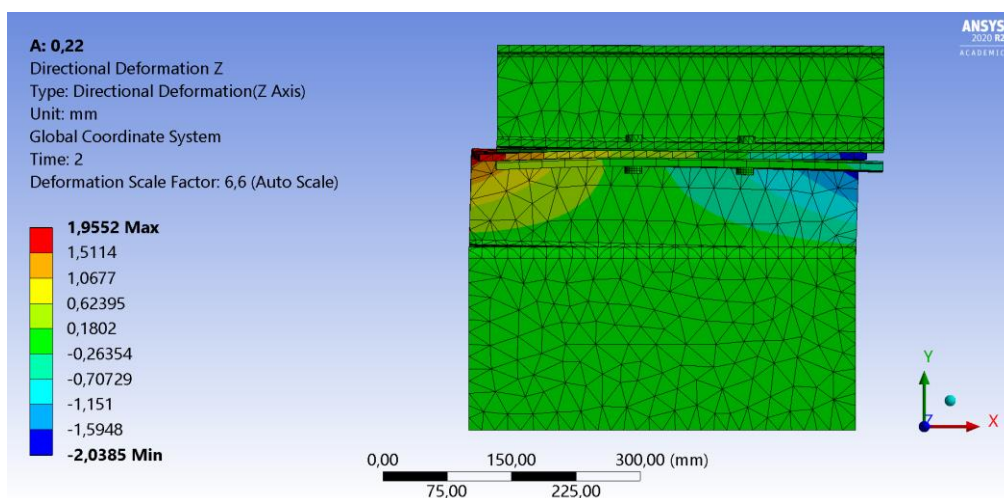


Figure 6-60 Deformation in Z-direction STH 2H M10 [mm]

Table 6-5 Force reaction and force probe for STD-2H with the dynamic friction coefficient

Bolt size	Friction coefficient	Force reaction [N]	Force probe 1 [N]	Force probe 2 [N]	Sum force probe [N]
M10	0,22	40 997	18 338	16 907	35 245

Figure 6-61 illustrates the equivalent stress in the anchor profile. The maximum stress is located around the holes. The maximum equivalent stress in the anchor profile is 548 MPa, but as seen in the figure it only happens in a small area. It is slightly lower than for the STD-1H with 657 MPa due to the lower preload.

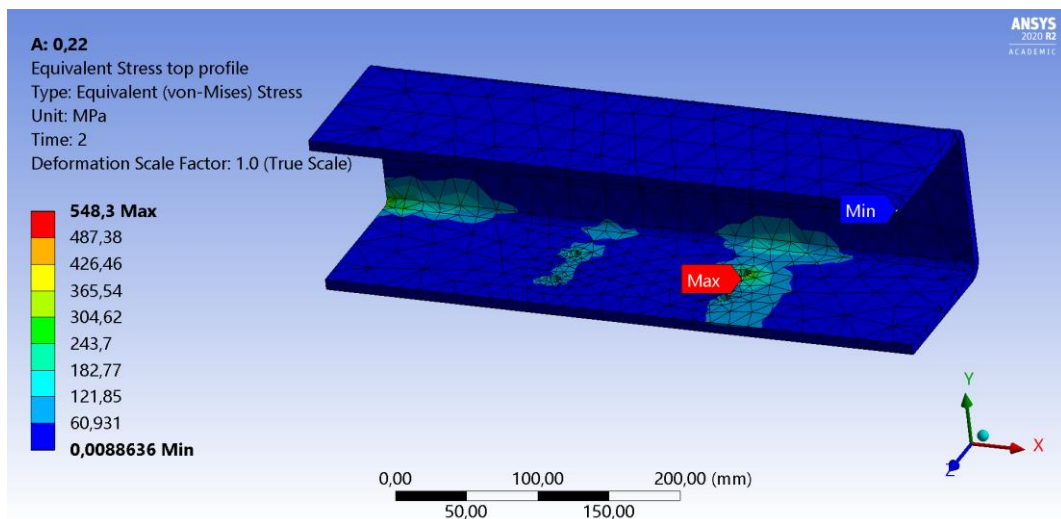


Figure 6-61 Equivalent stress in the anchor profile STD-2H [MPa]

Figure 6-62 illustrates the equivalent stress in the fixed profile. The largest stresses are located around the bolts, and the maximum is at the end of the slotted hole. There is also observed a stress around the bolts in the steel on each side of the slotted holes. This steel is narrow and is in danger of bending when the displacement in the anchor profile increases more than 5 mm.

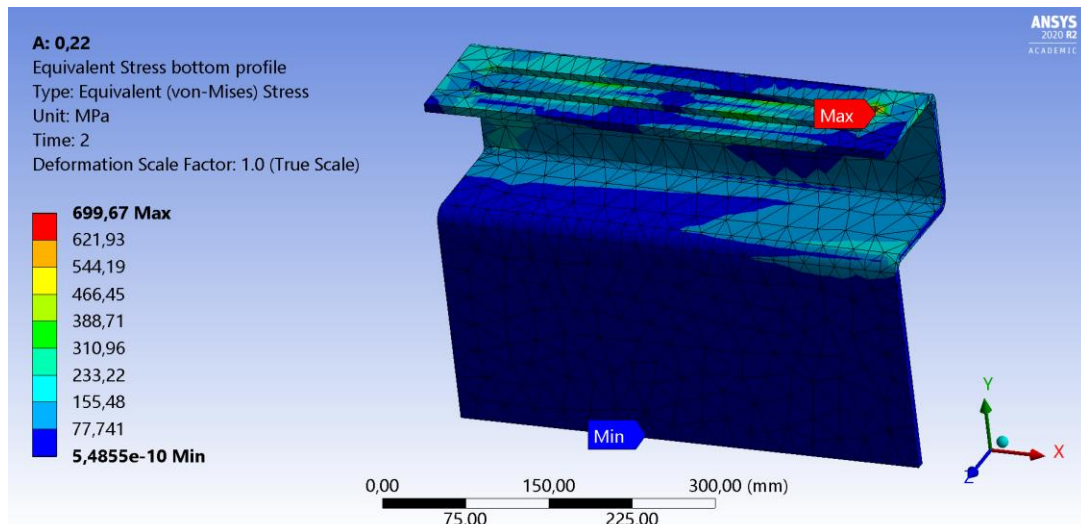


Figure 6-62 Equivalent stress in the fixed profile STD-2H [MPa]

The additional plate has a maximum equivalent stress in the same hole as the anchor profile seen in Figure 6-63. The maximum stress is 574 MPa and is in the right hole closest to the bend.

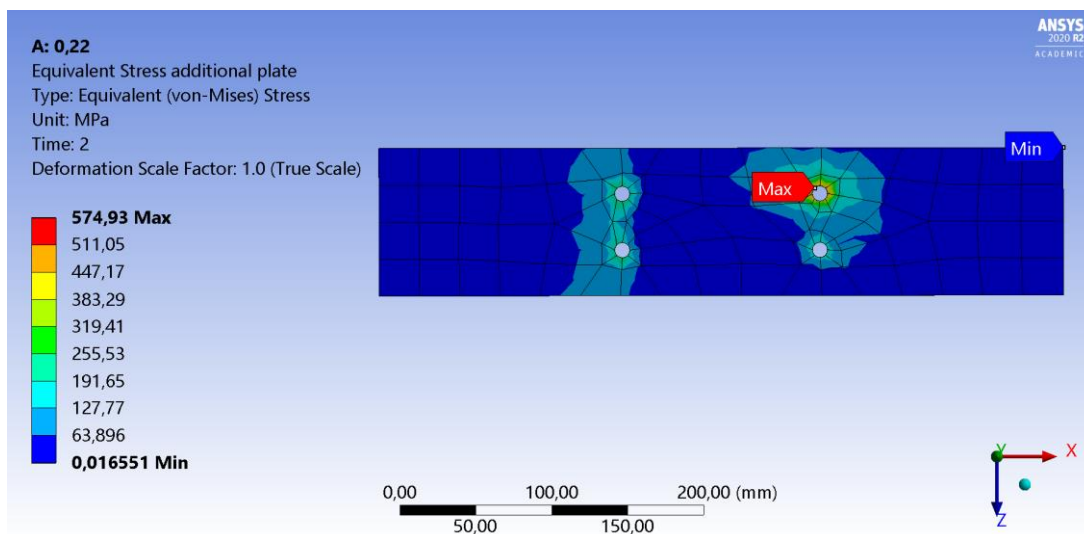


Figure 6-63 Equivalent stress in the additional plate STD-2H [MPa]

Figure 6-64 shows the contact status for friction surface 2 in STD-2H. *Sliding* status is observed around the holes and in the inner edge.

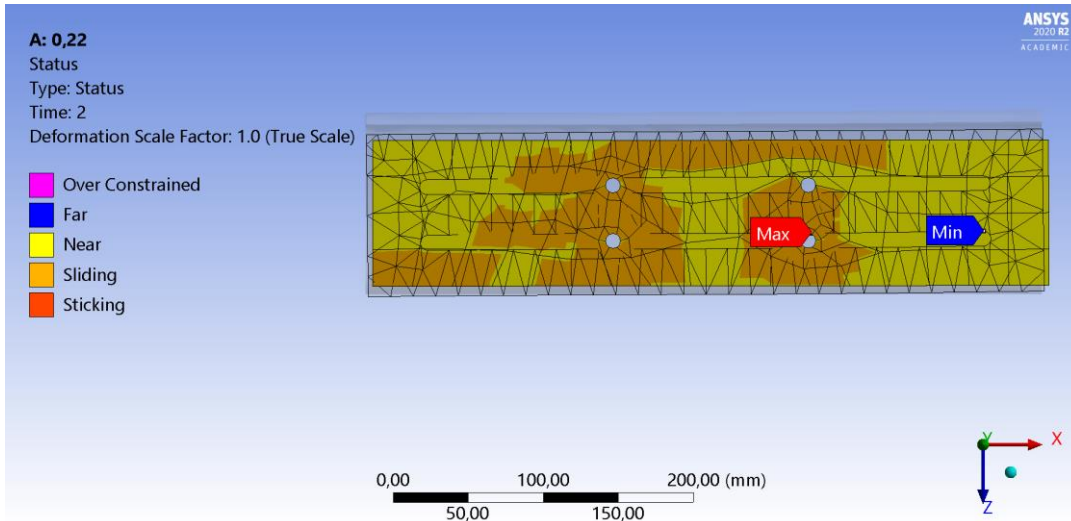


Figure 6-64 Contact status in friction surface 2 STD-2H

6.5.5 Hybrid

The Hybrid specimen appears like the ALT, but the fixed profile is mirrored, and the slotted hole is in the fixed profile. The deformation in Y-direction is exceedingly small with a maximum of 0,4 mm at the left side of the specimen with both M10 and M20 bolts, as seen in Figure 6-65 and Figure 6-66. This is a lower value than with the ALT M10 specimen, but the deformation occurs in the same place.

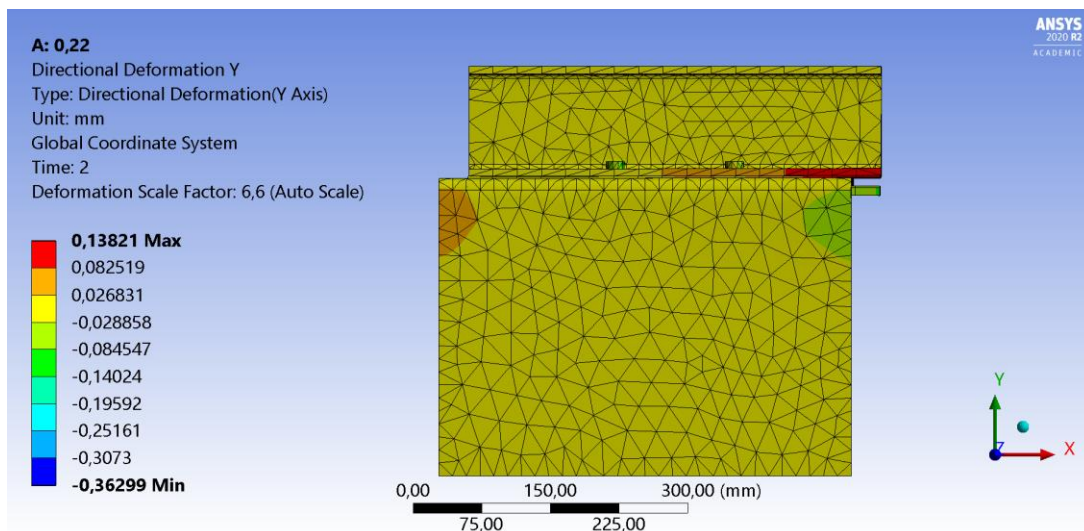


Figure 6-65 Deformation in Y-direction for Hybrid M10 [mm]

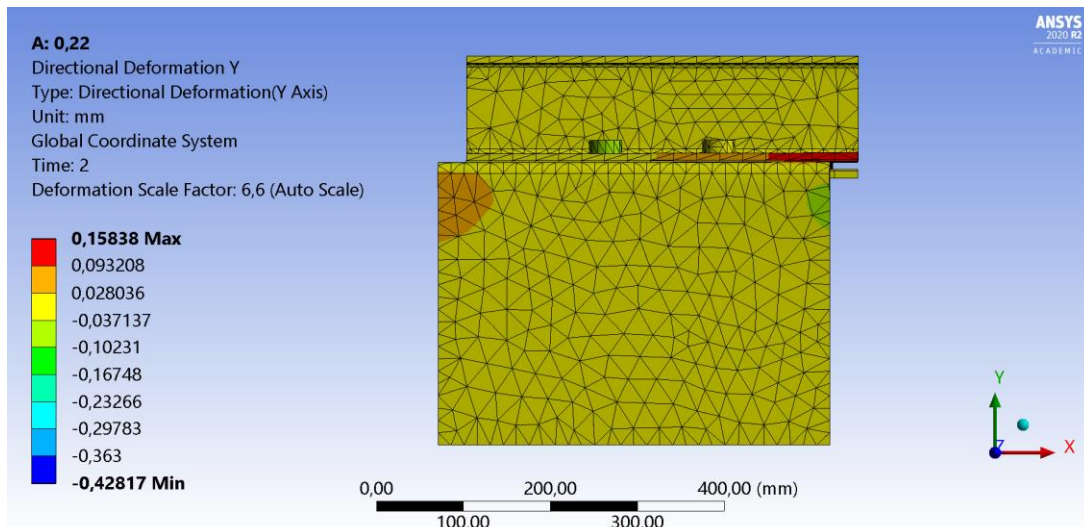


Figure 6-66 Deformation in Y-direction for Hybrid M20 [mm]

In Z-direction the deformation is the same on the right and left side but in different direction, as shown in Figure 6-67 and Figure 6-68. The deformation is 0,7 mm on the left side in the negative direction and 0,7 mm on the right side in the positive direction in the specimen with M10 bolts. In the specimen with M20 bolts, the deformation in Z-direction is 1,2 mm in the positive direction on the right side and 0,9 mm in the negative direction on the left side. The deformation in this direction is slightly higher in the M20 specimen.

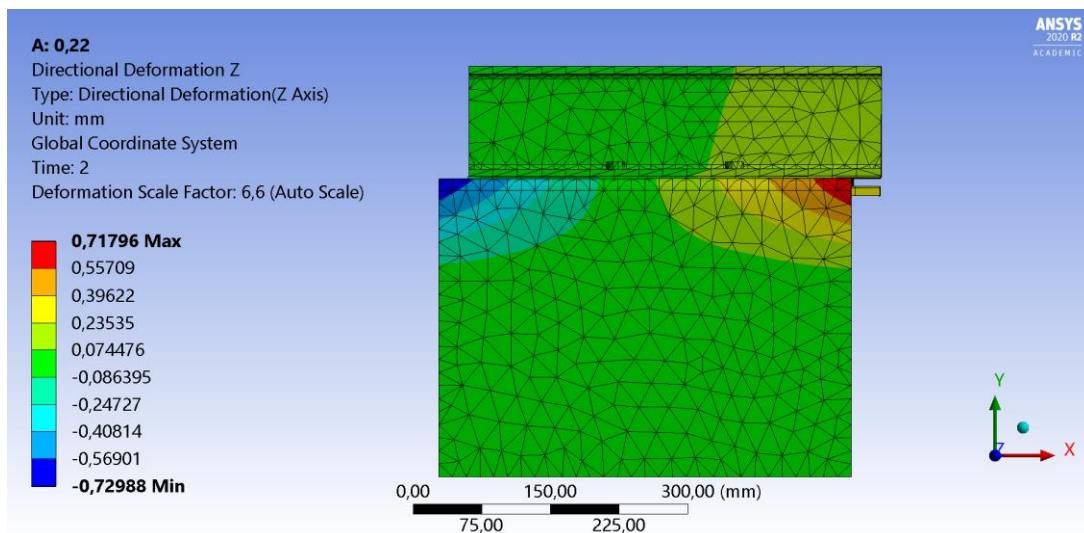


Figure 6-67 Deformation in Z-direction Hybrid M10 [mm]

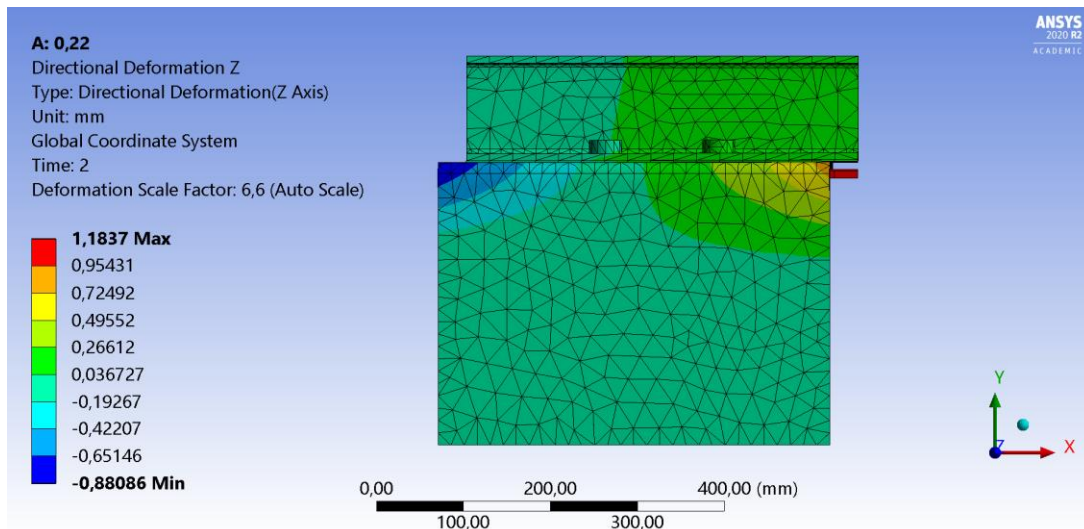


Figure 6-68 Deformation in Z-direction Hybrid M20 [mm]

Table 6-6 shows the force reaction and sum of force probe for the dynamic friction coefficient with M10 and M20 bolts. The force reaction and sum force probe are around 30 kN, as the theoretical slip friction force.

Table 6-6 Force reaction and force probe for Hybrid M10 and M20 with the dynamic friction coefficient

Bolt size	Friction coefficient	Force reaction [N]	Force probe 1 [N]	Force probe 2 [N]	Sum force probe [N]
M10	0,22	30 607	14 919	14 478	29 397
M20	0,22	29 692	14 880	14 490	29 370

In the anchor profile the maximum equivalent stress occurs in the bolted hole with both M10 and M20 bolts. The location of the maximum stress is shown in Figure 6-69 and Figure 6-70. It changes from the right hole in the specimen with the M10 bolts to the left hole with the M20 bolts. The maximum equivalent stress is 367 MPa with M10 bolts and 162 MPa with M20 bolts. The maximum stress is reduced by half with the M20 bolts. This is due to the larger area on the M20 bolts.

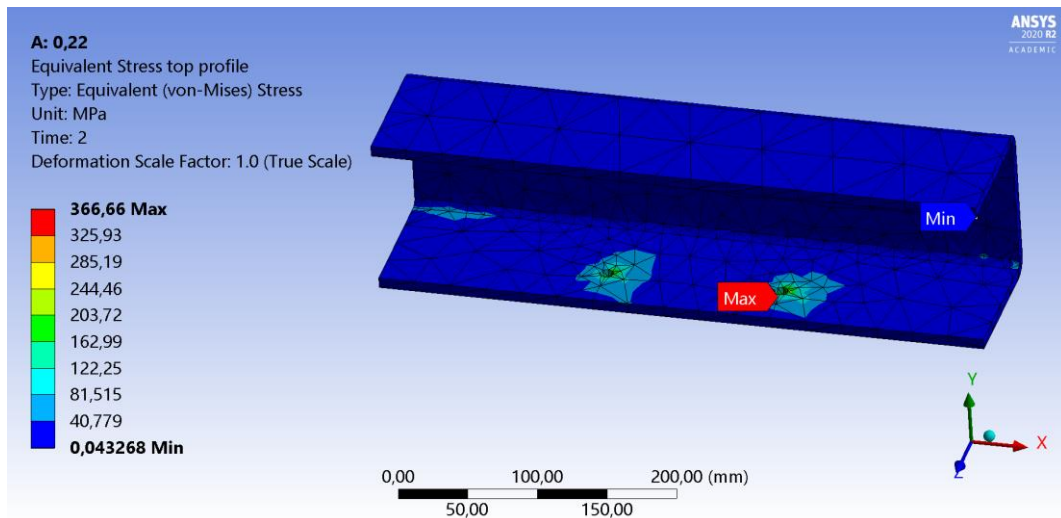


Figure 6-69 Equivalent stress in the anchor profile Hybrid M10 [MPa]

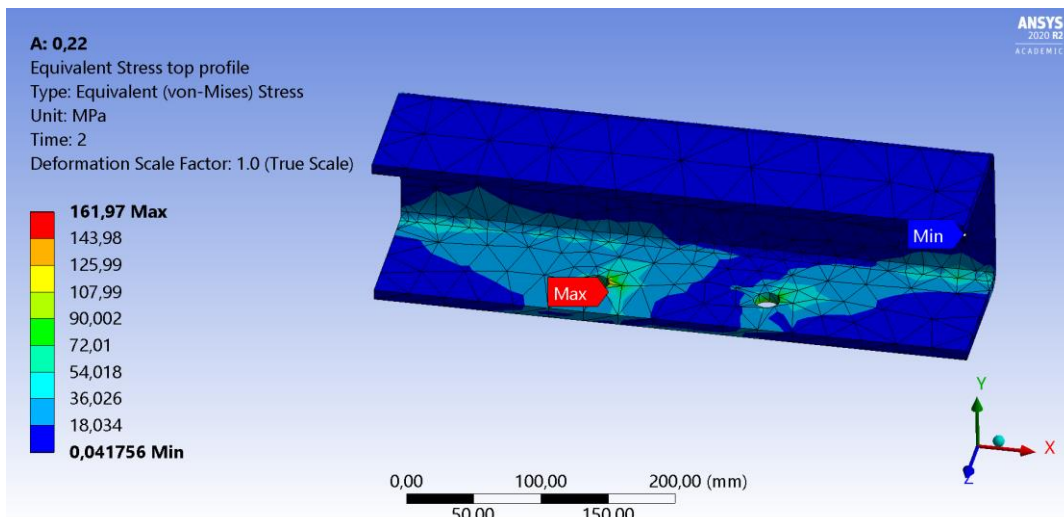


Figure 6-70 Equivalent stress in the anchor profile Hybrid M20 [MPa]

For the fixed profile, the maximum equivalent stress is around 180 MPa with both M10 and M20 bolts. With M10 bolts, the maximum stress occurs on the right side, as shown in Figure 6-71. The location of the maximum stress with the M20 bolt is shown in Figure 6-72, and it is in the bend of the profile.

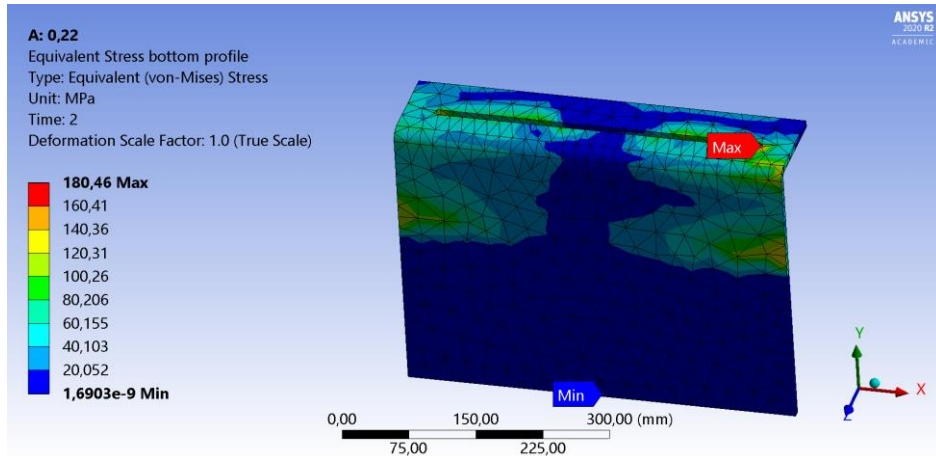


Figure 6-71 Equivalent stress in the fixed profile Hybrid M10 [MPa]

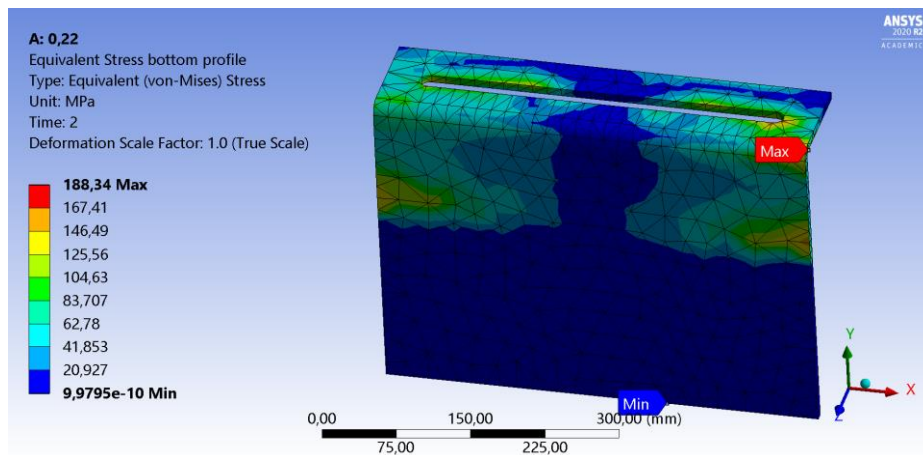


Figure 6-72 Equivalent stress in the fixed profile Hybrid M20 [MPa]

In Figure 6-73 the maximum equivalent stress in the additional plate with M10 bolts is shown. The stress is located around the bolted holes, and the maximum stress is 449 MPa in the right bolt hole. In the specimen with M20 bolts, the maximum equivalent stress in the additional plate is illustrated in Figure 6-74. The maximum stress is almost reduced by half compared to the specimen with M10 bolts.

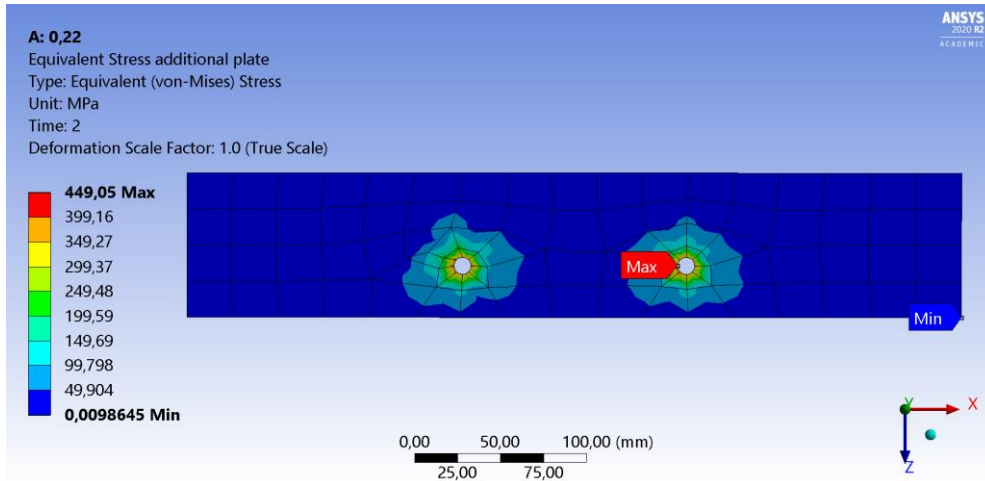


Figure 6-73 Equivalent stress in the additional plate Hybrid M10 [MPa]

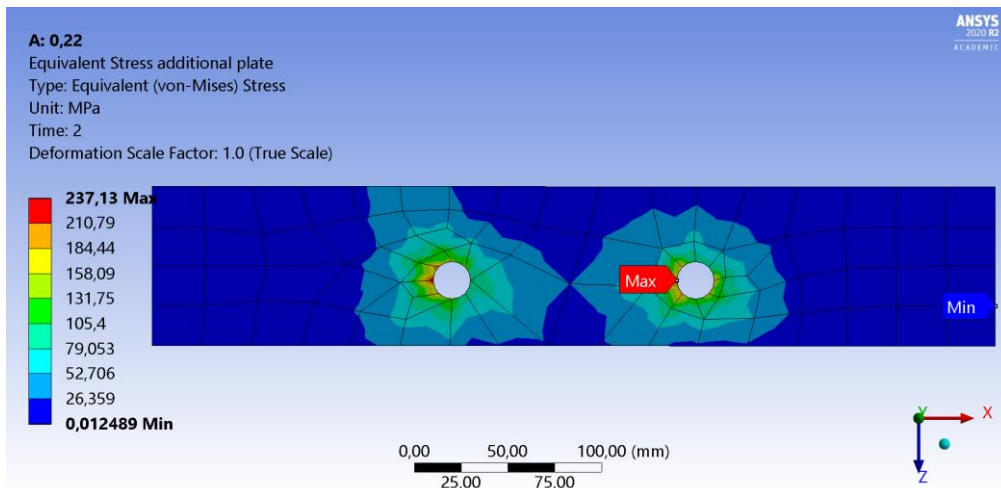


Figure 6-74 Equivalent stress in the additional plate Hybrid M20 [MPa]

Figure 6-75 and Figure 6-76 show the contact status for Hybrid M10 and M20. It is observed that the *sliding* status is only in a small area around the bolt holes.

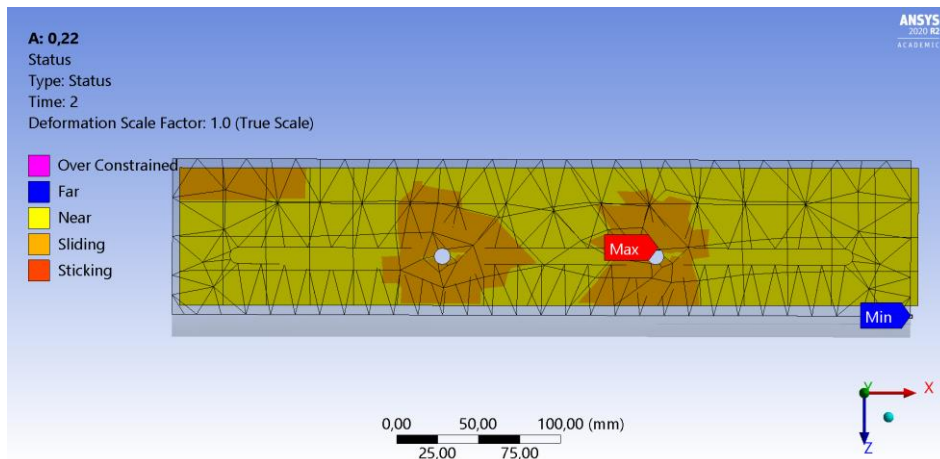


Figure 6-75 Contact status in friction surface 2 Hybrid M10

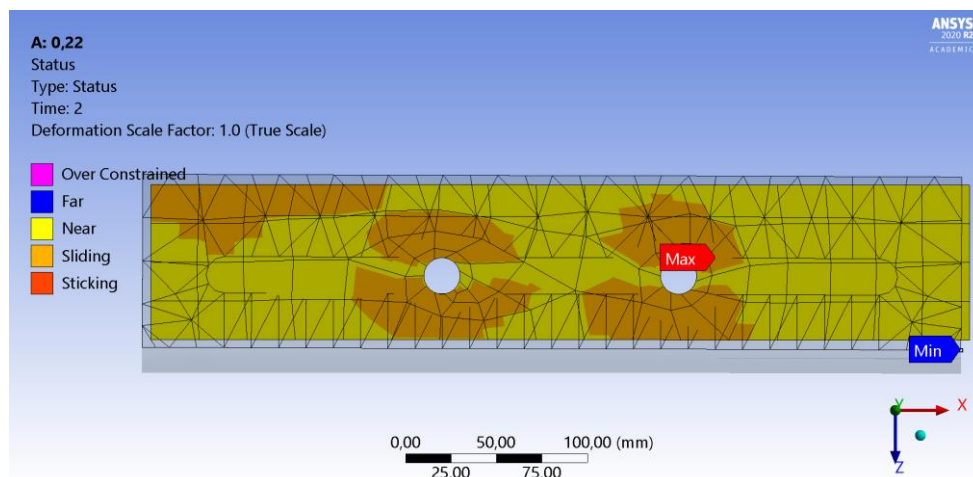


Figure 6-76 Contact status friction surface 2 Hybrid M20

6.5.6 Comparison

In Table 6-7 to Table 6-11 the force reaction and sum of force probe are listed for all the specimens with both the static- and dynamic friction coefficient. The wanted theoretical slip friction force is 30 kN with two bolts, two friction surfaces and the dynamic friction coefficient.

As seen from the tables, ALT and Hybrid specimen are closest to the theoretical 30 kN with both M10 and M20 bolts with the dynamic friction coefficient of 0,22. STD-2H is the specimen that reaches the highest force reaction and sum of force probes with the dynamic friction coefficient. As seen in chapter 6.5.4, the STD-2H specimen does not seem to slide,

and therefore reaches a higher force. For the other specimens, looking at the dynamic friction coefficient, the force reaction and force probe is almost the same with M10 and M20 bolts.

With the static friction coefficient of 0,39, the force reaction and force probe for all the specimens are over 50 kN. This indicates that the initial static part of the friction could damage the specimen and needs to be further investigated. The STD specimens reach a force close to 70 kN which is over twice the amount of the calculated 30 kN slip friction force. For specimen ALT and Hybrid, the change of bolt size did not influence the force. The force increases with less than 1 kN when the bolts are changed from M10 to M20 in specimen ALT and Hybrid. For the ALT-AS specimen the force reduces with around 3,5 kN changing from M10 to M20 bolts. Whereas for the STD-1H the force increases with 3 kN when changing from M10 to M20 bolts.

From the force reaction and force probe, seen in Table 6-7 to Table 6-11, the bolt size has a bigger impact in the static part than in the dynamic part, where the force is more stable and closer to the slip friction force of 30 kN. Although it has a bigger impact in the static part, the change of bolt size does not seem to affect the force reaction and sum of force probe.

Table 6-7 Force reaction and force probe in ALT specimen

ALT					
M10			M20		
Friction coefficient	Force reaction [N]	Sum force probe [N]	Friction coefficient	Force reaction [N]	Sum force probe [N]
0,22	30 862	30 594	0,22	30 392	30 551
0,39	53 270	52 715	0,39	53 516	53 656

Table 6-8 Force reaction and force probe in ALT-AS specimen

ALT-AS					
M10			M20		
Friction coefficient	Force reaction [N]	Sum force probe [N]	Friction coefficient	Force reaction [N]	Sum force probe [N]
0,22	31 511	31 571	0,22	31 993	31 366
0,39	57 756	57 692	0,39	54 946	54 107

Table 6-9 Force reaction and force probe in STD-1H specimen

STD-1H					
M10			M20		
Friction coefficient	Force reaction [N]	Sum force probe [N]	Friction coefficient	Force reaction [N]	Sum force probe [N]
0,22	38 782	34 083	0,22	37 079	33 294
0,39	73 200	64 393	0,39	72 090	67 492

Table 6-10 Force reaction and force probe in STD-2H specimen

STD-2H		
M10		
Friction coefficient	Force reaction [N]	Sum force probe [N]
0,22	40 997	35 245
0,39	80 167	73 566

Table 6-11 Force reaction and force probe in Hybrid specimen

HYBRID					
M10			M20		
Friction coefficient	Force reaction [N]	Sum force probe [N]	Friction coefficient	Force reaction [N]	Sum force probe [N]
0,22	30 607	29 397	0,22	29 692	29 370
0,39	53 071	51 875	0,39	53 965	52 760

In Table 6-12 to Table 6-16 the utilization rate for all the profiles in each specimen, with the two different friction coefficient is shown. It is listed in percent, where green indicates that the maximum stress is lower than the yielding strength of 355 MPa. As explained in the previous results, the M20 bolts give a lower stress due to the larger area than the M10 bolts and this can be seen in the tables. From the tables it can also be seen that the profiles with the bolted holes have a larger stress than the profiles with the slotted hole.

There are two specimens that are all green, the ALT M20 and the Hybrid M20. The ALT-AS M20 profile is only 3-7 % over the capacity. As shown in the previous results chapters the maximum equivalent stress only occurs in a small area. Since the area is so small the specimens are not expected to yield. The stress reduces in the profiles when the bolts are changed from M10 to M20 because the area is bigger with M20 bolts. The stress in the profiles is also affected by changing the friction coefficient. With the dynamic friction coefficient, the stress is lower than with the static friction coefficient. Still the change of bolt

size has a bigger impact in reaching a lower maximum equivalent stress in the specimens ALT, ALT-AS and Hybrid. For the STD specimens it seems that the friction coefficient is affecting the maximum stress more than the bolt size does. Again, this may be an indication that the specimens are not sliding, and therefore reaches a much higher stress than the other specimens.

Table 6-12 Utilization rate of the ALT specimen

ALT			
M10			
Friction coefficient	Max stress anchor profile [MPa]	Max stress fixed profile [MPa]	Max stress additional plate [MPa]
0,22	58 %	146 %	124 %
0,39	100 %	219 %	135 %
M20			
0,22	51 %	63 %	71 %
0,39	94 %	90 %	84 %

Table 6-13 Utilization rate of the ALT-AS specimen

ALT-AS				
M10				
Friction coefficient	Max stress anchor profile [MPa]	Max stress fixed profile [MPa]	Max stress additional plate [MPa]	Max stress alignment component [MPa]
0,22	82 %	109 %	153 %	104 %
0,39	150 %	127 %	193 %	163 %
M20				
0,22	53 %	103 %	73 %	85 %
0,39	88 %	107 %	81 %	86 %

Table 6-14 Utilization rate of the STD-1H specimen

STD-1H			
M10			
Friction coefficient	Max stress anchor profile [MPa]	Max stress fixed profile [MPa]	Max stress additional plate [MPa]
0,22	185 %	164 %	219 %
0,39	303 %	257 %	332 %
M20			
0,22	92 %	163 %	125 %
0,39	164 %	264 %	202 %

Table 6-15 Utilization rate of the STD-2H specimen

STD-2H			
M10			
Friction coefficient	Max stress anchor profile [MPa]	Max stress fixed profile [MPa]	Max stress additional plate [MPa]
0,22	154 %	197 %	162 %
0,39	261 %	322 %	270 %

Table 6-16 Utilization rate of the Hybrid specimen

HYBRID			
M10			
Friction coefficient	Max stress anchor profile [MPa]	Max stress fixed profile [MPa]	Max stress additional plate [MPa]
0,22	103 %	51 %	126 %
0,39	132 %	94 %	151 %
M20			
0,22	46 %	53 %	67 %
0,39	58 %	92 %	78 %

From the results done with Ansys the force for the STD-1H specimen reduces by around 1 kN when changing from M10 to M20 bolts. The stress also reduces with the M20 bolts. In the anchor profile and the additional plate, the stress reduces by around 500 MPa, most likely because the M20 bolts has a larger area and therefore reduces the stress.

STD-1H is the specimen that bends the most, which might be because of the bent design, that causes a bigger moment in the specimen. The bending deformation in the specimens is almost the same with the M10 and the M20 bolts, and therefore it seems that the bolts do not influence the bending. The force reaction for the specimen is around 38 kN and is also indicating that the specimen is bending and not sliding.

The behavior of the STD-2H is approximately the same as the STD-1H, where bending occurs due to the design of the fixed profile. In the STD-2H specimen, the preload on each bolt is reduced by half as the design has the double amount of M10 bolts. This reduced the stress concentration, especially around the bolt holes in the additional plate, and some reduction is also observed in the fixed profile and the anchor profile. Although the stress in the STD-2H specimen decreases with the double number of bolts, the achieved friction force is approximately the same. This design achieves a better stress distribution than STD-1H but reaches a higher force.

In the ALT specimen, the bending is almost non-existent compared to the STD specimens. The specimen seems to slide easier instead of bending like the STD. The force reaction is around 30 kN, and this indicates a more stable behavior of the specimen. Comparing the two different bolts, M10 and M20, the force is approximately the same, but the stress is lower with the M20 than the M10 bolts.

As for the ALT, the ALT-AS specimen also achieves a force reaction close to the theoretical slip force. The force reaction is around 31 kN with both M10 and M20 bolts. This indicates that also the ALT-AS specimen is behaving as desired. Equivalent stress in the specimen reduces by around half changing from M10 to M20 bolts. Looking at the two different friction coefficients, the stress increases around the bolted holes with the M10 bolts changing friction coefficient from 0,22 to 0,39. With the M20 bolts the stress is approximately the same with the two different coefficients.

With the Hybrid specimen the lowest force reaction with the dynamic friction coefficient is observed. It still reaches a force reaction over 50 kN with the static friction coefficient. In the dynamic friction part, the specimen reaches a force reaction below 30 kN. As seen from the other specimens the stress reduces when changing from M10 to M20 bolts. The same preload is used for the M20 and the M10 bolts. Using the same preload for both bolt sizes might be a problem due smaller amount of preload for the M20 compared to the capacity of the bolt.

From these results the STD specimens are expected to bend instead of slide, and therefore reach a higher slip friction force than 30 kN. For ALT, ALT-AS and Hybrid it is expected a better behavior with the M20 bolts than with the M10 bolts. These specimens seem to reach the theoretical slip friction force of 30 kN, and the two most promising specimens are ALT M20 and Hybrid M20. For the Hybrid specimen the top profile connected to the CLT-panel is not included in these tests, and that profile is like the STD with the bend. Therefore, this specimen might work better in these tests than in a full-scale test where the CLT-panel is included.

The contact status in friction surface 2 was presented for each specimen. ALT and ALT-AS specimen have a smaller contact area than STD and a larger part of the surface with *sliding* status. Hybrid had the least utilized surface with *sliding* of all the specimens.

7 Results and discussion: Experimental activity

This chapter shows the relevant results from the physical testing of the specimens. All graphs and results from every test can be found in Appendix C. In the first chapter, *Preliminary testing*, the old specimens with new Hardox 450 shim layers were tested in Instron100. These specimens were tested due to the late delivery of the new specimens. In chapter *Monotonic testing*, the results of the new specimen ALT are shown, where the washer sensors were tested for the first time. These tests were performed as monotonic in Instron100. In chapter *New testing campaign*, the results of all the new specimen are shown and the tests were performed in Instron300.

7.1 Preliminary testing

Tests 1 to 4 were done with the different old STD specimen seen in Table 4-3. Figure 7-1 shows that the tests gave similar result with a sudden increase in load, ending the test at 50 kN. STD-1H completed the most cycles but also reached 50 kN. There was observed large deformations in the specimens after the tests. The increasing force can be linked to these large deformations.

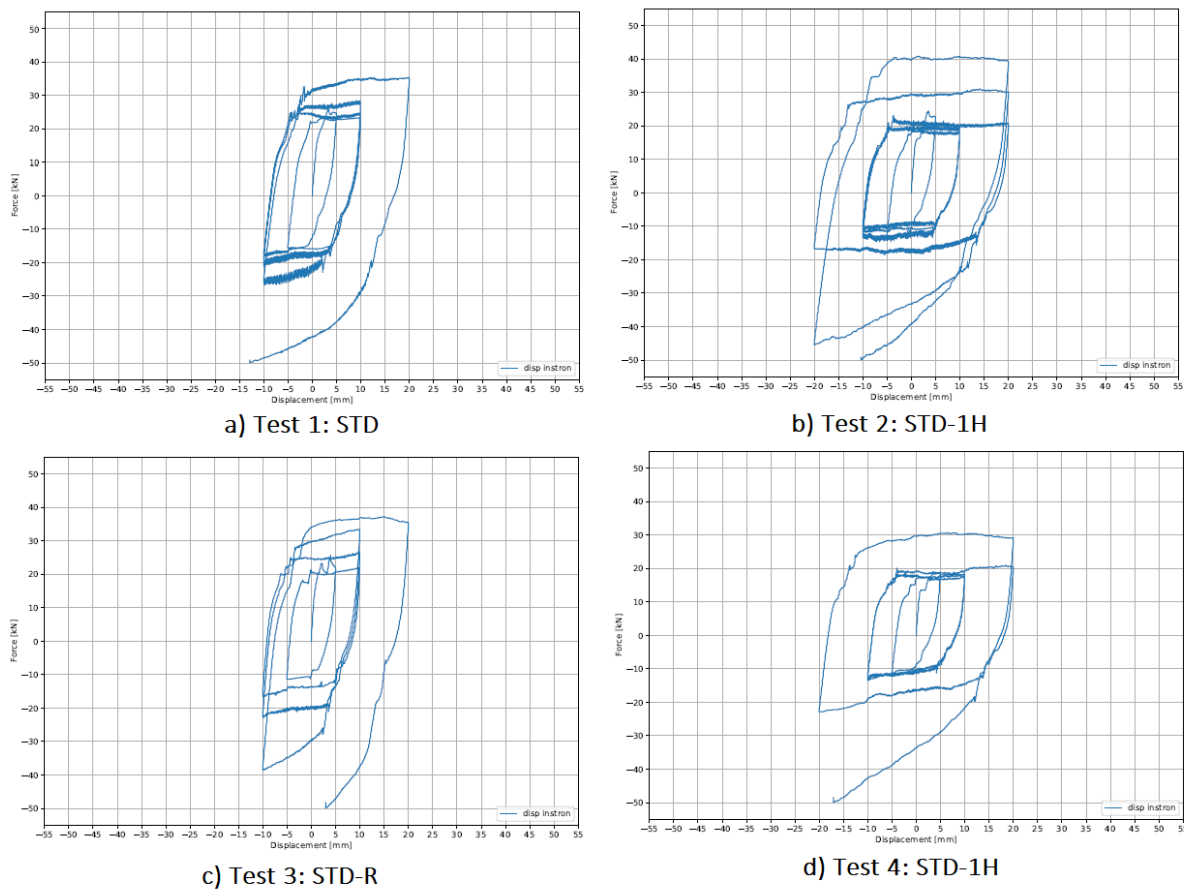


Figure 7-1 Hysteresis loop in a) test 1, b) test 2, c) test 3 and d) test 4

In test 5 (Table 4-3) the ALT specimen was tested. This test almost completed all the cycles, but also stopped when it reached 50 kN. When studying the hysteresis loop of the test in Figure 7-2 it is observed that the graph is not symmetric. The test passed 60 kN in the compression zone without ending. It was observed that when the test was concluded, there was still a load reading in the software of the press. The reading was about 5 kN and it kept increasing when the press was not in use.

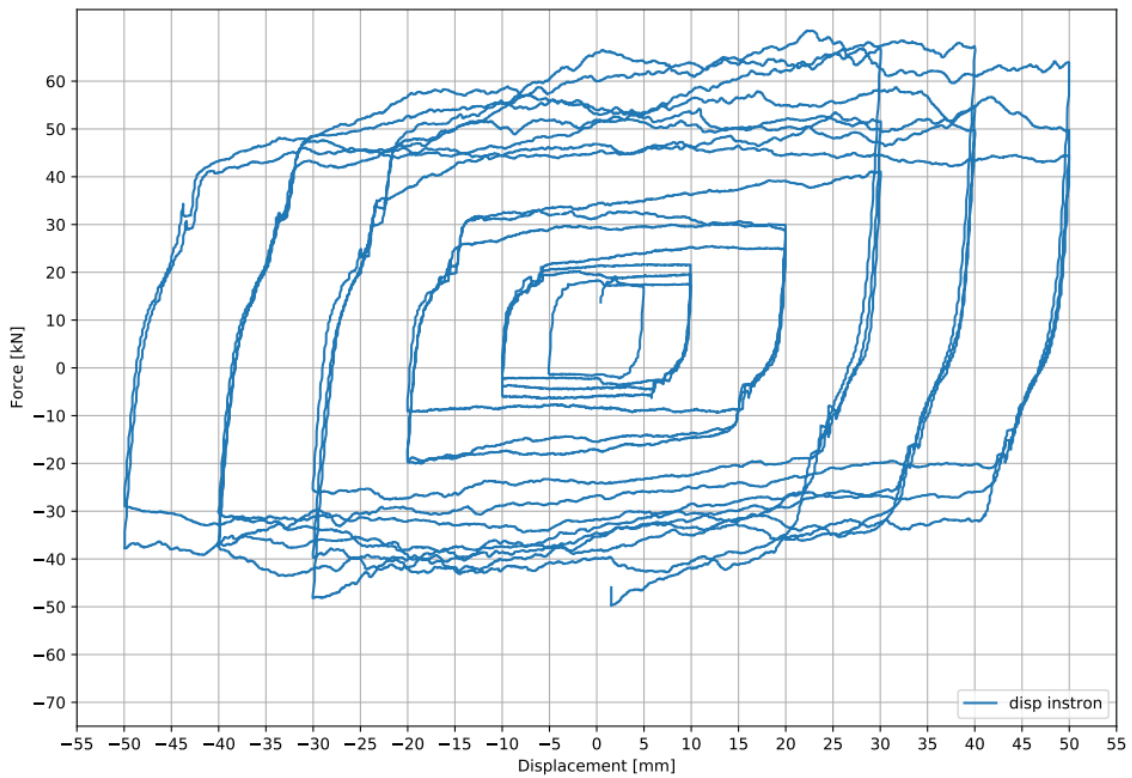


Figure 7-2 ALT hysteresis loop (test 5)

The computers and the press were then reset and a new test with the same ALT specimen was conducted, test 6 (Table 4-3). The shim layers were flipped before the new test, so that the unscratched side of the shim layer would face the frictional wear. The result of this test is seen in Figure 7-3. The press stopped at a random point when an error: “frame loop error: tripped severe” appeared on the software of the press. Again, after loosening the specimen, the press gave a reading of 5 kN. This can be seen in Figure 7-3 as the graph is asymmetric.

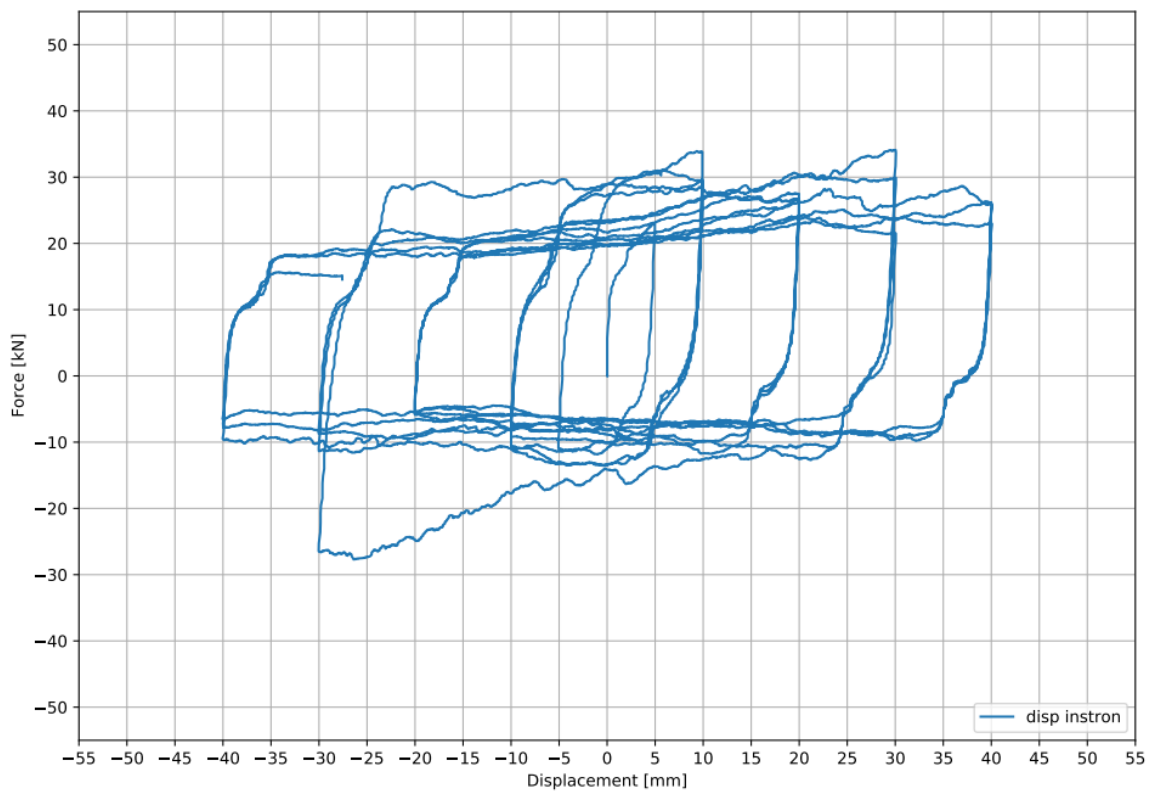


Figure 7-3 ALT hysteresis loop (test 6)

Since there was some problem with the load readings in the previous tests, it was decided to try a new load cell to investigate if that would solve the problem. The resulting hysteresis loop from the test can be seen in Figure 7-4 which still shows a clear asymmetric reading of the force. This result indicated that the problem was not related to the load cell, and the original load cell was therefore mounted again.

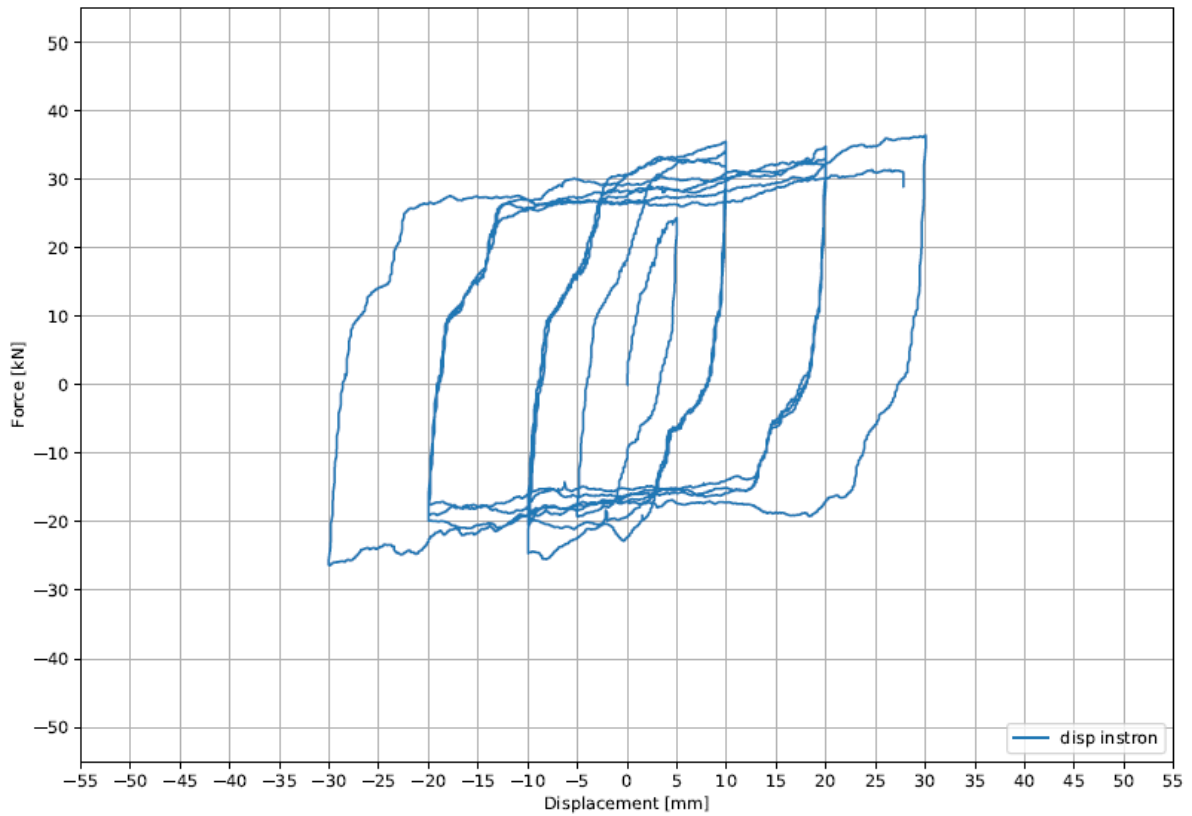


Figure 7-4 ALT hysteresis loop (test 7)

Test 8 (Table 4-3) was performed exactly the same way as Marthinsen's ALT test A [4, pp. 57] to be able to compare the results. The original load cell was mounted, and aluminum shim layers were used. Figure 7-5 shows the hysteresis loop for both the test of Marthinsen and test 8. It is clear from this result that the behavior has changed significantly. The previous test of Marthinsen was more stable and did not have the asymmetry as seen in test 8. The test stopped automatically when the same error code as in test 6 appeared.

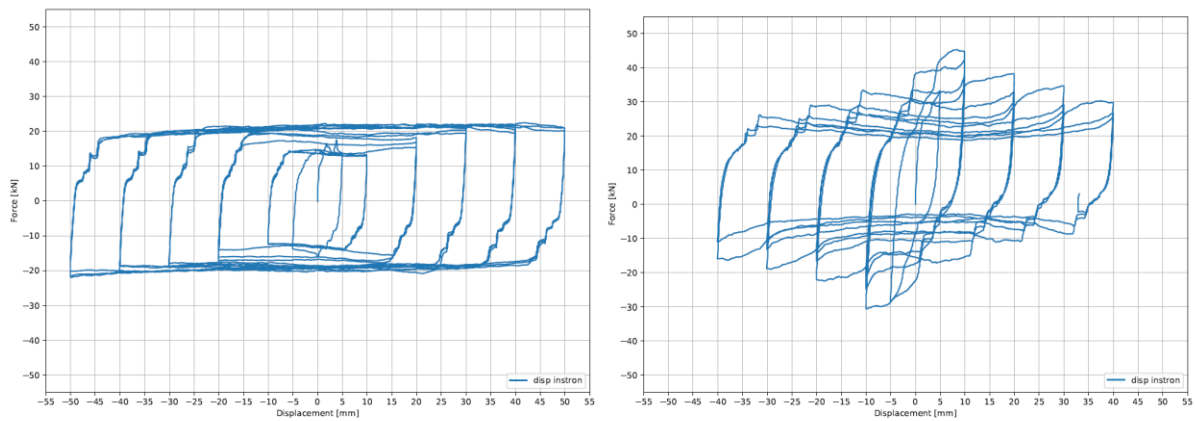


Figure 7-5 Hysteresis loop of Marthinsen's test (left) [4] and test 8 (right)

After examining the videos taken during the tests, it was observed that the press had a significant displacement of the frame, especially when the press went from the lowest position and was going up. This displacement was recorded in the top LDT sensor, as seen in the top right in Figure 4-1. The movement of the top column during test 2 (Table 4-3) is shown in blue in Figure 7-6. It is observed that the movement increases during the test and reaches a maximum displacement of -2 mm at the end of the test.

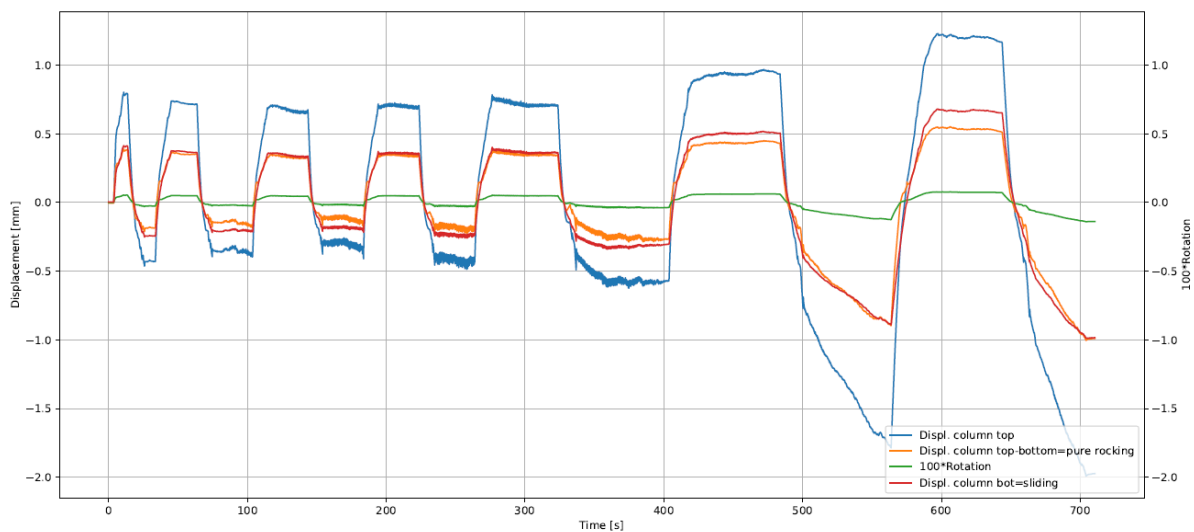


Figure 7-6 Displacement of the column in test 2

It was concluded that there was a problem with the load reading of the press with the observed asymmetry. In addition, the source of the error code was unknown. Further testing was therefore put on hold until the problems was solved.

7.2 Monotonic testing

The problems with the load reading in the Instron100 press was assumed to only occur when the press was lifted upwards. It was then decided to try monotonic tests with only compression applied. The monotonic testing was done to give an indication of the slip force in the new specimen and to test the new washer sensors. The washer sensors were initially tested in a specimen on the floor.

The applied torque would from theory give a preload of 34,1 kN. This initial test of the washer sensors gave the following load readings:

M10 top – 30,69 kN

M10 bot – 34,45 kN

M20 top – 36,91 kN

M20 bot – 32,58 kN

This result has a maximum of 3,41 kN difference from the theoretical 34,1 kN which corresponds to a deviation of 10 %. This result was promising, and it seemed like the sensors was working. It was therefore decided to try them in a monotonic test in the press.

Test 9.1 with the ALT M10 specimen (Table 4-4) was the first live test with the washer sensors. When applying the same preload as in the initial test above, the washer sensors gave a value of 13 kN at the top and 11 kN at the bottom. This was surprising and a new torquing of the bolts was done in the end of the mounting process, but they still gave the same result. Those readings were unexpected since they were tested only moments before with a totally different reading. It was decided to continue with the test. The development of force in the washer sensors during the test is shown in Figure 7-7. It shows an increasing force in the bottom bolt while the force in the top bolt decreases. Figure 7-8 shows a stable force of approximately 7,5 kN through the test. The Catman software was started 1-2 seconds late, so some results are missing from the beginning, therefore the initial preload does not match the value mentioned.

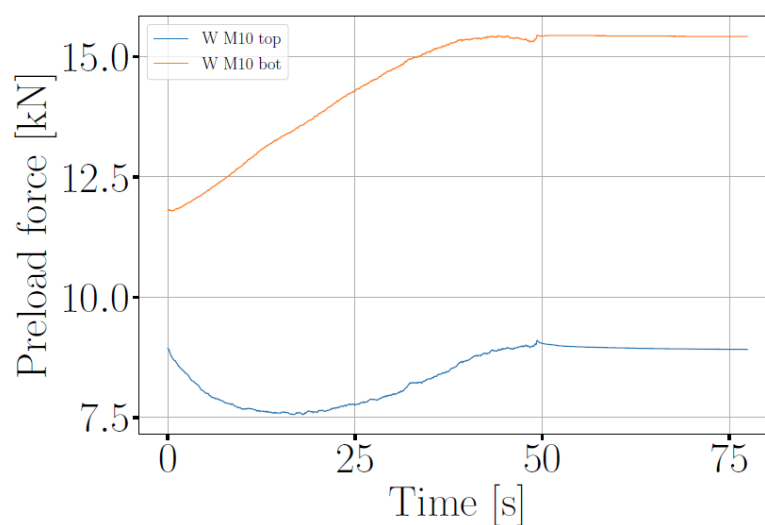


Figure 7-7 Preload force in the washer sensors in test 9.1

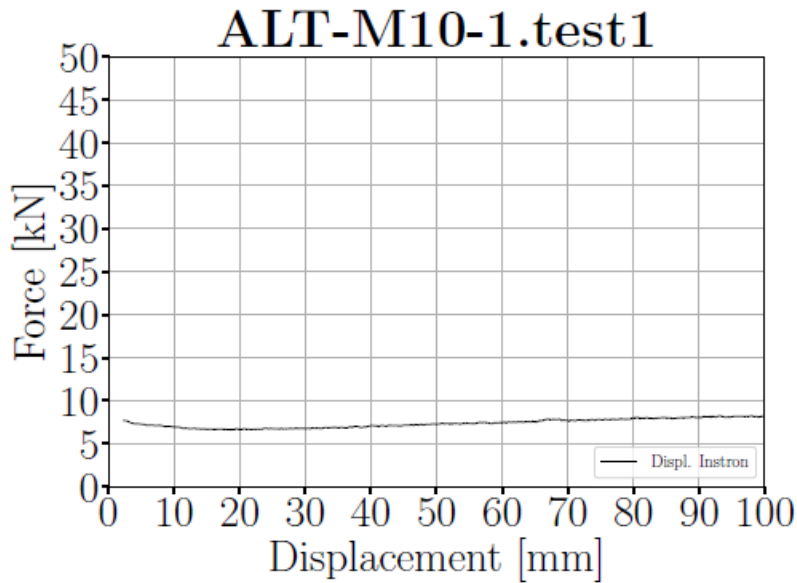


Figure 7-8 Load-displacement graph in test 9.1

In test 9.2 (Table 4-4), it was decided to try applying a slightly higher torque in the second torque step. This was done to be able to use the bigger torque wrench, which has the lowest possible torque value of 60 Nm, and investigate if the torque wrench was the reason for the problems. Figure 7-9 shows the development of the force in the washer sensors. The preload started with 29 kN in the top bolt and 21 kN in the bottom bolt. This reading is more like the theoretical preload than test 9.1. It is also observed from the figure that the preload in both the bolts dropped at the start of the test and slowly increased to the same value at the end of the test. Figure 7-10 shows a stable force of approximately 16 kN through the test.

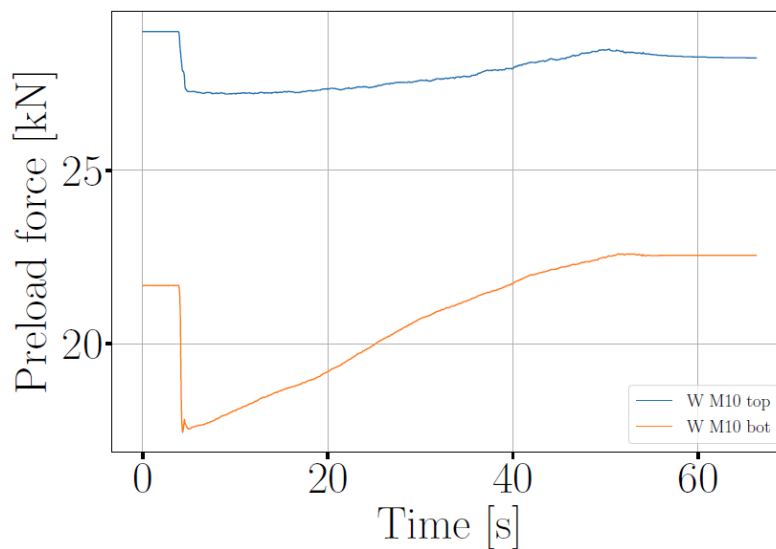


Figure 7-9 Preload force in the washer sensors in test 9.2

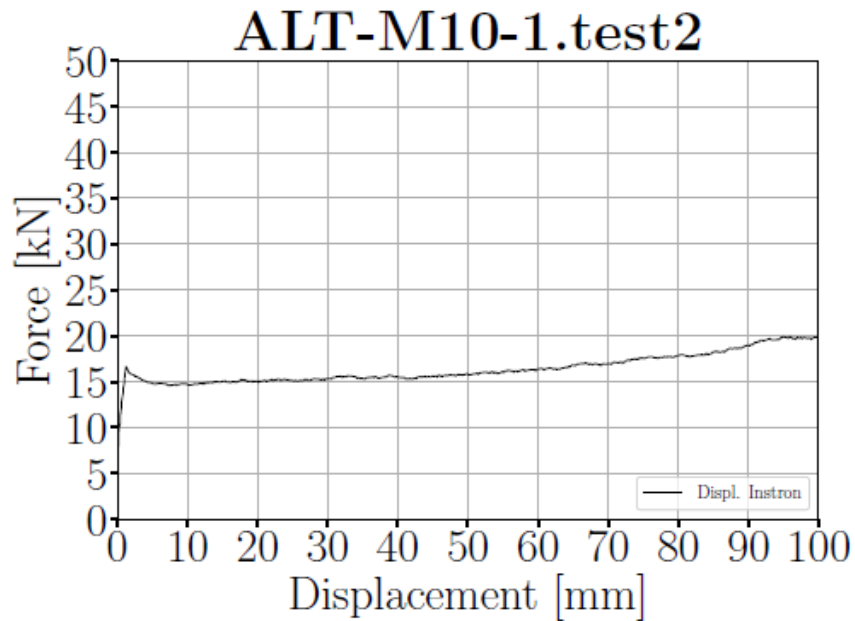


Figure 7-10 Load-displacement graph in test 9.2

Test 9.3 was conducted in the same way as test 9.1 (Table 4-4). Again, the force from the washer sensors were surprising. Starting with a value of 21 kN in the top bolt and 12 kN in the bottom bolt. The development in the preload can be seen in Figure 7-11. The preload in the top bolt increases significantly in the start of the test and the preload in the bottom bolt decreases by a small amount. Figure 7-12 shows a stable force in the test of approximately 12 kN. These three tests performed on the M10 washer sensors indicated that the results from the M10 washer sensors were highly unpredictable even with a stable force during the test.

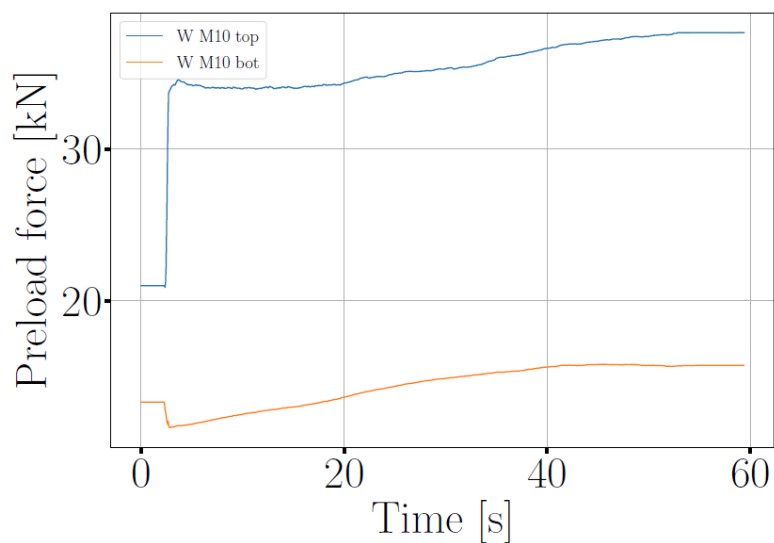


Figure 7-11 Preload force in the washer sensors in test 9.3

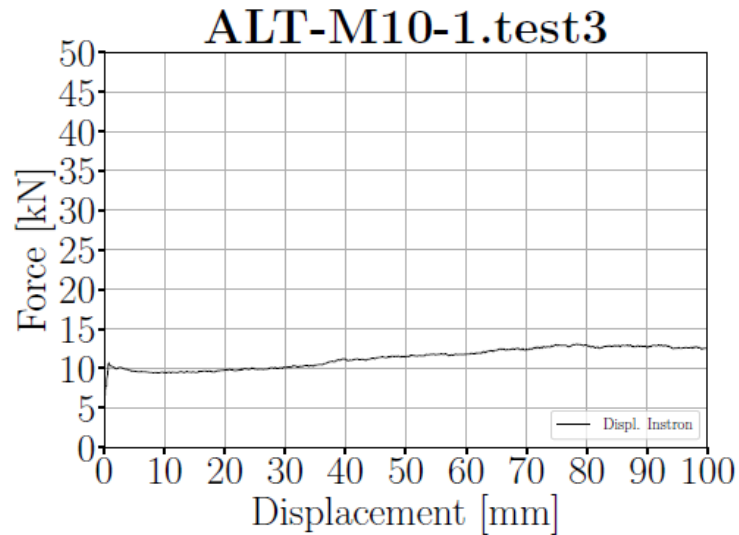


Figure 7-12 Load-displacement graph in test 9.3

Test 10.1, 10.2 and 10.3 (Table 4-4) were conducted the exact same way with the same ALT M20 specimen and with a theoretical preload of 34,1 kN. Figure 7-13 shows that the preload in the washer sensors during these three tests varies. This variation happens despite the stable force shown in Figure 7-14. These results show that for the M10 specimen, the preload in the washer sensors seem to be unpredictable and not behaving as expected. Both the start value of the preload and the development of the preload during the test varies.

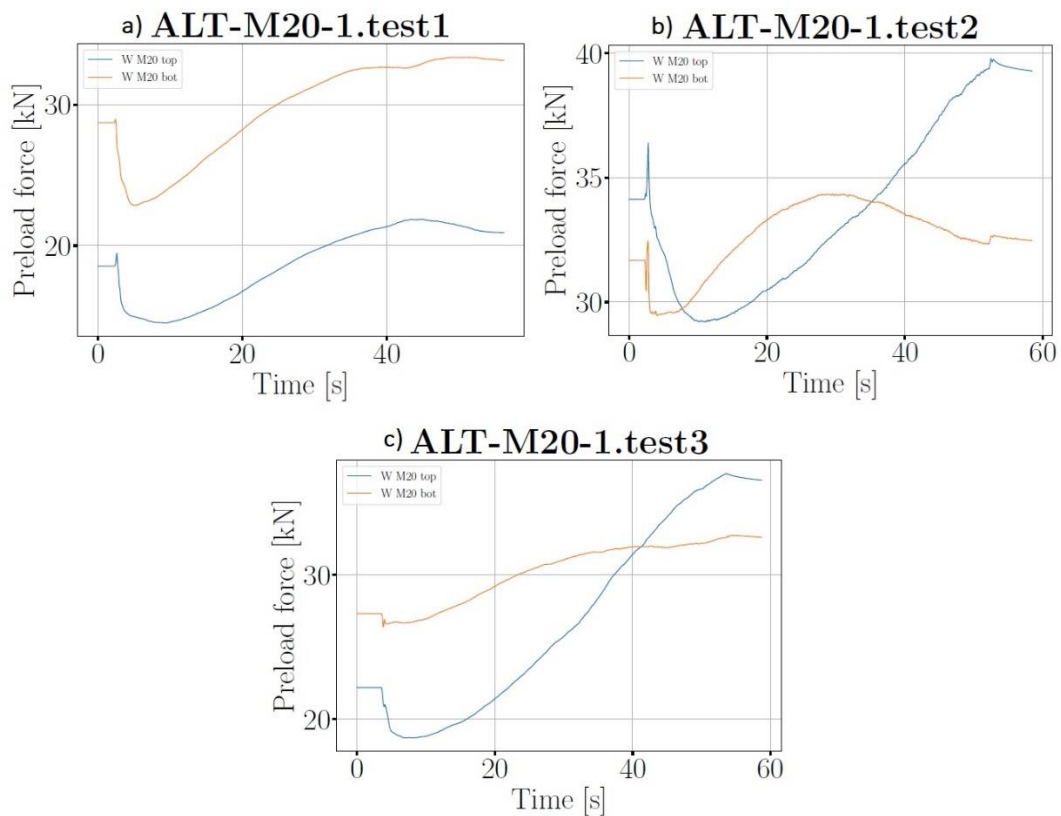


Figure 7-13 Preload force in the washer sensors in test a) 10.1, b) 10.2, c) 10.3

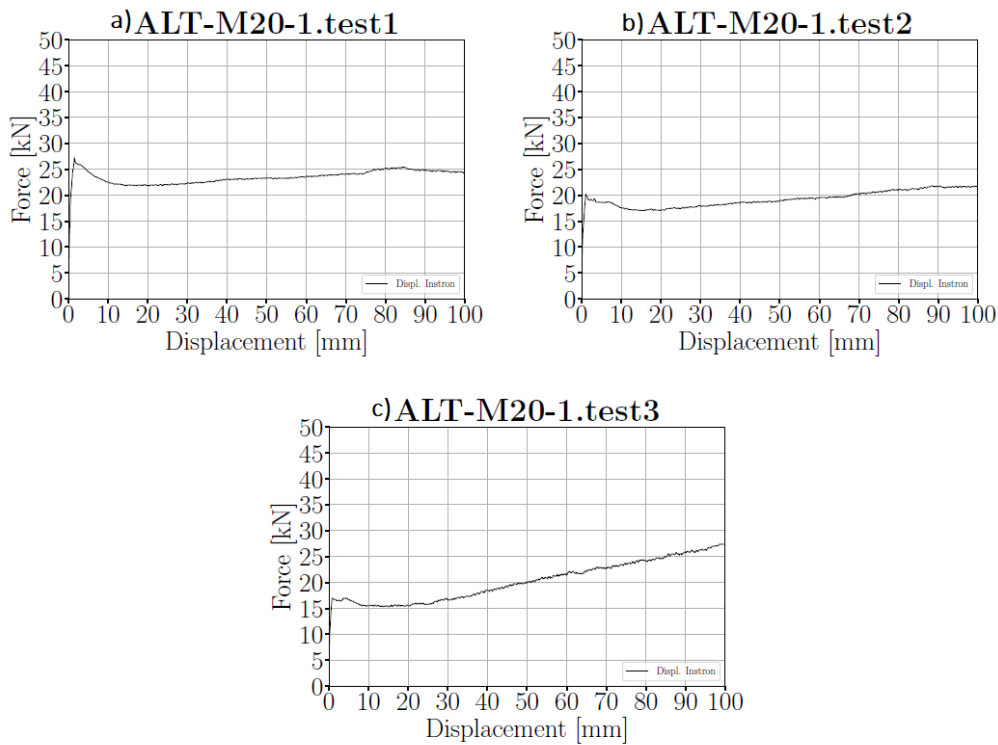


Figure 7-14 Load-displacement graph in tests a) 10.1, b) 10.2, c) 10.3

There are several sources of error which may lead to the unexpected reading in the washer sensors. The torque is applied using torque wrenches which are set to a specific torque value, makes a sound, and reaches a step when achieving the correct torque. The accuracy of these wrenches is not known, but human error while using it is highly possible and may lead to some variations in the applied torque. The k_m value used to calculate the torque of the M10 and M20 bolts is not provided by the supplier and might be inaccurate. In addition, these sensors are mainly made to monitor preload over a longer time span where they are calibrated on sight with small variations. Also, the tolerance of the washer sensors themselves is +/- 15 %. It was then concluded that the washer sensors could not be used as an accurate indication of preload in these tests.

7.3 New testing campaign

All the new specimens were tested in this new testing campaign. It was decided to make a standardized test to make comparable results. This standardized test was initially planned to give a slip force of 30 kN with the corresponding torque shown in Table 4-5. However, tests 11 to 14 with the ALT M20 and ALT M10 gave large forces. It was then decided to use 50 % of that torque corresponding to a slip force of 15 kN for the rest of the tests (15 to 21). The results from these tests are presented in this chapter.

7.3.1 ALT specimen

Figure 7-15 shows the load-displacement graph of tests 11 and 12. Test 11 reached close to 150 kN in the last cycle of 50 mm, resulting in an oscillating behavior in the columns of the press. Since this specimen ALT-M20_1 was already used in test 10.1 to 10.5 (Table 4-5) it was decided to try the new ALT-M20_2 specimen to investigate if the previous test of the specimen influenced the results. As seen in Figure 7-15 the result in test 12 was slightly better, but the force still reached 100 kN and seemed to increase significantly in the last cycle. It is also observed that the behavior remained stable until the cycle of 20 mm in test 12, but only until 10 mm in test 11. The graph is observed to be unsymmetric with a higher force reading when the press lifts the specimen upwards.

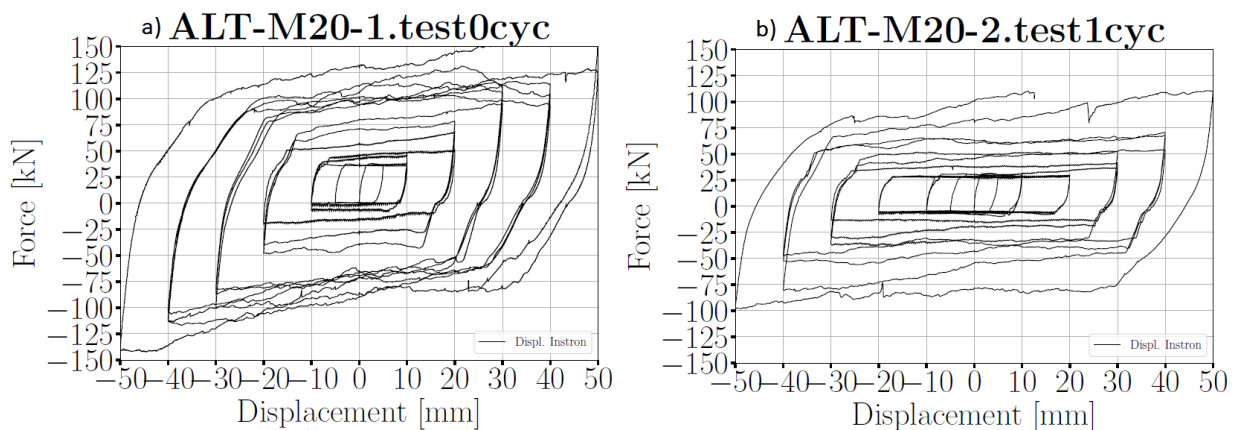


Figure 7-15 Load-displacement graph of a) test 11 and b) test 12

Two tests were conducted with the ALT-M10_1 specimen in the new testing campaign, test 13 which was cyclic and test 14 which was monotonic 100 mm (Table 4-5). The goal of those two tests was to achieve a slip force of 30 kN. This specimen had already been used in test 9.1 to 9.3 (Table 4-5). Figure 7-16 shows the result of tests 13 and 14. Catman stopped for a few seconds during test 13, resulting in a small part of the graph missing. The hysteresis loop

of test 13 shows a more stable behavior than for the ALT M20 in Figure 7-15, reaching a maximum of 75 kN even after being used in earlier testing. This result indicates that the M10 specimen has a more stable behavior after repeated testing. The result from the monotonic test shows a similar behavior as the first cycle in the cyclic test, with a slip force of around 25 kN. There is also observed a drop in force after reaching 70 mm displacement, which opens the question if the specimen would be able to maintain the force throughout the entire length of the slotted hole.

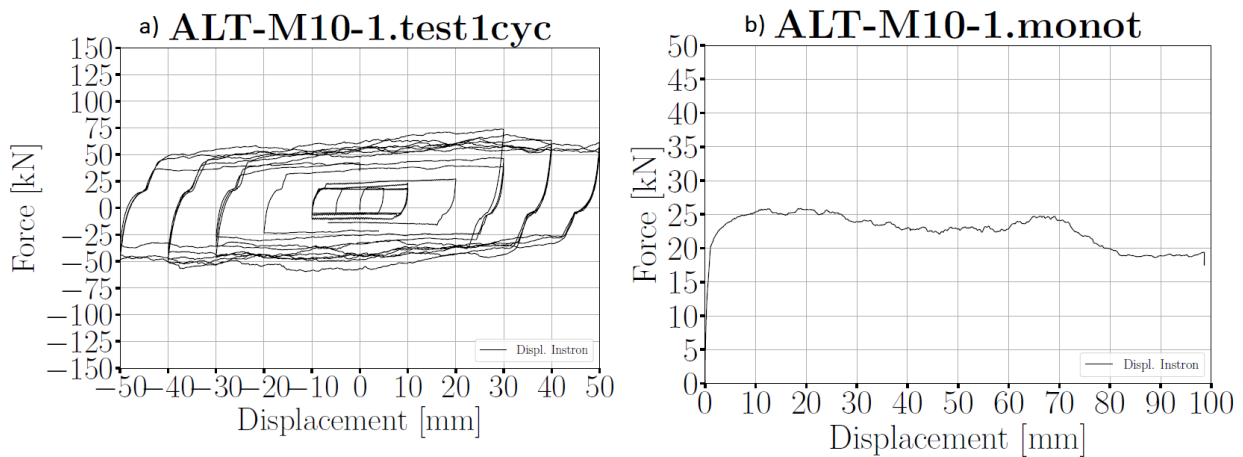


Figure 7-16 Load-displacement graph of a) test 13 and b) test 14

After test 11 and 12 it was observed that the ALT M20 twisted significantly more than the ALT M10, as seen in Figure 7-17. This was surprising as the ALT specimen used to have little twisting during earlier tests and in Ansys simulations. The reason for this larger twisting in the ALT M20 than in ALT M10 is because the slotted hole in the M20 specimen is made wider. The slotted hole in the M10 specimen is produced with a width of 12 mm which is 2 mm larger than the bolt. In the M20 specimen, the slotted hole is made with a width of 24 mm which is 4 mm wider than the bolts. This is done to have a tolerance in case of manufacturing defects. The twisting observed in the M20 specimen indicates that this added width to the slotted hole should be lower.

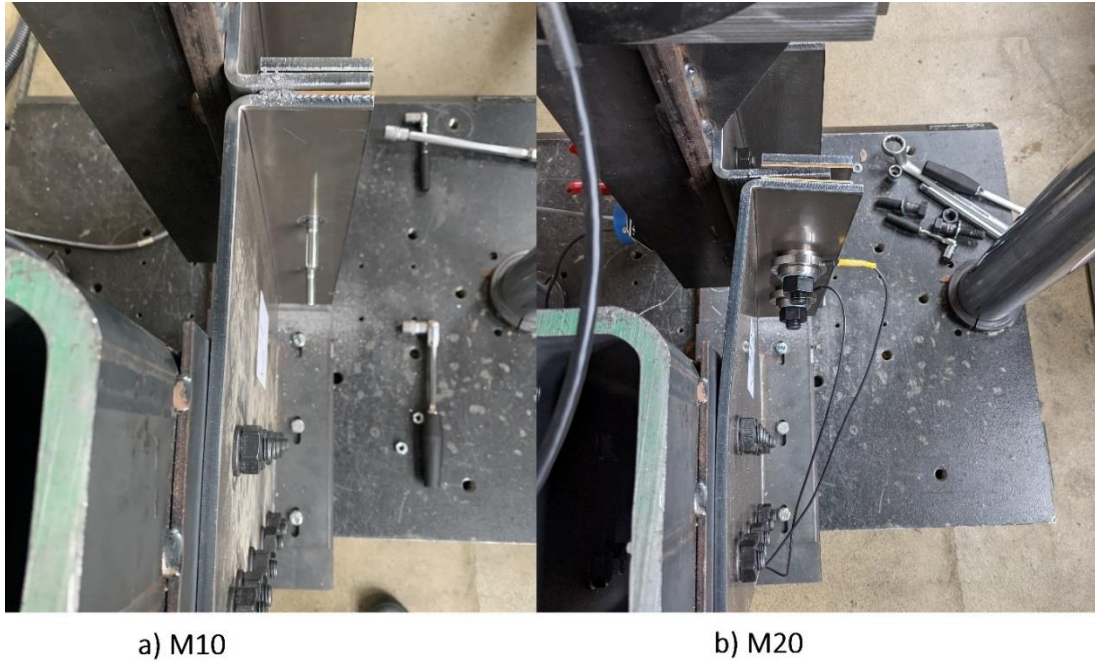


Figure 7-17 Twisting in a) ALT M10 and b) ALT M20

7.3.2 ALT-AS specimen

Since tests 11 to 14 gave a much larger force than expected, it was decided to reduce the preload by 50 % for the rest of the tests 15 to 21. Tests 15 and 16 was conducted with ALT-AS M10 and M20, as seen in Table 4-5. It was decided that the best mounting procedure for the ALT-AS was to first tighten connection G (Figure 4-2), adjust the alignment profile correctly, then tighten the bolts between the fixed profile and the alignment profile (Figure 4-2). It was problematic to fit the M16 bolts in the connection because of imperfections in the specimen. The part of the fixed profile which connects to the alignment component had an angle that moved the holes slightly. This prevented the bolt holes of being aligned as shown in Figure 7-18. With the M20 specimen, in test 16, it was necessary to loosen connection F (Figure 4-2) to insert the M16 bolts. On a construction site, this maneuver would be impractical, as the fixed profile would already be mounted to a CLT panel. This problem could be solved with wider holes for the M16 bolts or have a more accurate production of the specimens. It was observed less bending in the fixed profile of the ALT-AS than in the ALT specimen. This can be related to the alignment component making the fixed profile stiffer.



Figure 7-18 Imperfection in the ALT-AS specimen

Figure 7-19 shows the load-displacement graph for tests 15 and 16. Both the specimens have a stable behavior up until the 20 mm cycle with around 10 kN slip force. However, the M10 specimen reaches a max slip force of around 70 kN, while the M20 reaches 100 kN. This indicates that the M10 specimen is more stable than the M20. In these tests it was also observed more bending in the M20 specimen than in the M10 specimen.

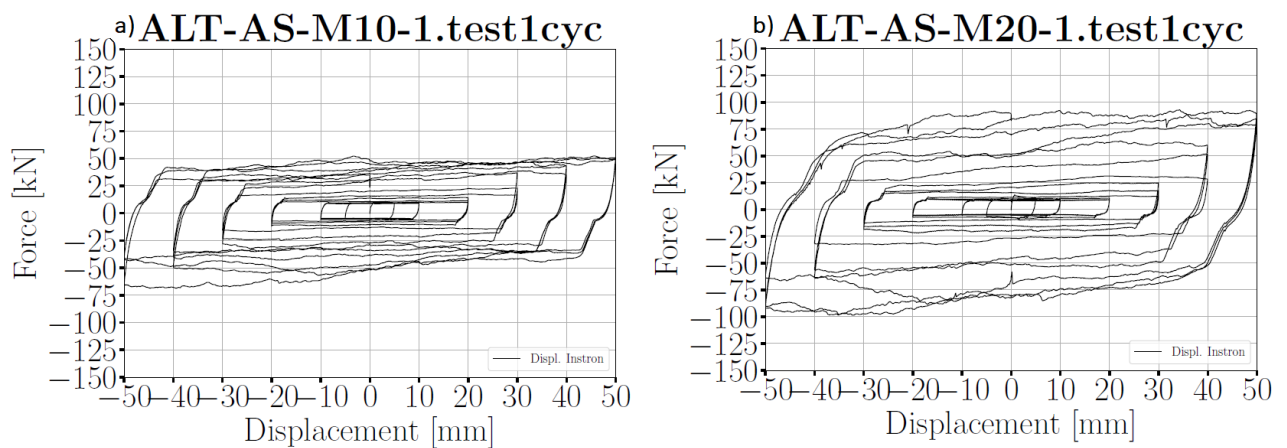


Figure 7-19 Load-displacement graph of a) test 15 and b) test 16

7.3.3 STD Specimen

The STD-1H M10 and M20 were tested in tests 17 and 18 (Table 4-5). Both specimens endured large bending deformations due to the twisting in the elements, and test 18 was stopped due to excessive amount of bending. Figure 7-20 shows the result of test 17 and 18. Due to bending in both elements, the force increases considerably during the test. However, the STD-1H M10 maintains a more stable behavior than the STD-1H M20. It is also observed from the figure that the STD-1H specimens have an asymmetric graph.

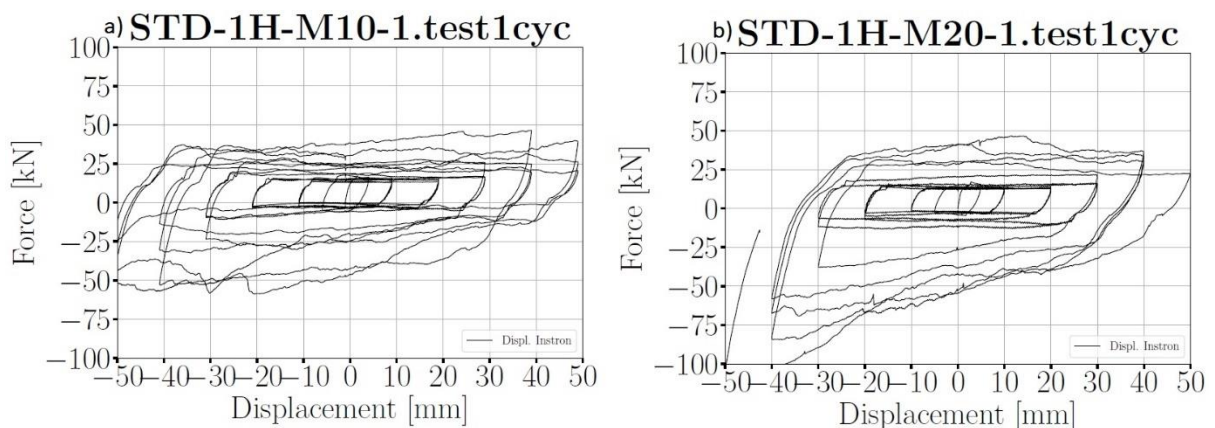


Figure 7-20 Load-displacement graph of a) test 17 and b) test 18

Figure 7-21 shows that there is a significant increase in twisting in STD-1H M10 compared to STD-1H M20. The test with the STD-1H M20 did not even reach the 50 mm cycles indicating that the wide slotted hole influenced the specimen.



Figure 7-21 Twisting in a) STD-1H M10 and b) STD-1H M20

STD-2H M10 was tested in test 19 (Table 4-5). This specimen only has the M10 version since there would not be enough space for four M20 bolts. The goal for the specimen was still to achieve 50 % preload, so the bolts were applied 25 % of the original preload in this test. The torque was calculated to 9.3 Nm and 14.1 Nm, but the torque wrench had a lower limit of 14 Nm. Therefore, it was decided to only preload in one step of 14 Nm. Figure 7-22 shows that the STD-2H has a stable behavior until 30 mm, before it starts twisting significantly and getting highly unstable. It is also observed that the graph is asymmetric as the other tests.

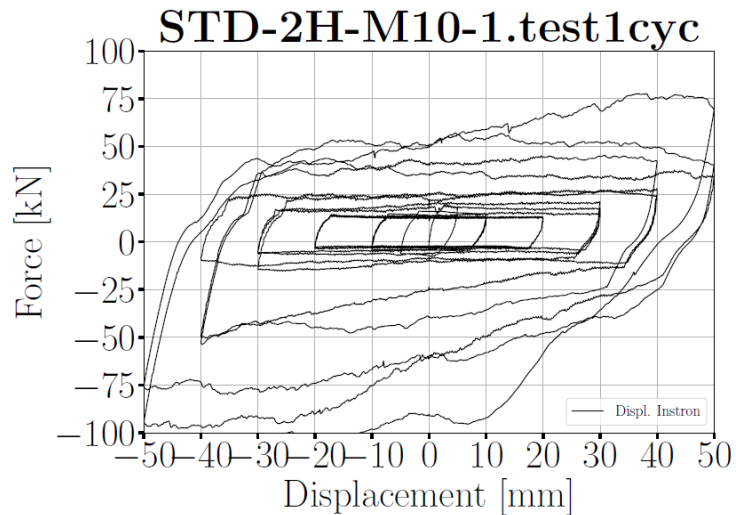


Figure 7-22 Load-displacement graph of test 19

Figure 7-23 shows the deformed shape in the specimen after test 19. The deformation in the slotted holes is significant. Two slotted holes makes the sliding surface have less steel to withstand the bolts pushing outwards.



Figure 7-23 Deformed shape of STD-2H in test 19

7.3.4 Hybrid Specimen

Tests 20 and 21 were performed with the Hybrid M10 and M20 (Table 4-5). Figure 7-24 shows the load-displacement graph of the tests done with the Hybrid specimen. The test done on the Hybrid M10 gave a stable behavior until the last cycle of 30 mm, then it started to have an increase in force, but with stable force in each cycle. Hybrid M20 had a more unstable behavior, with an increase in force starting in the 20 mm cycle. After passing the 20 mm cycle, the behavior became more unstable. In the second cycle of 50 mm, there was a loud “bang” from the specimen. That can be observed in Figure 7-24 as the sudden drop in force. Both the M10 and M20 specimens had an asymmetric load-displacement graph.

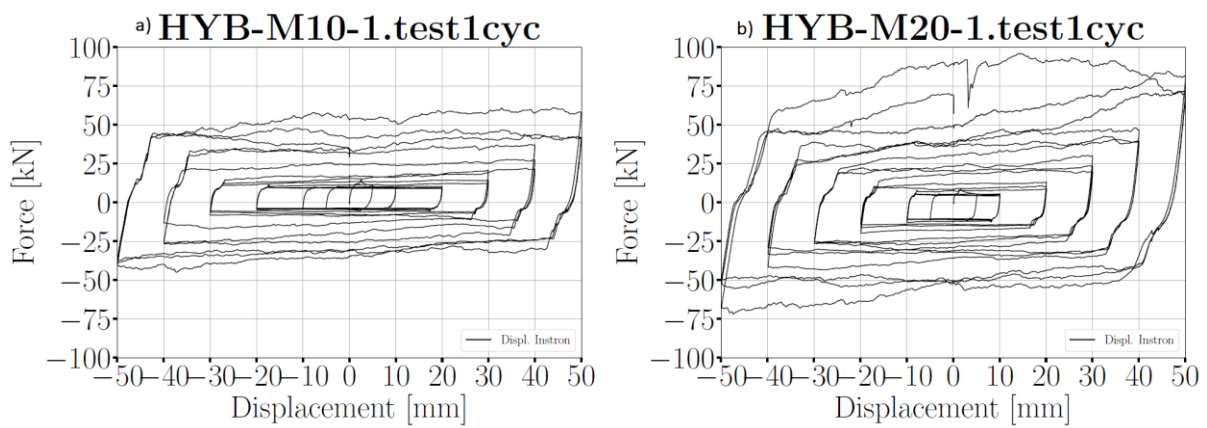


Figure 7-24 Load-displacement graph of a) test 20 and b) test 21

When mounting the Hybrid specimen to the CLT-panel the bolts can be hard to preload due to the limited access to the bolts, as seen in Figure 3-3.

7.4 Shim layer

For the specimens tested in this thesis it was decided to use shim layers of Hardox 450 rather than aluminum that have been tested earlier. It is presented in chapter 2.5 that a harder material as shim layer would give a more stable and reliable behavior of a friction connection. Tests 5 and 8 were done to the same ALT_2 specimens in the preliminary testing (Table 4-3). The only difference between these two tests was the shim layers and the value of torque shown in Table 4-3. Hardox 450 was used in test 5 and aluminum was used in test 8.

Specimen ALT_2 was used in tests 6 and 7 between test 5 and 8, which could influence the result of test 8. Figure 7-25 shows that the test with Hardox 450 shim layer has a more stable behavior in the early cycles before the force increase in each cycle after the 20 mm cycle.

Test 8 with the aluminum shim layer has a more unstable behavior in the early cycles but

seem to stabilize in the later cycles. The Hardox 450 shim layer also reaches a higher force than the aluminum, even with less preload, indicating a higher friction coefficient between Hardox and steel.

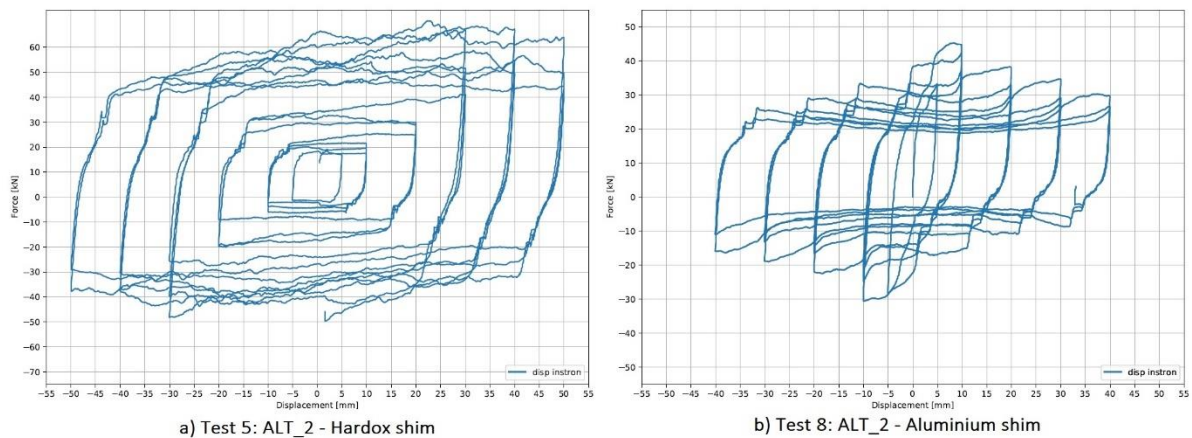


Figure 7-25 Load-displacement graph of a) test 5 and b) test 8

Figure 7-26 shows the damage to the shim layers in test 5 and 8. The aluminum shim layer have more damage to the surface than the Hardox 450. In addition, the holes in the aluminum shim layers are deformed.



Figure 7-26 Damage to the aluminum and Hardox 450 shim layer

A variation in wear on the shim layers was observed after the tests in the new testing campaign, tests 11 to 21 (Table 4-5). Figure 7-27, Figure 7-28 and Figure 7-29 show pictures of the shim layers of all the specimens after the tests. It is observed that the specimens with most twisting, like the different STD specimens, had less wear to the shim layers than the ALT, ALT-AS and Hybrid with less twisting. This observation indicates that the friction is more active during the ALT than the STD.

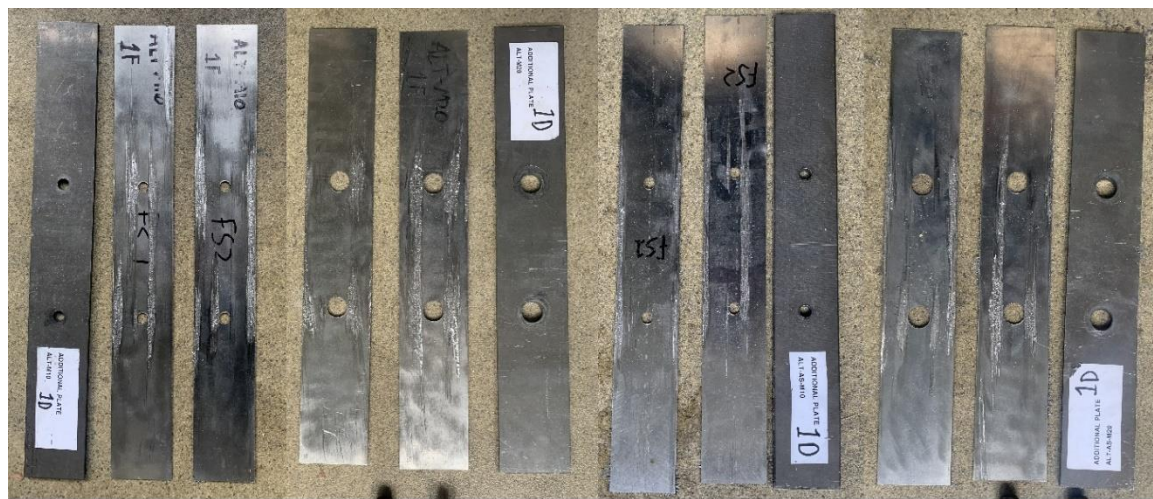


a) STD-1H M10

b) STD-1H M20

c) STD-2H M10

Figure 7-27 Damage to shim layers in the different STD specimen



a) ALT M10

b) ALT M20

c) ALT-AS M10

d) ALT-AS M20

Figure 7-28 Damage to shim layers in the different ALT and ALT-AS specimen



a) Hybrid M10

b) Hybrid M20

Figure 7-29 Damage to shim layers in the different Hybrid specimen

After tests with Hardox 450 shim layers it was a residue of magnetic dust attached to the surface as seen in Figure 7-30. This was not the case for the aluminum shim layers.



Figure 7-30 Magnetic Hardox steel residue on ALT M20

7.5 Bolt size

In all tests performed in the new test campaign, tests 11 to 21 (Table 4-5), M10 specimens gave a better behavior than the M20 specimens (see chapter 7.3). It was clear during the tests that the M20 specimens experienced more twisting. A possible explanation to this is the tolerance used in the slotted holes. The manufacture tolerance of the slotted hole in the M10 specimens are chosen to be +2 mm with a total width of 12 mm. In the M20 specimens this tolerance is chosen to be +4 mm with a total width of 24 mm. This free space of 4 mm enables the specimen to twist more during the tests. Figure 7-31 shows the load displacement graphs of test 10.3 to 10.5 (Table 4-4). These tests were done with the same specimen with 24 mm slotted hole with M20, M16 and M14 bolts. The preload was calculated accurately for the M16 and M14 bolts because the k_m was provided by the producer. Test 10.4 in Figure 7-31 c) with the M16 bolts show a surprisingly similar behavior as the test with the a) M20. However, there is a more unstable behavior at the start and end of the test, and it reaches a slightly higher force. In c) with the M14 bolts, the behavior is clearly affected by smaller bolts. The specimen bends more and reaches a much higher force, and has a sudden drop in force in the middle of the test. This confirms that the bolt size affects the twisting of the specimen.

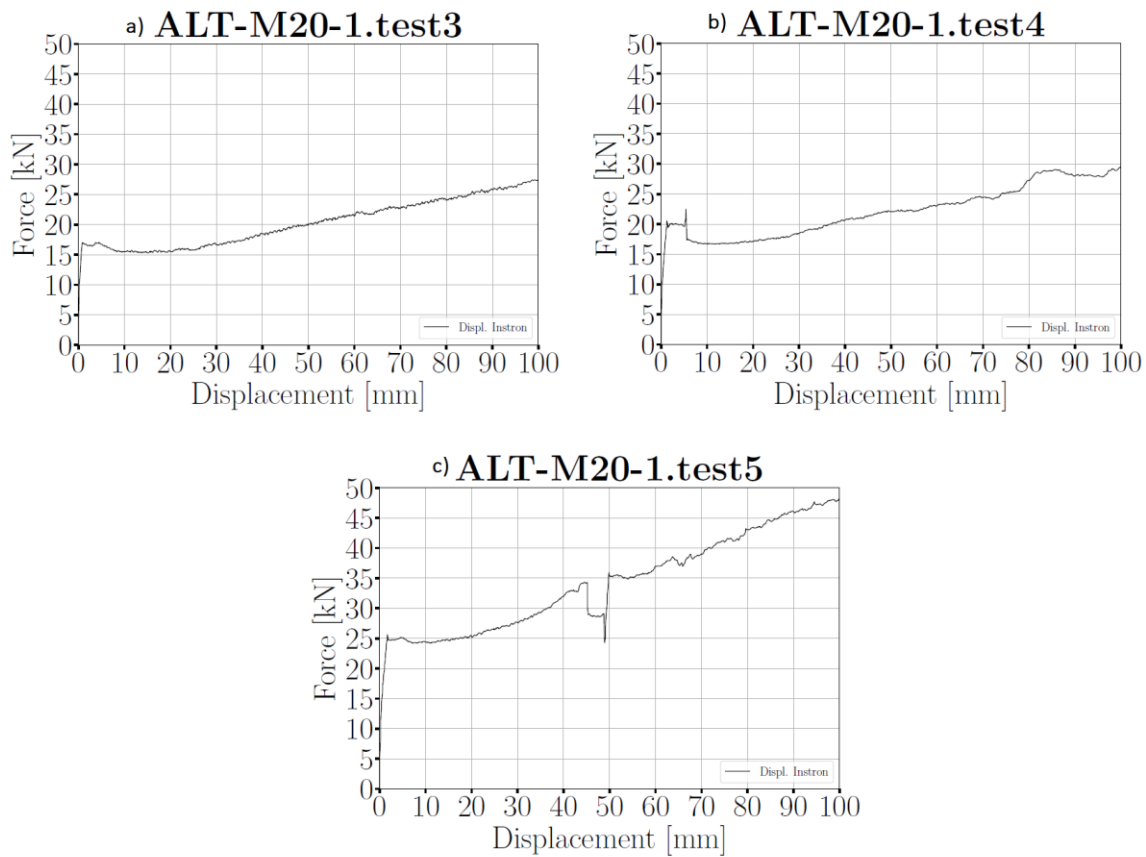


Figure 7-31 Load-displacement graph of a) test 10.3, b) test 10.4 and c) test 10.5

The bolts are forced into the sides of the slotted holes when the specimen twists. This makes the bolts in the STD- and Hybrid specimens more exposed to damage than the ALT and ALT-AS specimens. The M20 specimens tend to twist more than the M10 specimens, but that will not cause a problem for the bolts, as they are significantly stronger. Figure 7-32 shows the damage to the bolts in STD-2H and STD-1H. As observed from the figure, the M10 bolts become more damaged and bent compared to the M20. The deformation of the M10 bolts shows the connection applies an asymmetric load to the bolts as explained in chapter 2.4.



a) Test 19: STD-2H M10

b) Test 18: STD-1H M20

Figure 7-32 Damages to the bolts in a) test 19 and b) test 18

7.6 Temperature development

During the cyclic testing in tests 11 to 21 (Table 4-5) it was observed a temperature increase in all the specimens during the tests. The specimens ALT and ALT-AS had a steep temperature development, as seen in Figure 7-33. These specimens also had the most amount of wear to the shim layers after the testing. In the tests with ALT M10 and ALT M20 double amount of torque was applied, which can explain why the ALT M10 has a steeper temperature increase than the other ALT specimens. The temperature in ALT M20 matches the ALT-AS despite this higher preload.

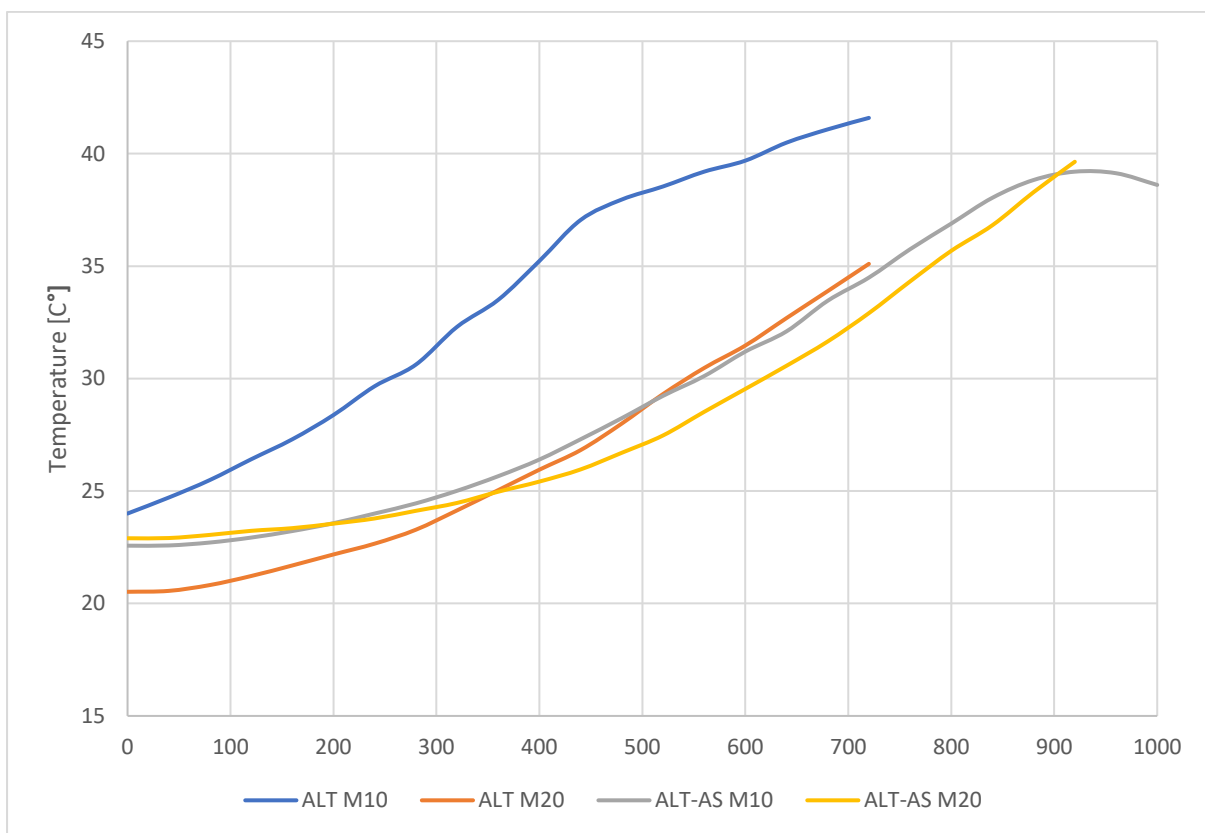


Figure 7-33 Temperature development for ALT and ALT-AS [C°]

The temperature increase during the tests was lower in the STD- and Hybrid specimens compared to the ALT specimens, as seen in Figure 7-34. These specimens also had less wear to the shim layers and experienced bending which reduced heat generated by friction.

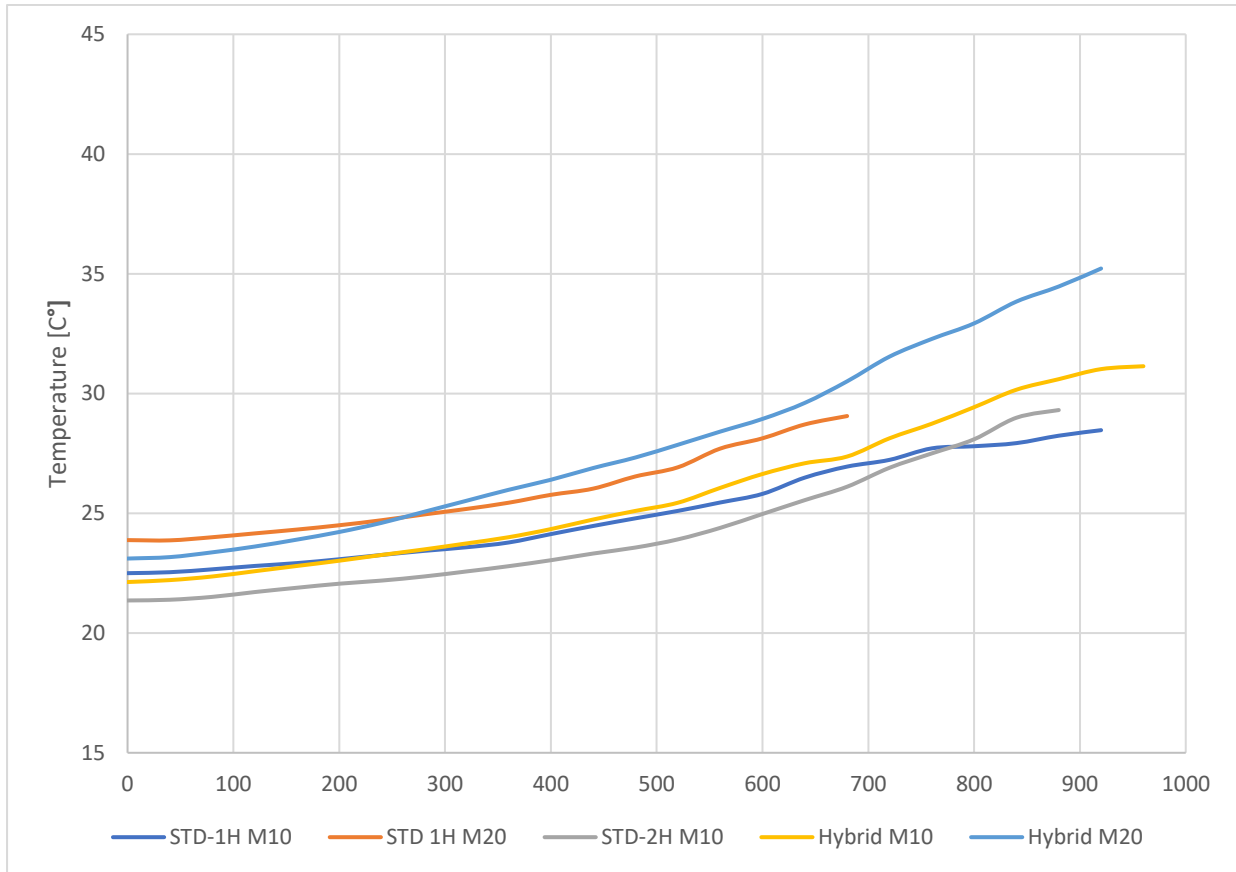


Figure 7-34 Temperature development for the STD-1H, STD-2H and Hybrid [C°]

Temperature is released as friction is generated between the layers. It is shown in this chapter that the ALT and ALT-AS specimen generate more heat during the tests. These specimens also had the most wear to the shim layers as seen in Figure 7-28. The released temperature is lower in the STD- and Hybrid specimen indicating that the friction is less utilized in the tests. In reality, these specimens would potentially have to slide 100 mm and possibly in a higher speed during an earthquake. This might lead to a temperature that could damage adjacent components in the structure.

8 Comparison: FEM-analysis and experimental activity

After performing both physical tests in the press and analysis in Ansys with the same specimens, there were observed several correlations between the Ansys results and the real-life behavior of the specimen.

The Ansys results gave a clear impression that the STD-1H and STD-2H would deform more than the ALT, ALT-AS and Hybrid in both Y- and Z-direction after the applied 5 mm displacement to the anchor profile. This indicated a better behavior of the ALT, ALT-AS and Hybrid. Figure 8-1 shows the maximum deformation in Y-direction in the different specimens. The deformation is the absolute maximum value, so direction is ignored. It is observed from the table that the STD specimens have significantly more bending.

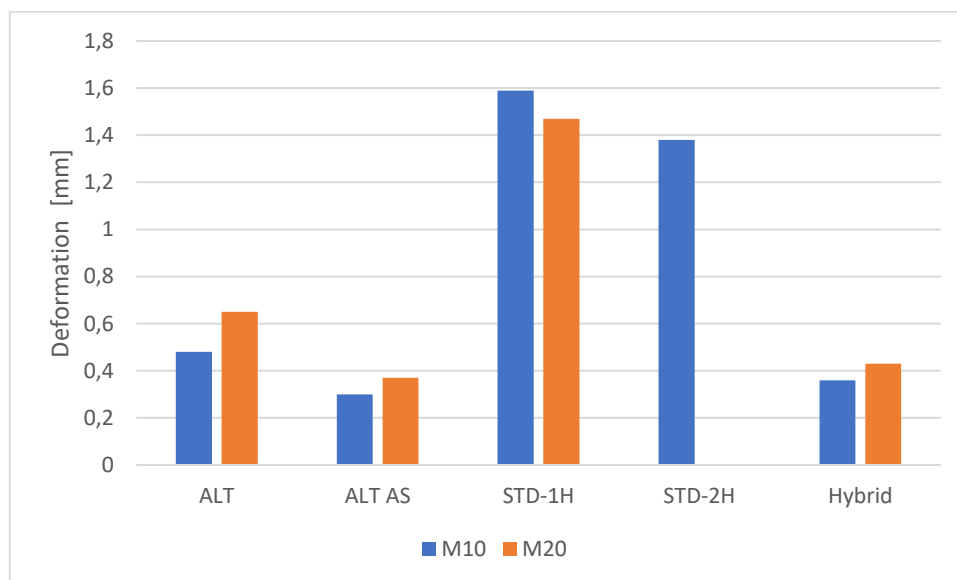


Figure 8-1 Deformation in Y-direction from Ansys [mm]

The inclinometer is placed on the T-shaped element and measures the rotation around the Z-axis which is comparable to the deformation in Y-direction from Ansys results as seen in Figure 8-2. Figure 8-3 shows the inclination of the specimens during the tests 11 to 21. The inclination is in absolute value, so the direction is ignored. From the figure it is observed that the specimen with the most deformation in Y-direction also has the most inclination. A surprising result was the STD-1H showed the largest deformation in Ansys but had a small inclination in the physical test. It is also observed in Figure 8-3 that the M20 specimens have more inclination in all the tests. This difference between Ansys and reality is due to the M20

bolts being 4 mm smaller than the slotted holes in the real specimen while in Ansys the slotted hole is the same size as the bolts.



Figure 8-2 Coordinate system in the press

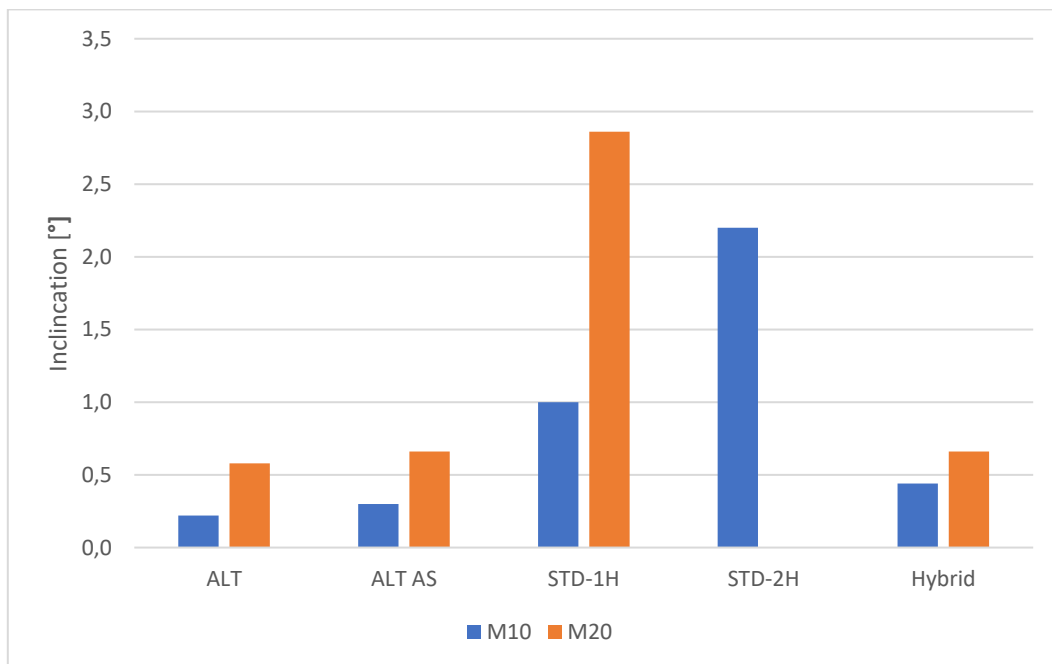


Figure 8-3 Maximum inclination from the inclinometer [°]

From the results in Ansys, it could be seen that the equivalent stress around several of the bolt holes exceeded the yielding strength of steel S355. However, the area with higher equivalent stress was always in a small spot with minimal probability of yielding. Figure 8-4 shows the damage to the additional plate in STD-1H M10 in Ansys and from test 13 (Table 4-5). This additional plate experienced the highest equivalent stress from all the simulations of 779 MPa. From test 13 there is only observed minor marks around the holes from the washers. This result confirmed that when the yielding strength of the steel is exceeded only in small areas, yielding will not occur.

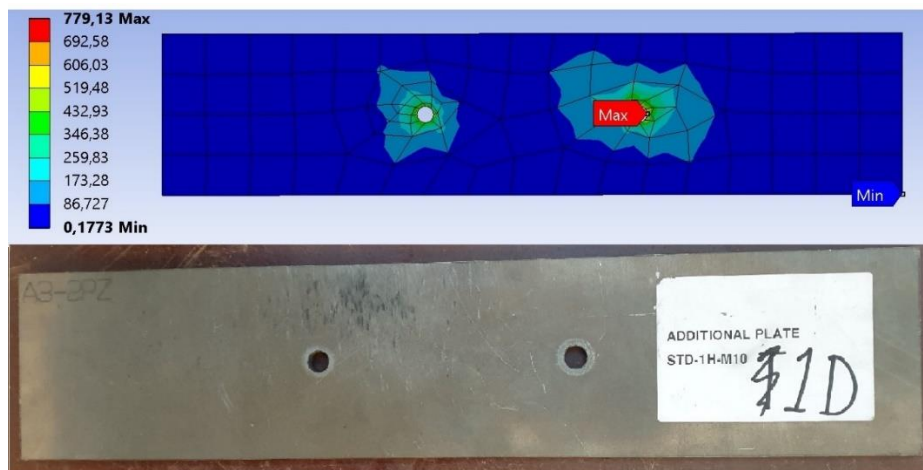


Figure 8-4 Comparison of damage to the additional plate STD-1H M10

Figure 8-5 and Figure 8-6 show the damage to the shim layer in reality and with contact status in Ansys. The damage is not exactly the same in both Ansys and reality. However, it is observed from the two figures that Ansys indicated more *sliding* in the ALT-AS than for Hybrid which corresponds to the physical testing.

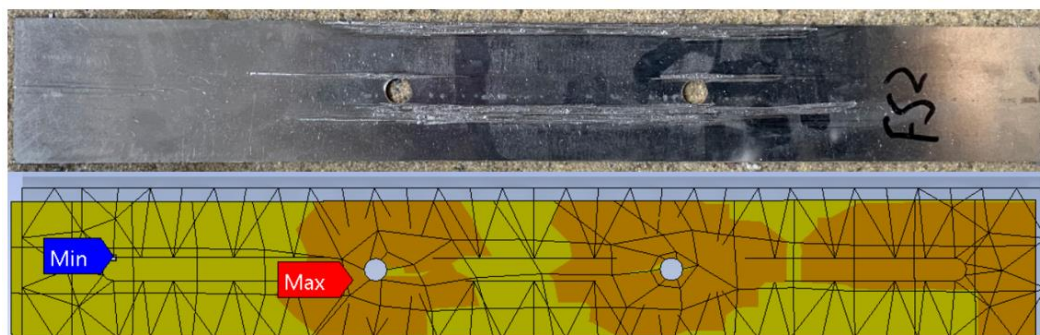


Figure 8-5 Comparison of damage to the shim layer ALT-AS M10

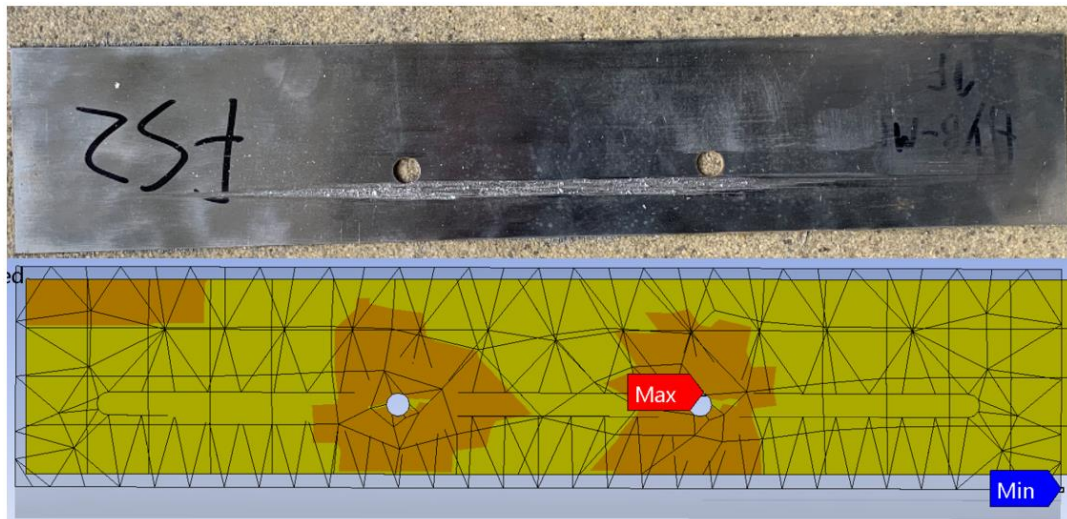


Figure 8-6 Comparison of damage to the shim layer in Hybrid M10

In the Ansys analysis it was chosen to compare the static friction coefficient of 0,39 with the dynamic friction coefficient of 0,22. It was built on the theory that a friction connection always needs to overcome this higher initial friction coefficient. In the monotonic tests 9.1 to 9.3 and 10.1 to 10.5 the effect of this behavior is studied. Figure 8-7 shows the load-displacement graph of the relevant test 9.2, 9.3, 10.1 and 10.3. Test 9.1 were not included because the Catman software was started too late, and the static effect was therefore not documented. 10.1 and 10.3 are chosen because they show the difference in behavior when the specimen is new and previously tested. As seen in the figure, all the monotonic tests have this static friction effect in the start of the sliding which stabilizes after few millimeters of displacement. It is observed that the static effect is bigger in test 10.1 when the specimen and the shim layers are new, than in test 10.3 when they are tested two times. In test 10.3 the force also increases, probably due to bending.

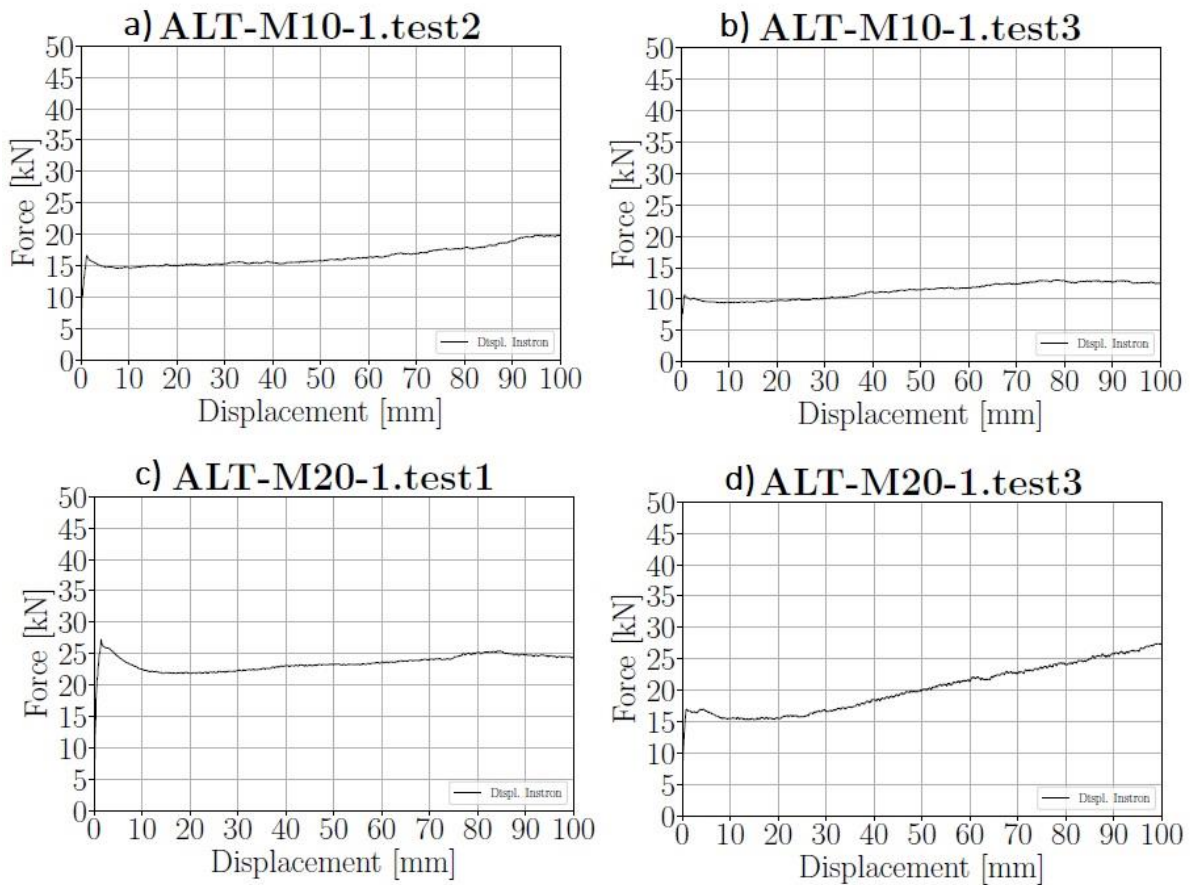


Figure 8-7 Load-displacement graph of a) test 9.2, b) test 9.3, c) test 10.1 and d) test 10.3

Most of the physical testing conducted in the press was as expected from the FEM-analysis. The STD-1H and STD-2H experienced bending and deformations which also was observed in the press. ALT, ALT-AS and Hybrid experienced small deformations and little bending both in the analysis and the press. A surprising result after performing the tests in the press was that the M20 specimens did not perform as expected from the analysis.

9 Conclusion

This thesis was part of a European project called e-SAFE. The project concerns seismic renovation using a system including CLT-panels in combination with friction connection to reduce damage during an earthquake. The focus in this thesis was on the friction connections used in the system. In this thesis a FEM-analysis and experimental activity was performed on five proposed designs: STD-1H, STD-2H, Hybrid, ALT and ALT-AS.

There was a clear correlation between the results from the analysis and the experiments. The difference between the model and physical testing was essentially related to simplifications made with the slotted hole. This way of defining the model in Ansys can be used as an initial evaluation of specimens to use in this system.

Specimens with M20 bolts had more twisting than those with M10 bolts. This was mainly related to the width of the slotted hole being 4 mm wider than the bolt diameter in the M20 specimens, while only 2 mm wider in the M10 specimens. From the simulations M20 bolts gave lower stresses than M10 bolts. The M20 specimens should therefore be produced with the same tolerance as the M10 specimens and should be tested further.

Use of Hardox 450 as shim layer material in the friction connection gave a stable hysteresis loop with repeated square shapes, without significant wear. Hardox 450 as shim layer is recommended for further testing.

STD-1H and STD-2H were majorly deformed in both the physical tests and the simulations. This is due to the bent part of the fixed profile, which is not stiff enough to withstand the forces. The STD specimens should not be included in further testing.

From physical testing and simulations, the Hybrid specimen showed a stable behavior and low stresses. Mounting of the Hybrid specimen could be problematic, as access to the bolts in the friction connection is limited. Therefore, the Hybrid specimen is not recommended for further testing.

ALT and ALT-AS had the best behavior of all the specimens in the physical testing, and simulations presented low stress and bending. ALT-AS was slightly stiffer in the fixed profile, due to the connection with the alignment profile. In addition, ALT-AS is optimized for easier mounting, and is therefore recommended for use in full-scale testing. The specimen should be produced with a high accuracy for the alignment profile connection or the M16 bolt holes should be expanded to minimize problems during mounting.

10 Further work

- The friction coefficient needs to be tested and investigated to optimize the preload of the bolts. The friction coefficient used in this thesis was assumed based on findings done by Golondrino et.al [22]. The static- and dynamic friction coefficient need to be studied closer to better understand the behavior of the connection.
- The washer sensors need to be controlled or repaired. This way they can be used to monitor the preload on the bolts and control that the right preload is applied.
- Perform tests with M10 and M20 bolts with a known k_m -value. This way the preload will be accurate. A more accurate way of applying the torque should be considered as the old torque wrench have an unknown accuracy. This way uncertainties with the preload will be eliminated in further tests.
- The specimens had a maximum applied displacement of 50 mm in the cyclic tests. For further testing the specimens should be investigated and tested with a higher displacement up to 100 mm. With this displacement it would be interesting to see if the behavior of the specimens remained stable through the entire length of 100 mm.
- In the tests done in this thesis the speed was set to 2 mm/s. The speed would be an interesting factor to change in further testing. By changing the speed, the temperature might rise, the force may increase, and the specimens could get more deformed.
- Perform a full-scale test with the entire system.
- To achieve a more stable behavior a suggestion would be to develop a specimen with a symmetrical friction connection. This might be a challenge because the CLT-panel and the connections are placed on the outer side of the existing walls, and the friction connection part can be difficult to preload due to limited access.

11 List of figures

Figure 1-1 e-SAFE [1]	1
Figure 1-2 Illustration of the CLT panel system.....	2
Figure 2-1 European seismic hazard map [12]	5
Figure 2-2 Example of a viscous damper [14].....	6
Figure 2-3 Static- and kinetic friction coefficient [19]	8
Figure 2-4 Symmetric friction connection [20]	9
Figure 2-5 Asymmetric friction connection [20]	9
Figure 2-6 Hysteresis loop shape for different materials [22]	11
Figure 2-7 Set up of the sliding bolt component [23].....	12
Figure 2-8 Hysteresis curves for G300, G80 and G400 shims [23].....	13
Figure 2-9 Variation of the friction coefficient with increased hardness [22].....	14
Figure 2-10 Hysteresis loop of AFC specimen with different sliding lengths [22].....	14
Figure 2-11 Hexa and tetra meshing shape.....	17
Figure 3-1 STD specimen	20
Figure 3-2 ALT and ALT-AS specimen.....	21
Figure 3-3 Hybrid specimen	22
Figure 4-1 Set up in Instron100	25
Figure 4-2 Set up in Instron300	26
Figure 4-3: Wire sensor	27
Figure 4-4: Washer sensor	27
Figure 4-5: Inclinator sensor	28
Figure 4-6 Thermocouple	28
Figure 4-7 LDT sensor.....	29
Figure 4-8 Interface of the Labview software.....	30
Figure 4-9 Interface of the Catman software	31
Figure 4-10 Set up of the washer sensor test.	36
Figure 5-1 Sliding surface indicated with red.....	40
Figure 5-2 Restraints in the model.....	41
Figure 5-3 Bonded contact between bolt and nut	43
Figure 5-4 Application of the bolt pretension function	43
Figure 5-5 Mesh in the bolt.....	44
Figure 5-6 Fixed surfaces.....	44

Figure 5-7 Geometry of the simple model.....	45
Figure 5-8 Load steps.....	45
Figure 5-9 Geometry of the real model.....	46
Figure 5-10 Rotation point in the middle of the anchor profile.....	47
Figure 5-11 Rotation point in the middle.....	47
Figure 5-12 Rotation point on the top of the press profile.....	48
Figure 5-13 Rotation point at the top.....	48
Figure 5-14 XY-plane in Ansys (STD-1H)	49
Figure 5-15: YX-plane in Ansys (STD-1H)	50
Figure 5-16 Free DOF in case A.....	50
Figure 5-17 Free DOF in case B	51
Figure 6-1 Normal stress in the bolt [MPa]	53
Figure 6-2 Normal elastic strain in the bolt [MPa]	54
Figure 6-3 Deformation in X-direction [mm].....	55
Figure 6-4 Maximum equivalent stress along the slotted hole [MPa].....	55
Figure 6-5 Maximum equivalent stress in the fixed profile [MPa]	56
Figure 6-6 Deformation in X-direction [mm].....	57
Figure 6-7 Maximum equivalent stress along the slotted hole [MPa].....	57
Figure 6-8 Maximum equivalent stress in the fixed profile [MPa]	58
Figure 6-9 Maximum equivalent stress in the additional plate [MPa].....	58
Figure 6-10 Deformation in Y-direction with remote displacement in the middle [mm]	59
Figure 6-11 Deformation in Y-direction with remote displacement in the top [mm]	60
Figure 6-12 Restraints in case A	60
Figure 6-13 STD-1H Case A, deformation in Y-direction [mm]	61
Figure 6-14 ALT Case A, deformation in Y-direction [mm]	61
Figure 6-15 Restraints in case B	61
Figure 6-16 STD-1H Case B, deformation in Y-direction [mm].....	62
Figure 6-17 ALT Case B, deformation in Y-direction [mm].....	62
Figure 6-18 Restraints in case C	63
Figure 6-19 STD-1H Case C, deformation in Y-direction [mm].....	63
Figure 6-20 ALT Case C, deformation in Y-direction [mm].....	63
Figure 6-21 Deformation in Y-direction ALT M10 [mm].....	65
Figure 6-22 Deformation in Y-direction ALT M20 [mm].....	65
Figure 6-23 Deformation in Z-direction ALT M10 [mm].....	66

Figure 6-24 Deformation in Z-direction ALT M20 [mm]	66
Figure 6-25 Equivalent stress in the fixed profile ALT M10 [MPa]	67
Figure 6-26 Equivalent stress in the fixed profile ALT M20 [MPa]	67
Figure 6-27 Equivalent stress in the additional plate ALT M10 [MPa]	68
Figure 6-28 Equivalent stress in the additional plate ALT M20 [MPa]	68
Figure 6-29 Equivalent stress in the anchor profile ALT M10 [MPa]	69
Figure 6-30 Contact status in friction surface 2 ALT M10	70
Figure 6-31 Contact status in friction surface 2 ALT M20	70
Figure 6-32 Deformation in Y-direction ALT-AS M10 [mm]	71
Figure 6-33 Deformation in Y-direction ALT-AS M20 [mm]	71
Figure 6-34 Deformation in Z-direction ALT-AS M10 [mm].....	72
Figure 6-35 Deformation in Z-direction ALT-AS M20 [mm].....	72
Figure 6-36 Equivalent stress in the anchor profile ALT-AS M10 [MPa]	73
Figure 6-37 Equivalent stress in the anchor profile ALT-AS M20 [MPa]	73
Figure 6-38 Equivalent stress in the additional plate ALT-AS M10 [MPa].....	74
Figure 6-39 Equivalent stress in the additional plate ALT-AS M20 [MPa].....	74
Figure 6-40 Equivalent stress in the fixed profile ALT-AS M10 [MPa].....	75
Figure 6-41 Equivalent stress in the fixed profile ALT-AS M20 [MPa].....	75
Figure 6-42 Equivalent stress in the alignment component ALT-AS M10 [MPa].....	76
Figure 6-43 Equivalent stress in the alignment component ALT-AS M20 [MPa].....	76
Figure 6-44 Contact status in friction surface 2 ALT-AS M10	77
Figure 6-45 Contact status in friction surface 2 ALT-AS M20	77
Figure 6-46 Contact status between alignment component and fixed profile, ALT-AS M10.	78
Figure 6-47 Contact status between alignment component and fixed profile, ALT-AS M20.	78
Figure 6-48 Deformation in Y-direction STH 1H M10 [mm]	79
Figure 6-49 Deformation in Y-direction STD-1H M20 [mm].....	79
Figure 6-50 Deformation in Z-direction STH 1H M10 [mm]	80
Figure 6-51 Deformation in Z-direction STD-1H M20 [mm]	80
Figure 6-52 Equivalent stress in the anchor profile STH 1H M10 [MPa].....	81
Figure 6-53 Equivalent stress in the anchor profile STD-1H M20 [MPa]	82
Figure 6-54 Equivalent stress in the additional plate STD-1H M10 [MPa]	82
Figure 6-55 Equivalent stress in the additional plate STD-1H [MPa].....	83
Figure 6-56 Equivalent stress in the fixed profile STH 1H M10 [MPa]	83
Figure 6-57 Contact status in friction surface 2 STD-1H M10	84

Figure 6-58 Contact status in friction surface 2 STD-1H M20	84
Figure 6-59 Deformation in Y-direction STH 2H M10 [mm].....	85
Figure 6-60 Deformation in Z-direction STH 2H M10 [mm]	85
Figure 6-61 Equivalent stress in the anchor profile STD-2H [MPa].....	86
Figure 6-62 Equivalent stress in the fixed profile STD-2H [MPa].....	87
Figure 6-63 Equivalent stress in the additional plate STD-2H [MPa].....	87
Figure 6-64 Contact status in friction surface 2 STD-2H	88
Figure 6-65 Deformation in Y-direction for Hybrid M10 [mm]	88
Figure 6-66 Deformation in Y-direction for Hybrid M20 [mm]	89
Figure 6-67 Deformation in Z-direction Hybrid M10 [mm]	89
Figure 6-68 Deformation in Z-direction Hybrid M20 [mm]	90
Figure 6-69 Equivalent stress in the anchor profile Hybrid M10 [MPa].....	91
Figure 6-70 Equivalent stress in the anchor profile Hybrid M20 [MPa].....	91
Figure 6-71 Equivalent stress in the fixed profile Hybrid M10 [MPa].....	92
Figure 6-72 Equivalent stress in the fixed profile Hybrid M20 [MPa].....	92
Figure 6-73 Equivalent stress in the additional plate Hybrid M10 [MPa].....	93
Figure 6-74 Equivalent stress in the additional plate Hybrid M20 [MPa].....	93
Figure 6-75 Contact status in friction surface 2 Hybrid M10	94
Figure 6-76 Contact status friction surface 2 Hybrid M20	94
Figure 7-1 Hysteresis loop in a) test 1, b) test 2, c) test 3 and d) test 4	101
Figure 7-2 ALT hysteresis loop (test 5).....	102
Figure 7-3 ALT hysteresis loop (test 6).....	103
Figure 7-4 ALT hysteresis loop (test 7).....	104
Figure 7-5 Hysteresis loop of Marthinsen's test (left) [4] and test 8 (right).....	105
Figure 7-6 Displacement of the column in test 2	106
Figure 7-7 Preload force in the washer sensors in test 9.1.....	107
Figure 7-8 Load-displacement graph in test 9.1	108
Figure 7-9 Preload force in the washer sensors in test 9.2.....	108
Figure 7-10 Load-displacement graph in test 9.2	109
Figure 7-11 Preload force in the washer sensors in test 9.3.....	109
Figure 7-12 Load-displacement graph in test 9.3	110
Figure 7-13 Preload force in the washer sensors in test a) 10.1, b) 10.2, c) 10.3.....	110
Figure 7-14 Load-displacement graph in tests a) 10.1, b) 10.2, c) 10.3	111
Figure 7-15 Load-displacement graph of a) test 11 and b) test 12	112

Figure 7-16 Load-displacement graph of a) test 13 and b) test 14	113
Figure 7-17 Twisting in a) ALT M10 and b) ALT M20.....	114
Figure 7-18 Imperfection in the ALT-AS specimen.....	115
Figure 7-19 Load-displacement graph of a) test 15 and b) test 16	115
Figure 7-20 Load-displacement graph of a) test 17 and b) test 18	116
Figure 7-21 Twisting in a) STD-1H M10 and b) STD-1H M20.....	116
Figure 7-22 Load-displacement graph of test 19	117
Figure 7-23 Deformed shape of STD-2H in test 19.....	117
Figure 7-24 Load-displacement graph of a) test 20 and b) test 21	118
Figure 7-25 Load-displacement graph of a) test 5 and b) test 8	119
Figure 7-26 Damage to the aluminum and Hardox 450 shim layer.....	119
Figure 7-27 Damage to shim layers in the different STD specimen.....	120
Figure 7-28 Damage to shim layers in the different ALT and ALT-AS specimen	120
Figure 7-29 Damage to shim layers in the different Hybrid specimen.....	120
Figure 7-30 Magnetic Hardox steel residue on ALT M20	121
Figure 7-31 Load-displacement graph of a) test 10.3, b) test 10.4 and c) test 10.5.....	122
Figure 7-32 Damages to the bolts in a) test 19 and b) test 18.....	122
Figure 7-33 Temperature development for ALT and ALT-AS [C°]	123
Figure 7-34 Temperature development for the STD-1H, STD-2H and Hybrid [C°].....	124
Figure 8-1 Deformation in Y-direction from Ansys [mm]	125
Figure 8-2 Coordinate system in the press.....	126
Figure 8-3 Maximum inclination from the inclinometer [°]	126
Figure 8-4 Comparison of damage to the additional plate STD-1H M10	127
Figure 8-5 Comparison of damage to the shim layer ALT-AS M10.....	127
Figure 8-6 Comparison of damage to the shim layer in Hybrid M10.....	128
Figure 8-7 Load-displacement graph of a) test 9.2, b) test 9.3, c) test 10.1 and d) test 10.3.	129

12 List of tables

Table 3-1 Description of specimens	23
Table 4-1 Procedure of the monotonic test	30
Table 4-2 Procedure of the cyclic test.....	30
Table 4-3 Overview of the preliminary testing.....	35
Table 4-4 Overview of the monotonic testing in Instron100.....	37
Table 4-5 Overview of the new testing campaign with Instron300.....	38
Table 5-1 Material Properties in Ansys	40
Table 5-2 Definition of friction surface 1 and 2	42
Table 5-3 Restraints in case A, B and C	51
Table 6-1 Summary of the force reaction and deformation in Y-direction in case A, B and C for specimen STD-1H and ALT	64
Table 6-2 Force reactions in ALT M10 and M20.....	66
Table 6-3 Force reaction and force probe with the dynamic friction coefficient for ALT-AS M10 and M20.....	73
Table 6-4 Force reactions in STD-1H M10 and M20.....	81
Table 6-5 Force reaction and force probe for STD-2H with the dynamic friction coefficient 86	
Table 6-6 Force reaction and force probe for Hybrid M10 and M20 with the dynamic friction coefficient	90
Table 6-7 Force reaction and force probe in ALT specimen	95
Table 6-8 Force reaction and force probe in ALT-AS specimen.....	95
Table 6-9 Force reaction and force probe in STD-1H specimen	96
Table 6-10 Force reaction and force probe in STD-2H specimen	96
Table 6-11 Force reaction and force probe in Hybrid specimen	96
Table 6-12 Utilization rate of the ALT specimen	97
Table 6-13 Utilization rate of the ALT-AS specimen	97
Table 6-14 Utilization rate of the STD-1H specimen	98
Table 6-15 Utilization rate of the STD-2H specimen	98
Table 6-16 Utilization rate of the Hybrid specimen	98

13 References

- [1] CORDIS. "Energy and seismic renovation: the European H2020 programme finances the e-SAFE project." Available online: <https://cordis.europa.eu/article/id/422585-energy-and-seismic-renovation-the-european-h2020-programme-finances-the-e-safe-project> (accessed Apr. 26, 2021).
- [2] e-SAFE. "ENERGY AND SEISMIC RENOVATION: THE EUROPEAN H2020 PROGRAMME." Available online: <http://esafe-buildings.eu/en/news/news-3/> (accessed May. 26, 2021).
- [3] M. R. Hatletveit, "Mechanical assessment of a steel dissipation system for RC buildings retrofitting with CLT panels," Master's thesis, Norwegian University of Life Sciences, Ås, 2020.
- [4] M. B.-A. Marthinsen, "Experimental assessment of a steel dissipating system," Master's thesis, Norwegian University of Life Sciences, Ås, 2020.
- [5] NORSAR. "Hva er et jordskjelv." Available online: <https://www.jordskjelv.no/om-jordskjelv/hva-er-et-jordskjelv/> (accessed Feb. 5, 2021).
- [6] B. A. Bolt. "Earthquake." Available online: <https://www.britannica.com/science/earthquake-geology> (accessed Feb. 4, 2021).
- [7] NORSAR. "Hvordan blir jordskjelv registrert? Hvordan blir jordskjelv målt? Hvordan blir størrelsen av et jordskjelv bestemt?" Available online: <https://www.jordskjelv.no/jordskjelv/om-jordskjelv/faq/maaling-av-styrke-og-intensitet/hvordan-blir-jordskjelv-registrert-hvordan-blir-jordskjelv-malt-hvordan-blir-storrelsen-av-et-jordskjelv-bestemt-article1014-941.html> (accessed Feb. 4, 2021).
- [8] USGS. "Earthquake Magnitude, Energy Release, and Shaking Intensity." Available online: https://www.usgs.gov/natural-hazards/earthquake-hazards/science/earthquake-magnitude-energy-release-and-shaking-intensity?qt-science_center_objects=0#qt-science_center_objects (accessed May. 26, 2021).
- [9] USGS. "Earthquake Glossary." Available online: <https://earthquake.usgs.gov/learn/glossary/?term=acceleration> (accessed Feb. 4, 2021).
- [10] COMSOL. "Response Spectrum Analysis." Available online: <https://www.comsol.com/multiphysics/response-spectrum-analysis> (accessed Feb 26, 2021).
- [11] *Design of structures for earthquake resistance*, EN 1998, CEN, 2004.
- [12] D. Giardini, J. Wössner, and L. Danciu, "Mapping Europe's Seismic Hazard," *Eos, Transactions American Geophysical Union*, vol. 95, no. 29, pp. 261-262, 2014, doi: <https://doi.org/10.1002/2014EO290001>.
- [13] M. Rak, D. Mestrovic, and A. Nizic, "Damping and its importance to structure," *WIT Transactions on The Built Environment*, vol. 81, 2005.
- [14] A. A. Shabana, *Theory of vibration: an introduction*, 3. ed. Springer, 2019.
- [15] T. L. Schmitz and K. S. Smith, *Mechanical Vibrations: Modeling and Measurement*. Springer, 2012.
- [16] H. Ormestad. "friksjon." Available online: <https://snl.no/friksjon> (accessed May. 26, 2021).
- [17] P. J. Blau, "The significance and use of the friction coefficient," *Tribology International*, vol. 34, no. 9, pp. 585-591, 2001.
- [18] Britannica. "Coefficient of friction." Available online: <https://www.britannica.com/science/force-physics> (accessed May. 26, 2021).
- [19] H. Kanamori and E. E. Brodsky, "The Physics of Earthquakes," 2004, doi: 10.1088/0034-4885/67/8/R03.
- [20] H.-H. Khoo, C. Clifton, G. Macrae, H. Zhou, and S. Ramhormozian, "Proposed design models for the asymmetric friction connection," *Earthquake Engineering & Structural Dynamics*, vol. 44, no. 8, pp. 1309-1324, 2015, doi: 10.1002/eqe.2520.

- [21] W. Y. Loo, P. Quenneville, and N. Chouw, "A new type of symmetric slip-friction connector," *Journal of Constructional Steel Research*, vol. 94, pp. 11-22, 2014, doi: 10.1016/j.jcsr.2013.11.005.
- [22] J. C. Golondrino, G. MacRae, and C. Clifton, "Behaviour of Asymmetrical Friction Connections using different shim materials," in *Proceedings of the New Zealand Society for Earthquake Engineering Conference*, 2012.
- [23] H.-H. Khoo, C. Clifton, J. Butterworth, G. MacRae, and G. Ferguson, "Influence of steel shim hardness on the Sliding Hinge Joint performance," *Journal of Constructional Steel Research*, vol. 72, pp. 119-129, 2012/05/01/ 2012, doi: <https://doi.org/10.1016/j.jcsr.2011.11.009>.
- [24] Medium. "Bolts, Preload Explained." Available online: <https://bananajutsu.medium.com/bolted-joint-preload-9ead1f81511b> (accessed Mar. 17, 2021).
- [25] *Execution of steel structures and aluminium structures - Part 2: Technical requirements for steel structures*, EN 1090-2, CEN, 2018.
- [26] *Design of steel structures - Part 1-8: Design of joints*, EN 1993, CEN, 2005.
- [27] *High-strength structural bolting assemblies for preloading - Part 1: General requirements*, EN 14399-1, CEN, 2015.
- [28] Ansys. "Structural Analysis & Simulation Software Solutions." Available online: <https://www.ansys.com/products/structures> (accessed Feb. 15, 2021).
- [29] Ansys. "Finite Element Analysis (FEA) Software for Structural Engineering." Available online: <https://www.ansys.com/products/structures/ansys-mechanical> (accessed Apr. 29, 2021).
- [30] Ansys. "Ansys Meshing - Influencing Accurate Results." Available online: <https://www.ansys.com/products/meshing> (accessed Feb. 15, 2021).
- [31] Ansys. "Ansys SpaceClaim - 3D Modeling Software." Available online: <https://www.ansys.com/products/3d-design/ansys-spaceclaim> (accessed Feb. 15, 2021).
- [32] Ansys. "Workbench User's Guide." Available online: https://ansyshelp.ansys.com/account/secured?returnurl=/Views/Secured/corp/v202/en/wb2_help/wb2_help.html (accessed Mar. 11, 2021).

Appendix

Appendix A:
Nominal torque

Tabell 3: Nominelt tiltrekningsmoment (Mv) i Nm for stålskruer

Gjenge d	Stigning P mm	Spenningsareal As mm ²	Fasthetsklasse				
			4.6	5.8	8.8	10.9	12.9
1,6	0,35	1,27	0,065	0,1	0,17	0,24	0,29
1,8	0,35	1,7	0,096	0,16	0,25	0,36	0,43
2	0,4	2,07	0,13	0,22	0,35	0,49	0,58
2,2	0,45	2,48	0,17	0,29	0,46	0,64	0,77
2,5	0,45	3,39	0,26	0,44	0,7	0,98	1,2
3	0,5	5,03	0,46	0,77	1,2	1,7	2,1
3,5	0,6	6,78	0,73	1,2	1,9	2,7	3,3
4	0,7	8,78	1,1	1,8	2,9	4	4,9
4,5	0,75	11,3	1,6	2,6	4,1	5,8	7
5	0,8	14,2	2,2	3,6	5,7	8,1	9,7
6	1	20,1	3,7	6,1	9,8	14	17
8	1,25	36,6	8,9	15	24	33	40
10	1,5	58	17	29	47	65	79
12	1,75	84,3	30	51	81	114	136
14	2	115	48	80	128	181	217
16	2	157	74	123	197	277	333
18	2,5	192	103	172	275	386	463
20	2,5	245	144	240	385	541	649
22	2,5	303	194	324	518	728	874
24	3	353	249	416	665	935	1120
27	3	459	360	600	961	1350	1620
30	3,5	561	492	819	1310	1840	2210
33	3,5	694	663	1100	1770	2480	2980
36	4	817	855	1420	2280	3210	3850
39	4	976	1100	1830	2930	4120	4940
42	4,5	1121	1360	2270	3640	5110	6140
45	4,5	1306	1690	2820	4510	6340	7610
48	5	1473	2040	3400	5450	7660	9190
52	5	1758	2620	4370	6990	9830	11800
56	5,5	2030	3270	5440	8710	12200	14700
60	5,5	2362	4050	6750	10800	15200	18200
64	6	2676	4900	8170	13100	18400	22000
68	6	3055	5910	9860	15800	22200	26600
72	6	3460	7060	11800	18800	26500	31800
76	6	3889	8340	13900	22200	31300	37500
80	6	4344	9770	16300	26100	36600	44000
85	6	4948	11800	19600	31400	44200	53000
90	6	5591	14000	23400	37400	52700	63200
95	6	6273	16600	27600	44200	62200	74600
100	6	6995	19400	32300	51700	72700	87300
ReL eller Rp0,2 N/mm2 nominelt			240	400	640	900	1080
$\frac{k}{\chi \left(1 + \frac{S_F}{F_{FM}}\right)} \cdot \sigma_s \text{ N/mm}^2$			26,16	43,6	69,76	98,1	117,72

Appendix B:
Measurements and drawings of the
specimen

ANCHOR PROFILE STD	length	t	h1	h2	k	A1	A2	B (at A1)	B (at F1 and F2)	C (at D1)	C (at D2)	D1	D2	E1
Drawing E	450,0	8,0	11,0	15,0	5,0	121,0	121,0	113,0	113,0	104,0	104,0	120,0	120,0	60,0
STD 1H-M10 1A	450,0	8,0	10,9	14,9	5,0	120,2	120,2	112,0	112,0	104,0	104,0	121,5	121,8	60,7
Drawing G	450,0	8,0	21,0	15,0	5,0	121,0	121,0	113,0	113,0	104,0	104,0	120,0	120,0	60,0
STD 1H-M20 1B	450,0	8,1	20,9	15,0	5,0	120,0	120,0	112,0	112,0	104,0	106,0	121,4	122,5	60,9
Drawing J	450,0	8,0	11,0	15,0	5,0	121,0	121,0	113,0	113,0	104,0	104,0	120,0	120,0	60,0
STD 2H-M10 1A	450,0	8,0	10,7	14,8	5,0	120,5	119,8	112,0	111,0	101,0	101,0	118,4	118,8	59,3

E2	F1	F2	H1	H2	H3	H4	H5	G(1/2)	I	J	X
60,0	54,0	54,0	90,0	90,0	90,0	90,0	90,0	67,0	54,0	160,0	130,0
60,2	53,6	53,6	89,8	89,9	89,9	89,9	89,8	65,5	54,2	159,9	129,9
60,0	54,0	54,0	90,0	90,0	90,0	90,0	90,0	67,0	54,0	160,0	130,0
60,3	53,5	53,5	89,9	90,1	90,1	90,1	90,0	66,6	54,0	159,9	129,9
60,0	35,5	37,0	90,0	90,0	90,0	90,0	90,0	35,5/48,5	37,0	160,0	130,0
58,6	35,1	37,3	89,9	89,8	89,8	89,8	89,9	36,3/47,4	31,5	159,8	129,7

FREE PROFILE STD	length	height	t	h2	h3	k	A1	A2	B (at A1)	B (at F1 and F2)	C (at D1)	C (at D2)	D1	G(1/2)
Drawing F	450,0	325	8,0	15,0	12,0	5,0	121,0	121,0	113,0	113,0	104,0	104,0	120,0	67,0
STD 1H-M10 1B	450,0	323	8,1	15,0	11,6	5,0	119,2	120,0	111,0	112,0	104,0	104,0	119,7	66,6
Drawing H	450,0	325	8,0	15,0	24,0	5,0	121,0	121,0	113,0	113,0	104,0	104,0	120,0	67,0
STD 1H-M20 1B	450,0	327	8,0	14,8	23,1	5,0	120,7	121,0	111,0	112,0	105,0	106,0	120,8	66,1
Drawing K	450,0	325	8,0	15,0	12,0	5,0	121,0	121,0	113,0	113,0	104,0	104,0	120,0	35,5/48,5
STD 2H-M10 1B	449,0	327	8,1	14,8	12,0	5,0	122,7	121,9	116,0	115,0	104,0	104,0	121,2	35,6/52,3

I	L	J	N	O	P	Q	R	S	T	U
54,0	205,0	213,0	58,0	37,1	74,2	111,3	84,0	63,0	370,0	40,0
53,8	206,0	211,0	58,1	37,6	74,0	111,5	83,9	61,5	371,4	39,8
54,0	205,0	213,0	58,0	37,1	74,2	111,3	84,0	63,0	370,0	40,0
53,5	204,0	213,0	57,9	36,8	74,0	111,2	83,9	61,4	369,9	39,7
37,0	205,0	213,0	58,0	37,1	74,2	111,3	84,0	63,0	370,0	40,0
31,0	204,0	210,0	58,0	37,0	74,1	111,3	83,9	60,4	370,0	40,2

ANCHOR PROFILE ALT	length	t	h1	h2	k	A1	A2	B (at A1)	B (at F1 and F2)	C (at D1)	C (at D2)	D1	D2	E1
Drawing L	450,0	8,0	12,0	15,0	5,0	78,5	78,5	70,5	70,5	103,9	103,9	120,0	120,0	60,0
ALT-M10 1A	449,0	8,1	11,0	14,8	5,0	77,4	77,4	69,0	68,0	103,0	102,9	120,7	120,4	59,4
Drawing N	450,0	8,0	24,0	15,0	5,0	93,0	93,0	85,0	85,0	103,9	103,9	120,0	120,0	60,0
ALT-M20 1A	450,0	8,0	23,1	14,9	5,0	91,2	92,0	84,0	84,0	103,0	103,0	119,0	119,0	59,6

E2	F1	F2	H1	H2	H3	H4	H5	G	I	U	T
60,0	30,0	48,5	90,0	90,0	90,0	90,0	90,0	48,5	30,0	40,0	370,0
59,9	29,4	46,9	91,9	90,1	90,1	90,1	91,9	47,0	29,4	39,5	370,0
60,0	40,0	40,0	90,0	90,0	90,0	90,0	90,0	53,0	40,0	40,0	370,0
61,3	39,1	39,1	90,0	90,0	90,0	90,0	90,0	51,9	39,6	39,6	369,9

FREE PROFILE ALT	length	height	t	h2	h3	k	A1	A2	F1/F1	F2	G	I	N	O
Drawing M	450,0	325	8,0	15,0	11,0	5,0	78,5	78,5	30/34,5	48,5	48,5	30,0	58,0	37,1
ALT-M10 1B	450,0	325	8,1	14,8	11,0	5,0	77,7	77,7	30,1	48,2	47,0	29,4	57,7	37,0
Drawing P	450,0	325	8,0	15,0	21,0	5,0	93,0	93,0	40/34,5	48,5	53,0	40,0	58,0	37,1
ALT-M20 1B	451,0	324	8,1	15,0	20,9	5,0	93,5	93,3	39,5/35	53,0	51,9	39,6	58,2	37,2

P	Q	R	S	J	X
74,2	111,3	84,0	183,0	160,0	130,0
73,9	111,3	83,7	182,4	160,2	130,0
74,2	111,3	84,0	183,0	160,0	130,0
74,2	111,5	84,0	182,5	160,3	129,9

ANCHOR PROFILE ALT-AS	length	t	h1	h2	k	A1	A2	B (at A1)	B (at F1 and F2)	C (at D1)	C (at D2)	D1	D2	E1
Drawing Q	450,0	8,0	12,0	15,0	5,0	78,5	78,5	70,5	70,5	103,9	103,9	120,0	120,0	60,0
ALT-AS-M10 1A	450,0	8,0	11,1	15,0	5,1	76,7	76,7	68,7	68,7	103,6	103,9	120,4	119,7	60,3
Drawing T	450,0	8,0	24,0	15,0	5,0	93,0	93,0	85,0	85,0	103,9	103,9	120,0	120,0	60,0
ALT-AS-M20 1A	450,0	8,1	23,9	15,1	5,0	91,8	91,8	83,0	82,0	104,0	103,0	120,9	120,2	60,0

E2	F1	F2	H1	H2	H3	H4	H5	G	I	U	T
60,0	30,0	48,5	90,0	90,0	90,0	90,0	90,0	48,5	30,0	40,0	370,0
60,3	29,5	46,7	90,0	90,0	90,0	90,0	90,0	46,5	29,4	39,4	372,9
60,0	40,0	40,0	90,0	90,0	90,0	90,0	90,0	53,0	40,0	40,0	370,0
60,7	39,8	40,9	90,0	90,0	90,0	90,0	90,0	53,0	39,8	35,5	370,1

FREE PROFILE ALT-AS	length	height	t	h2	h3	A1	F1/F1	F2	H	I	J	N	O	P
Drawing S	466,0	317	8,0	15,0	17,0	78,5	35,3	43,3	70,5	32,5	50,0	66,0	37,1	74,2
ALT-AS-M10 1B	466,0	317	8,2	14,7	16,8	78,4L/78,2R	35,4	43,0	70,5	32,7B/32,4T	49,9	65,7	37,0	74,1
Drawing V	466,0	317	8,0	15,0	17,0	93,0	42,5	50,5	85,0	32,5	50,0	66,0	37,1	74,2
ALT-AS-M20 1B	466,0	316	8,0	15,0	17,2	92,7L/92,7R	49,3	49,3	85,0	31,3	48,0	65,8	36,9	74,8

Q	M	R	S
111,3	58,0	84,0	175,0
111,3	57,9	83,7	174,4
111,3	58,0	84,0	175,0
111,4	57,9	84,0	174,5

ALIGNMENT COMPONENT ALT-AS	length	t	h4	k	A1	D1	Q	W	Y	Z	V	F1	F2	J
Drawing R	450,0	8,0	11,0	5,0	70,5	123,0	23,5	17,0	34,0	18,0	15,5	35,3	35,3	160,0
ALT-AS-M10 1C	449,0	8,0	10,6	5,0	69,0	122,9	23,8	16,9	33,6	16,2	15,6	35,3	35,3	159,3
Drawing U	450,0	8,0	21,0	5,0	85,0	123,0	23,5	17,0	34,0	18,0	15,5	42,5	42,5	160,0
ALT-AS-M20 1C	448,0	8,1	21,0	5,0	84,2	122,9	23,6	17,3	34,0	15,9	15,3	42,4	42,2	159,2

X	G	I	L
130,0	40,5	30,0	434,0
129,6	39,8	29,9	432,0
130,0	45,0	40,0	434,0
130,0	44,4	40,0	432,0

ANCHOR PROFILE HYBRID	length	t	h1	h2	k	A1	A2	B (at A1)	B (at F1 and F2)	C (at D1)	C (at D2)	D1	D2	E1
Drawing W	450,0	8,0	11,0	15,0	5,0	108,0	108,0	100,0	100,0	103,9	103,9	120,0	120,0	60,0
HYBRID-M10 1A	450,0	8,1	11,0	15,0	5,0	107,4	108,0	99,0	99,0	103,0	104,0	120,3	121,2	60,3
Drawing Y	450,0	8,0	21,0	15,0	5,0	108,0	108,0	100,0	100,0	103,9	103,9	120,0	120,0	60,0
HYBRID-M20 1A	450,0	8,1	20,8	14,9	5,0	108,2	107,4	99,0	99,0	103,0	102,0	120,3	119,3	60,5

E2	F1	F2	H1	H2	H3	H4	H5	G	I	J	X
60,0	36,0	59,0	90,0	90,0	90,0	90,0	90,0	72,0	36,0	160,0	130,0
60,0	36,0	57,8	90,0	90,0	90,0	90,0	90,0	70,8	36,0	160,0	130,0
60,0	40,0	55,0	90,0	90,0	90,0	90,0	90,0	68,0	40,0	160,0	130,0
59,8	35,9	58,4	89,9	89,9	89,9	89,9	89,9	71,4	35,9	156,9	123,9

FREE PROFILE HYBRID	length	height	t	h2	h3	k	A1	F1(I)/F1	F2/G	N	O	P	Q	R
Drawing X	450,0	325,0	8,0	15,0	12,0	5,0	108,0	49/35	59,0	58,0	37,1	74,2	111,3	84,0
HYBRID-M10 1B	450,0	324,0	8,0	14,8	10,9	5,0	108,5	49,9/33	58,4	57,8	37,0	74,0	111,2	84,0
Drawing Z	450,0	325,0	8,0	15,0	24,0	5,0	108,0	53/33	55,0	58,0	37,1	74,2	111,3	84,0
HYBRID-M20	450,0	323,0	8,0	14,7	22,8	5,0	106,8	53,9	54,2	57,8	36,9	74,0	111,2	83,7

S	U	T
183,0	40,0	370,0
181,4	39,5	373,1
183,0	40,0	370,0
180,4	39,4	370,2

STD-1H-M10	length	height	h1	L1	L2	L3	b1	b2
Drawing	450,0	98,0	11,0	160,0	130,0	160,0	49,0	49,0
Additional plate 1D	449,0	97,0	10,9	159,8	129,9	154,5	49,5	48,8
Shim layer 1F	449,0	97,0	10,9	159,8	129,9	154,5	49,5	48,8

STD-1H-M20	length	height	h1	L1	L2	L3	b1	b2
Drawing	450,0	98	21,0	160,0	130,0	160,0	49,0	49,0
Additional plate 1D	450,0	98	20,8	160,0	129,8	159,8	48,8	48,8
Shim layer 1F	450,0	98	20,8	160,0	129,8	159,8	48,8	48,8

STD-2H-M10	length	height	h1	L1	L2	L3	b1	b2	b3
Drawing	450,0	97,0	11,0	160,0	130,0	160,0	30,0	37,0	30,0
Additional plate 1D	450,0	96,8	11,1	160,0	130,1	160,0	30,1	37,2	30,1
Shim layer 1F	450,0	96,8	11,1	160,0	130,1	160,0	30,1	37,2	30,1

HYBRID-M10	length	height	h1	L1	L2	L3	b1	b2
Drawing	450,0	84,0	11,0	160,0	130,0	160,0	30,0	54,0
Additional plate 1D	450,0	83,9	11,0	154,4	119,0	154,4	24,5	48,5
Shim layer 1F	450,0	83,9	11,0	154,4	119,0	154,4	24,5	48,5

HYBRID-M20	length	height	h1	L1	L2	L3	b1	b2
Drawing	450,0	85,0	21,0	160,0	130,0	160,0	35,0	50,0
Additional plate 1D	450,0	85,2	20,8	159,4	129,8	159,7	29,7	55,5
Shim layer 1F	450,0	85,0	21,0	159,4	129,8	159,7	35,0	49,9

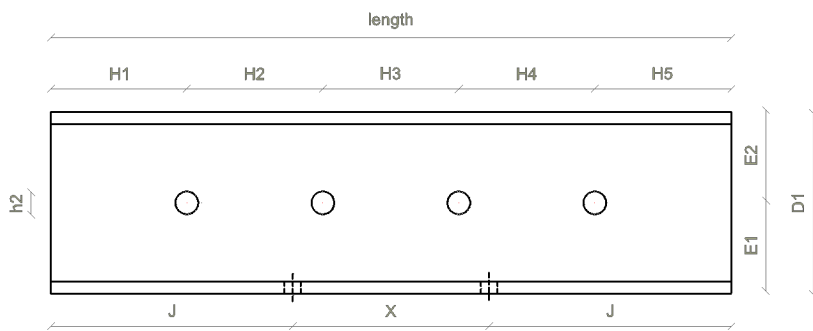
ALT-M10	length	height	h1	L1	L2	L3	b1	b2
Drawing	450,0	60,0	11,0	160,0	130,0	160,0	30,0	30,0
Additional plate 1D	449,0	59,9	10,9	159,9	129,9	159,8	30,0	30,0
Shim layer 1F	449,0	59,9	10,9	159,9	129,9	159,8	30,0	30,0

ALT-M20	length	height	h1	L1	L2	L3	b1	b2
Drawing	450,0	70,0	21,0	160,0	130,0	160,0	35,0	35,0
Additional plate 1D	450,0	70,1	20,8	159,9	130,0	170,5	35,0	35,1
Shim layer 1F	450,0	70,1	20,8	159,9	130,0	170,5	35,0	35,1

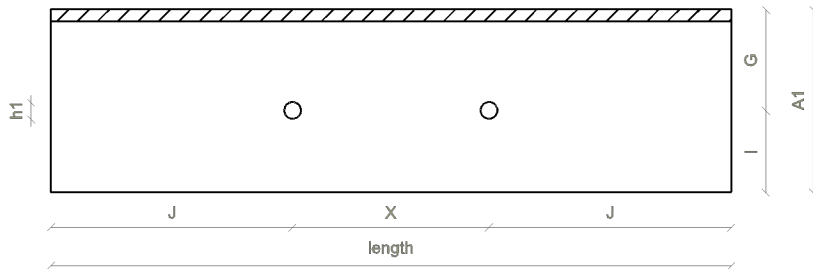
ALT-AS-M10	length	height	h1	L1	L2	L3	b1	b2
Drawing	450,0	60,0	11,0	160,0	130,0	160,0	30,0	30,0
Additional plate 1D	450,0	60,0	11,0	159,8	130,0	159,8	29,9	30,3
Shim layer 1F	450,0	60,0	11,0	159,8	130,0	159,8	29,9	30,3

ALT-AS-M20	length	height	h1	L1	L2	L3	b1	b2
Drawing	450,0	70,0	21,0	160,0	130,0	160,0	35,0	35,0
Additional plate 1D	449,0	70,0	20,8	159,9	129,9	159,8	34,8	35,0
Shim layer 1F	449,0	70,0	20,8	159,9	129,9	159,8	34,8	35,0

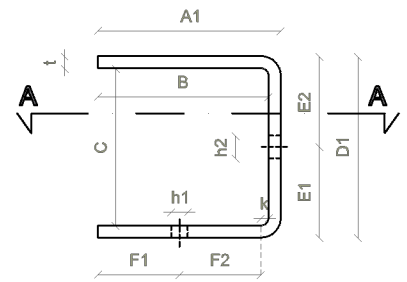
ANCHOR PROFILE



Front view



Section A-A



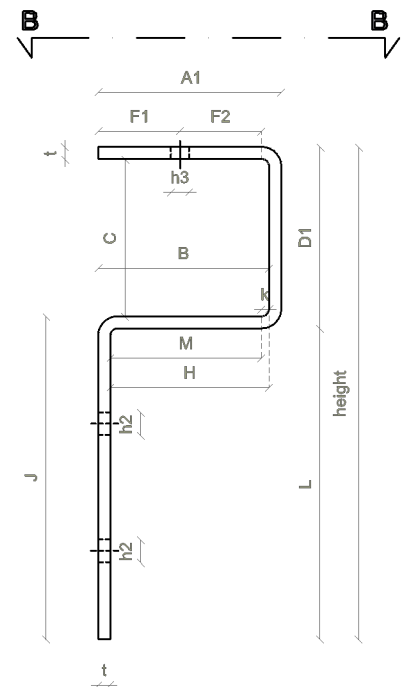
Lateral view

E

FREE PROFILE

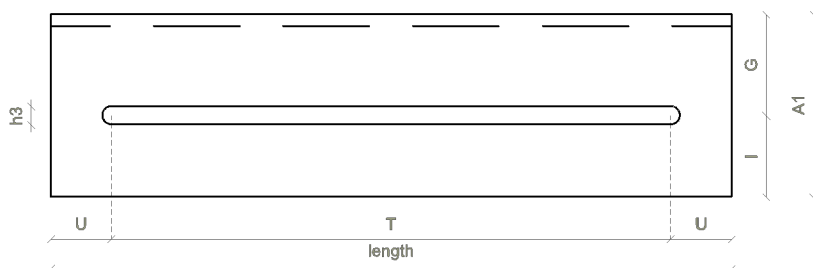


Front view



Lateral view

F

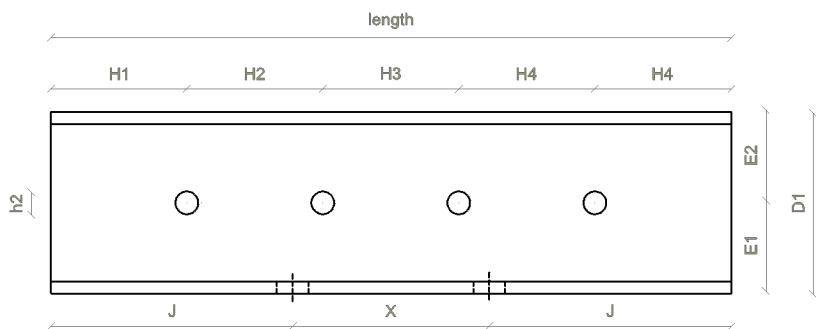


View B-B

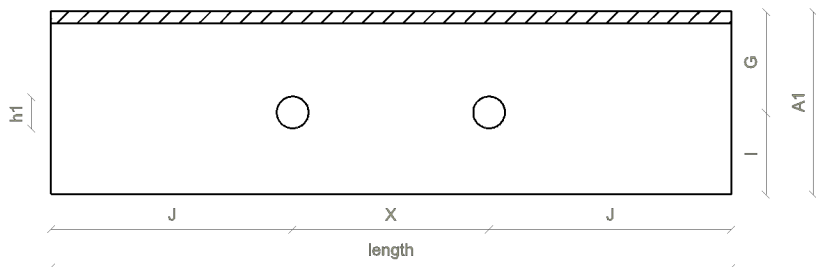
Prototype

STD-1H-M10

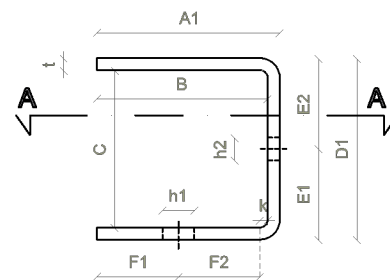
ANCHOR PROFILE



Front view



Section A-A



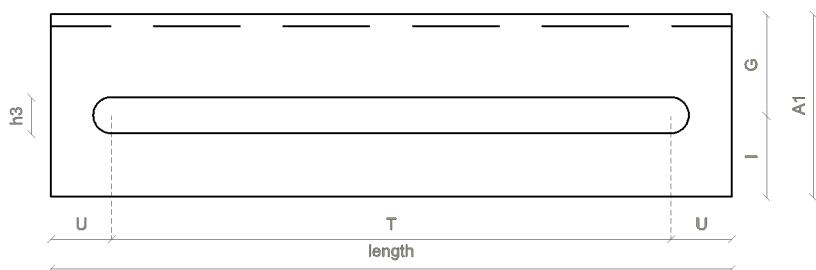
Lateral view

G

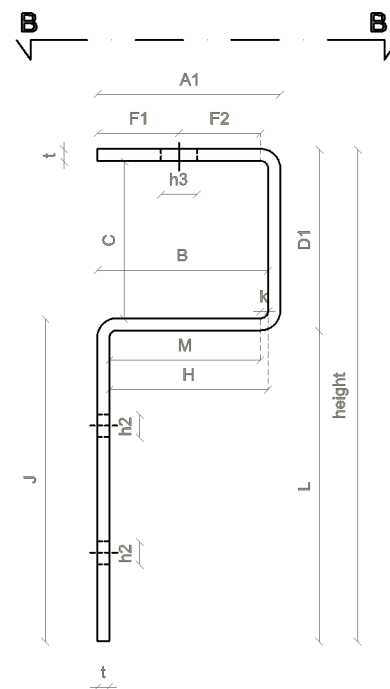
FREE PROFILE



Front view



View B-B



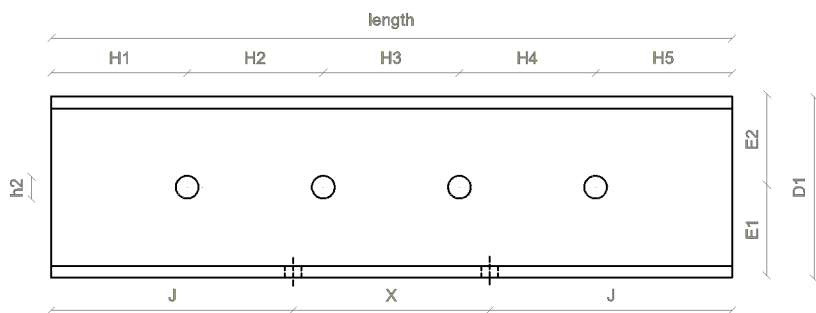
Lateral view

H

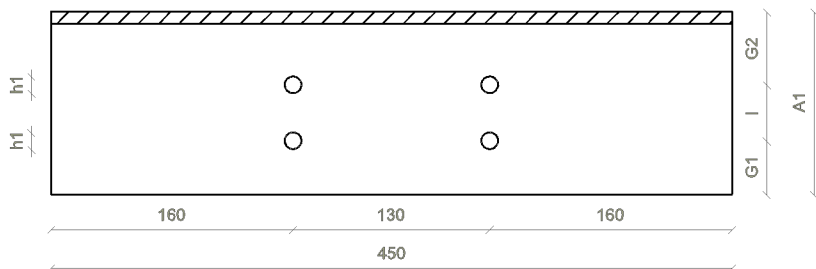
Prototype

STD-1H-M20

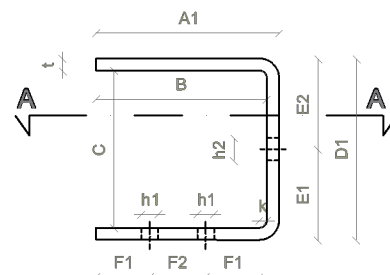
ANCHOR PROFILE



Front view



Section A-A



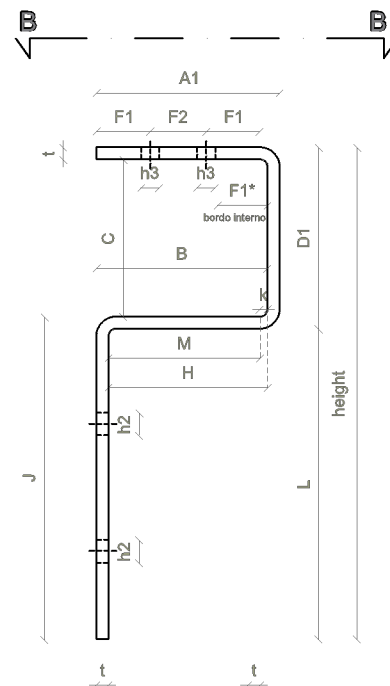
Lateral view

J

FREE PROFILE



Front view



Lateral view

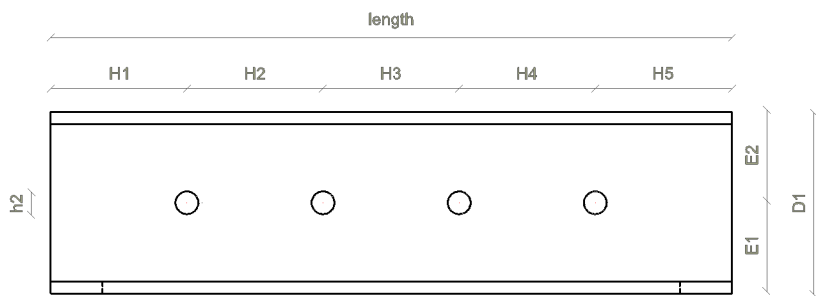


View B-B

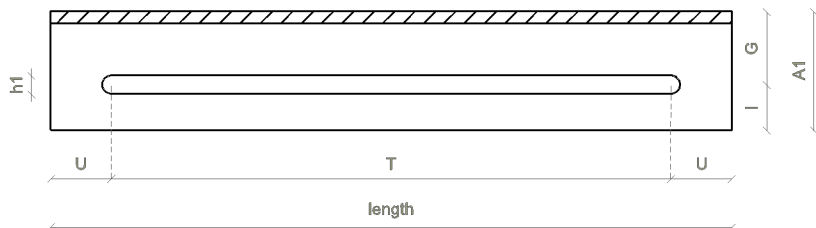
K

Prototype
STD-2H-M10

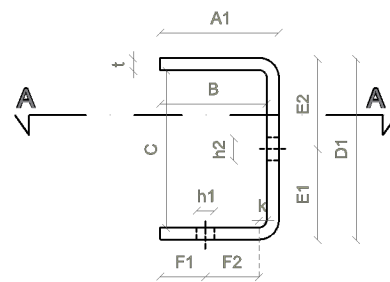
ANCHOR PROFILE



Front view



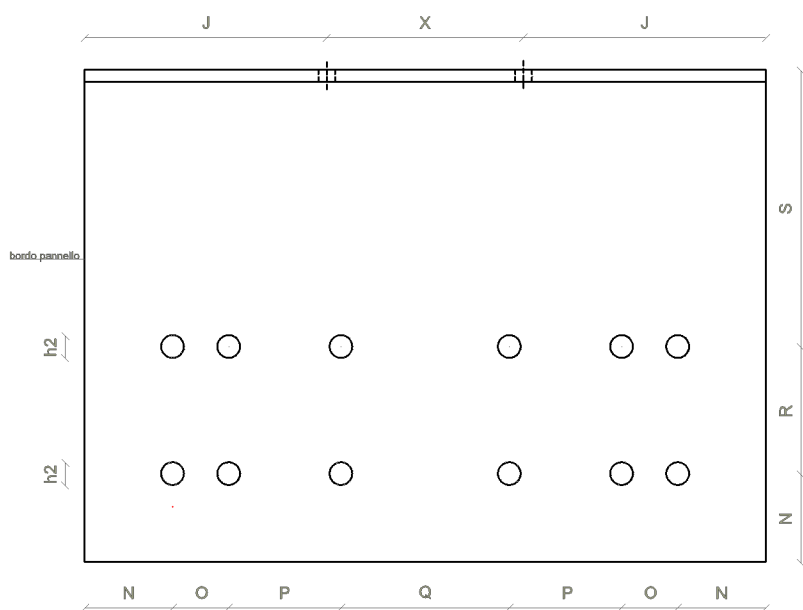
Section A-A



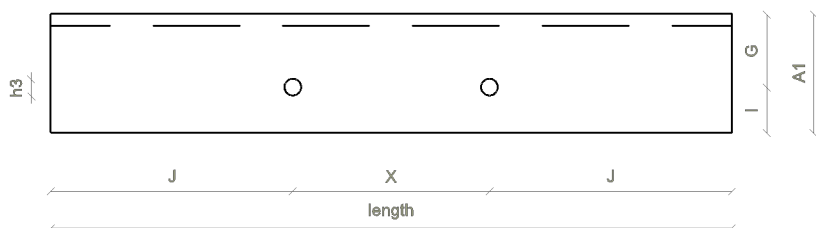
Lateral view



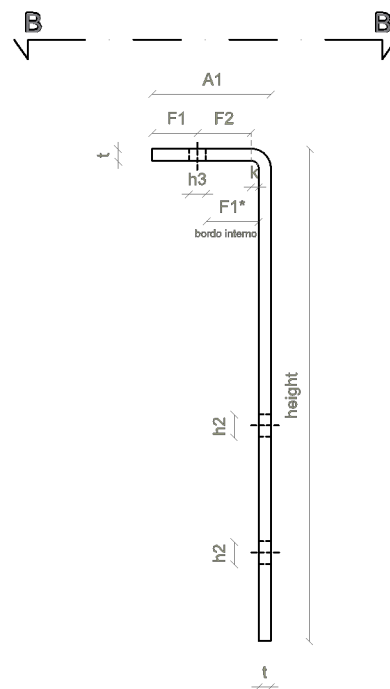
FREE PROFILE



Front view



View B-B



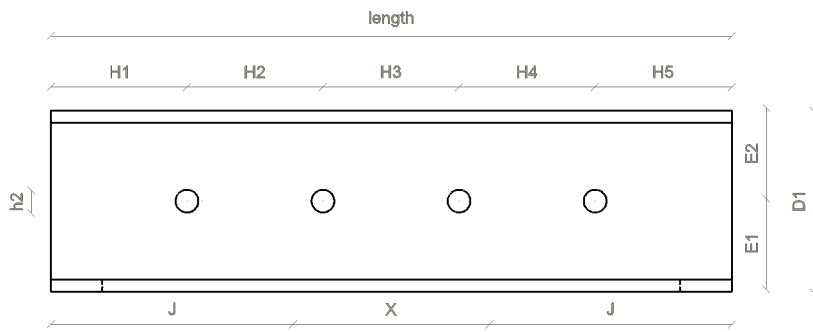
Lateral view



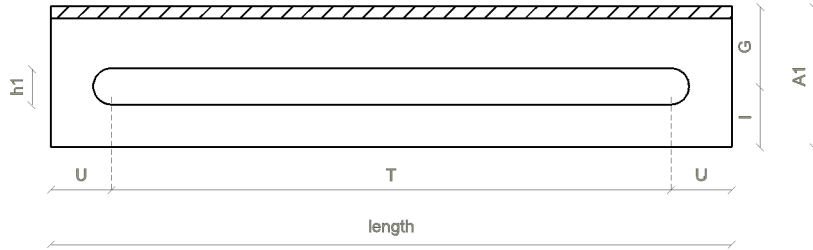
Prototype

ALT-M10

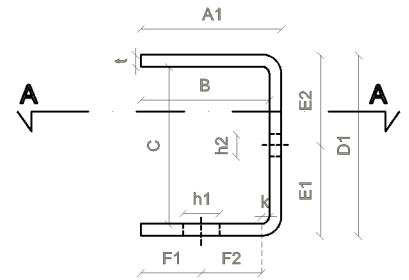
ANCHOR PROFILE



Front view



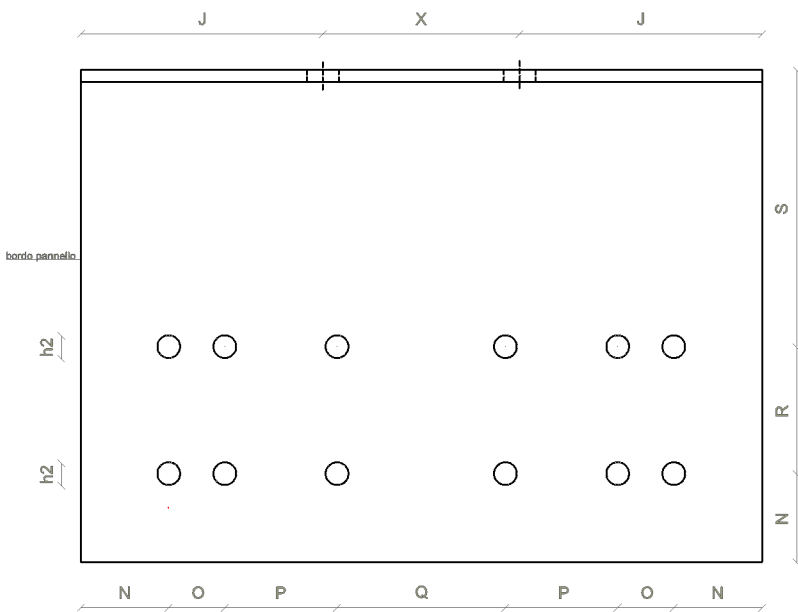
Section A-A



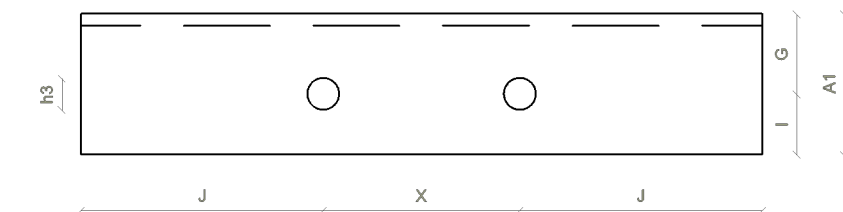
Lateral view

N

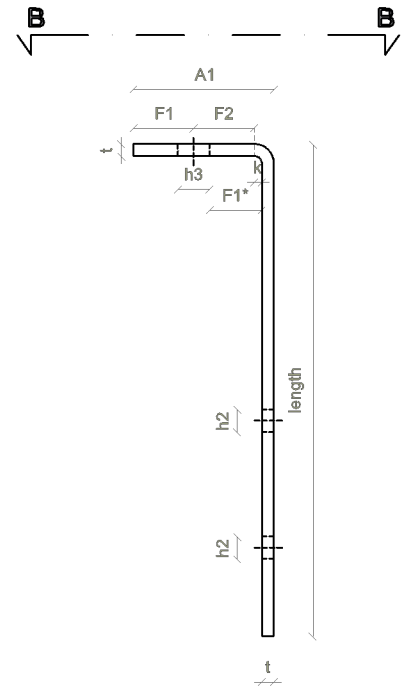
FREE PROFILE



Front view



View B-B

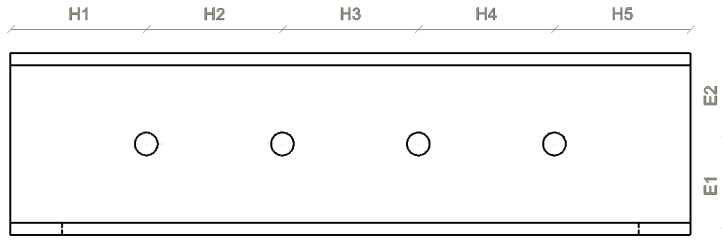


Lateral view

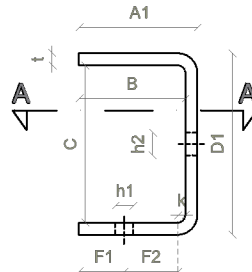
P

Prototype
ALT-M20

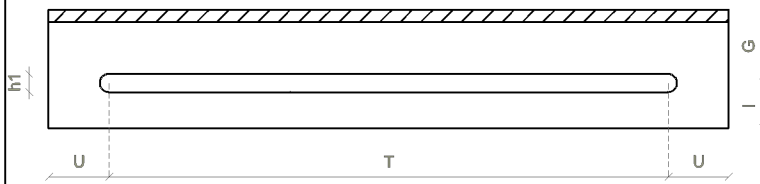
ANCHOR PROFILE



Front view



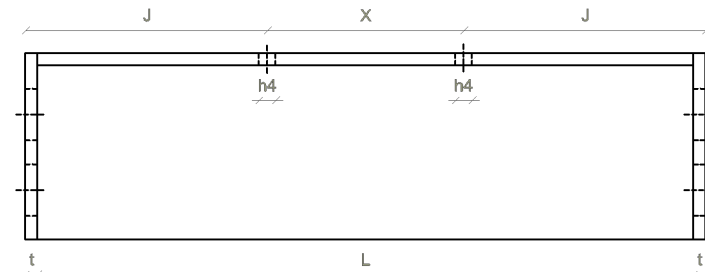
Lateral view



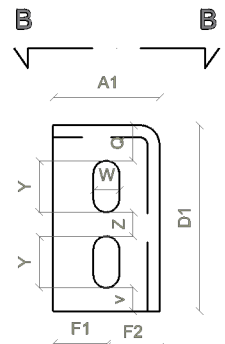
Section A-A

Q

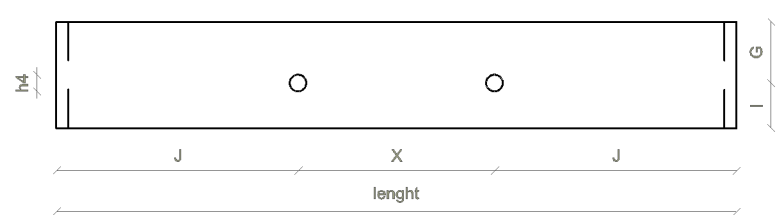
ALIGNMENT COMPONENT



Front view



Lateral view (right and left)



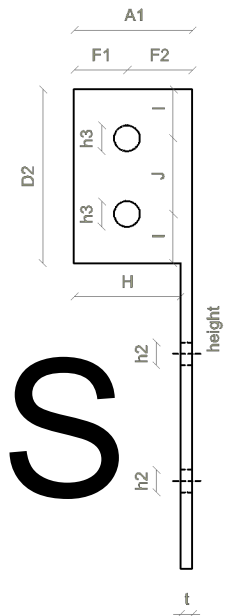
View B-B

R

FREE PROFILE



Front view



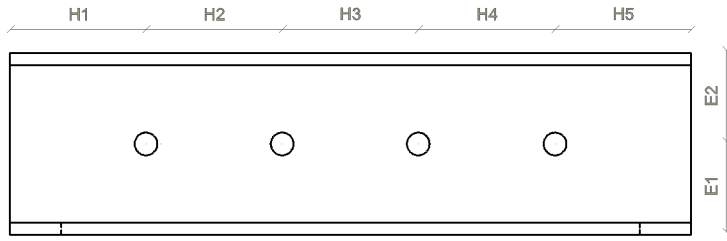
Lateral view (right and left)

S

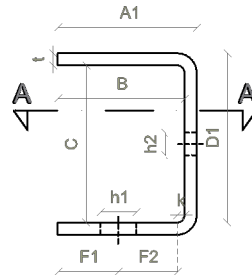
Prototype

ALT-AS-M10

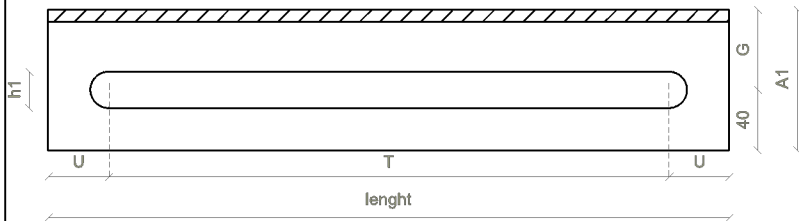
ANCHOR PROFILE



Front view



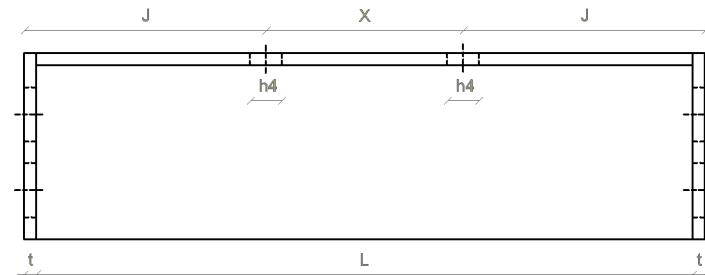
Lateral view



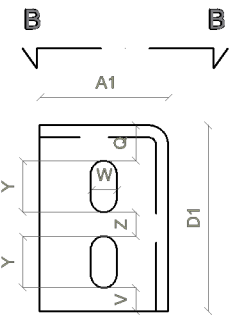
Section A-A



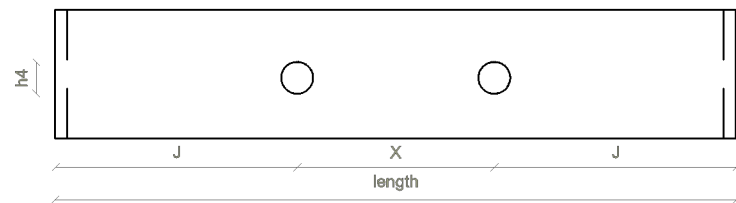
ALIGNMENT COMPONENT



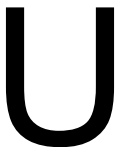
Front view



Lateral view
(right and left)



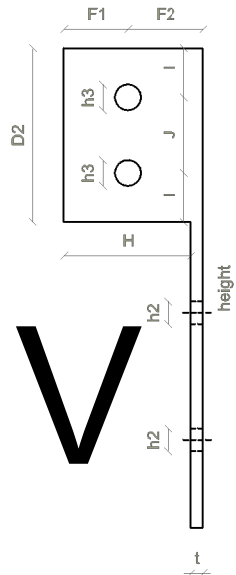
View B-B



FREE PROFILE



Front view

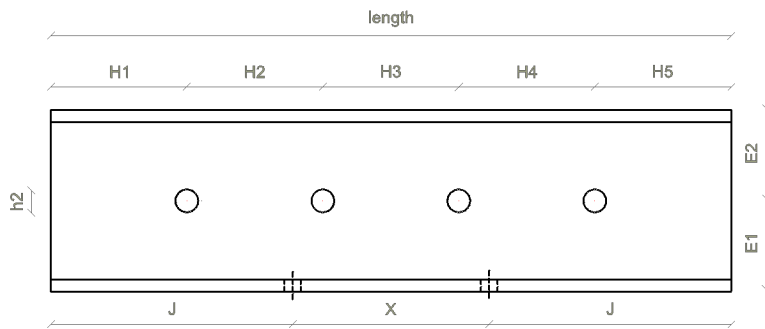


Lateral view
(right and left)

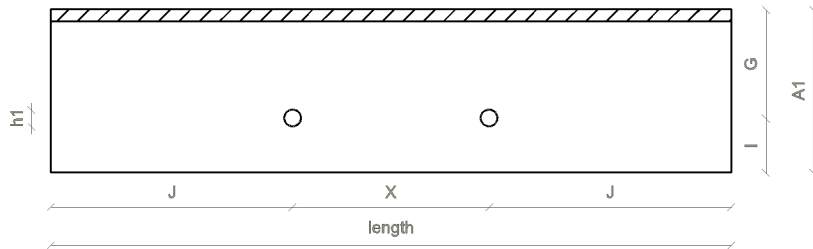
Prototype

ALT-AS-M20

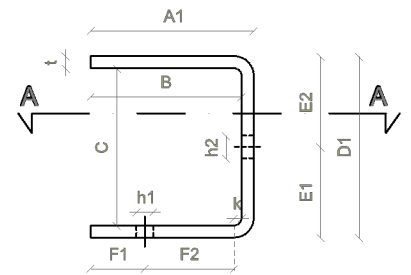
ANCHOR PROFILE



Front view



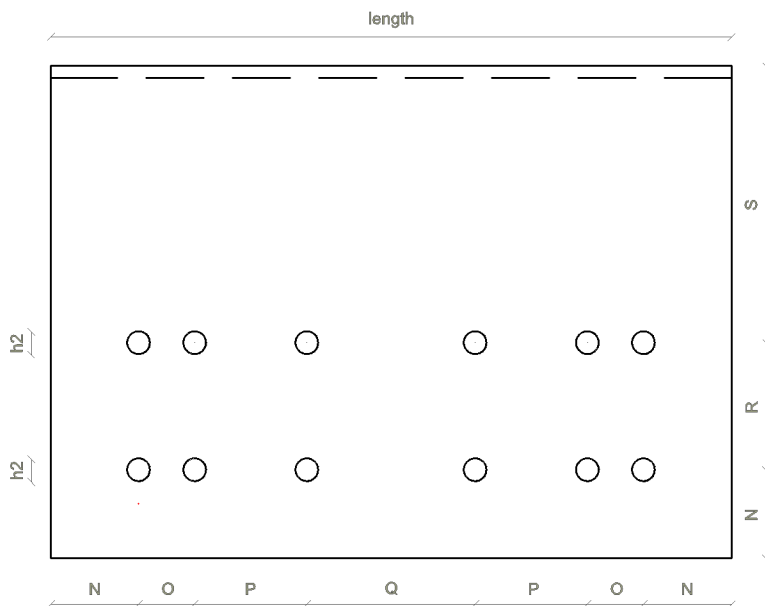
Section A-A



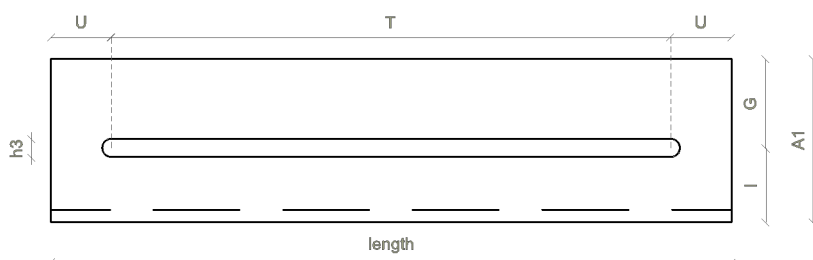
Lateral view



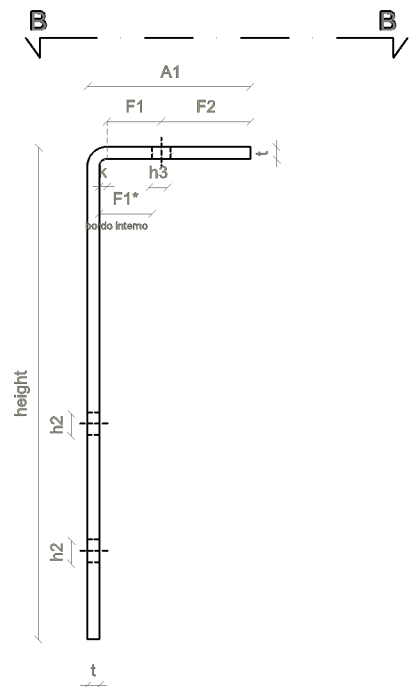
FREE PROFILE



Front view



View B-B

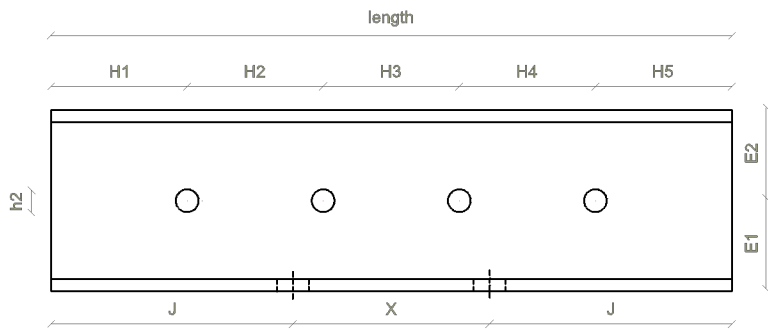


Lateral view

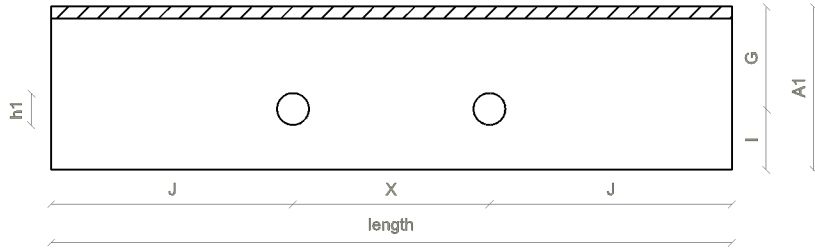


Prototype
HYBRID-M10

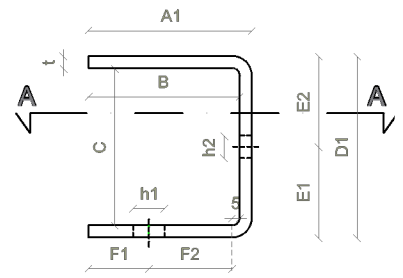
ANCHOR PROFILE



Front view



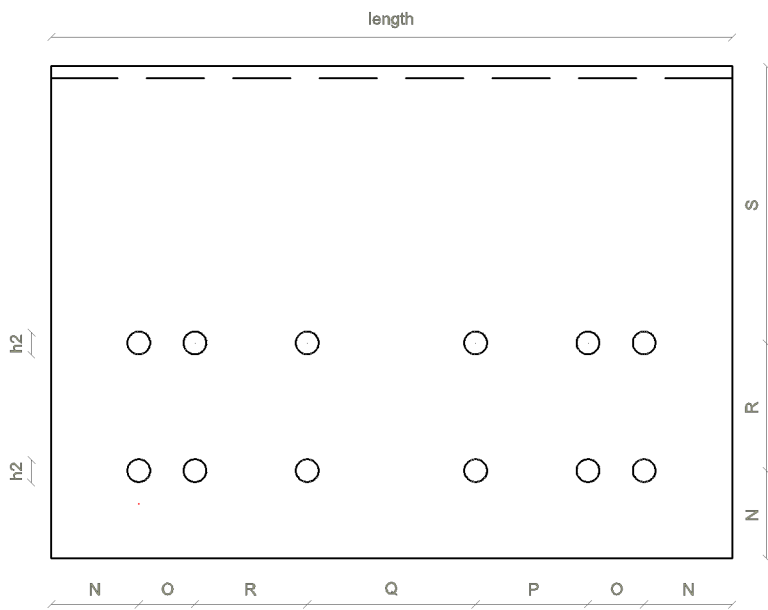
Section A-A



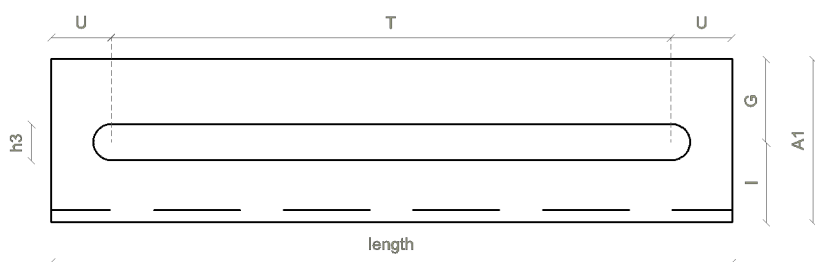
Lateral view



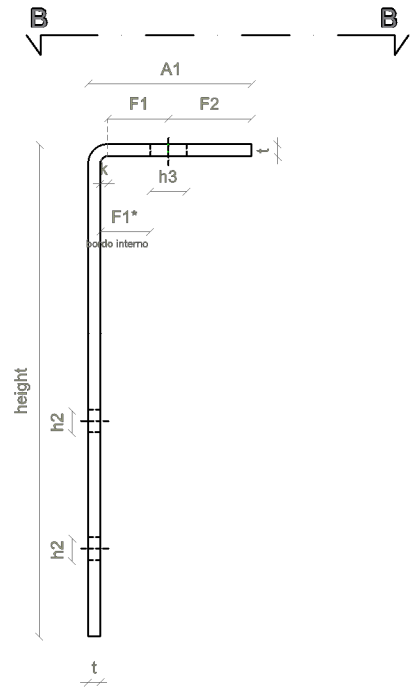
FREE PROFILE



Front view



View B-B



Lateral view

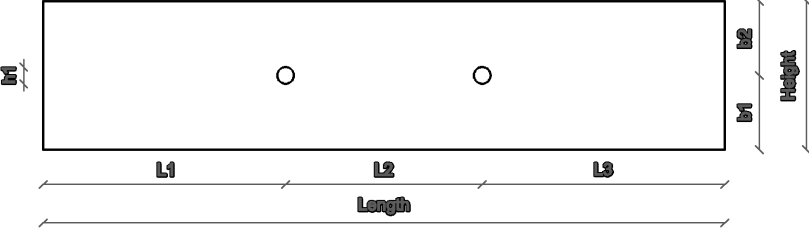


Prototype

HYBRID-M20

Additional plates (thickness: 8 mm)

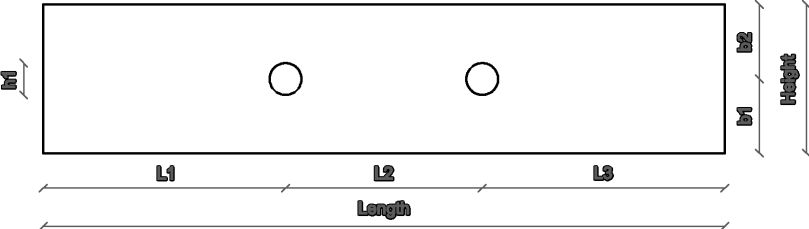
STD-1H-M10



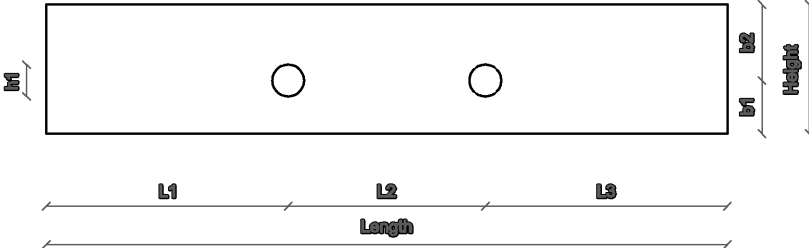
HYBRID-M10



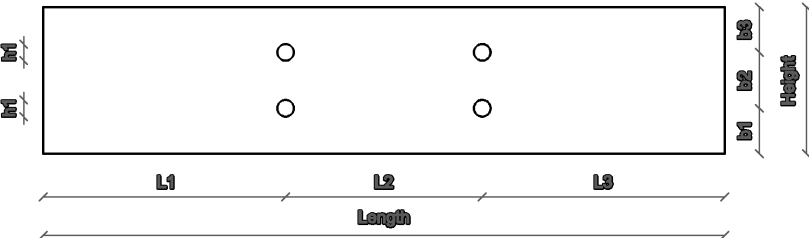
STD-1H-M20



HYBRID-M20

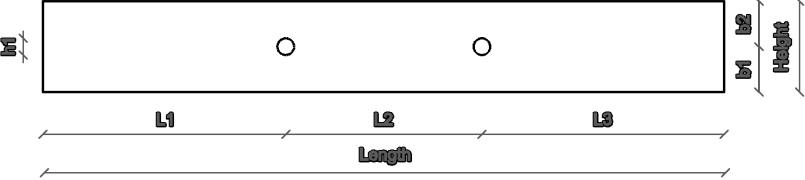


STD-2H-M10



Additional plates (thickness: 8 mm)

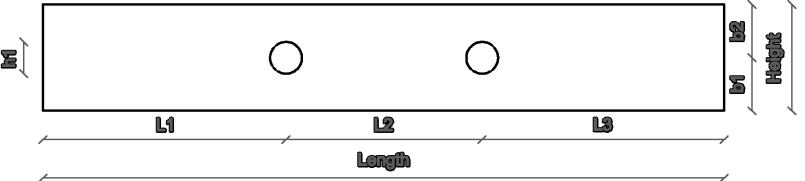
ALT-M10



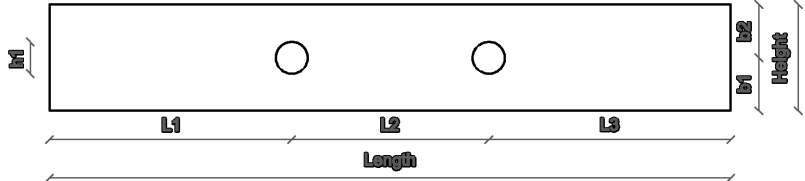
ALT-AS-M10



ALT-M20



ALT-AS-M20



Appendix C:

Results from experimental testing

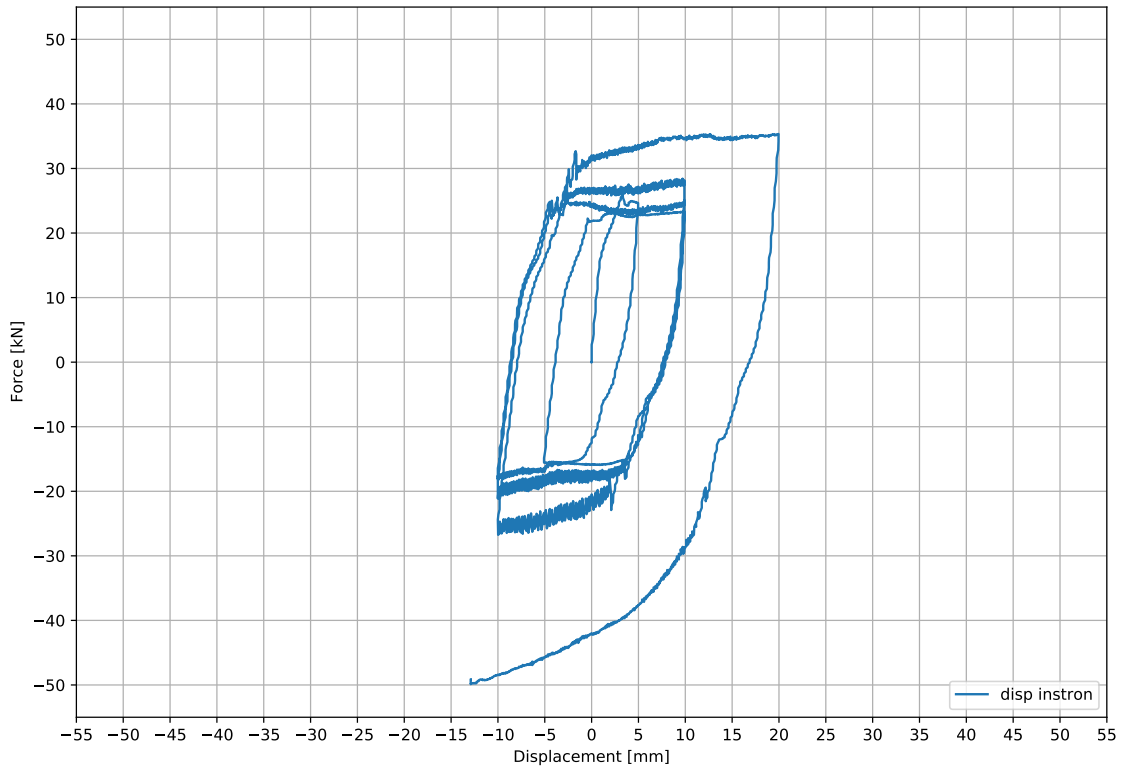
Contents

1 Test 1 - STD 3 - 08.02.21	2
2 Test 2 - STD-1H 2 - 08.02.21	6
3 Test 3 - STD-R 2 - 09.02.21	10
4 Test 4 - STD-1H 3 - 09.02.21	14
5 Test 5 - ALT 2 - 09.02.21	18
6 Test 6 - ALT 2 - 10.02.21	22
7 Test 7 - ALT 2 - 11.02.21	26
8 Test 8 - ALT 2 - 12.02.21	30
9 Test 9.1 to 9.3 - ALT-M10 1 - 22.04.21	34
9.1 Test 9.1	34
9.2 Test 9.2	39
9.3 Test 3	43
10 Test 10.1 to 10.5 - ALT-M20 1 - 23.04.21	47
10.1 Test 10.2	52
10.2 Test 10.3	56
10.3 Test 10.4	60
10.4 Test 10.5	63
11 Test 11 - ALT-M20 1 - 14.05.21	68
12 Test 12 - ALT-M20 2 - 15.05.21	73
13 Test 13 - ALT-M10 1 - 15.05.21	78
14 Test 14 - ALT-M10 1 - 16.05.21	83
15 Test 15 - ALT-AS-M10 1 - 16.05.21	88
16 Test 16 - ALT-AS-M20 1 - 16.05.21	93
17 Test 17 - STD-1H-M10 1 - 16.05.21	98
18 Test 18 - STD-1H-M20 1 - 16.05.21	103
19 Test 19 - STD-2H-M10 1 - 18.05.21	108
20 Test 20 - HYBRID-M10 1 - 18.05.21	113
21 Test 21 - HYBRID-M20 1 - 18.05.21	118

Chapter 1

Test 1 - STD_3 - 08.02.21

Force-Displacement



Force-Displacement

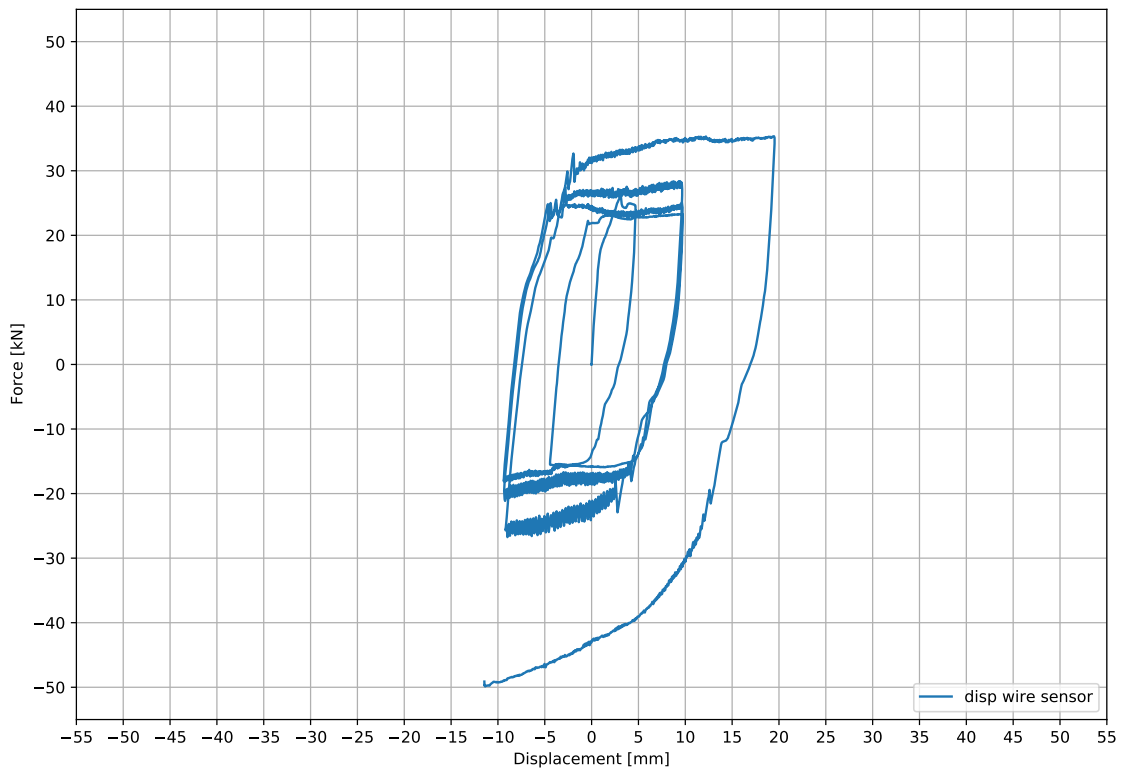


Figure 1.1: Load displacement graph.

Difference displacements - Time

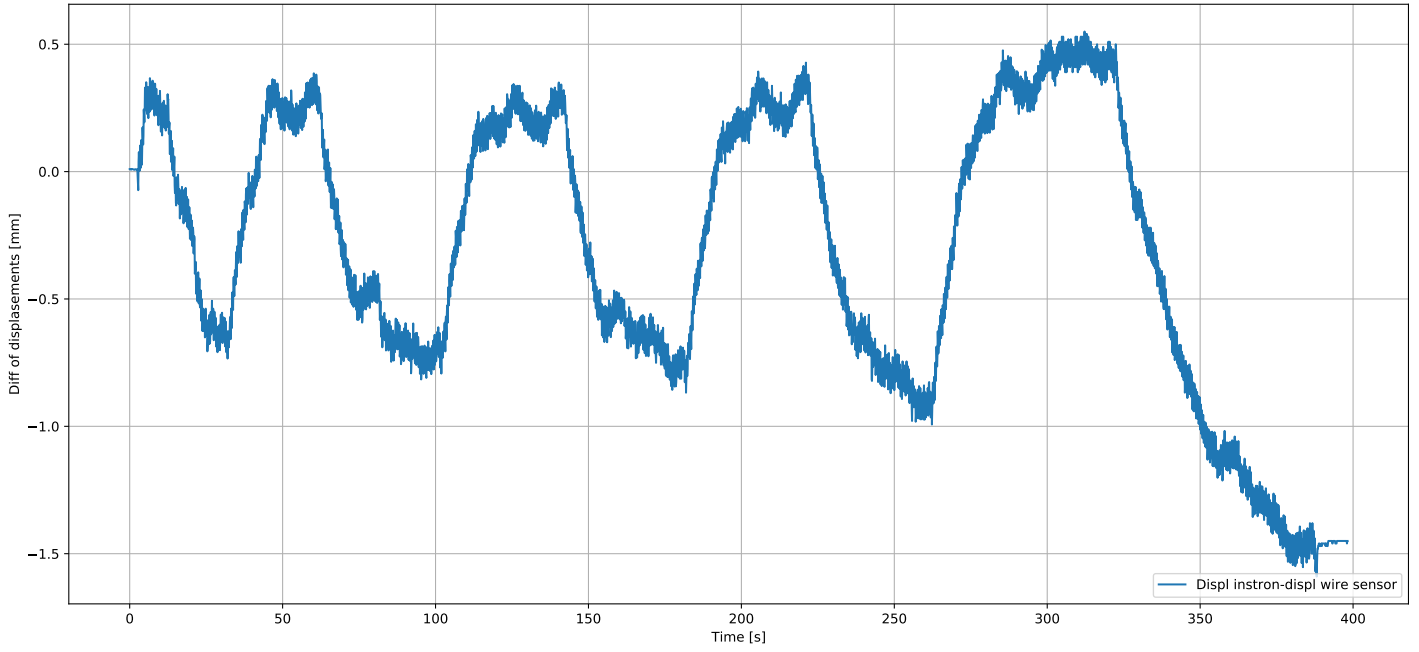


Figure 1.2: Difference of displacement between instron press and wire sensor.

Displacement of columns

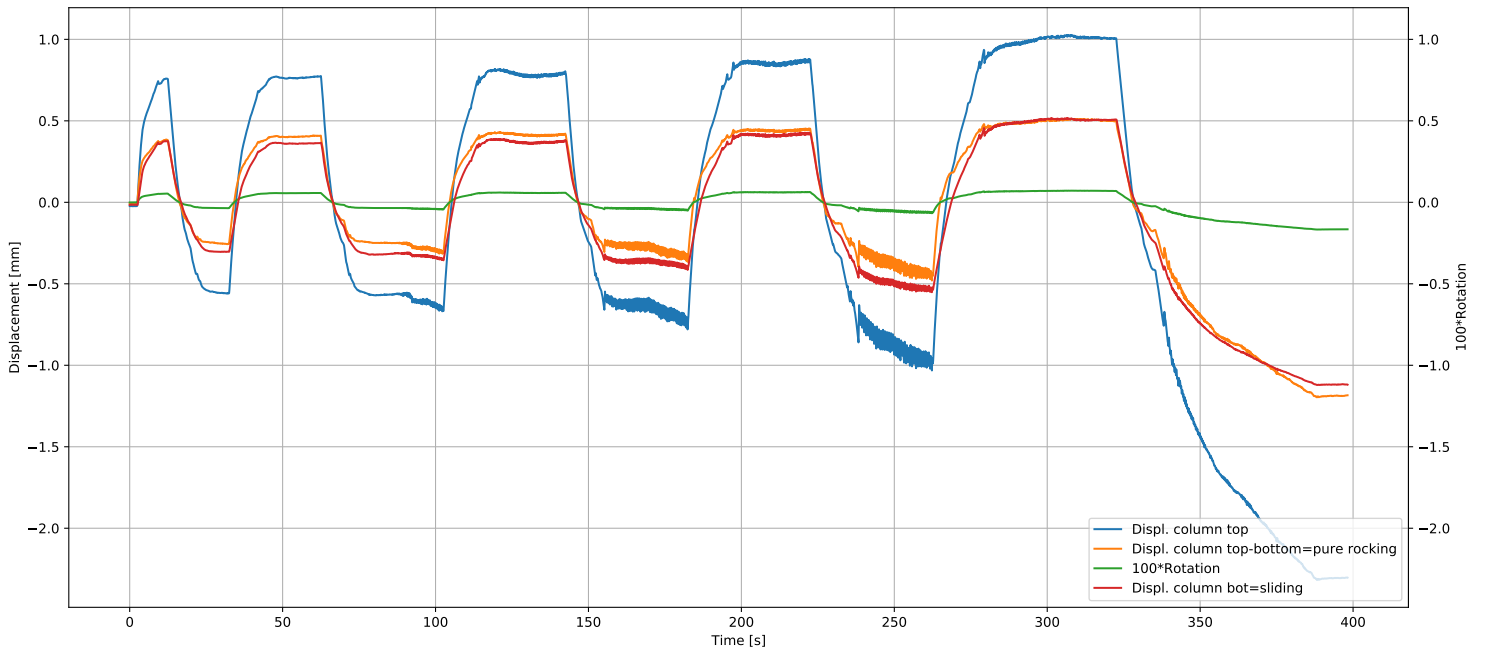


Figure 1.3: Movements of the column.

Force and displacements - time

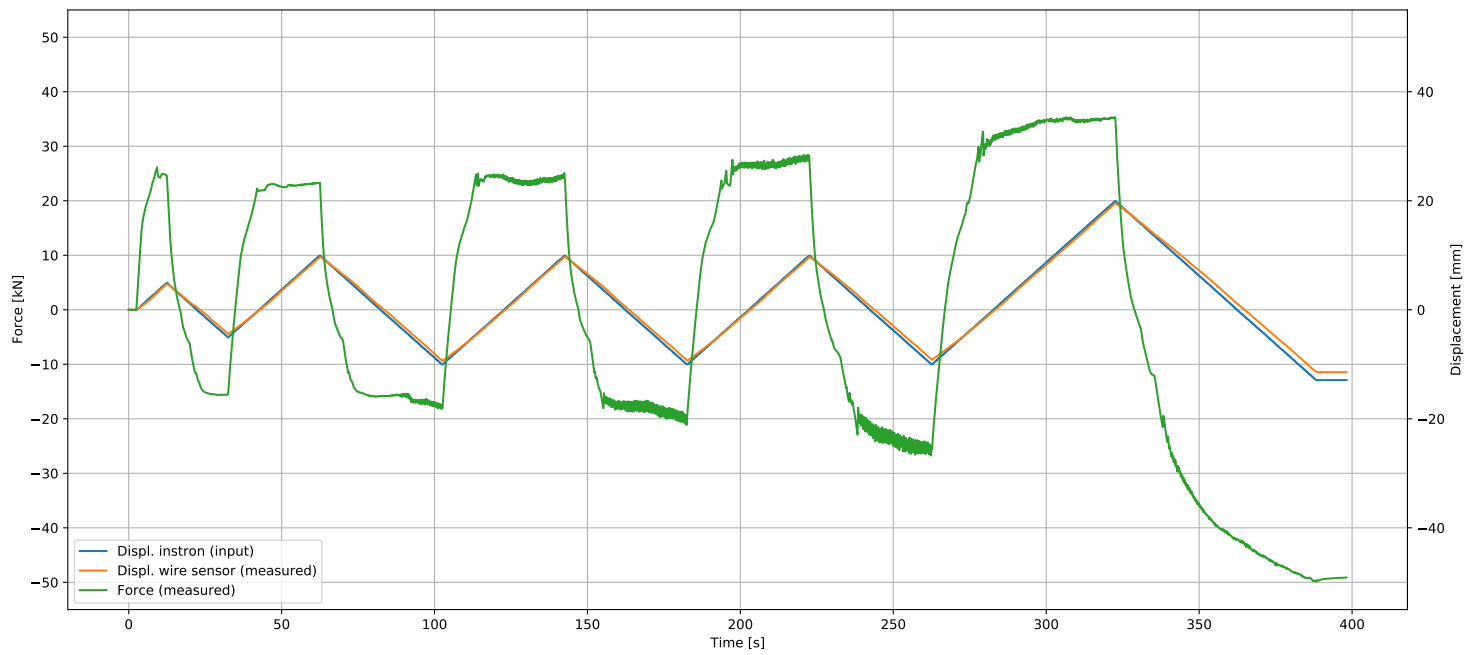
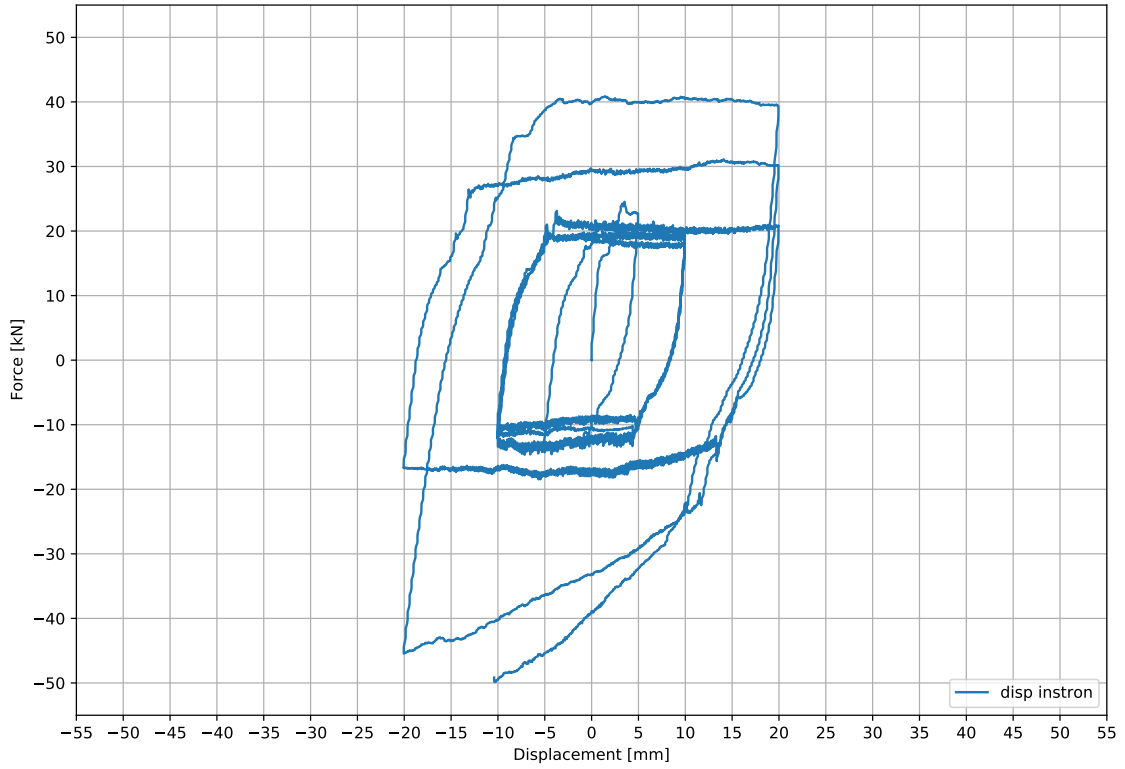


Figure 1.4: Force and displacement plotted against time.

Chapter 2

Test 2 - STD-1H_2 - 08.02.21

Force-Displacement



Force-Displacement

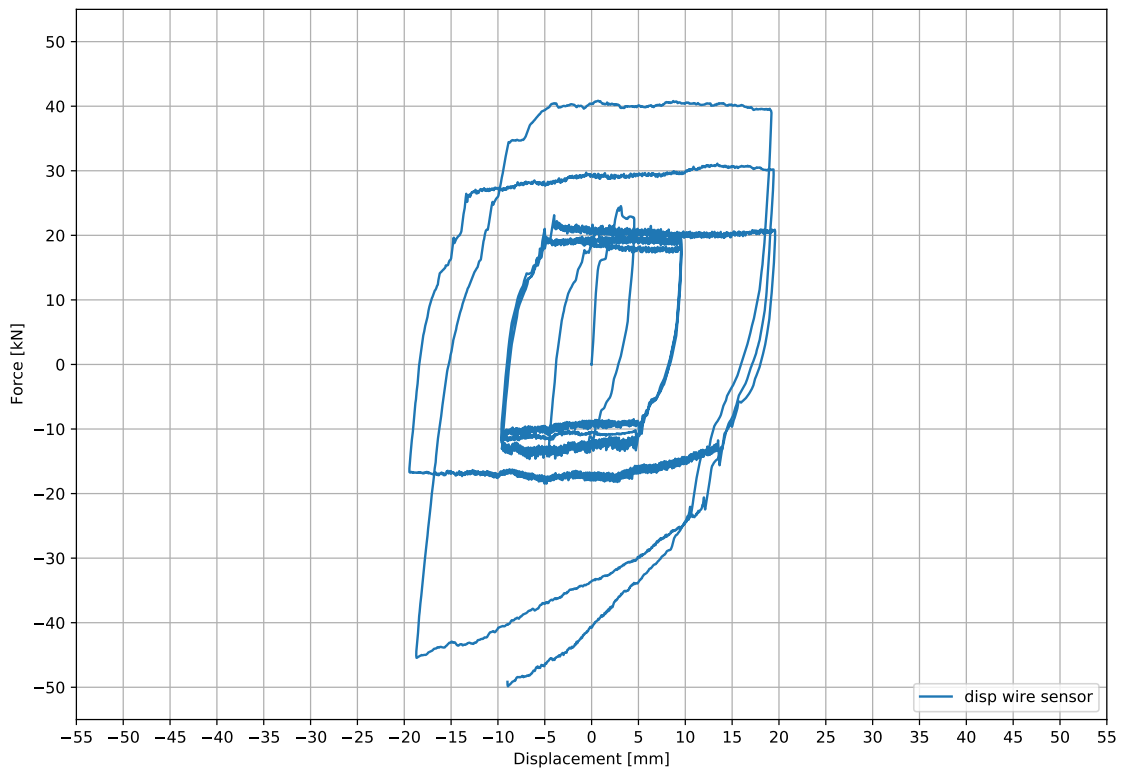


Figure 2.1: Load displacement graph.

Difference displacements - Time

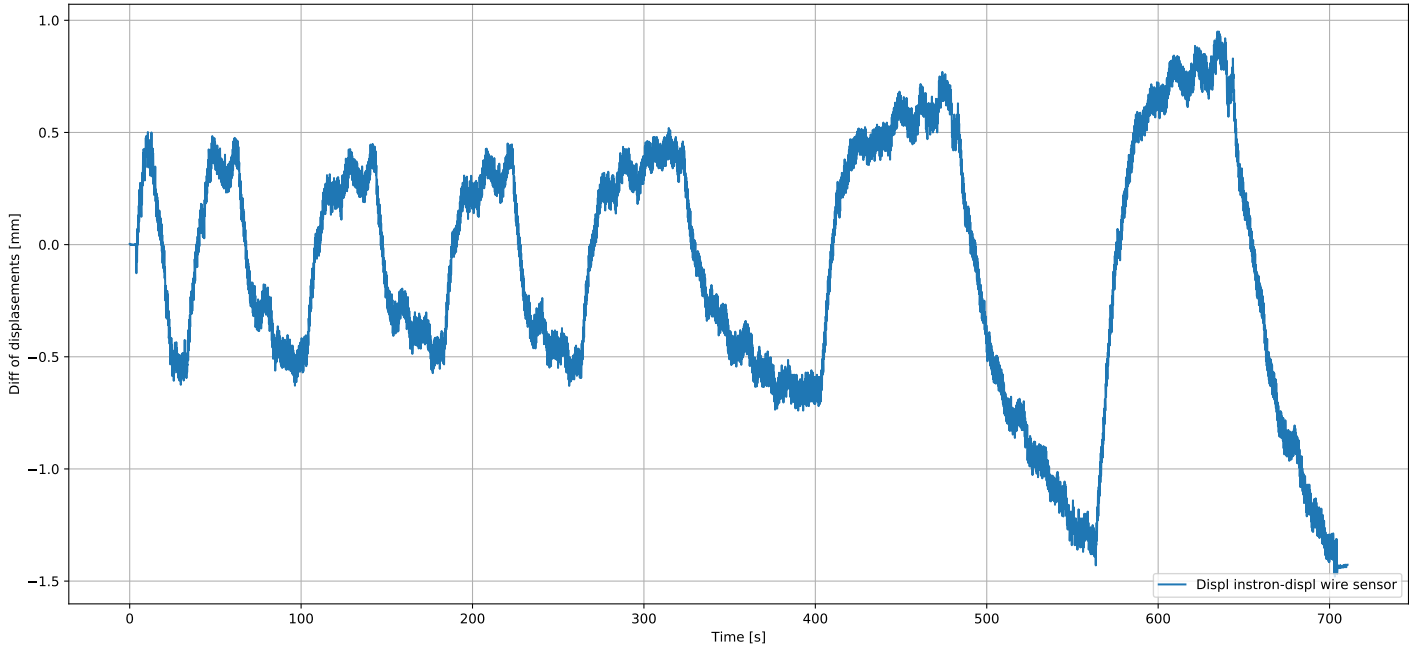


Figure 2.2: Difference of displacement between instron press and wire sensor.

Displacement of columns

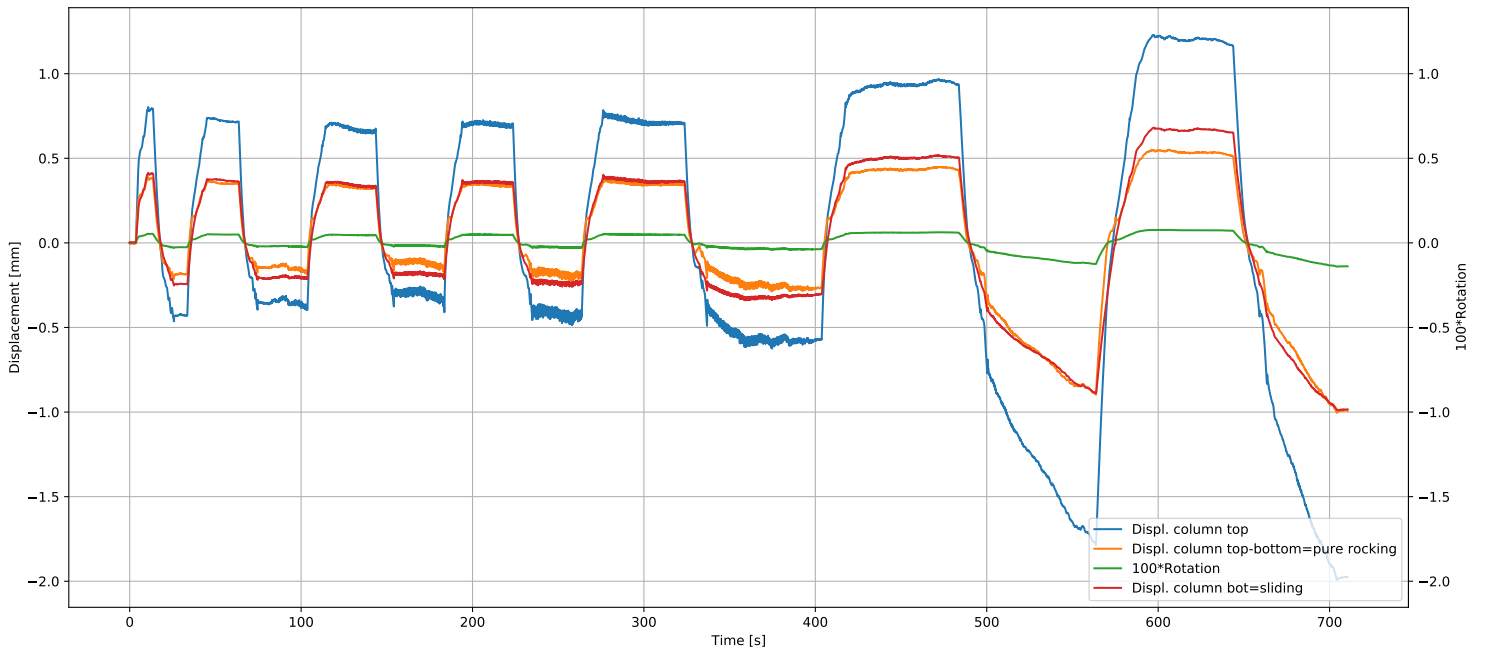


Figure 2.3: Movements of the column.

Force and displacements - time

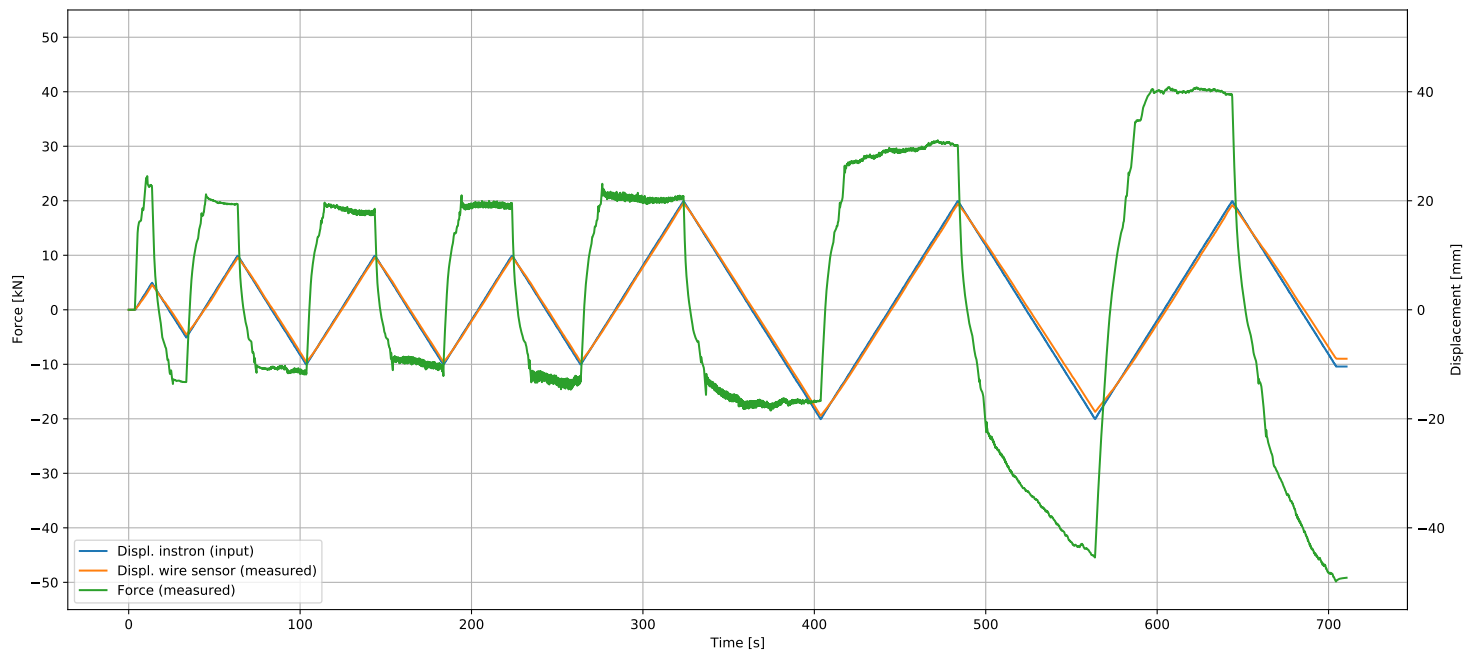
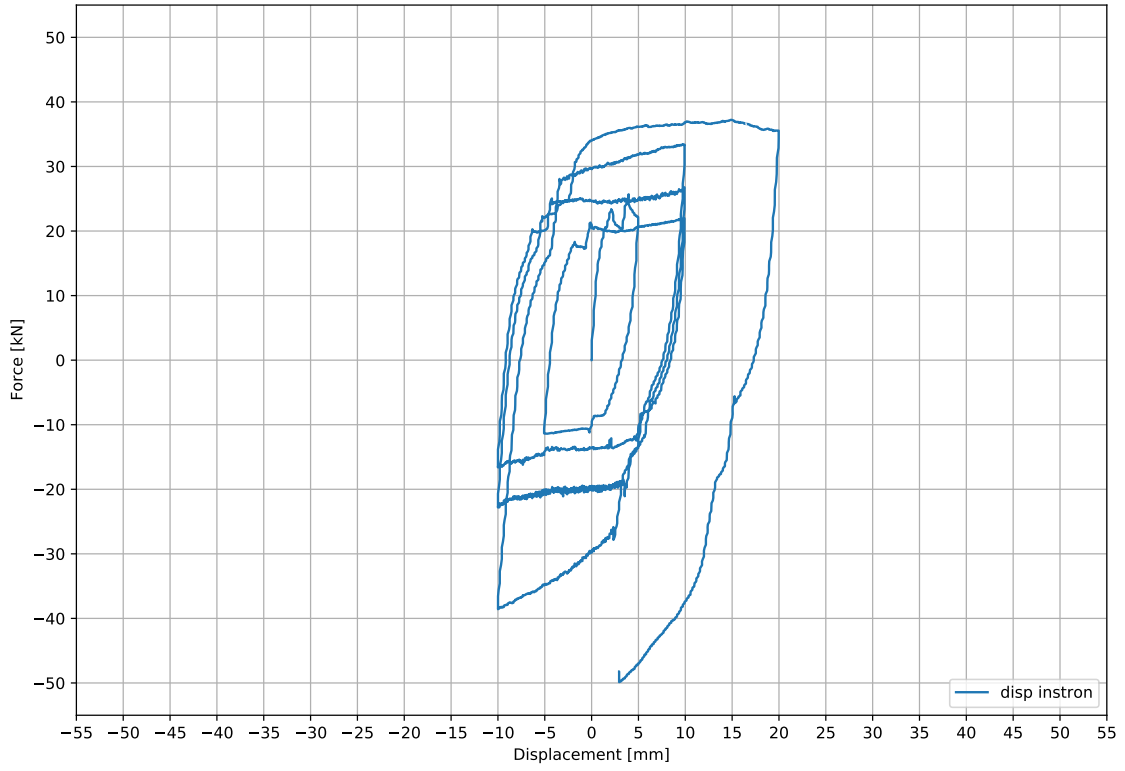


Figure 2.4: Force and displacement plotted against time.

Chapter 3

Test 3 - STD-R_2 - 09.02.21

Force-Displacement



Force-Displacement

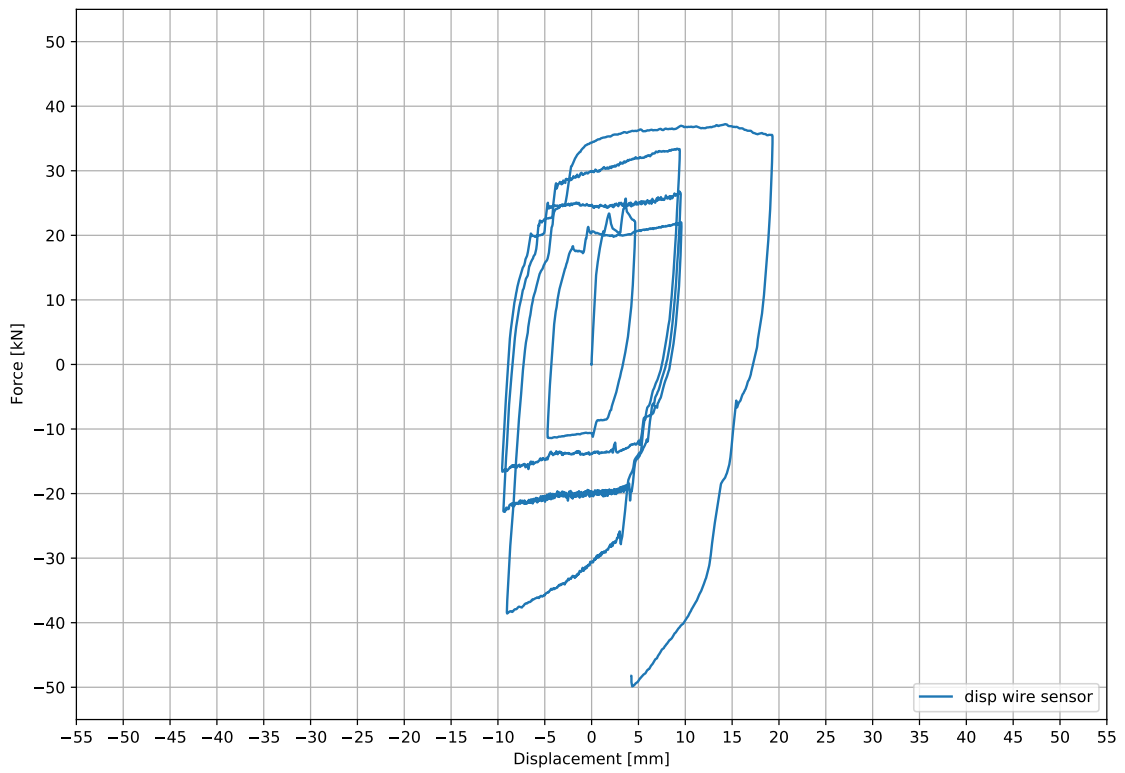


Figure 3.1: Load displacement graph.

Difference displacements - Time

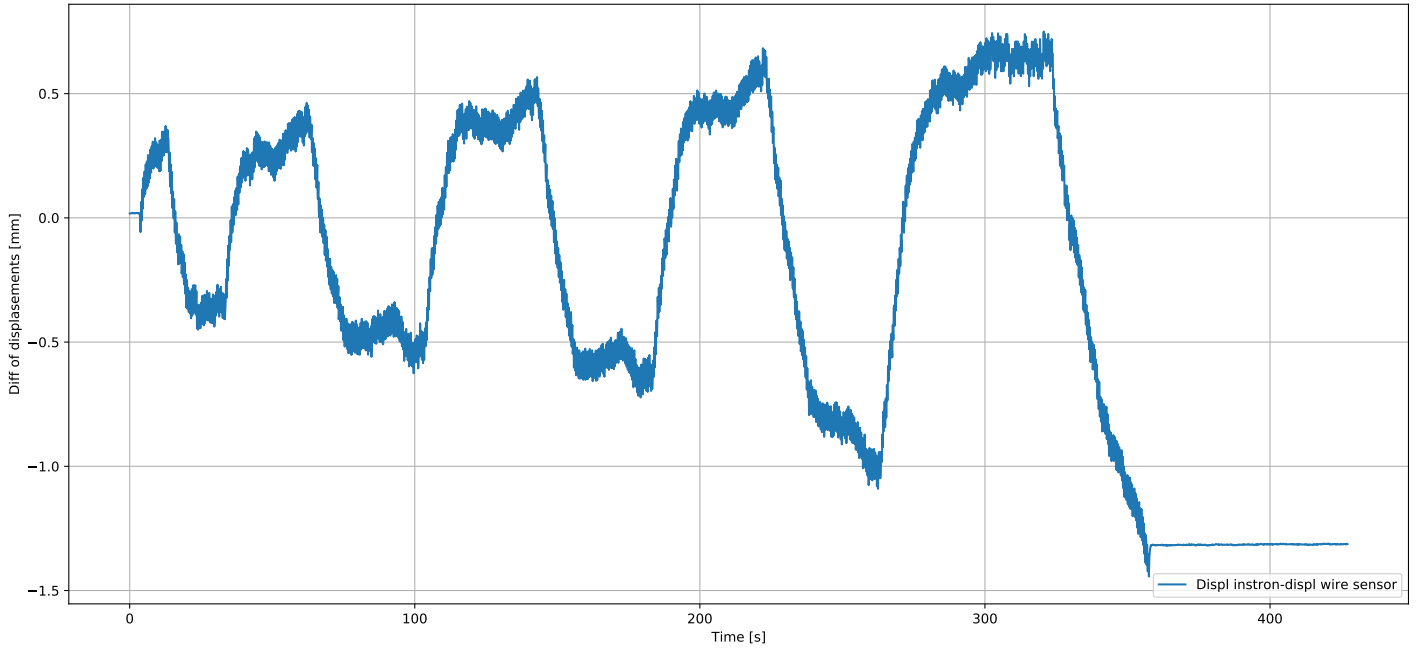


Figure 3.2: Difference of displacement between instron press and wire sensor.

Displacement of columns

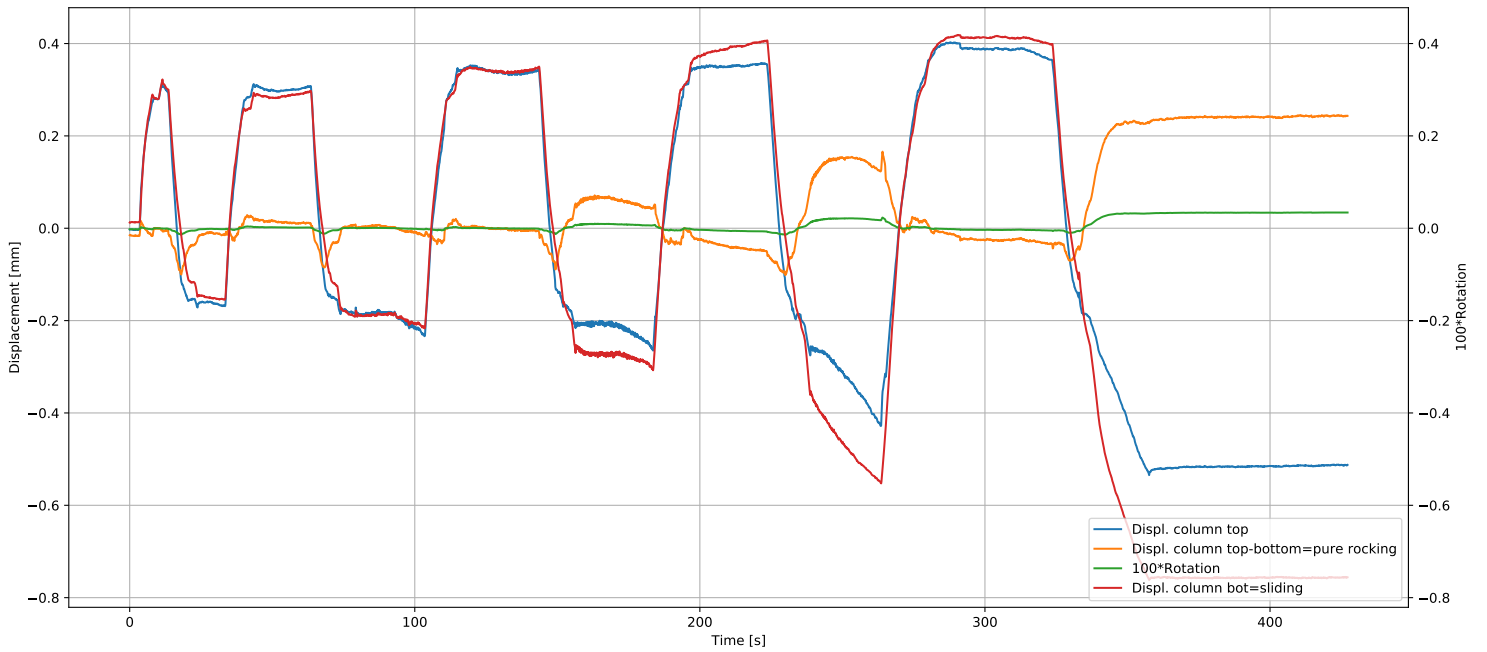


Figure 3.3: Movements of the column.

Force and displacements - time

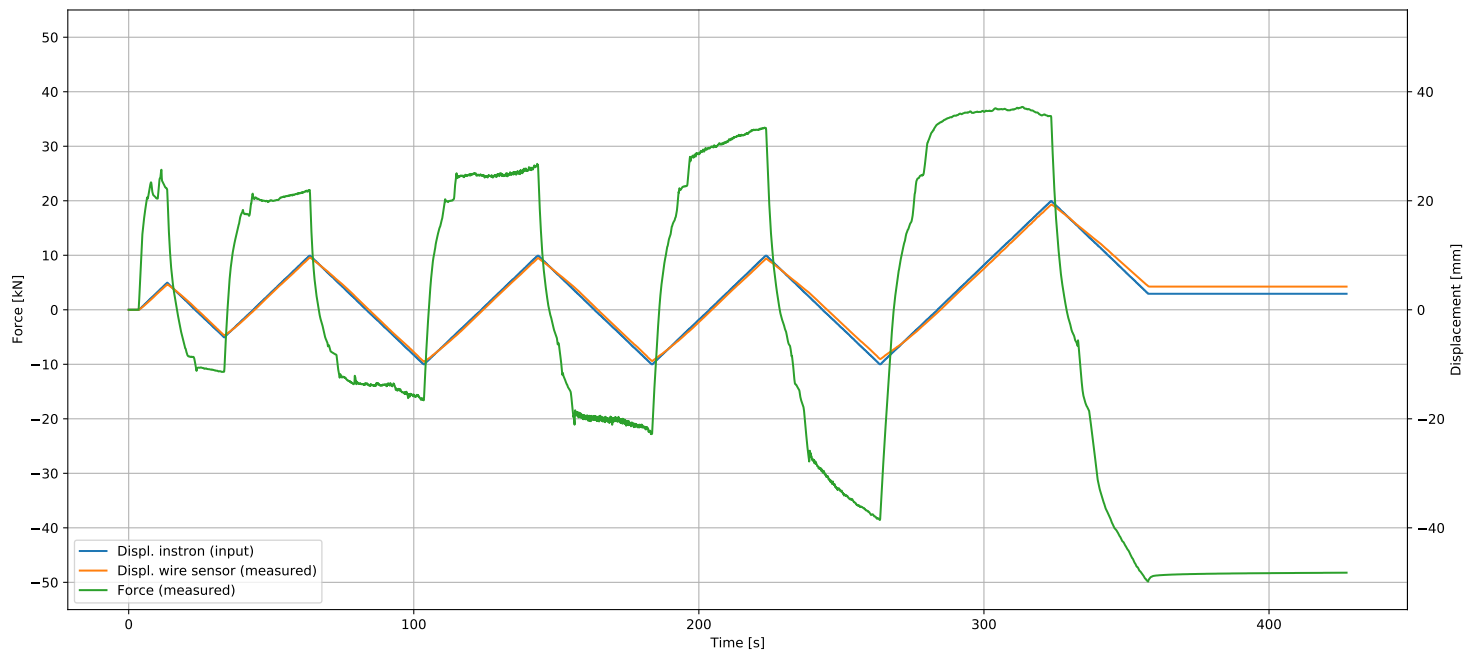
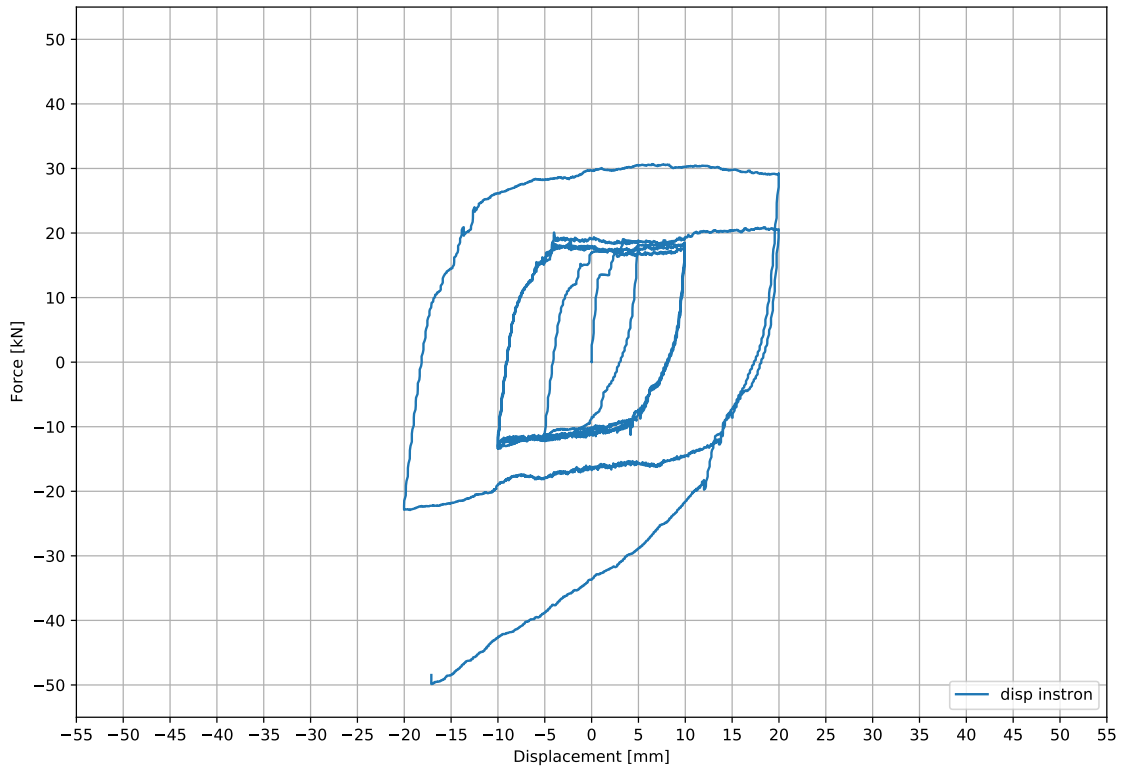


Figure 3.4: Force and displacement plotted against time.

Chapter 4

Test 4 - STD-1H_3 - 09.02.21

Force-Displacement



Force-Displacement

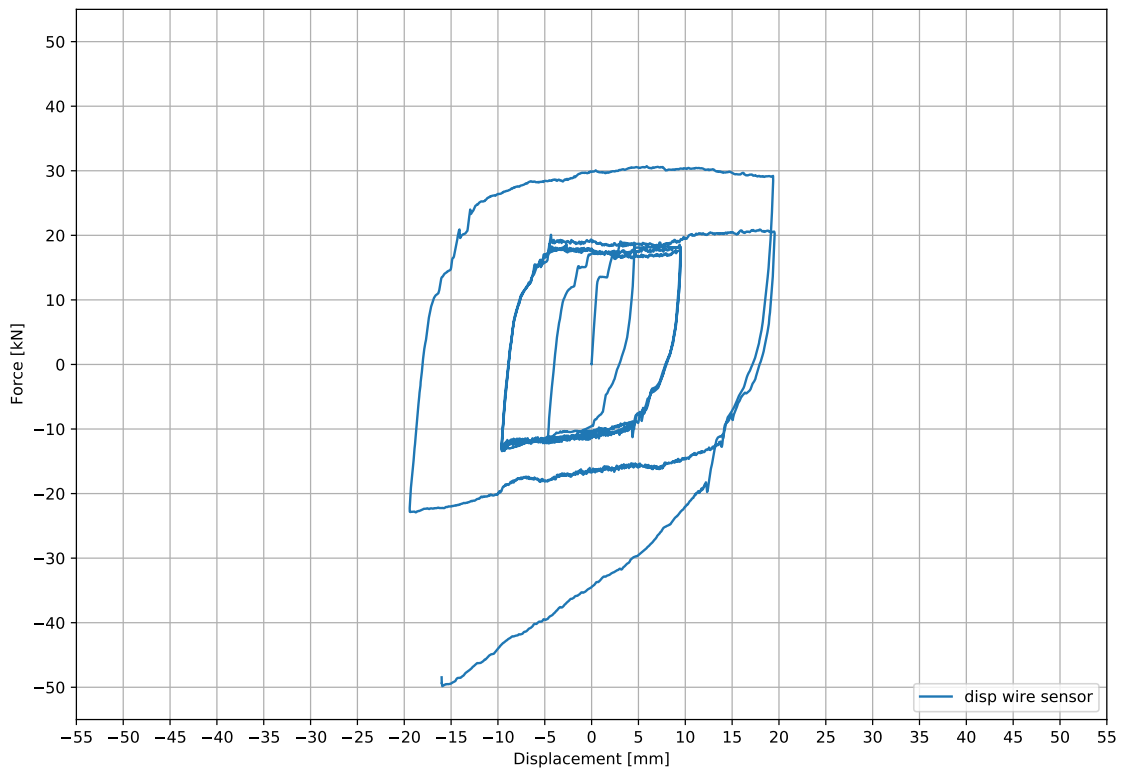


Figure 4.1: Load displacement graph.

Difference displacements - Time

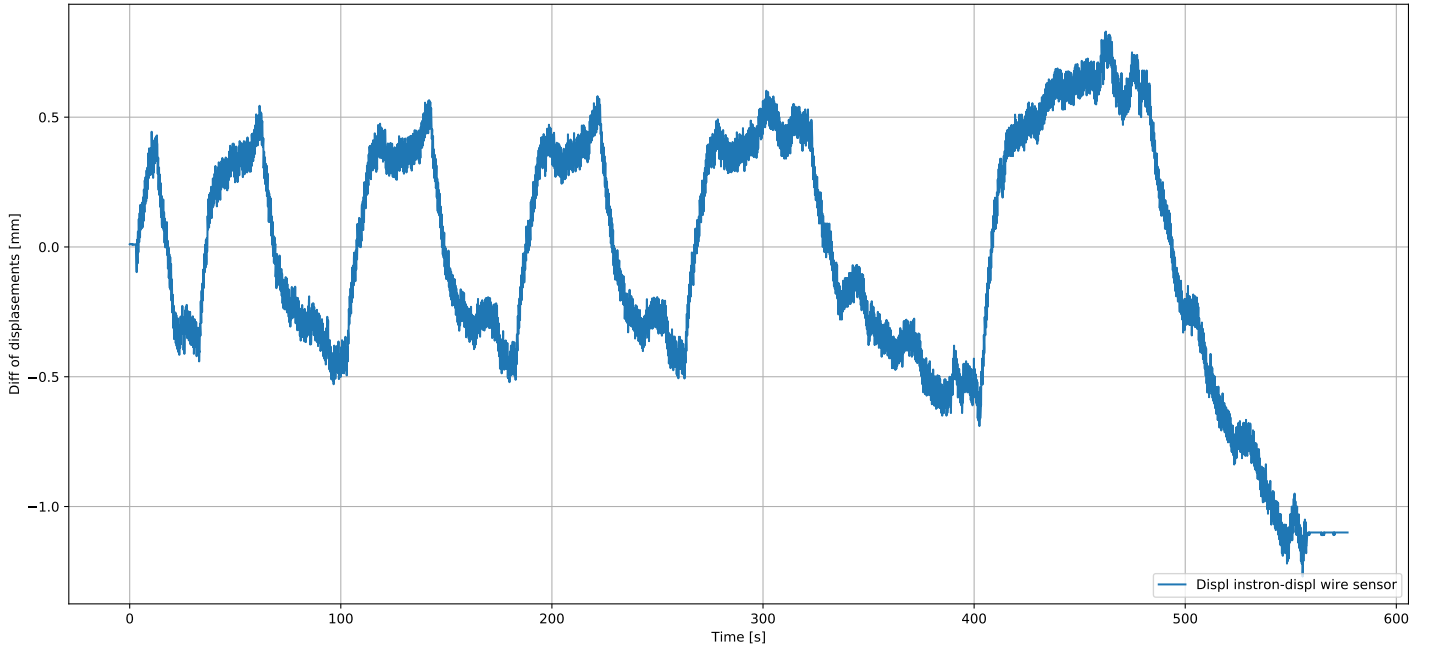


Figure 4.2: Difference of displacement between instron press and wire sensor.

Displacement of columns

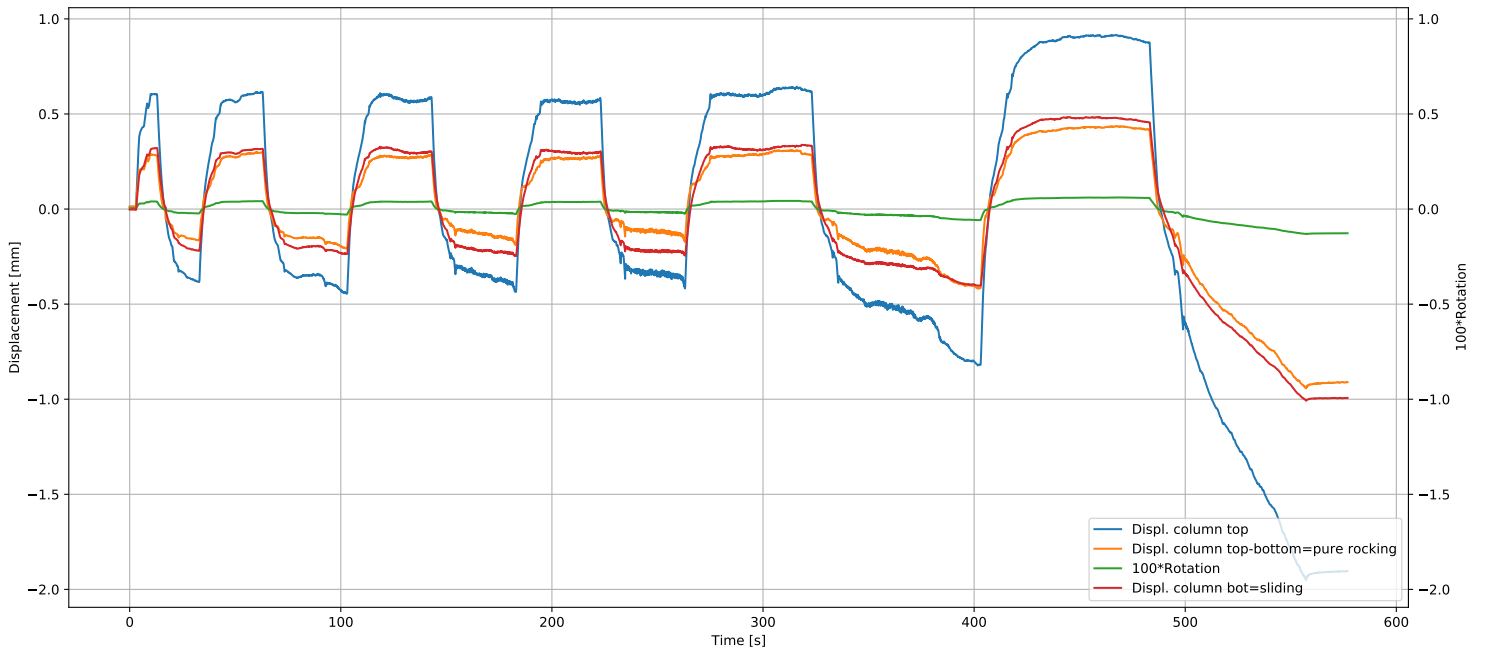


Figure 4.3: Movements of the column.

Force and displacements - time

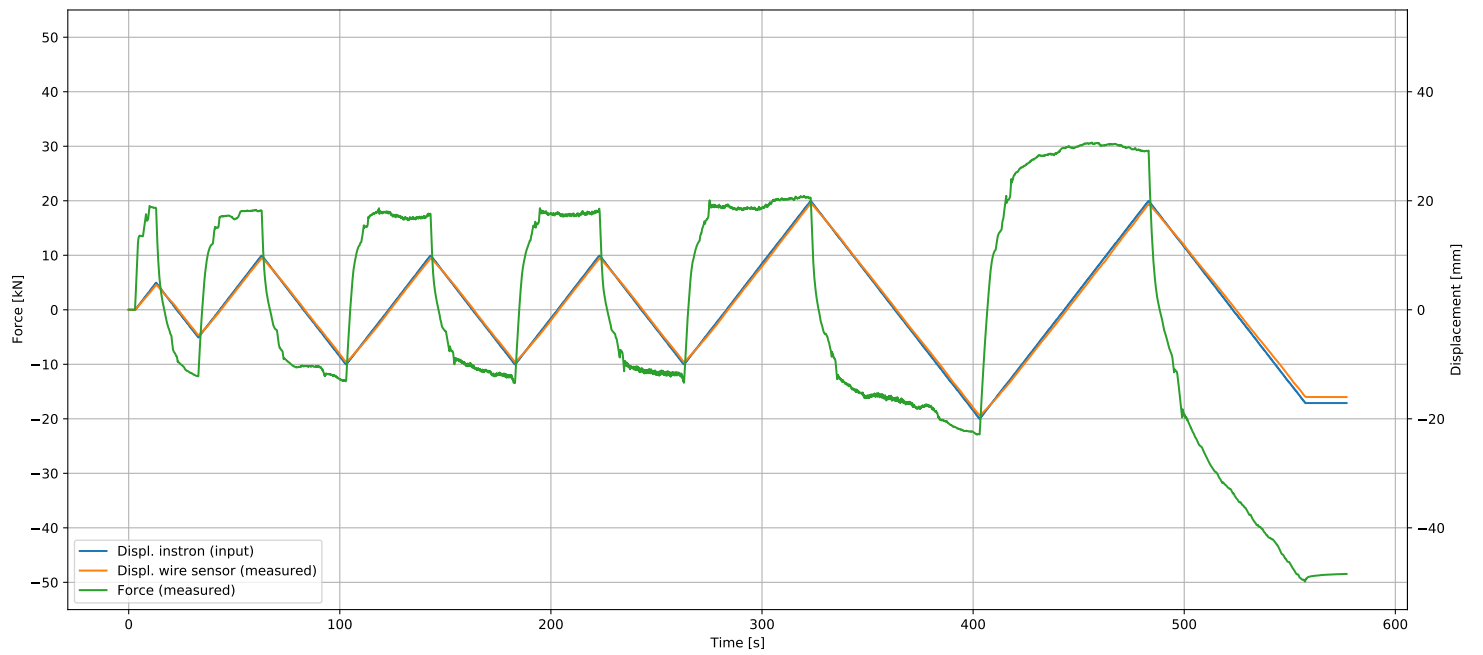
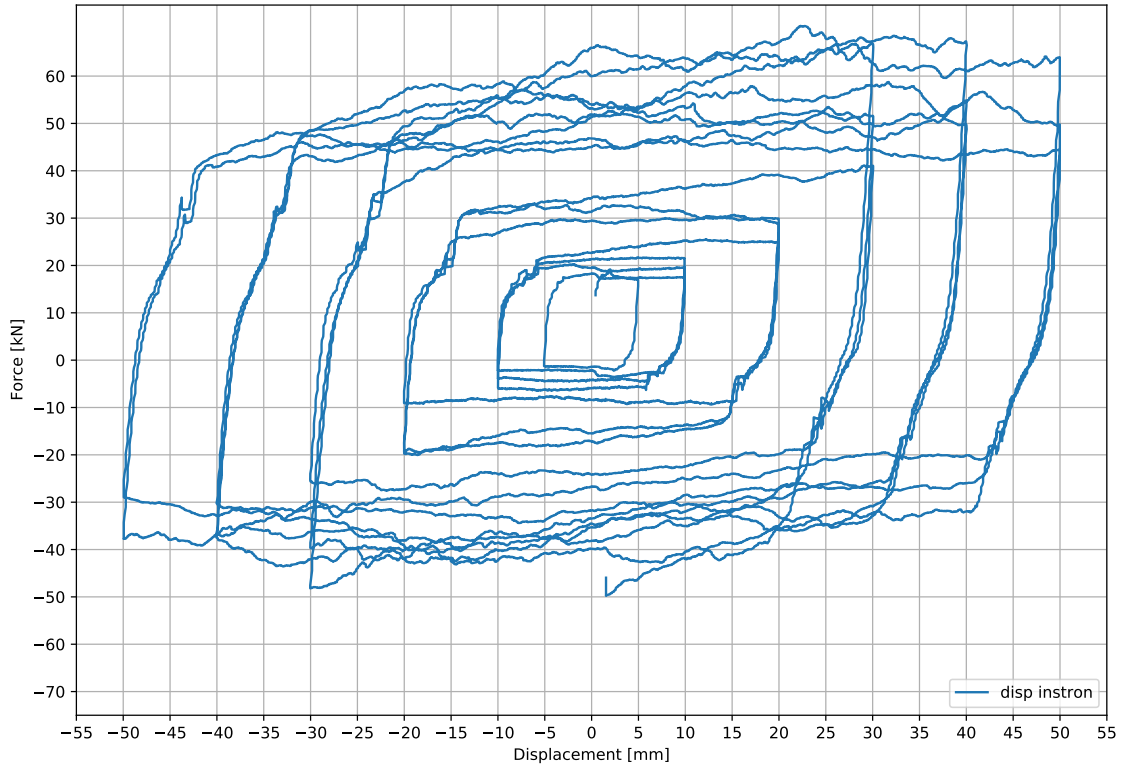


Figure 4.4: Force and displacement plotted against time.

Chapter 5

Test 5 - ALT_2 - 09.02.21

Force-Displacement



Force-Displacement

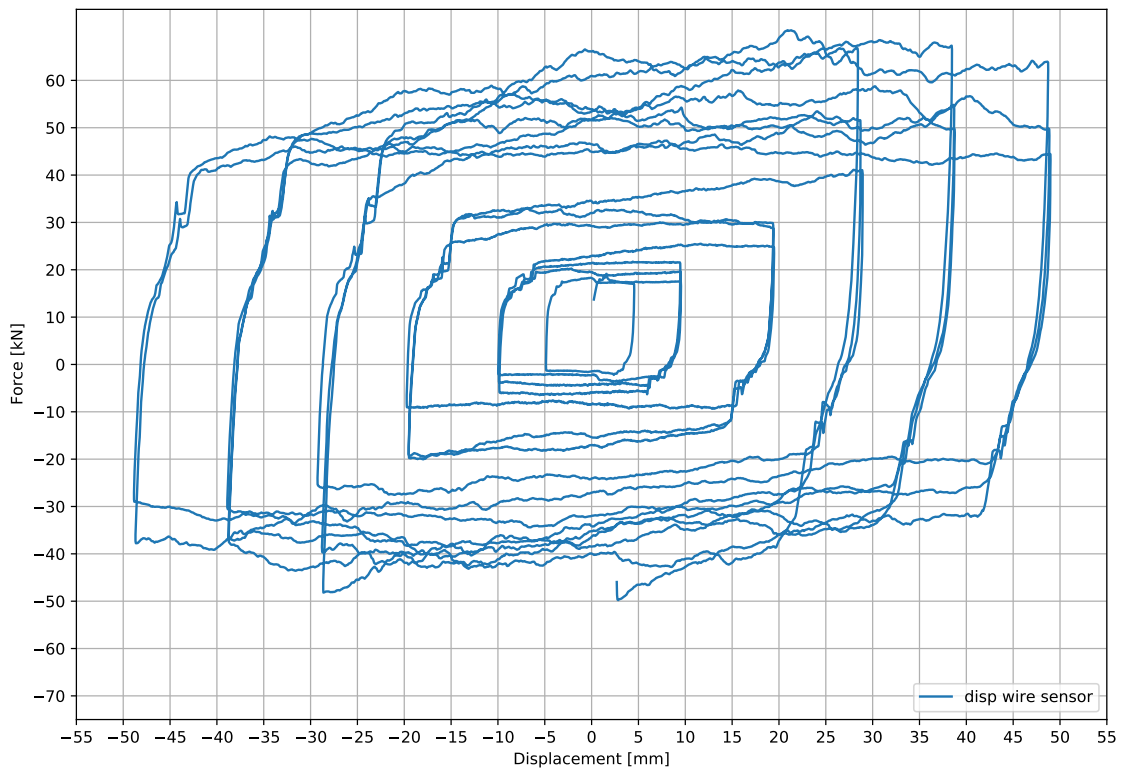


Figure 5.1: Load displacement graph.

Difference displacements - Time

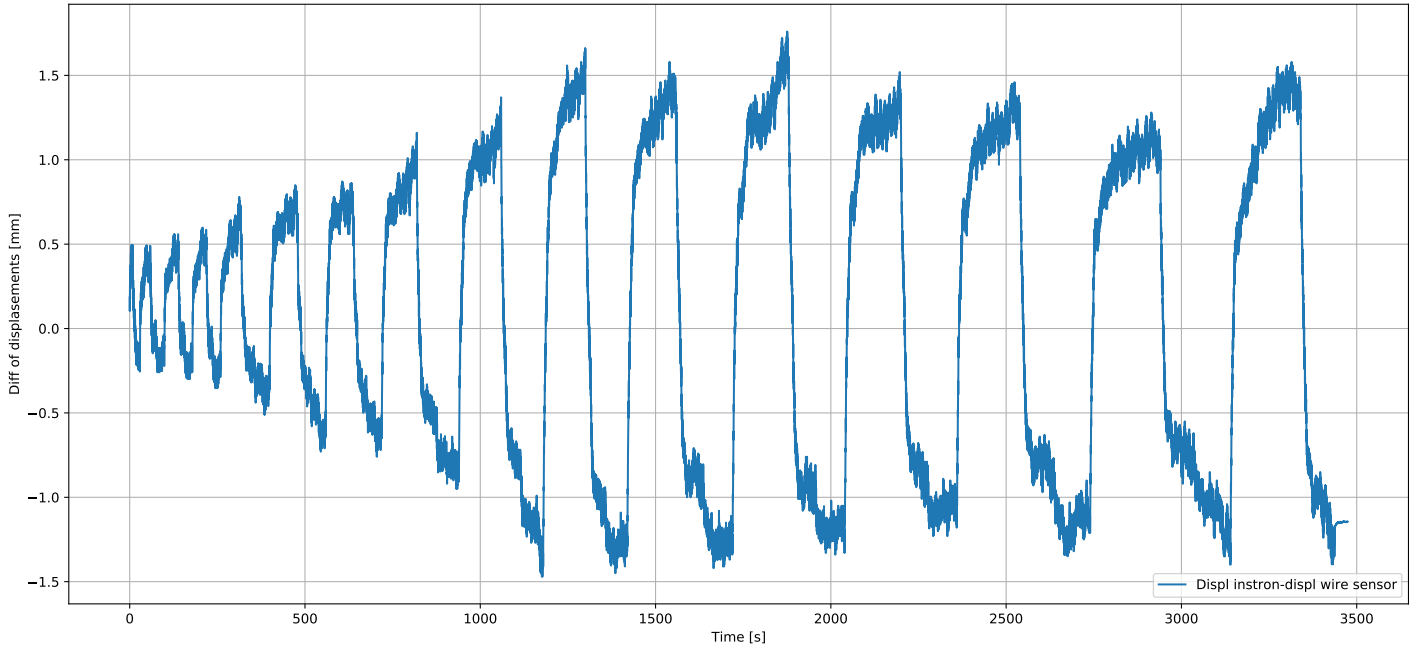


Figure 5.2: Difference of displacement between instron press and wire sensor.

Displacement of columns

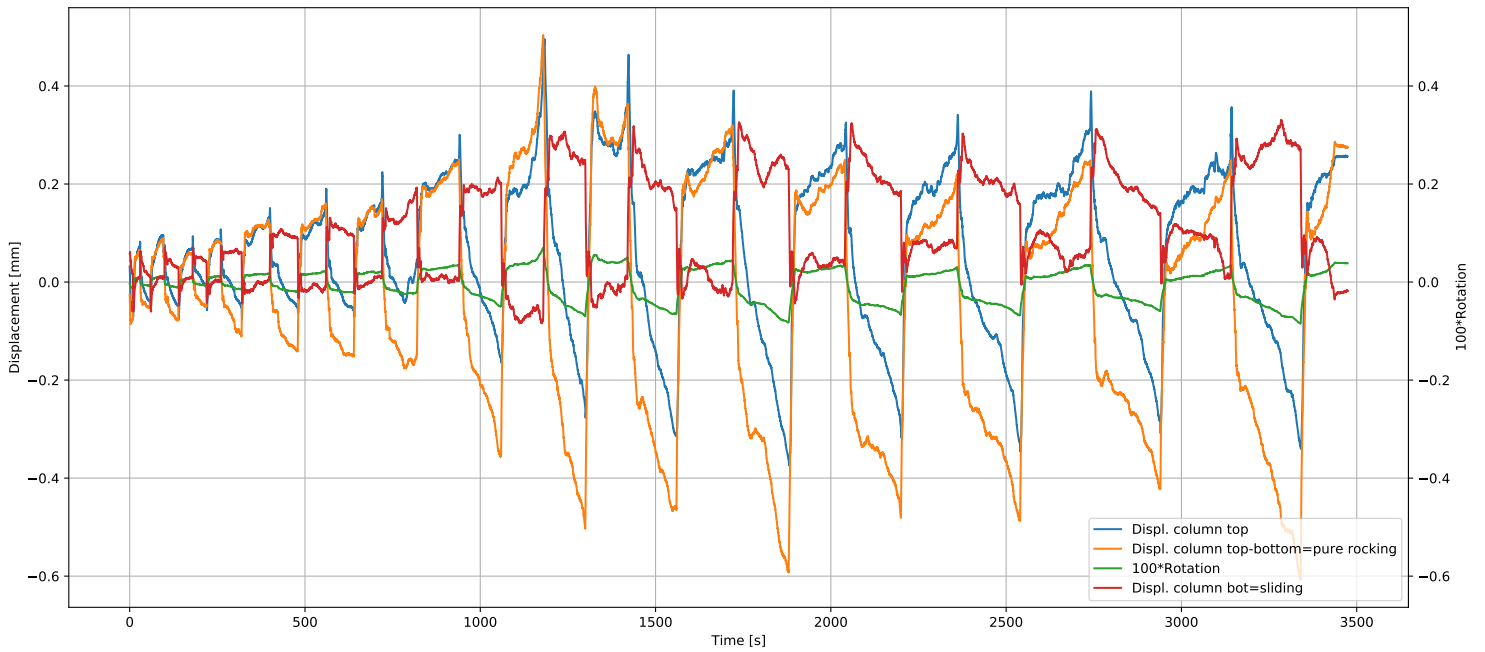


Figure 5.3: Movements of the column.

Force and displacements - time

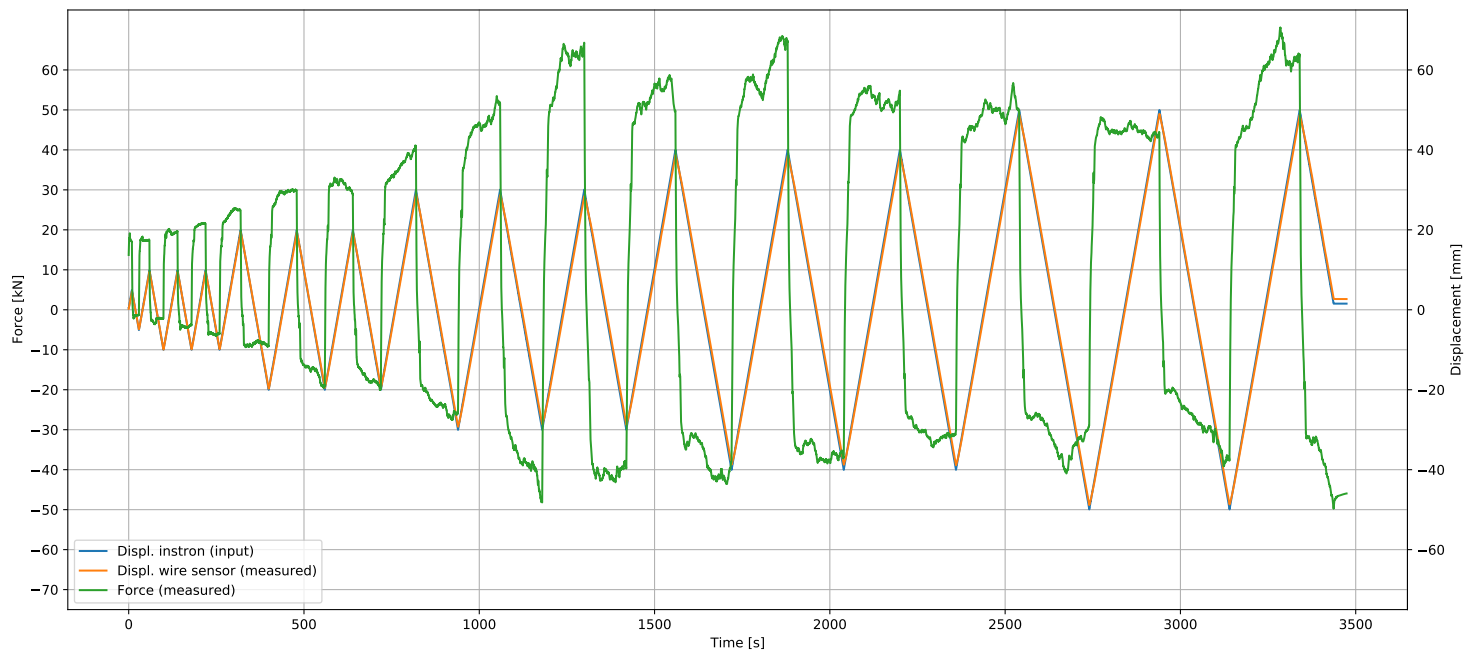
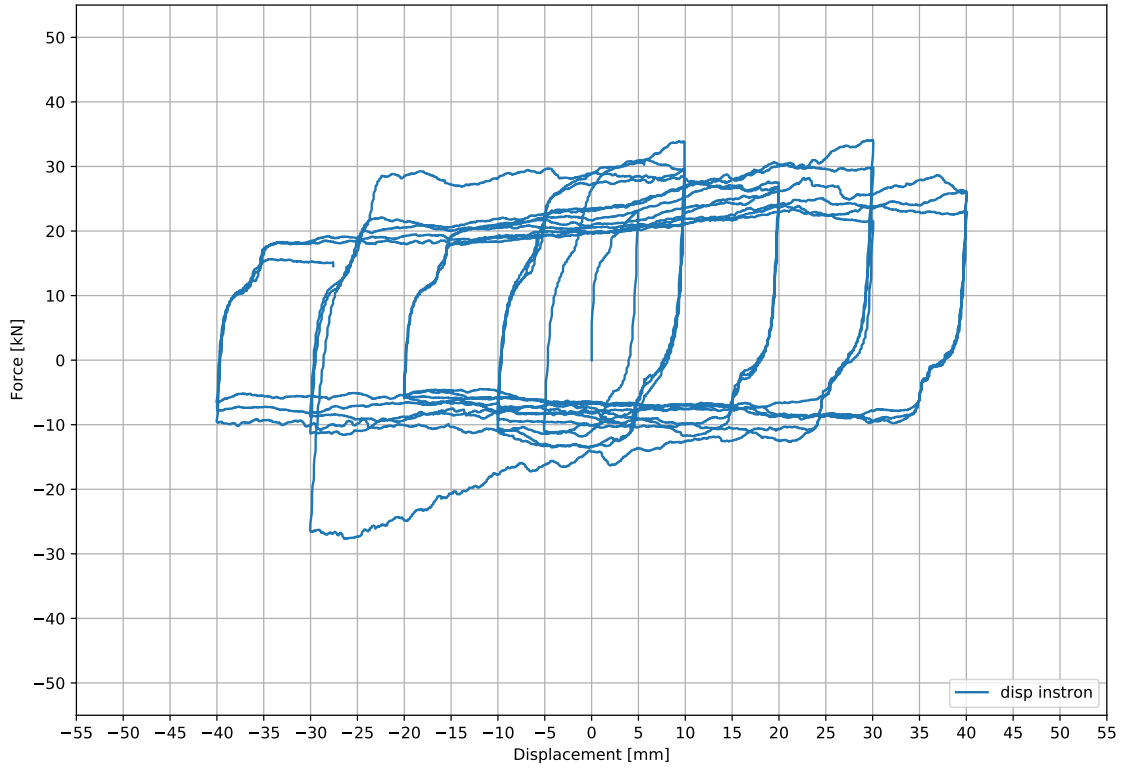


Figure 5.4: Force and displacement plotted against time.

Chapter 6

Test 6 - ALT_2 - 10.02.21

Force-Displacement



Force-Displacement

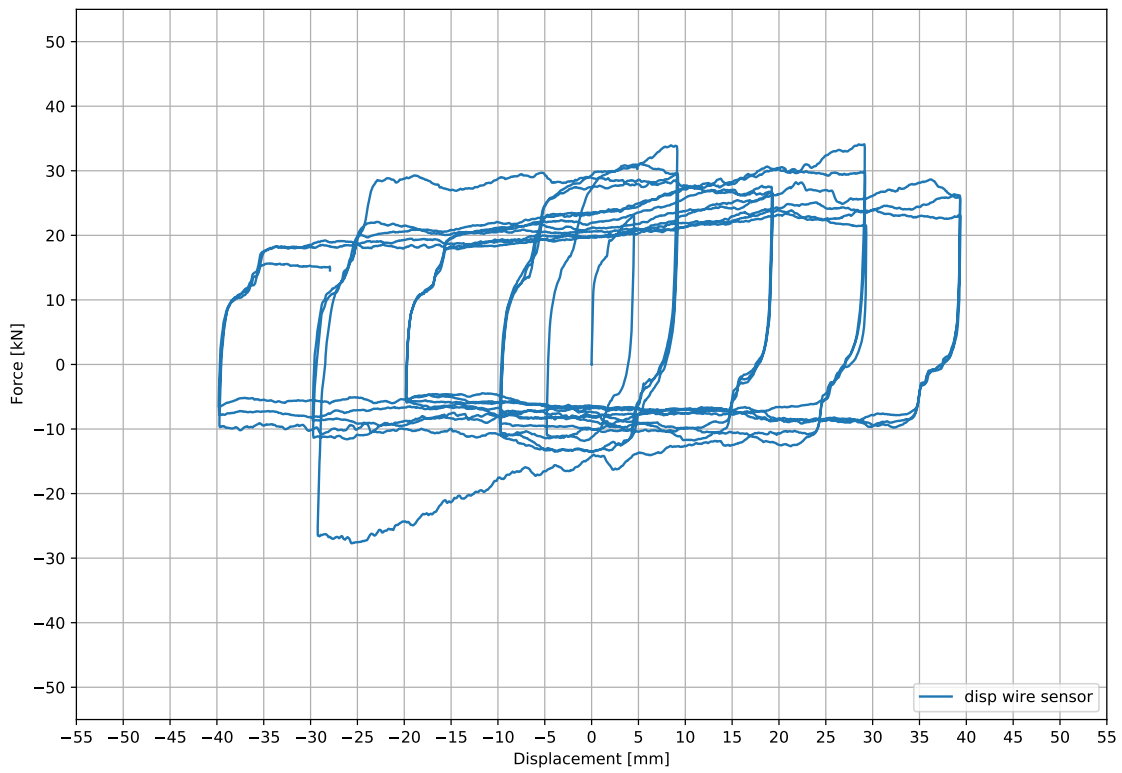


Figure 6.1: Load displacement graph.

Difference displacements - Time

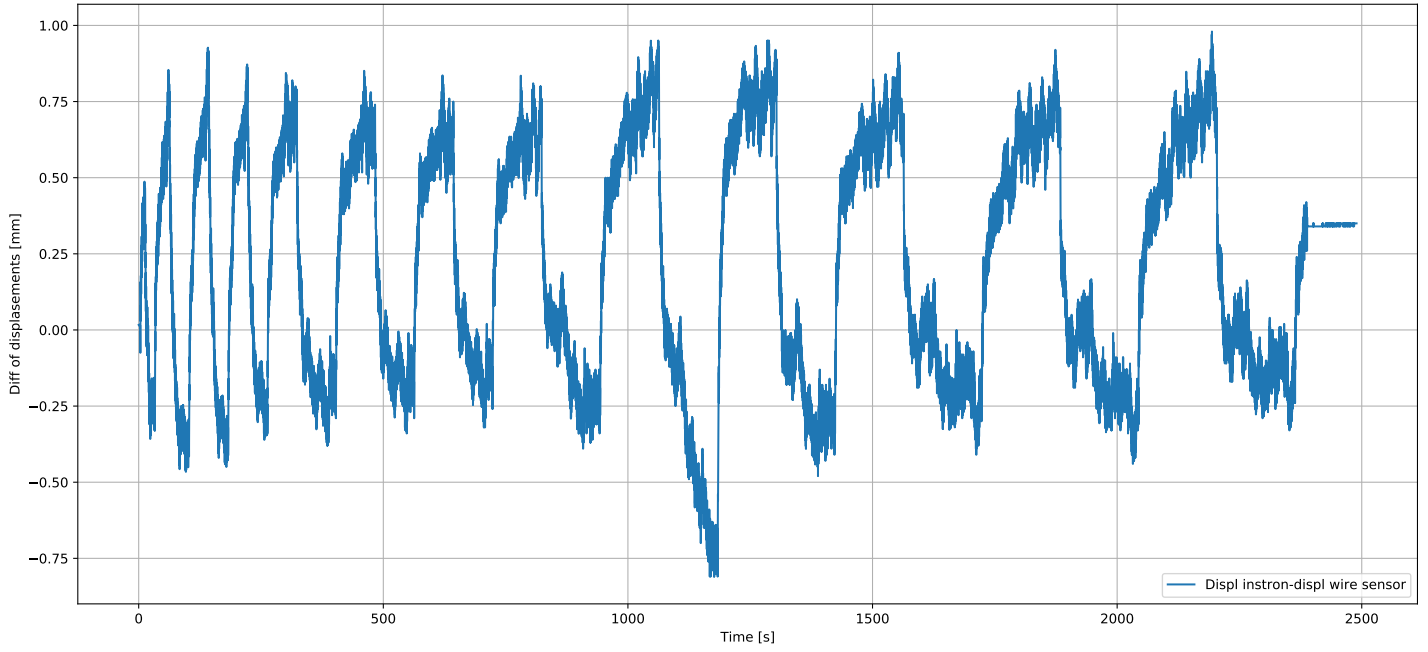


Figure 6.2: Difference of displacement between instron press and wire sensor.

Displacement of columns

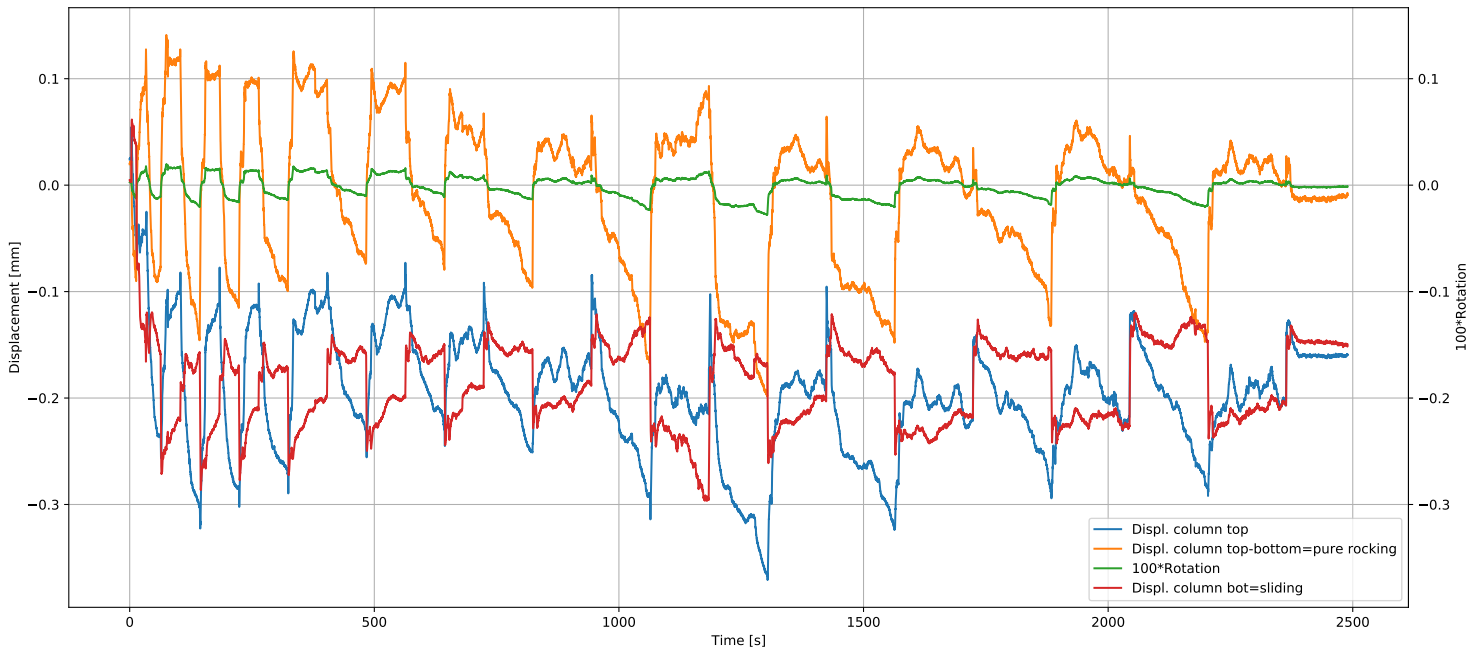


Figure 6.3: Movements of the column.

Force and displacements - time

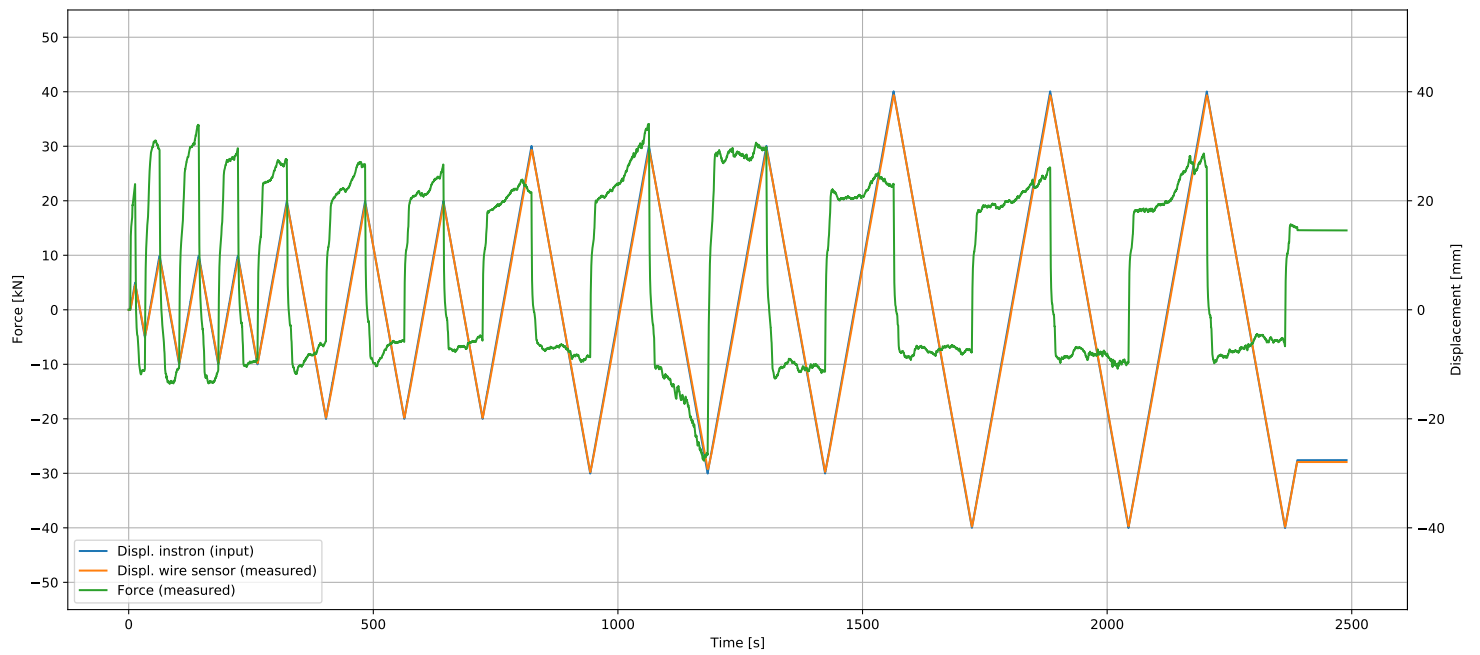
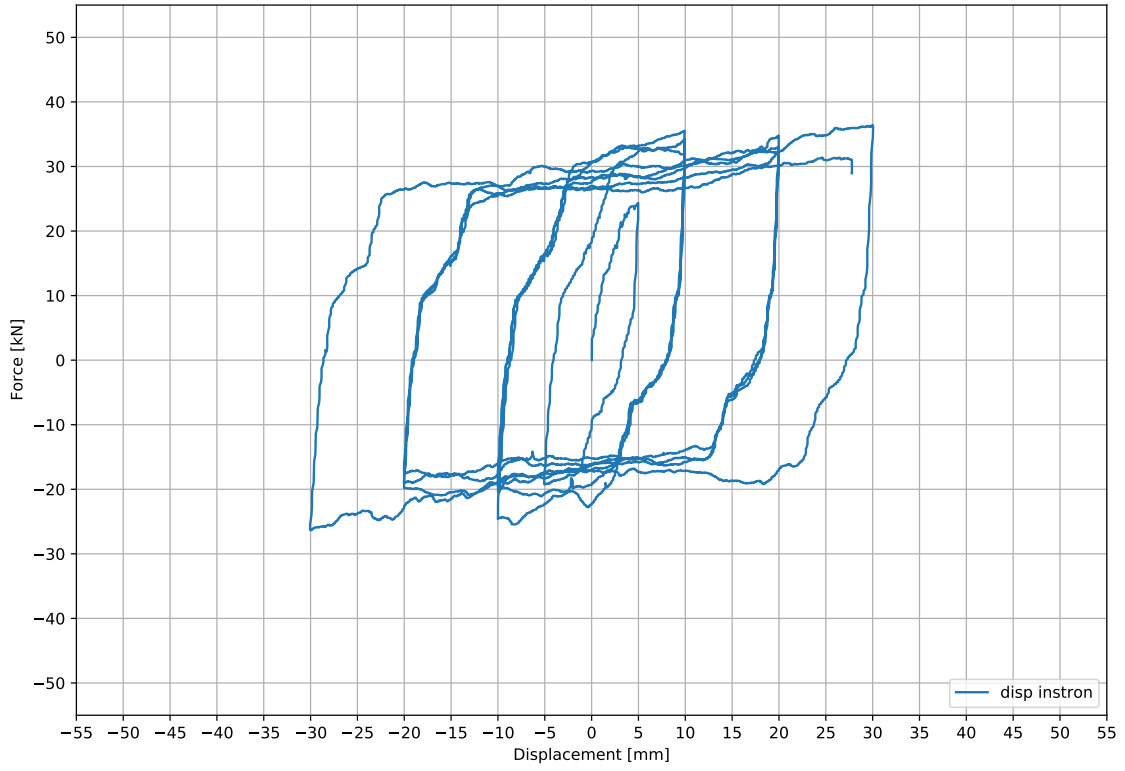


Figure 6.4: Force and displacement plotted against time.

Chapter 7

Test 7 - ALT_2 - 11.02.21

Force-Displacement



Force-Displacement

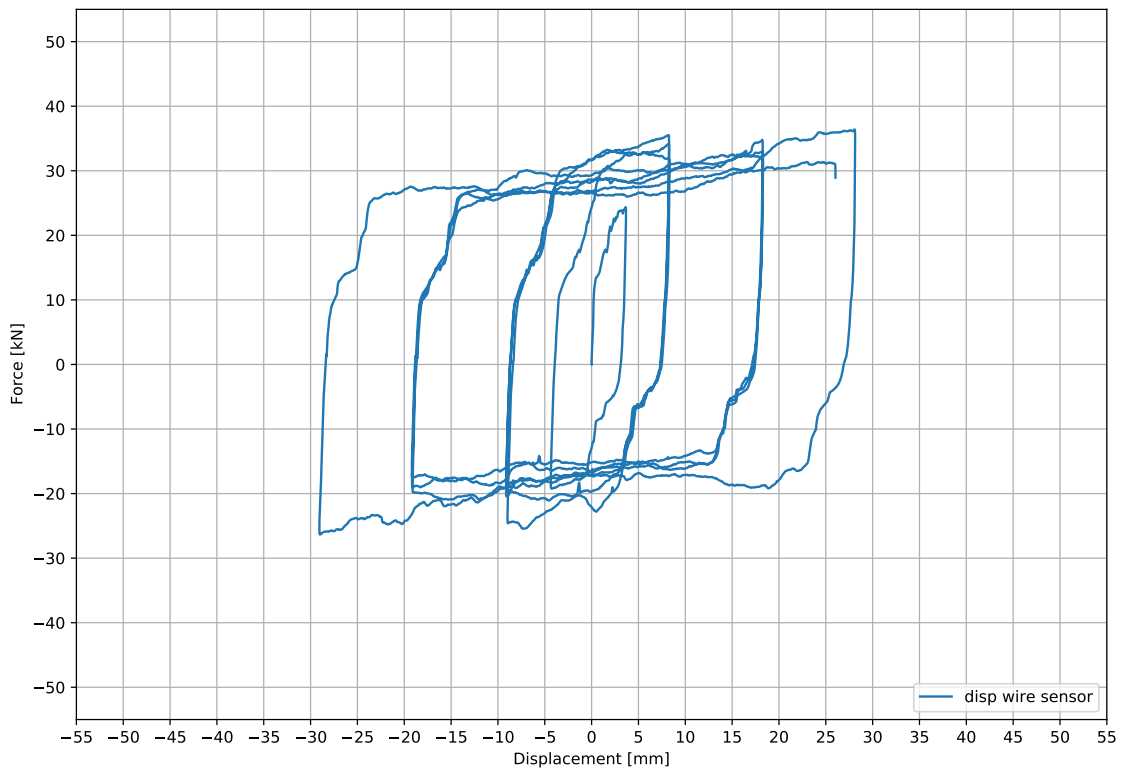


Figure 7.1: Load displacement graph.

Difference displacements - Time

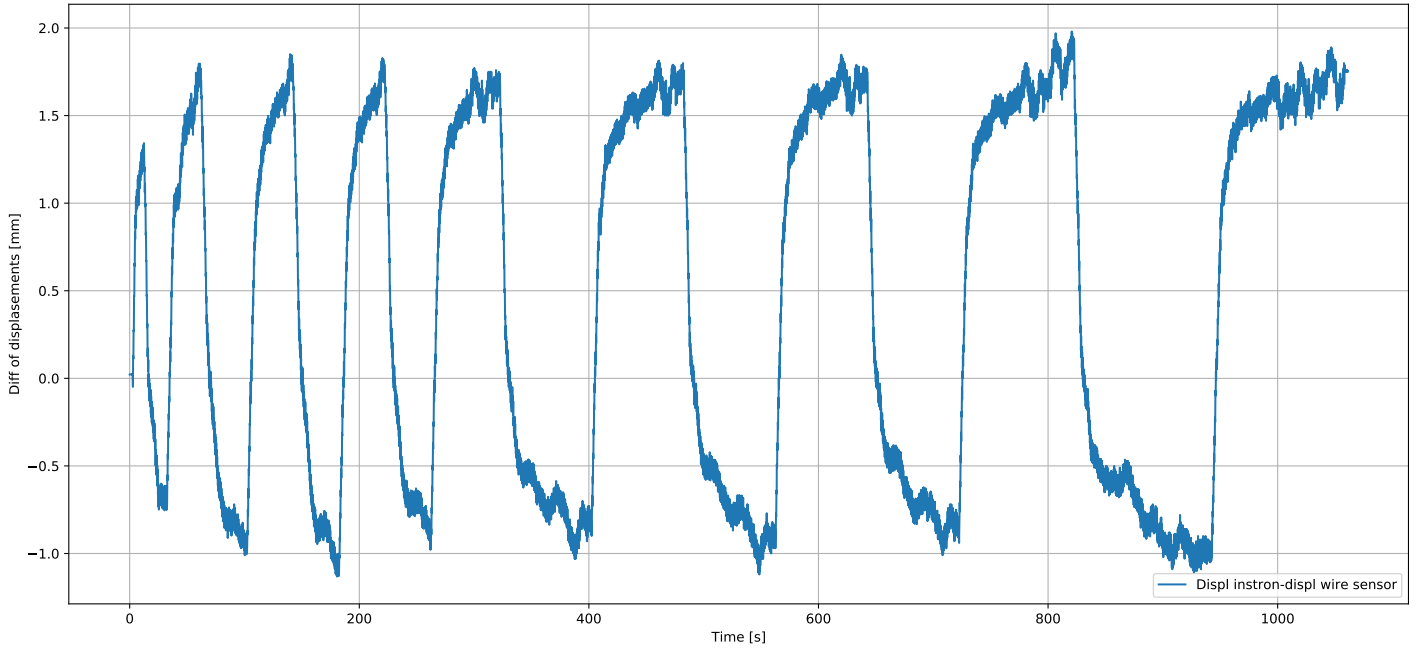


Figure 7.2: Difference of displacement between instron press and wire sensor.

Displacement of columns

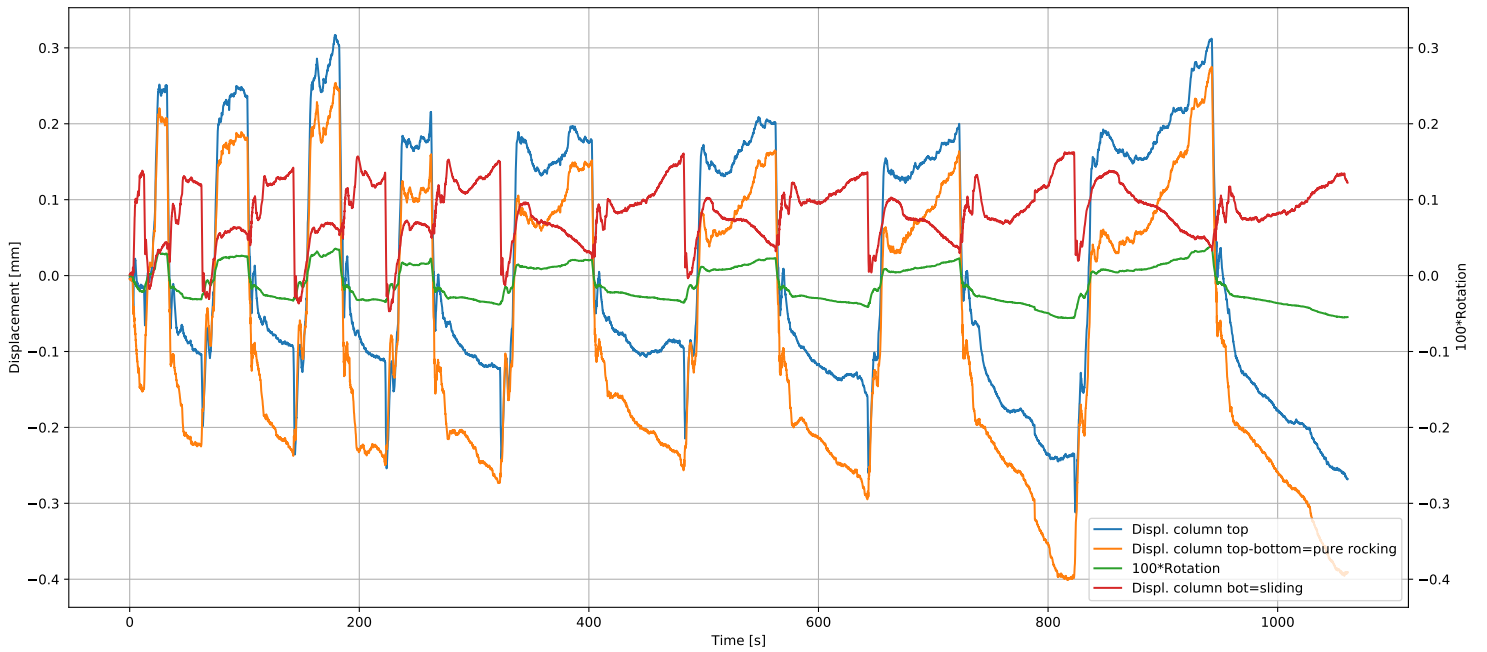


Figure 7.3: Movements of the column.

Force and displacements - time

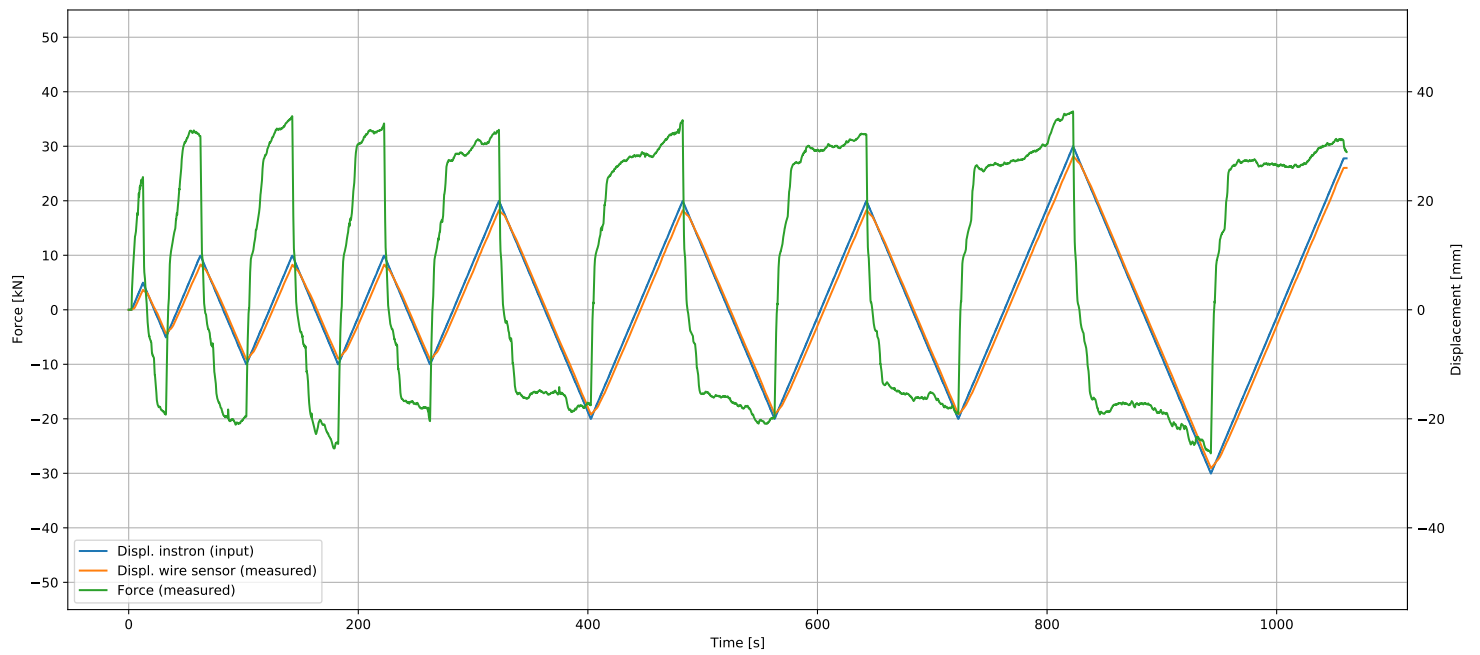
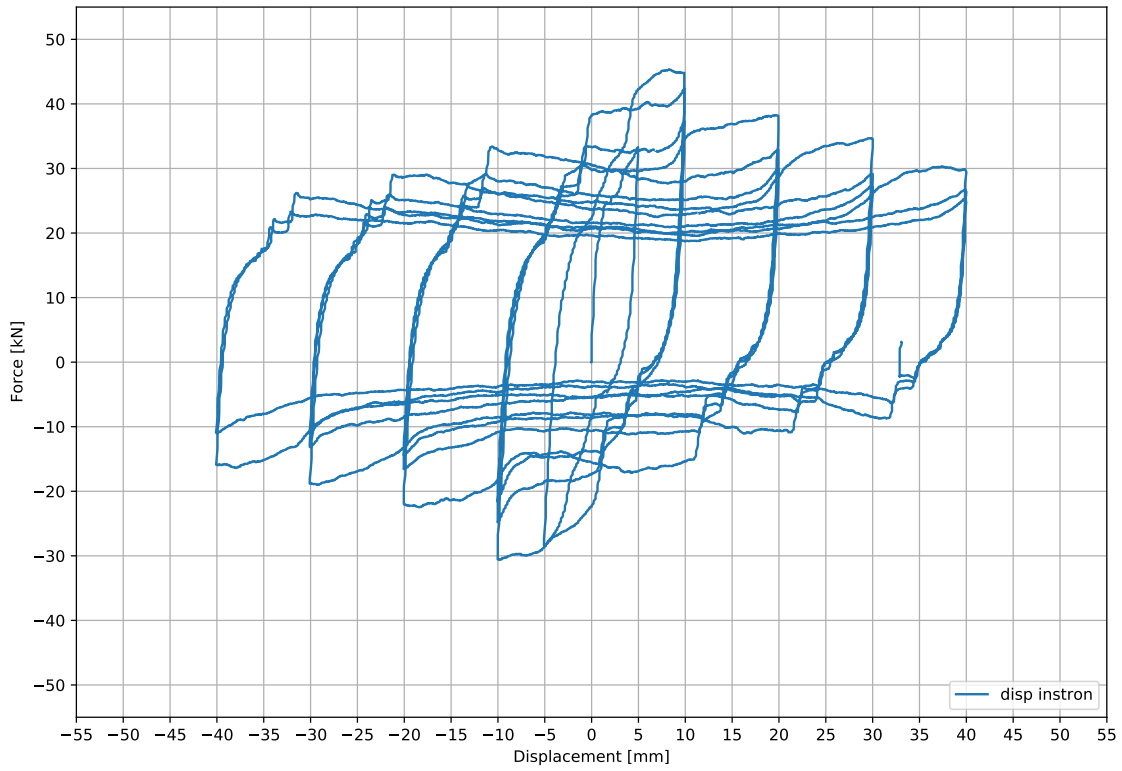


Figure 7.4: Force and displacement plotted against time.

Chapter 8

Test 8 - ALT_2 - 12.02.21

Force-Displacement



Force-Displacement

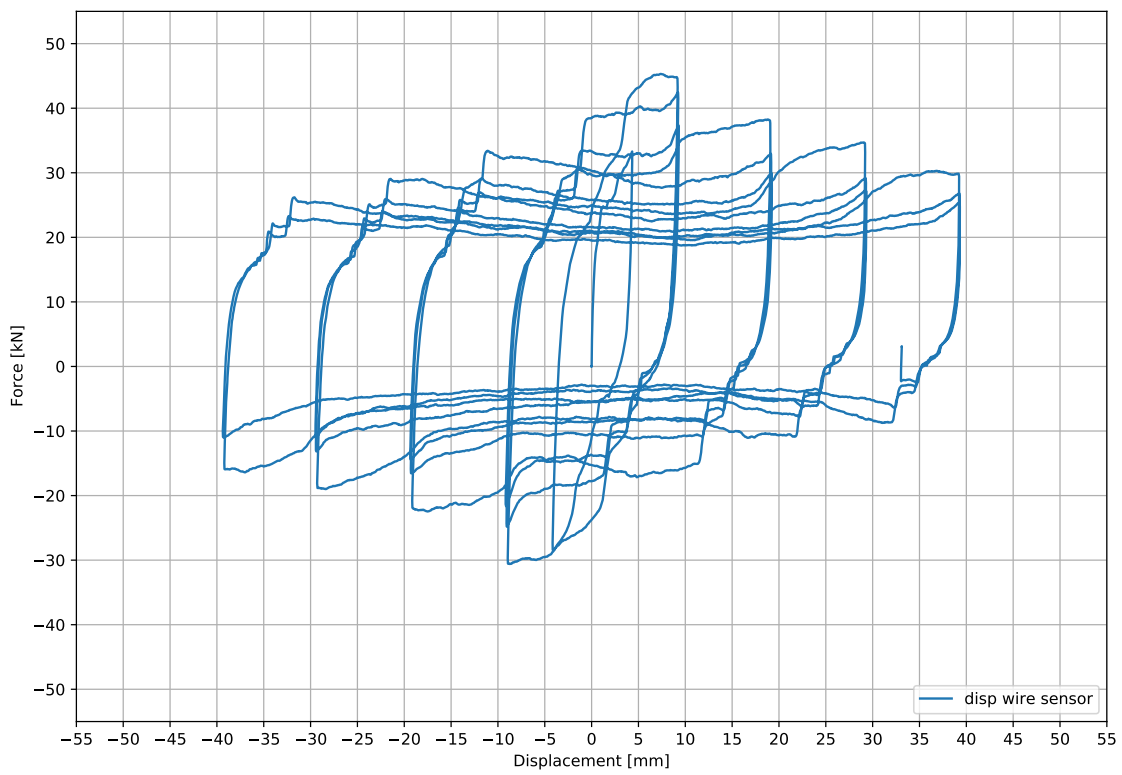


Figure 8.1: Load displacement graph.

Difference displacements - Time

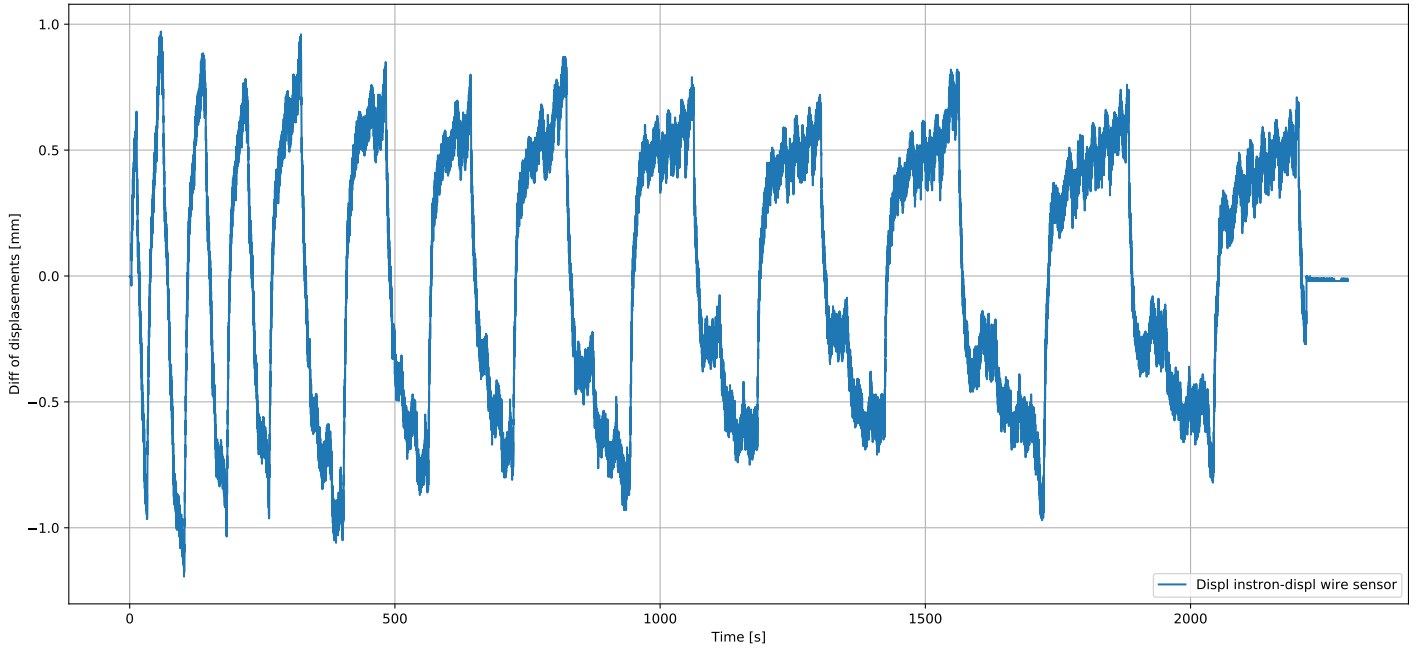


Figure 8.2: Difference of displacement between instron press and wire sensor.

Displacement of columns

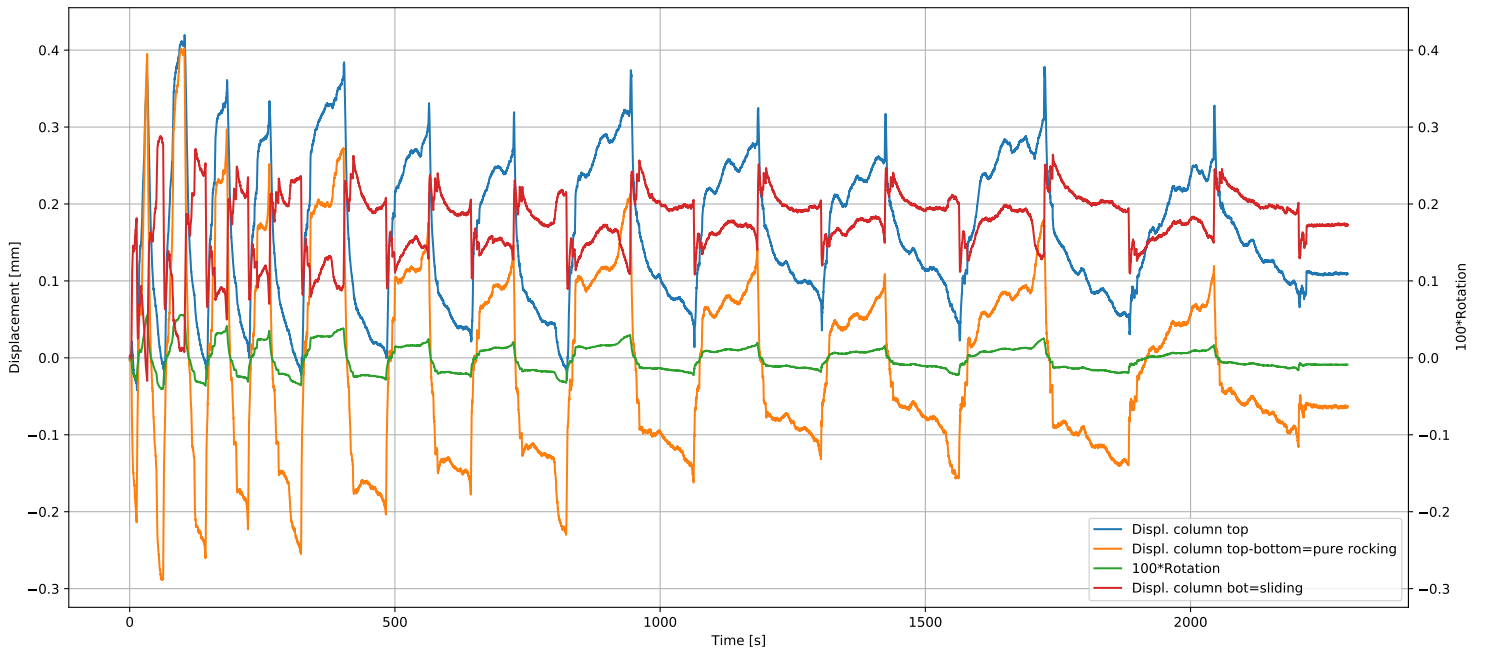


Figure 8.3: Movements of the column.

Force and displacements - time

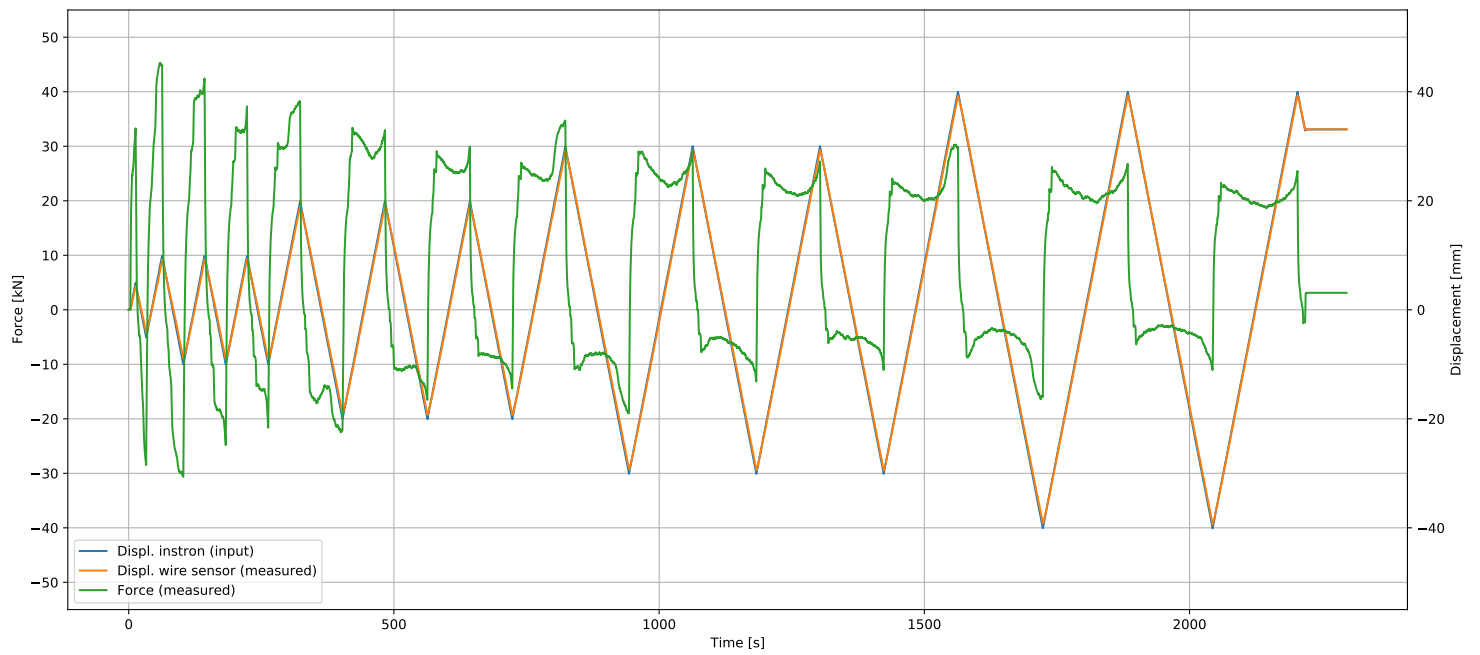


Figure 8.4: Force and displacement plotted against time.

Chapter 9

Test 9.1 to 9.3 - ALT-M10_1 - 22.04.21

9.1 Test 9.1

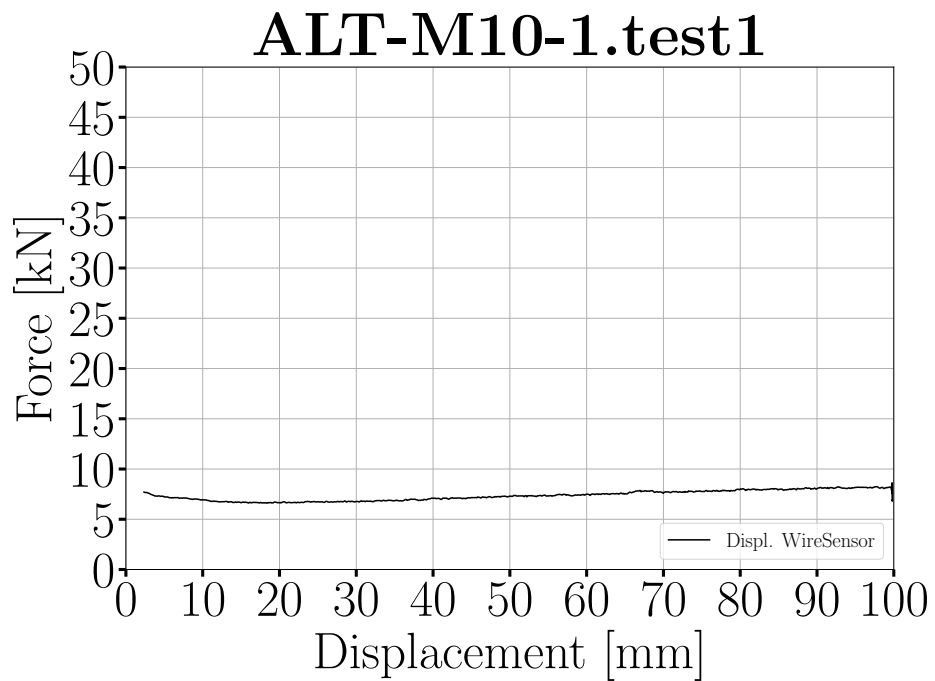
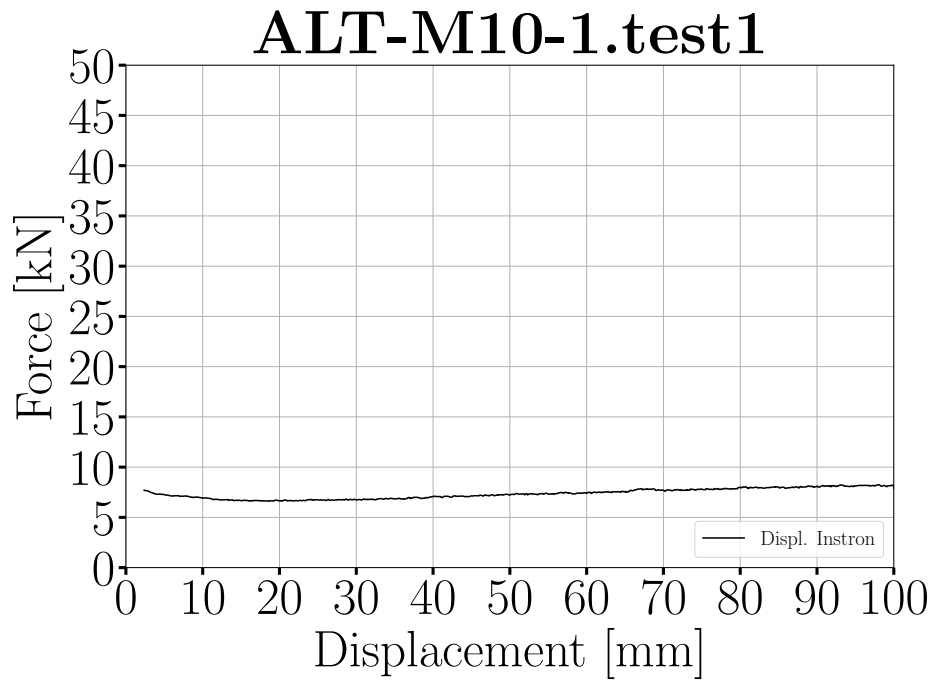


Figure 9.1: Load displacement graph.

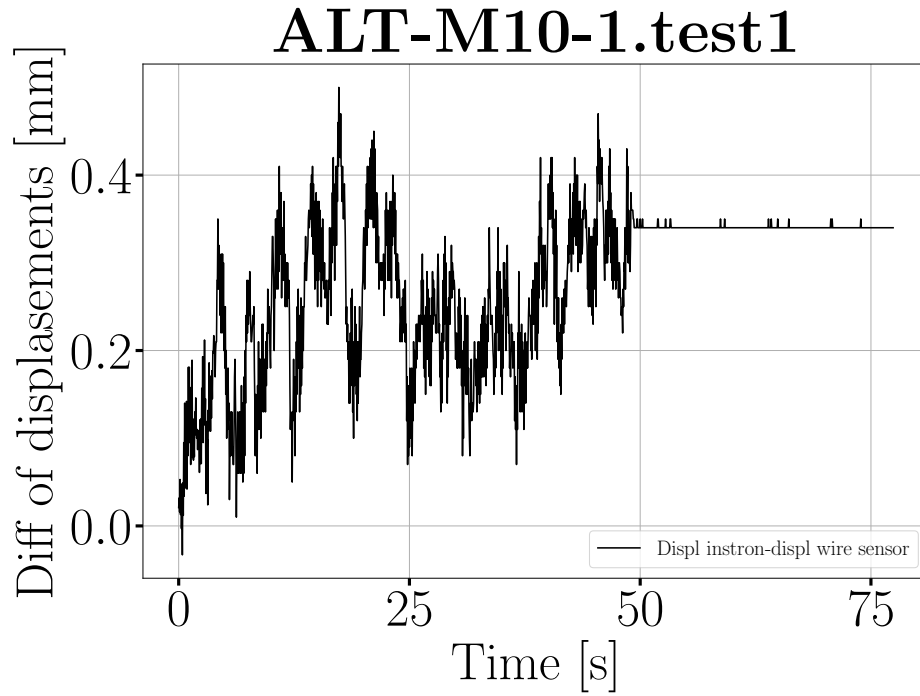


Figure 9.2: Difference of displacement between instron press and wire sensor.

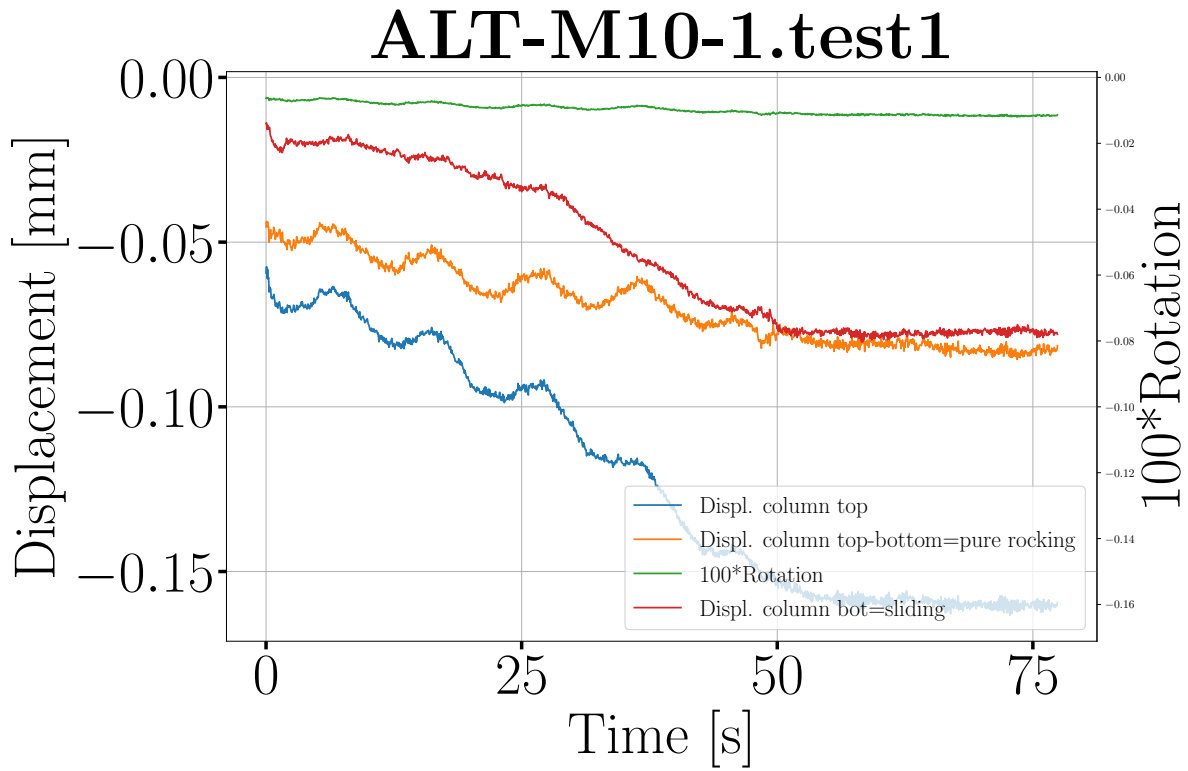


Figure 9.3: Movements of the column.

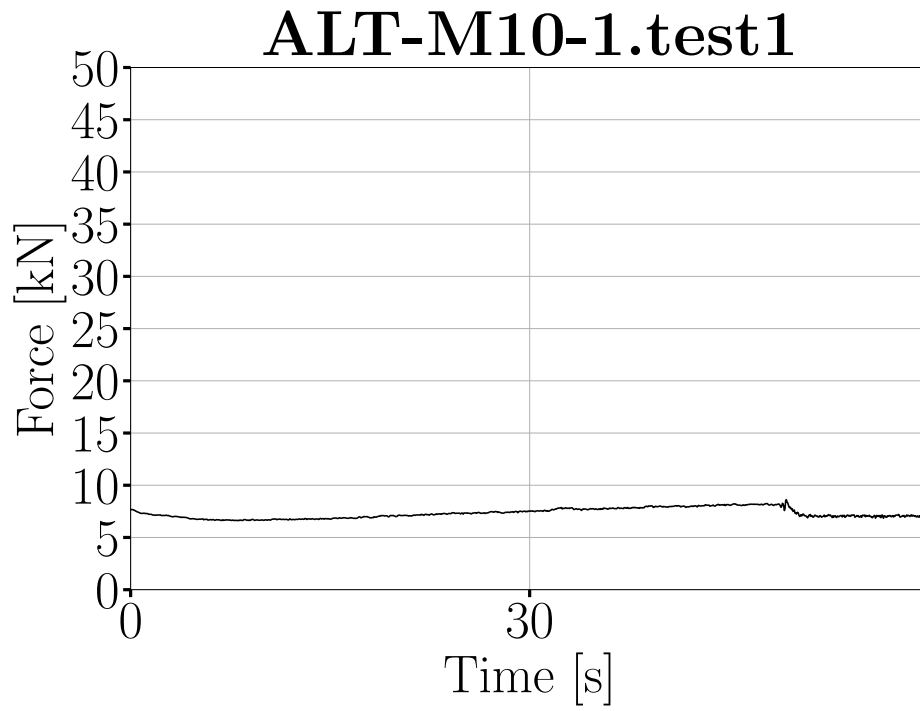


Figure 9.4: Force plotted against time.

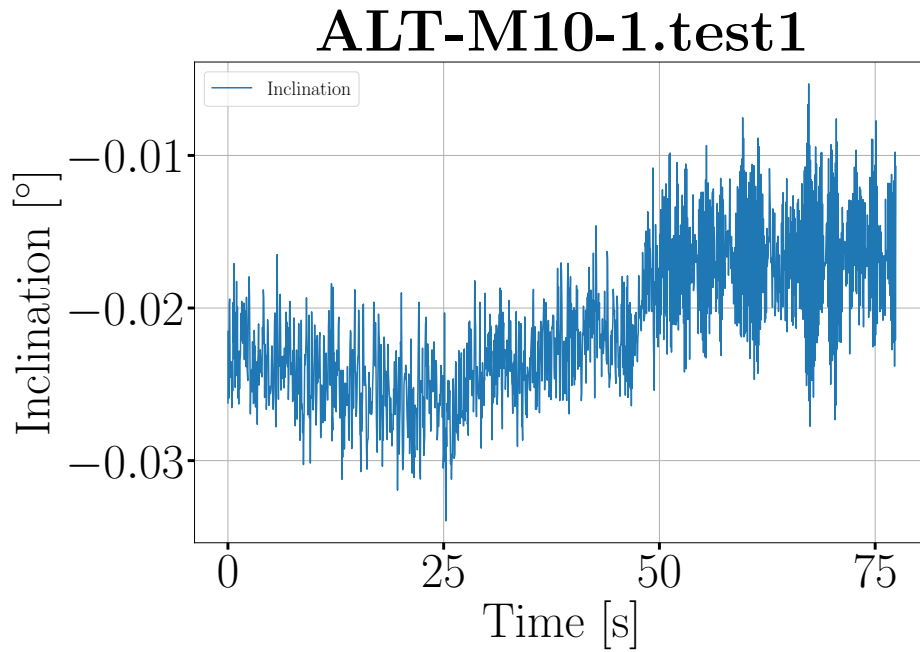


Figure 9.5: Inclination plotted against time.

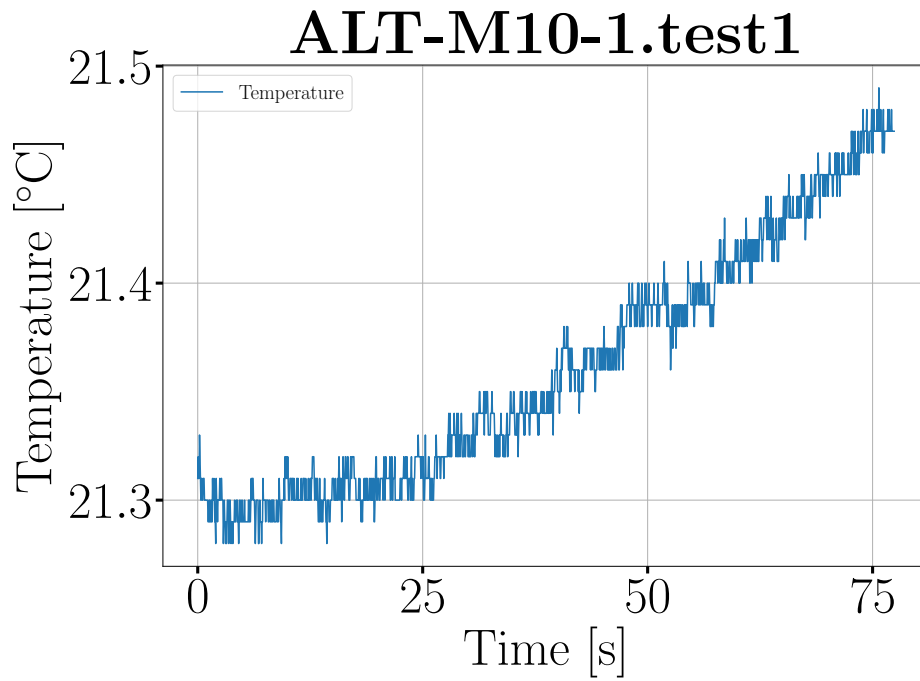


Figure 9.6: Temperature plotted against time.

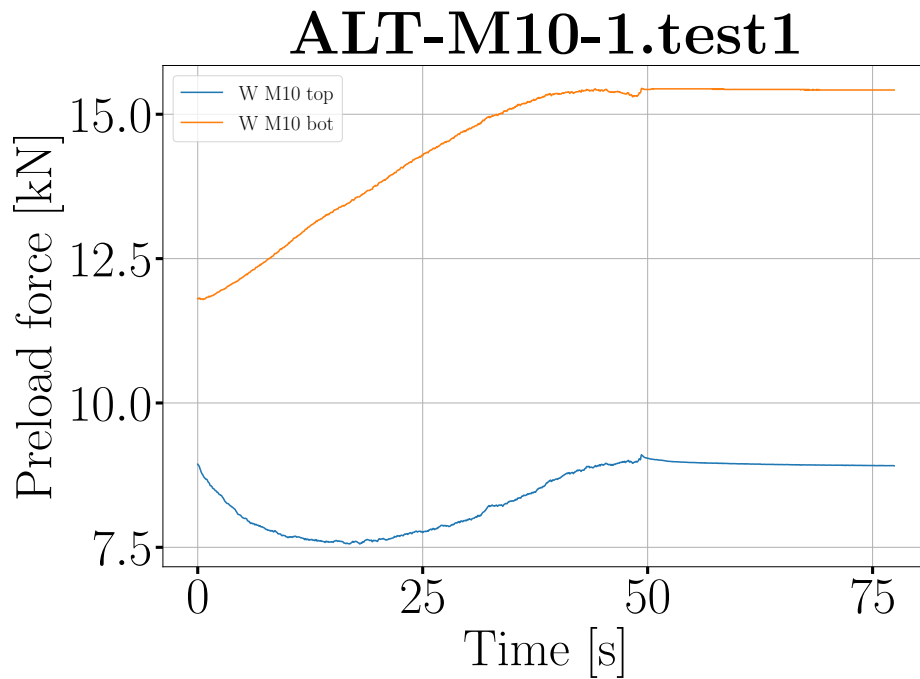


Figure 9.7: Preload in bolts.

9.2 Test 9.2

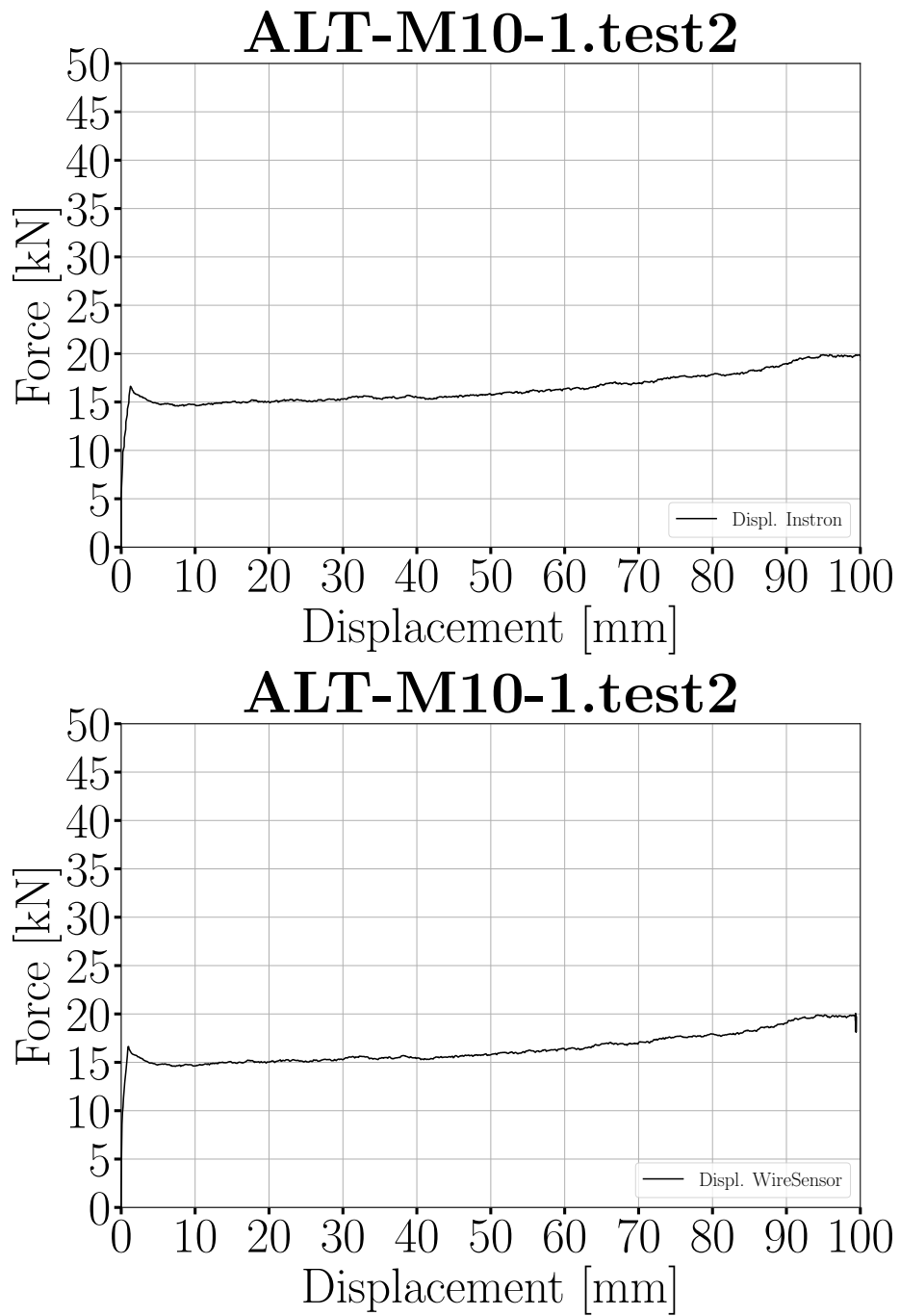


Figure 9.8: Load displacement graph.

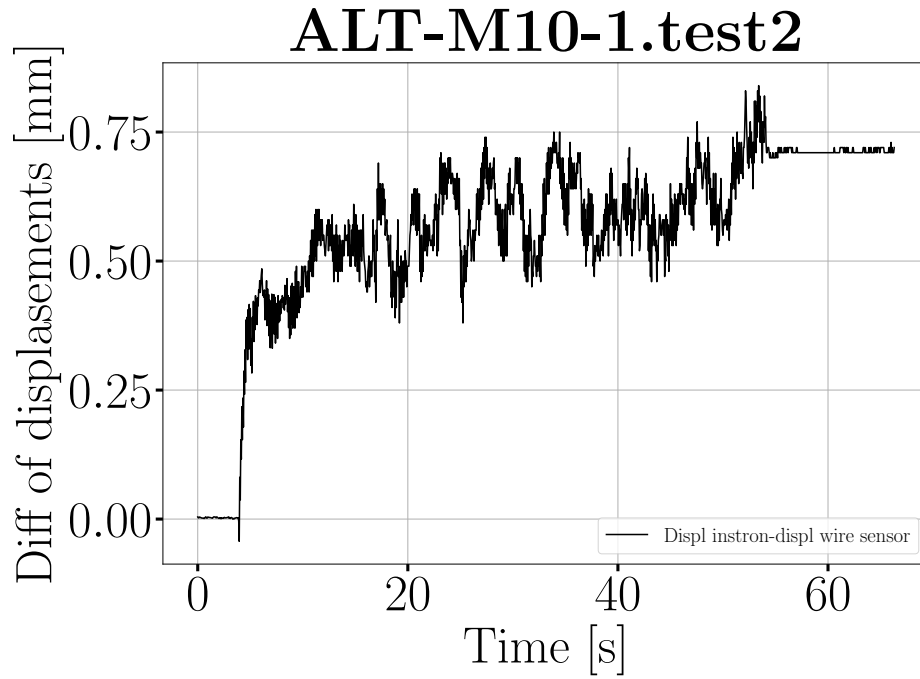


Figure 9.9: Difference of displacement between instron press and wire sensor.

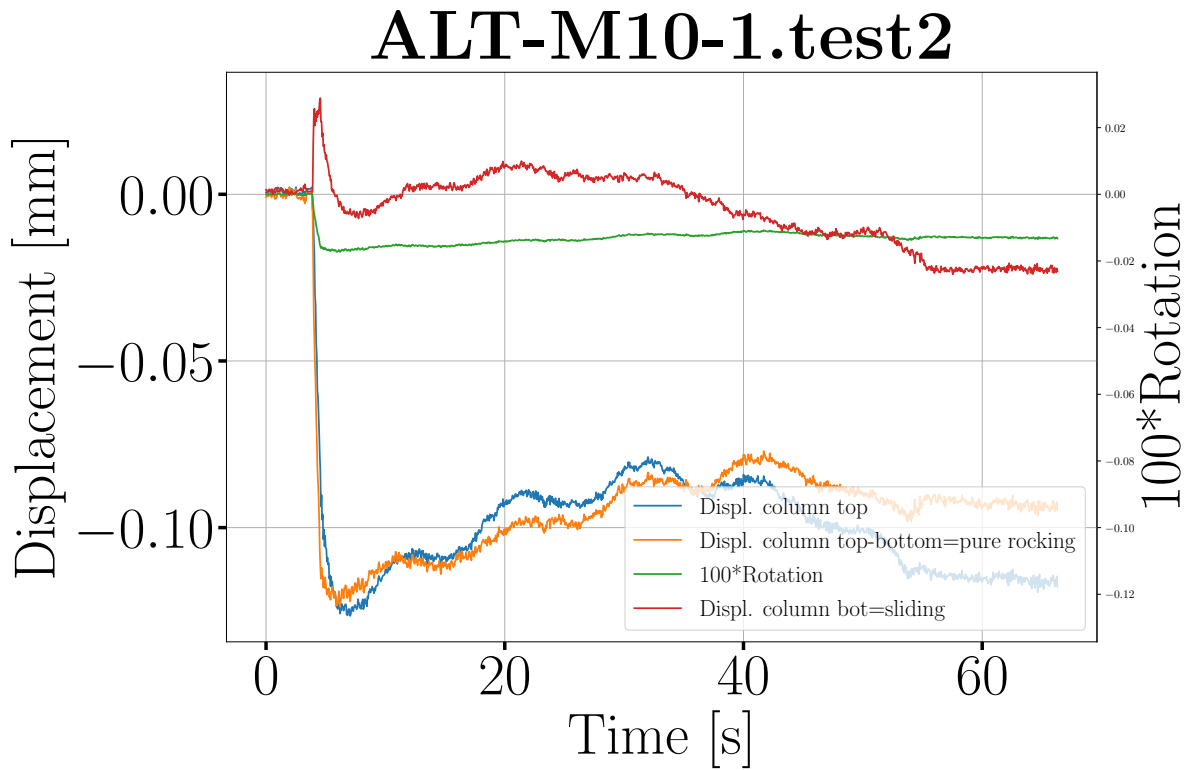


Figure 9.10: Movements of the column.

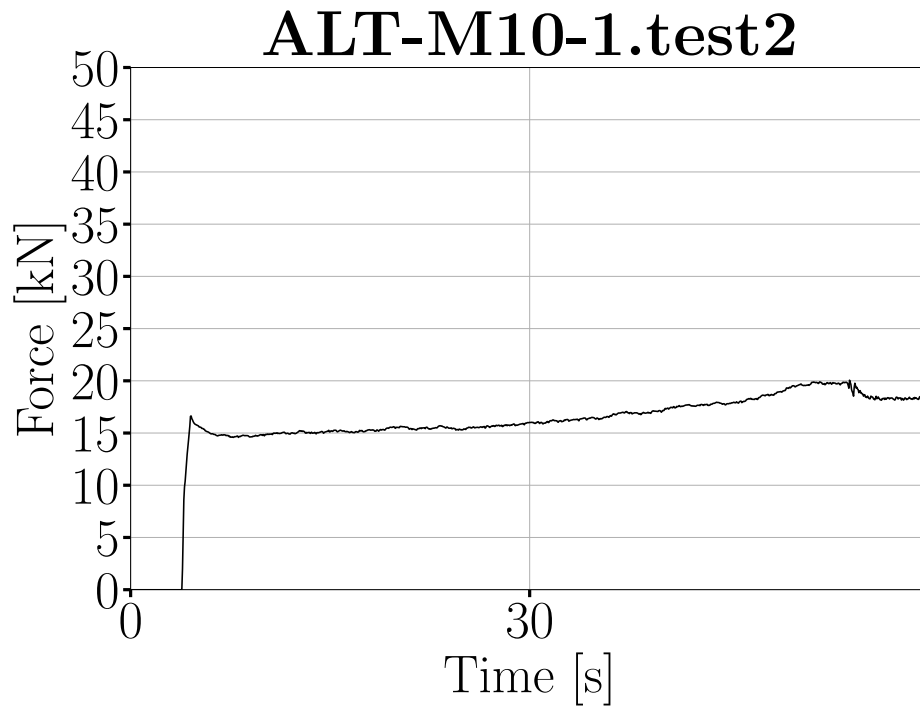


Figure 9.11: Force plotted against time.

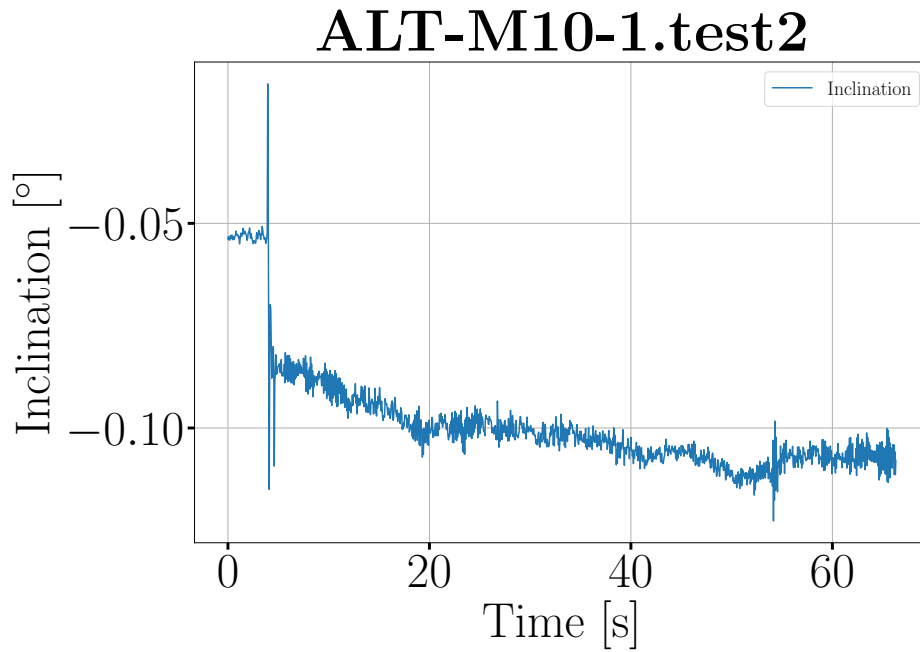


Figure 9.12: Inclination plotted against time.

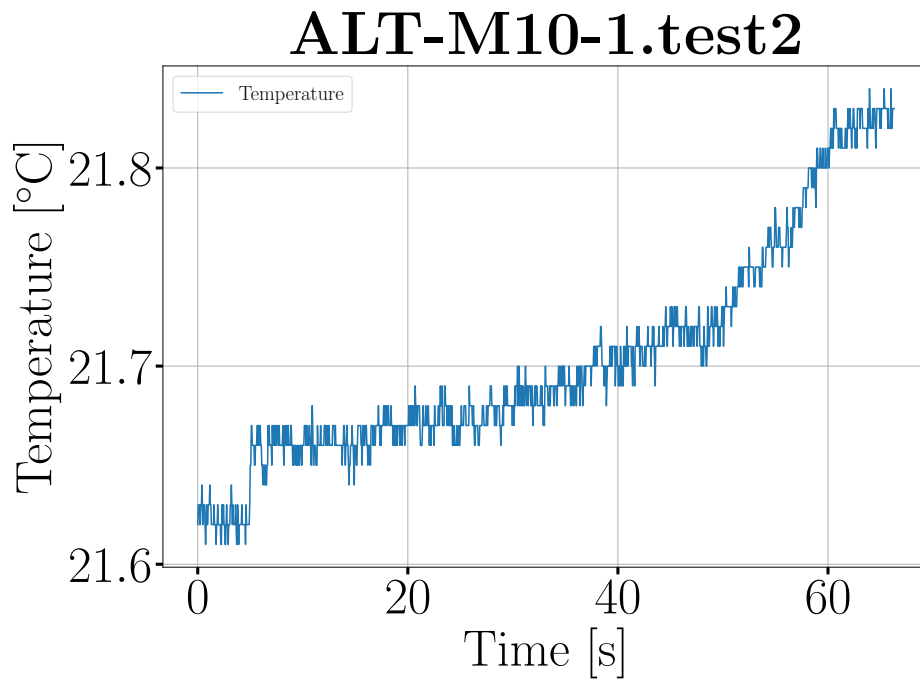


Figure 9.13: Temperature plotted against time.

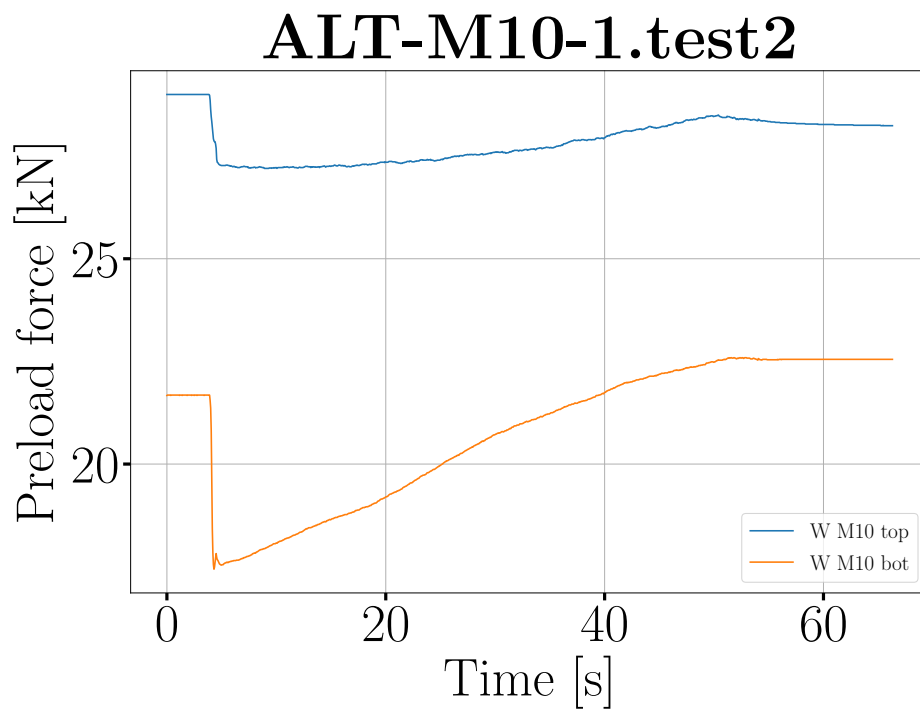


Figure 9.14: Preload in bolts.

9.3 Test 3

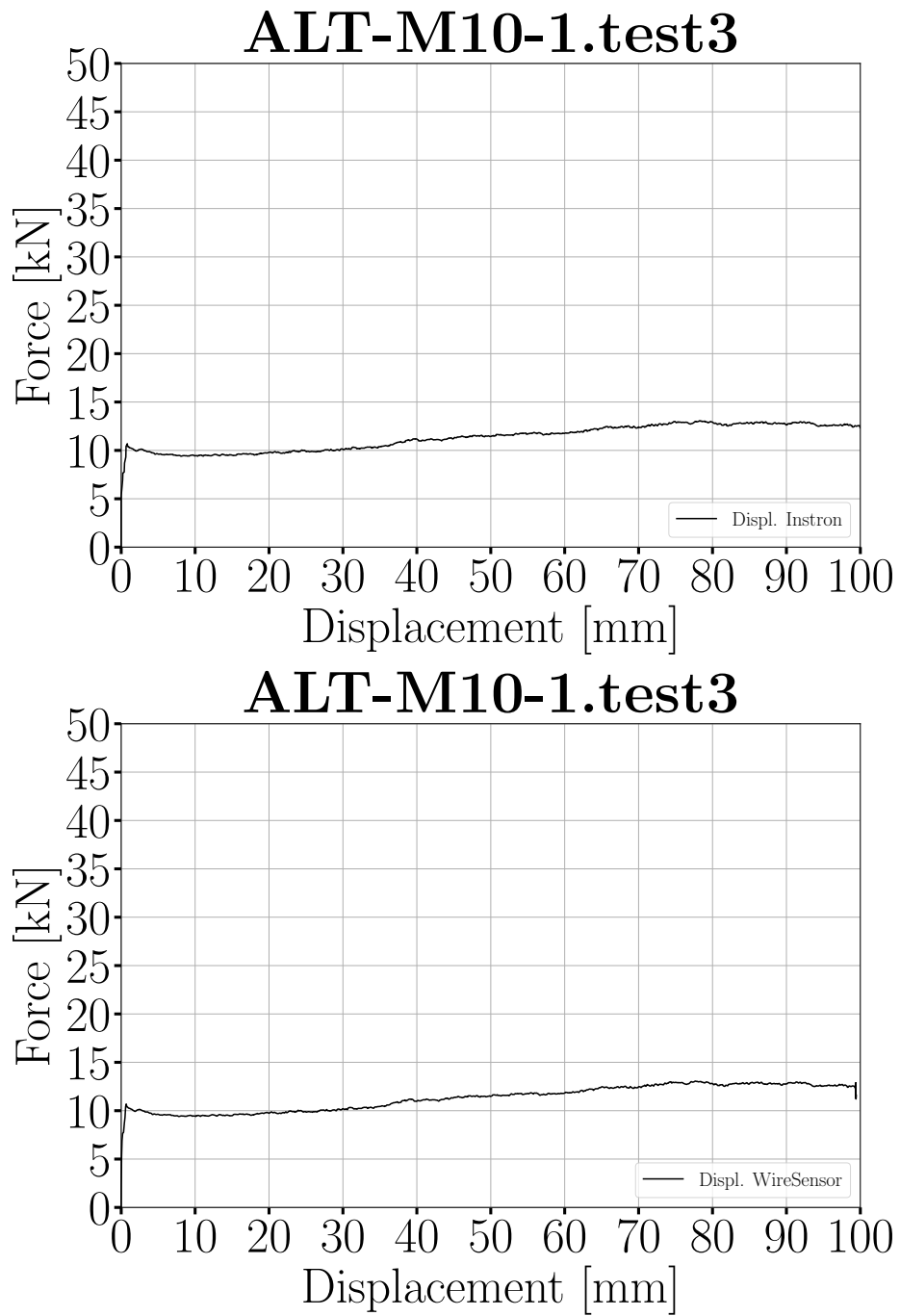


Figure 9.15: Load displacement graph.

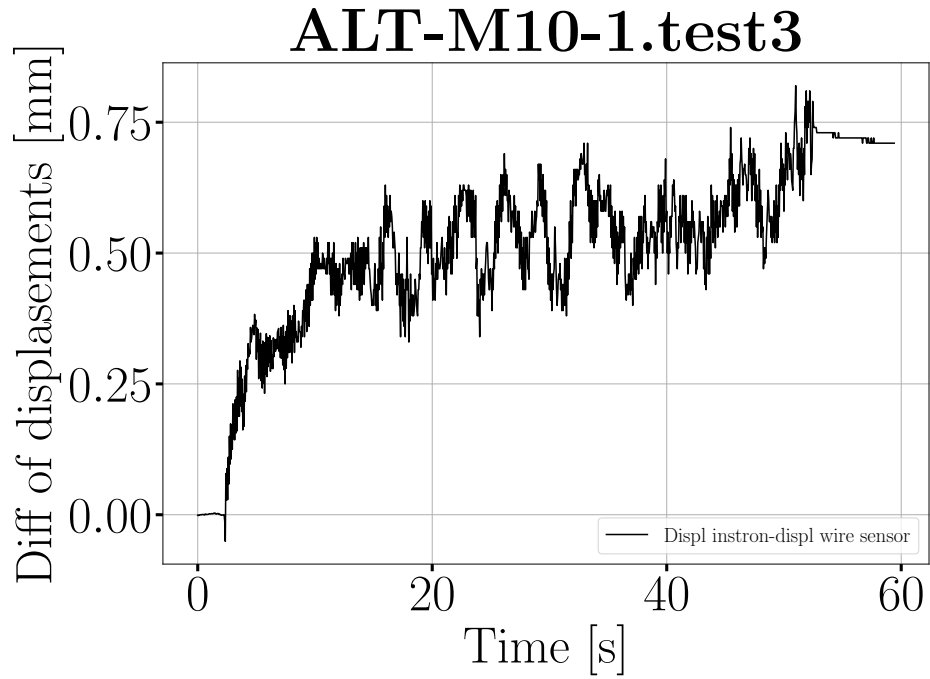


Figure 9.16: Difference of displacement between instron press and wire sensor.

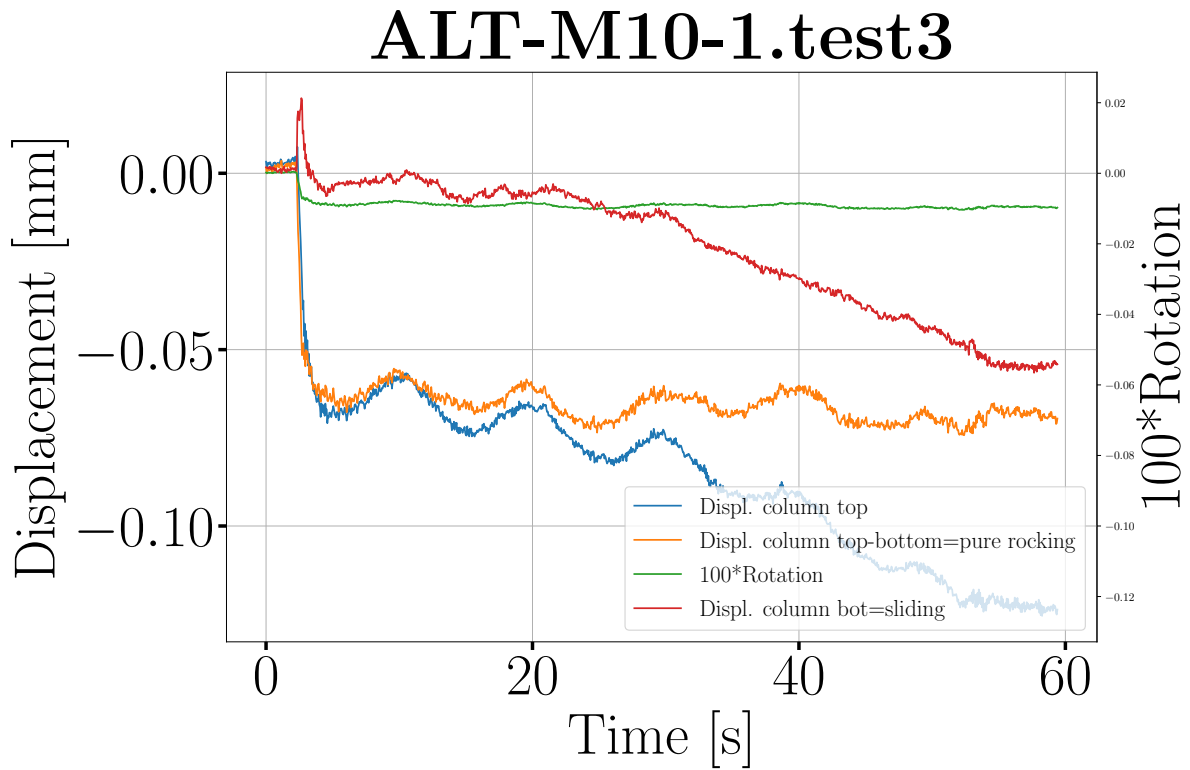


Figure 9.17: Movements of the column.

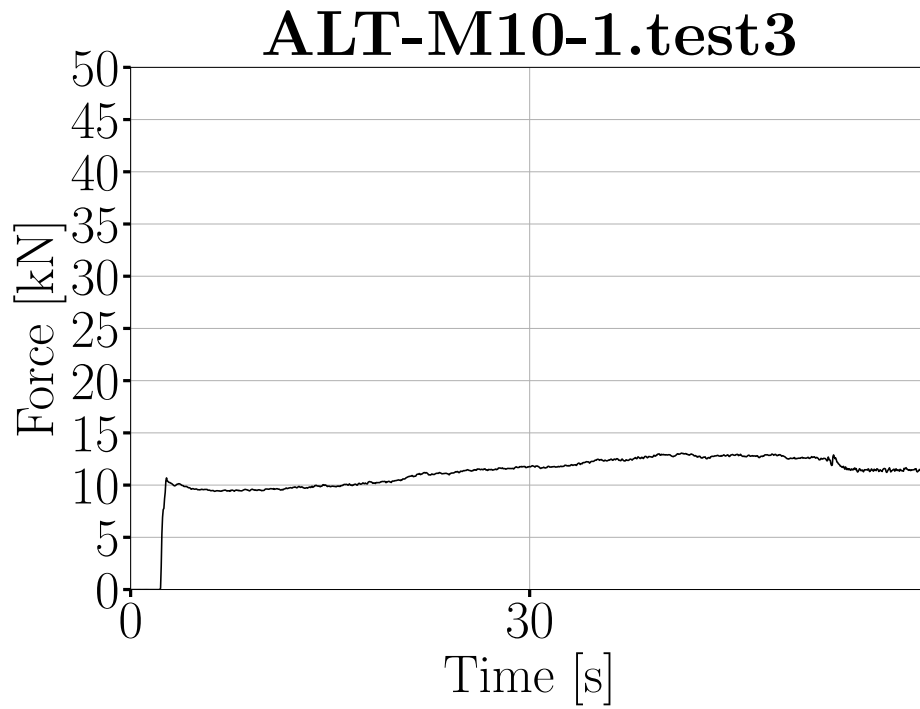


Figure 9.18: Force plotted against time.

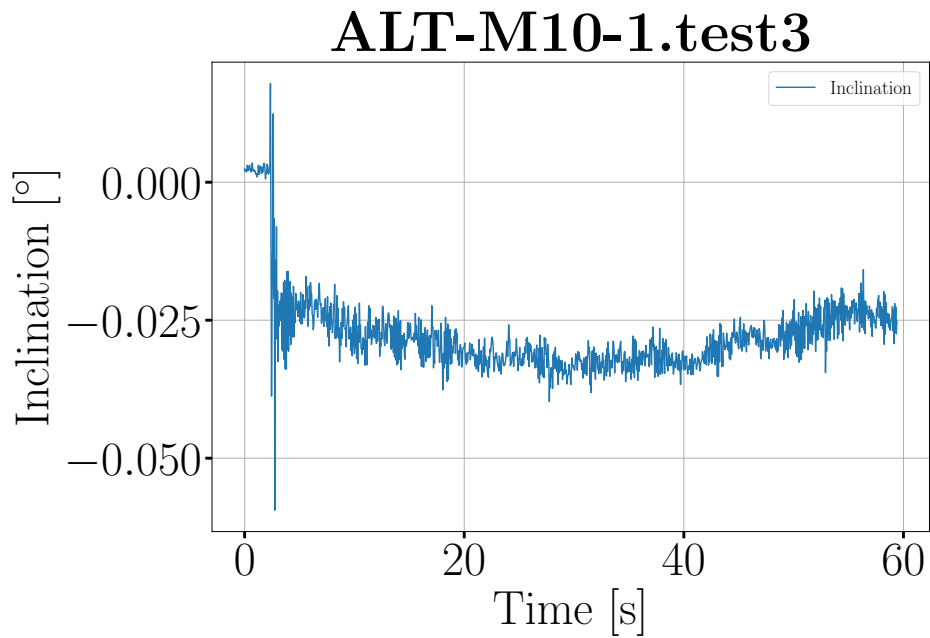


Figure 9.19: Inclination plotted against time.

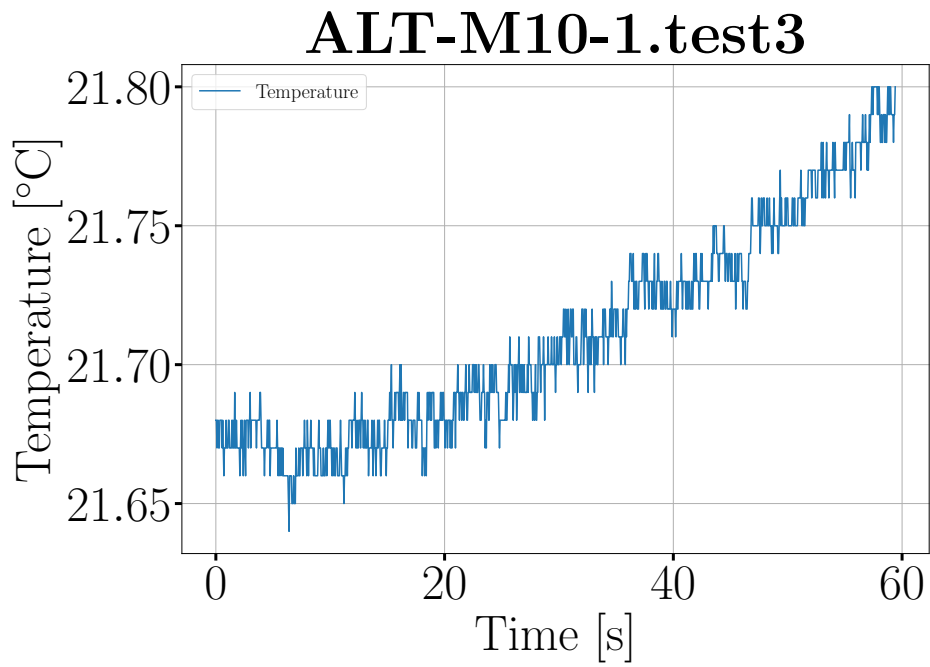


Figure 9.20: Temperature plotted against time.

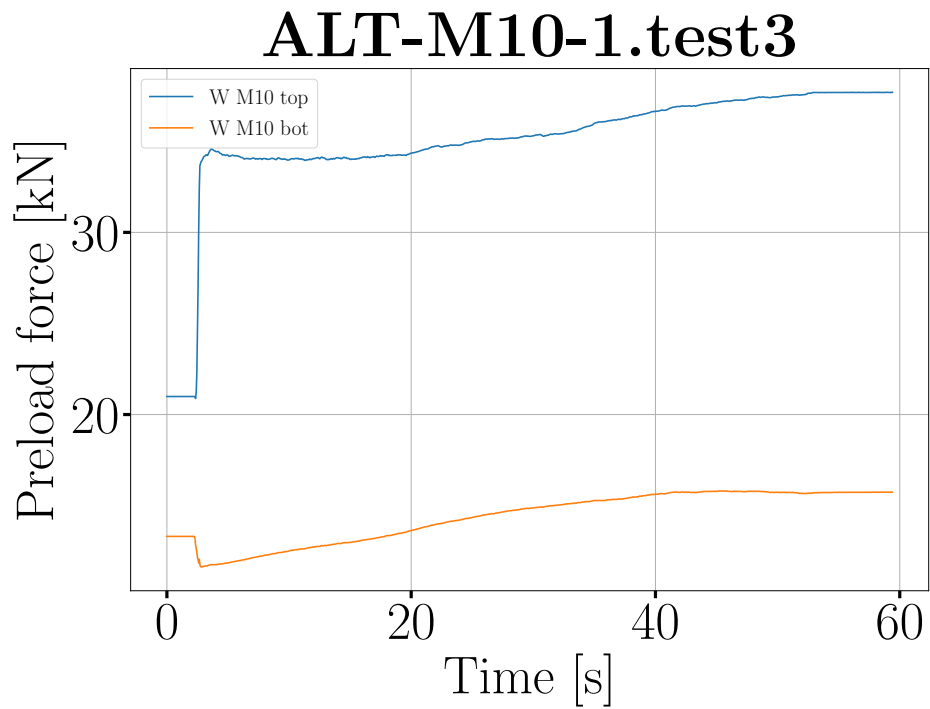


Figure 9.21: Preload in bolts.

Chapter 10

Test 10.1 to 10.5 - ALT-M20_1 - 23.04.21

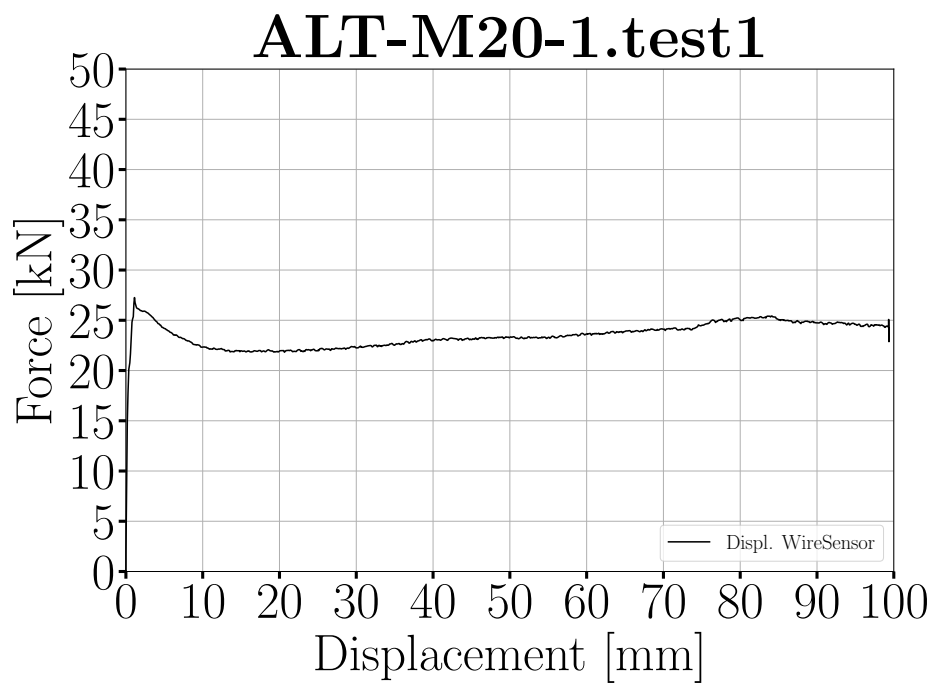
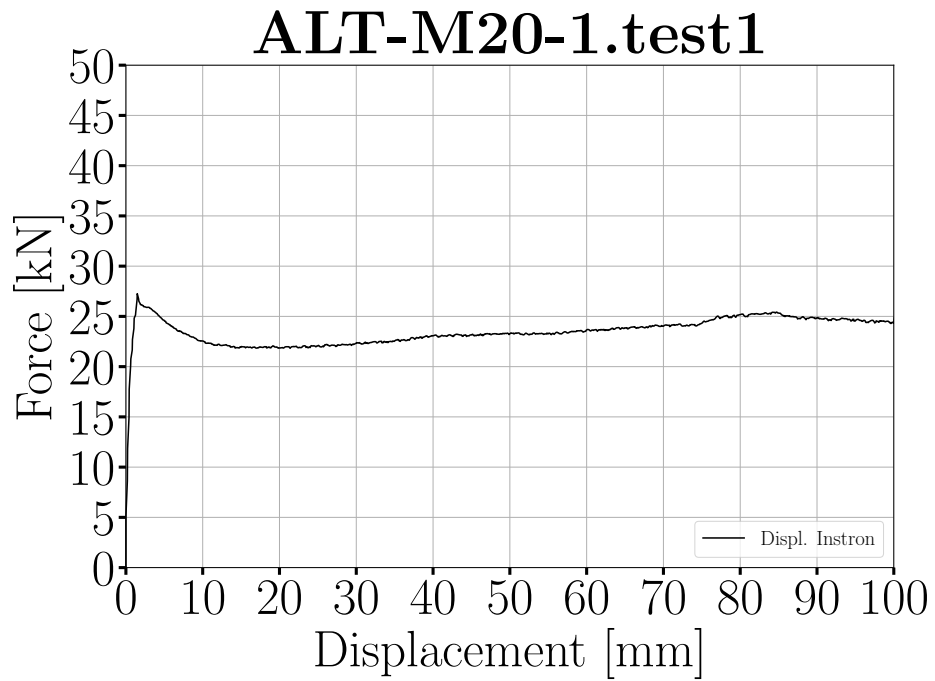


Figure 10.1: Load displacement graph.

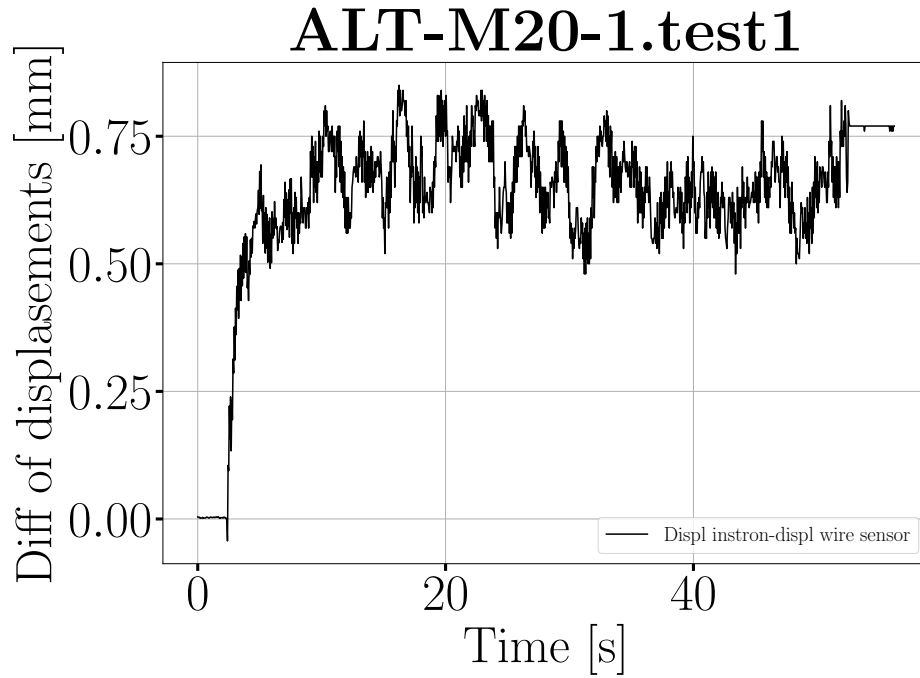


Figure 10.2: Difference of displacement between instron press and wire sensor.

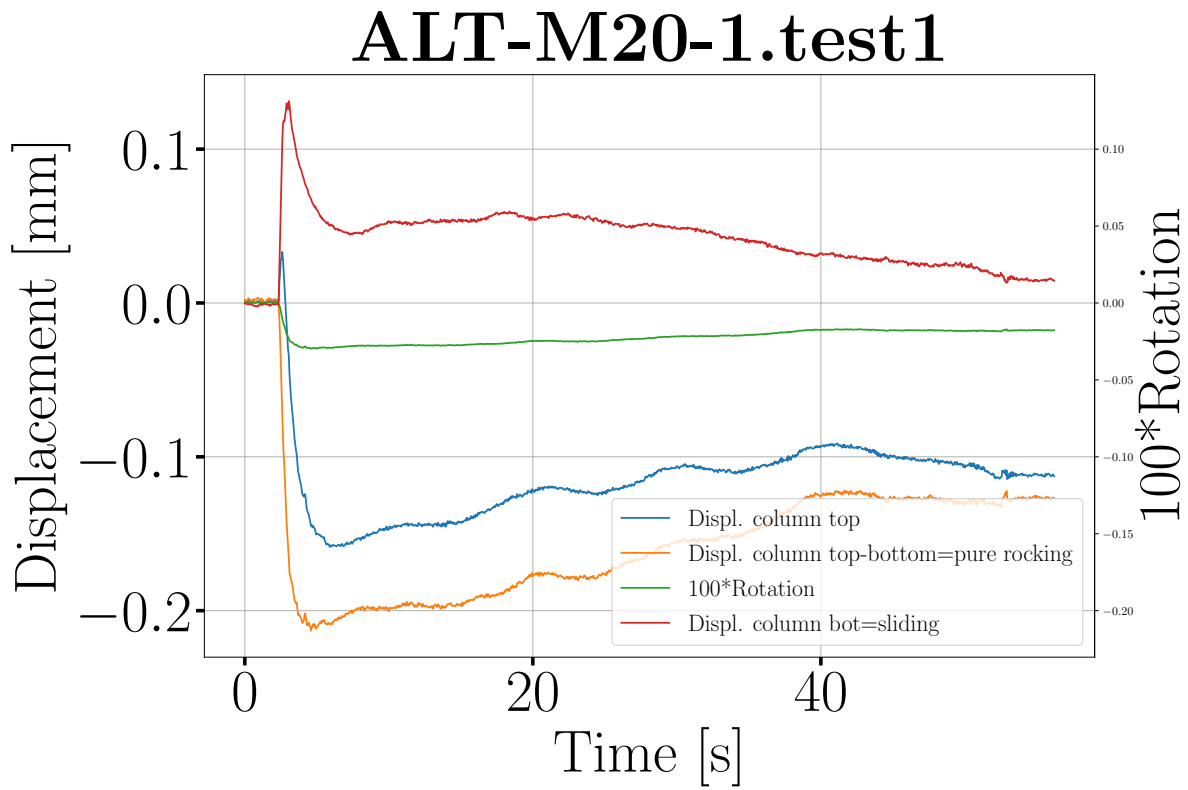


Figure 10.3: Movements of the column.

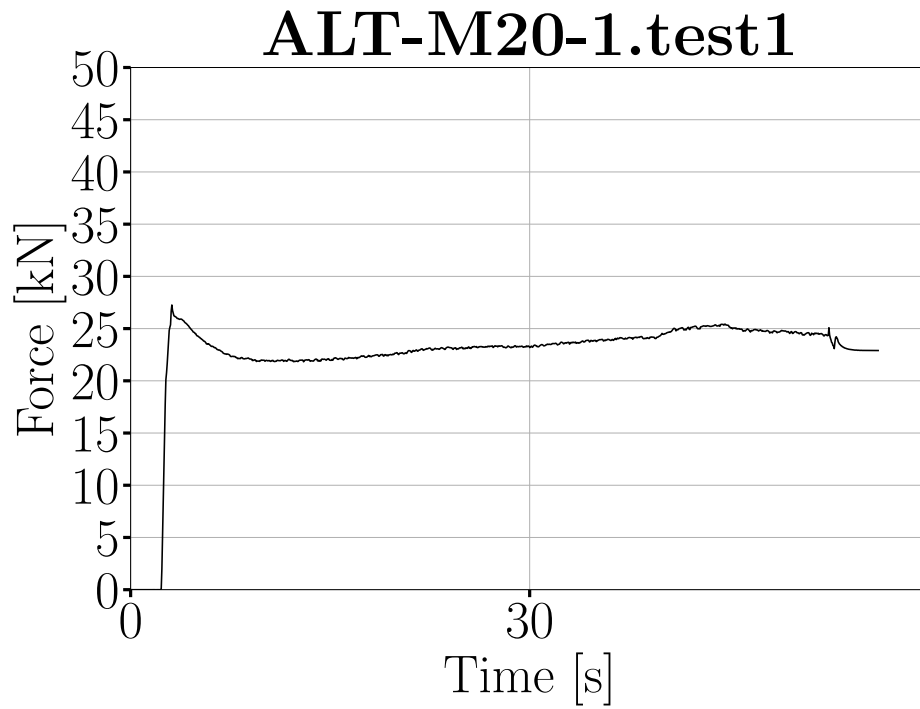


Figure 10.4: Force plotted against time.

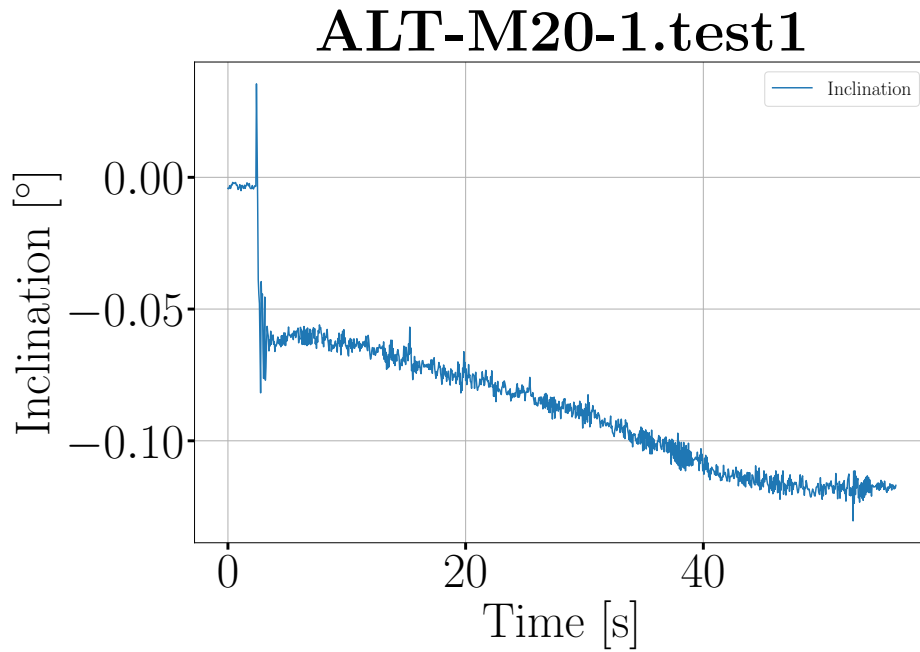


Figure 10.5: Inclination plotted against time.

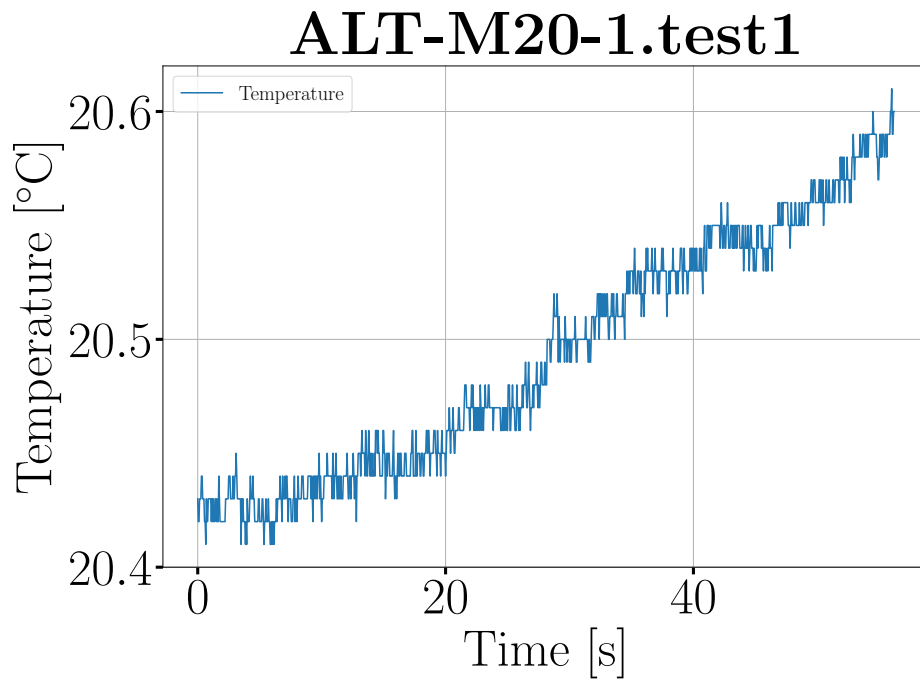


Figure 10.6: Temperature plotted against time.

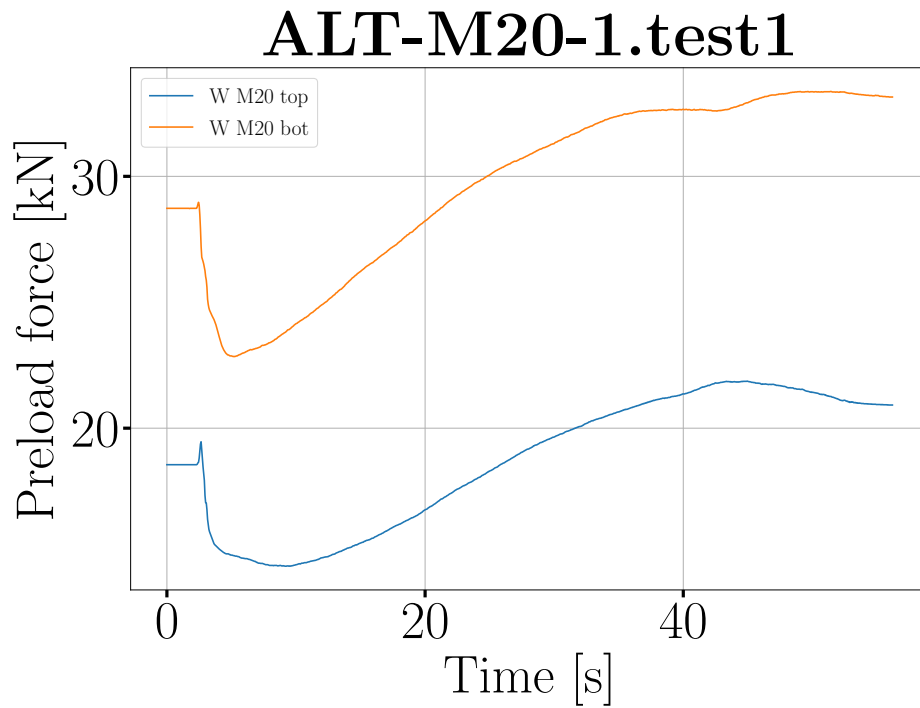


Figure 10.7: Preload in bolts.

10.1 Test 10.2

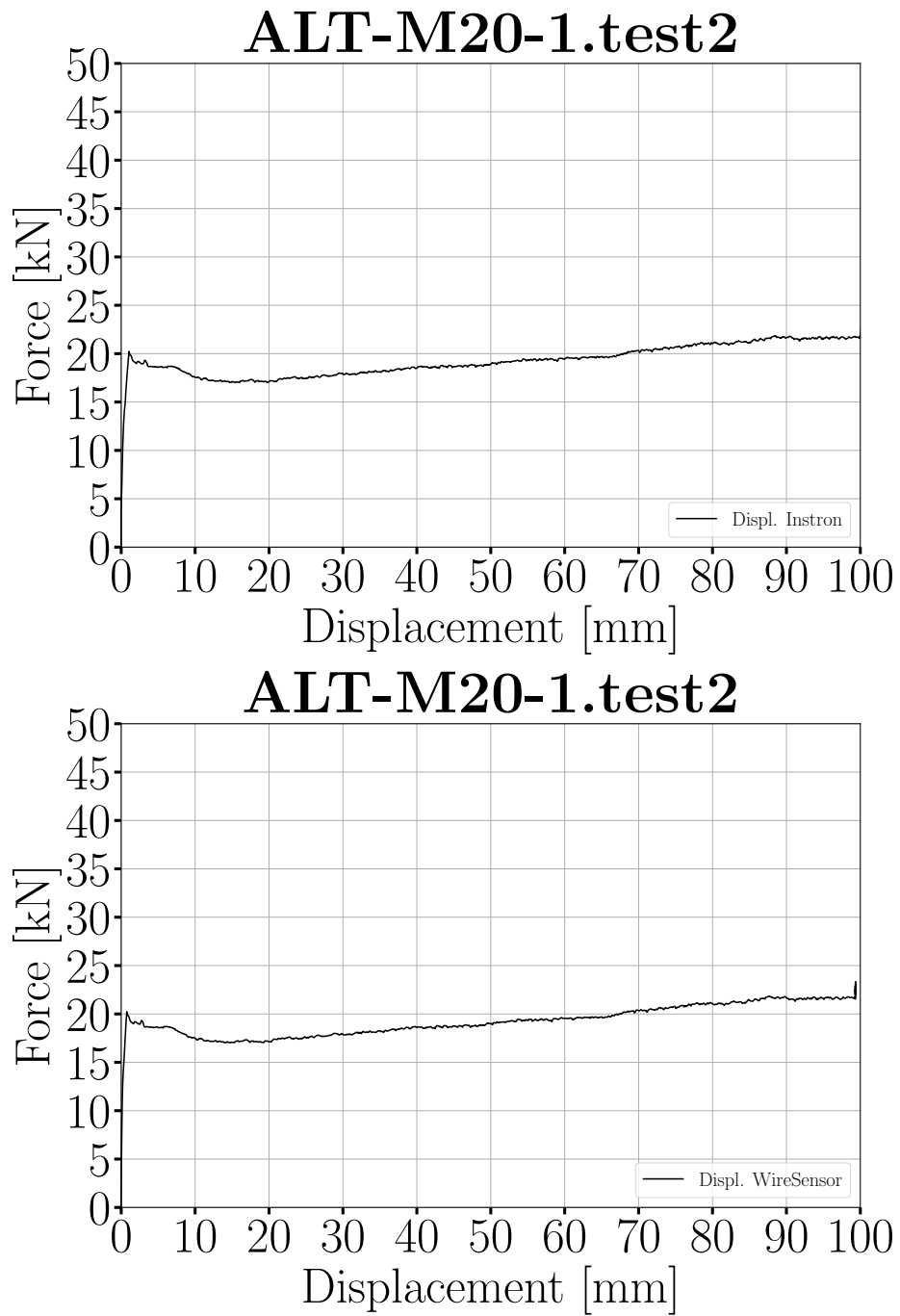


Figure 10.8: Load displacement graph.

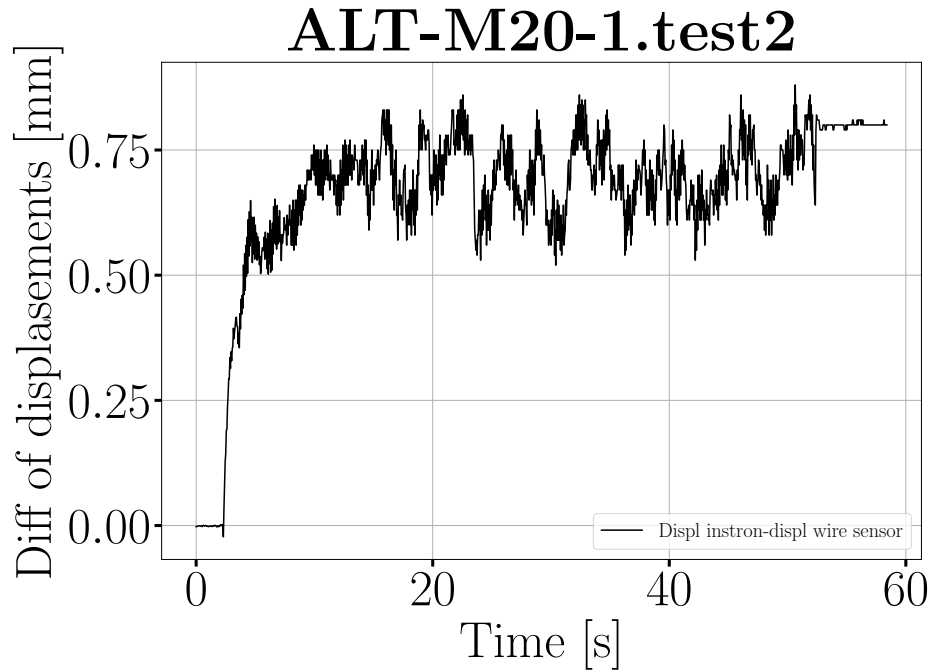


Figure 10.9: Difference of displacement between instron press and wire sensor.

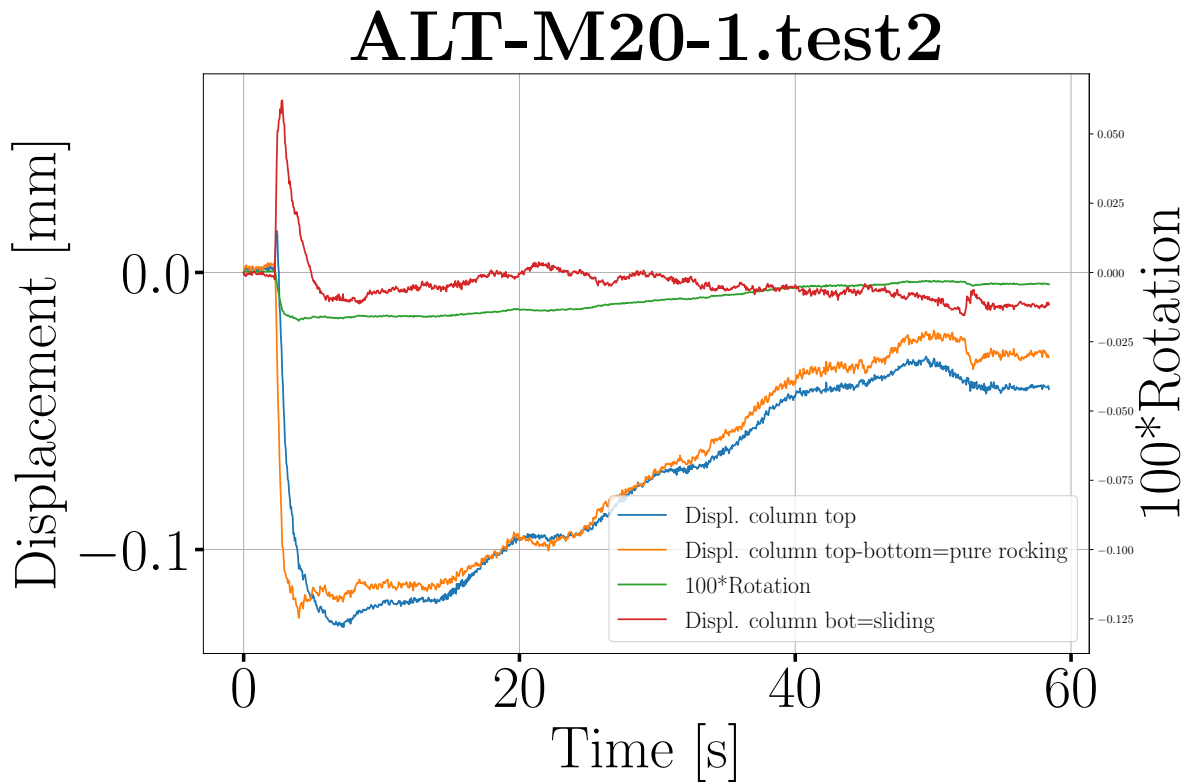


Figure 10.10: Movements of the column.

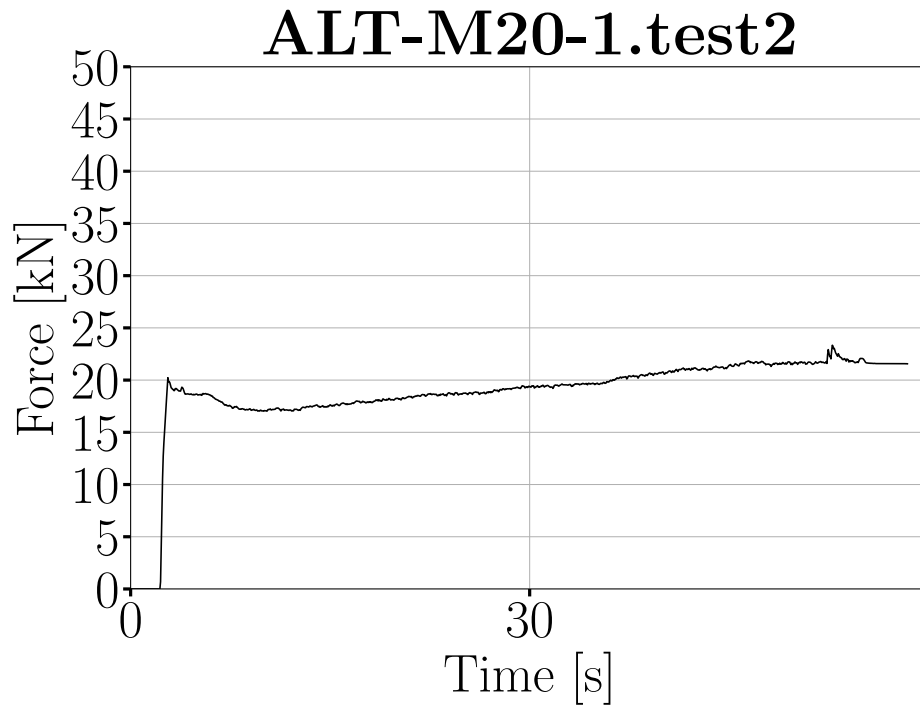


Figure 10.11: Force plotted against time.

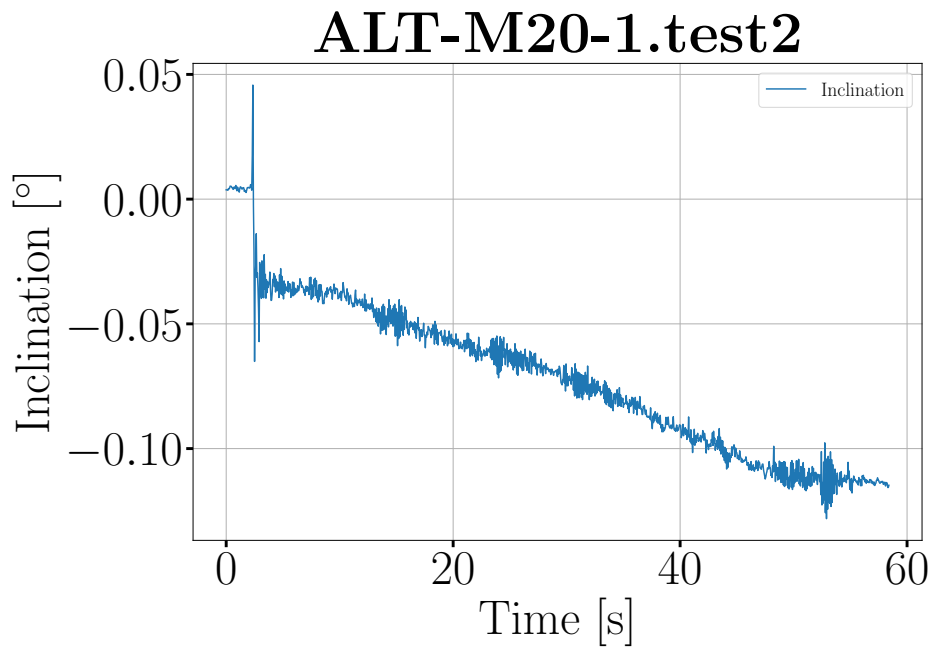


Figure 10.12: Inclination plotted against time.

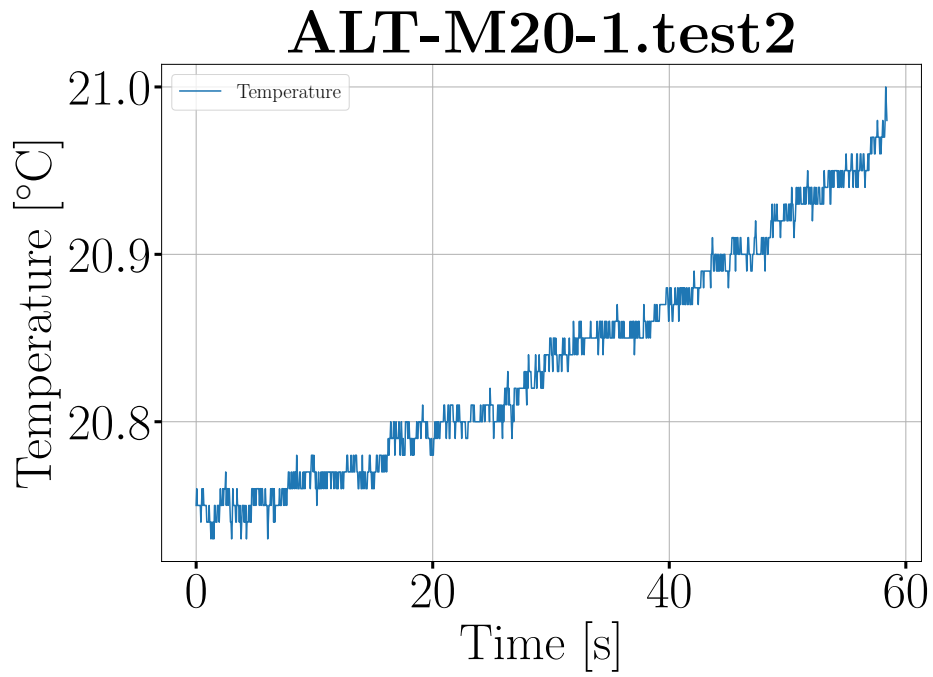


Figure 10.13: Temperature plotted against time.

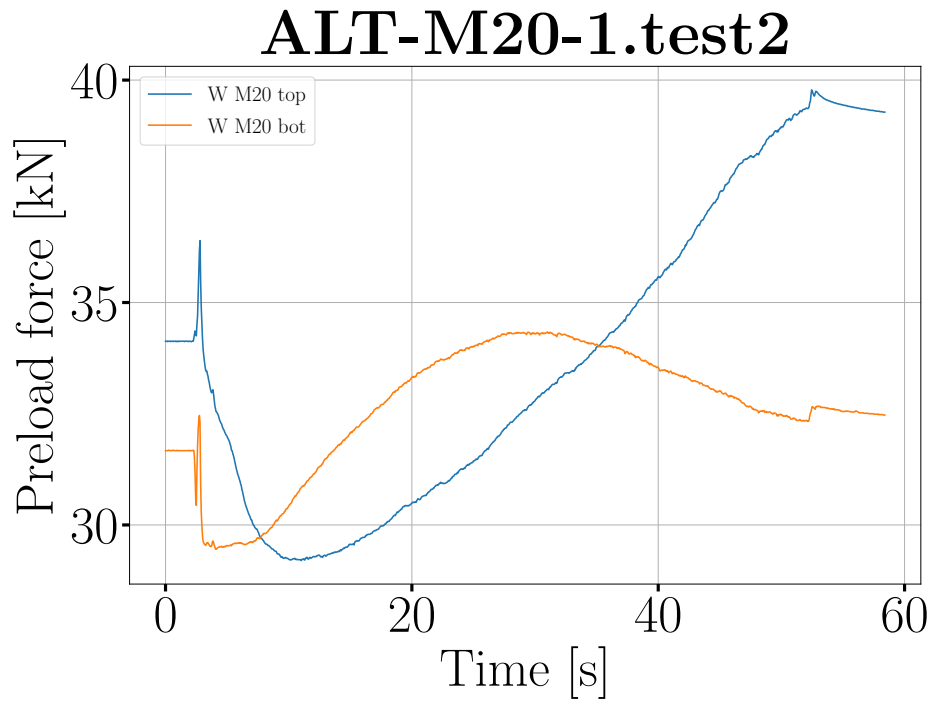


Figure 10.14: Preload in bolts.

10.2 Test 10.3

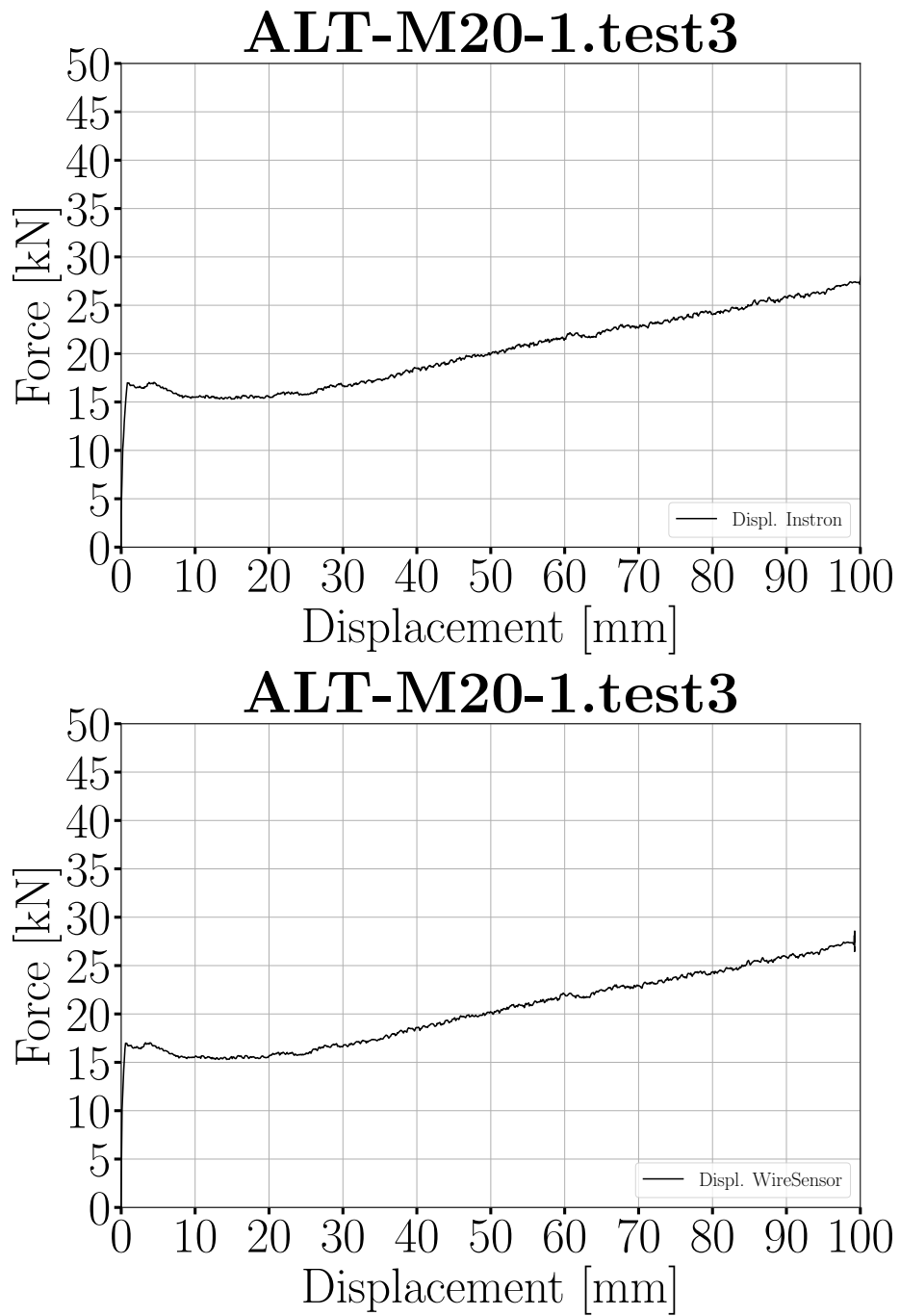


Figure 10.15: Load displacement graph.

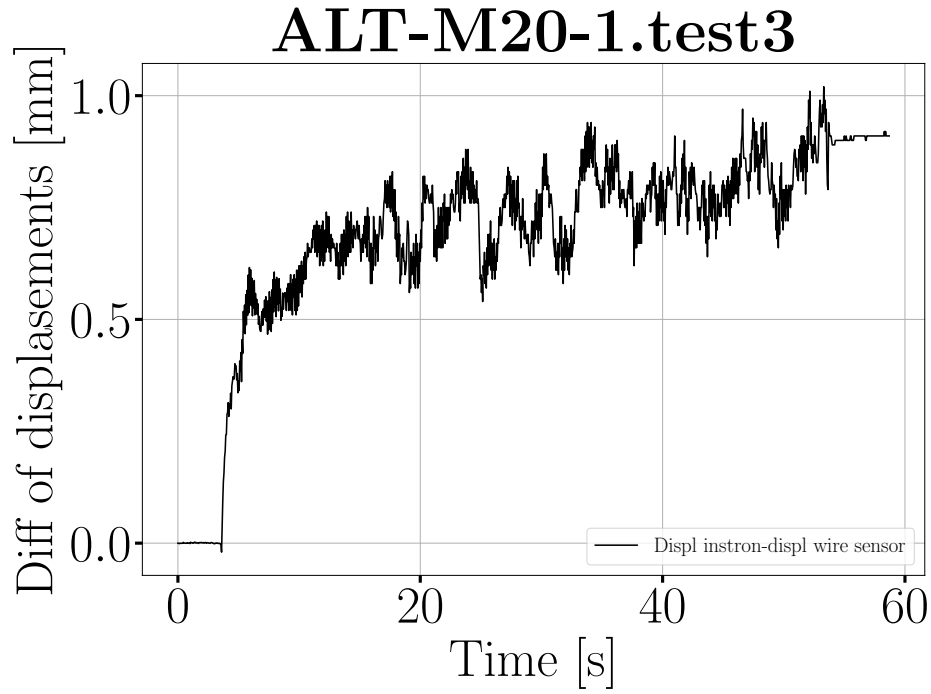


Figure 10.16: Difference of displacement between instron press and wire sensor.

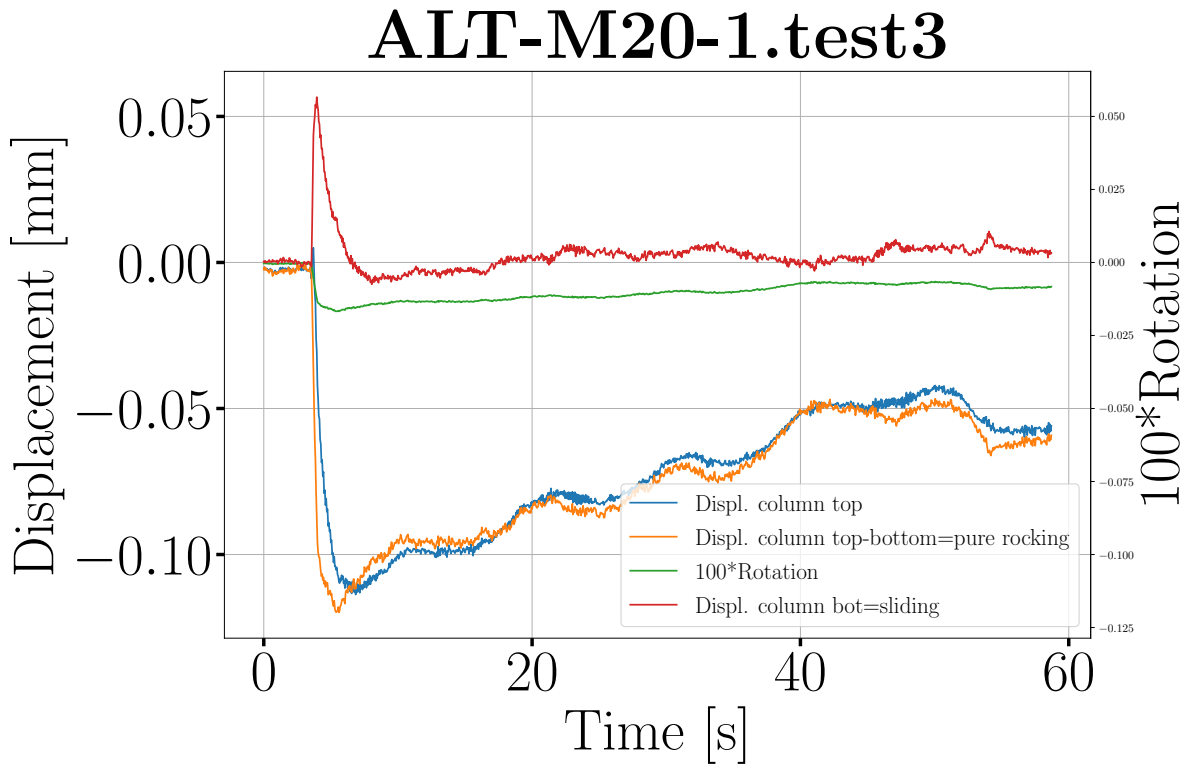


Figure 10.17: Movements of the column.

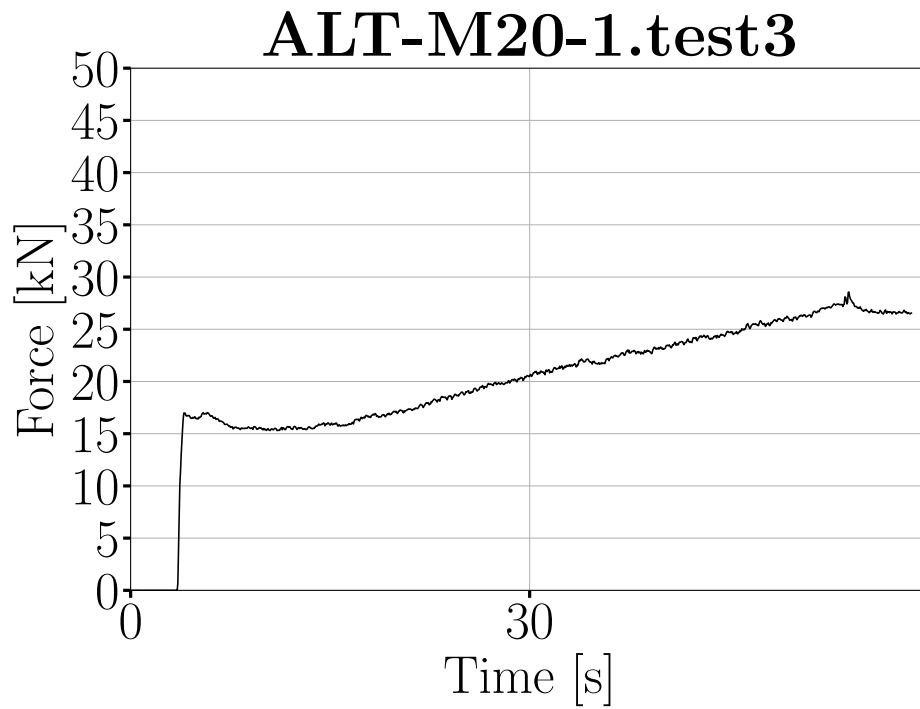


Figure 10.18: Force plotted against time.

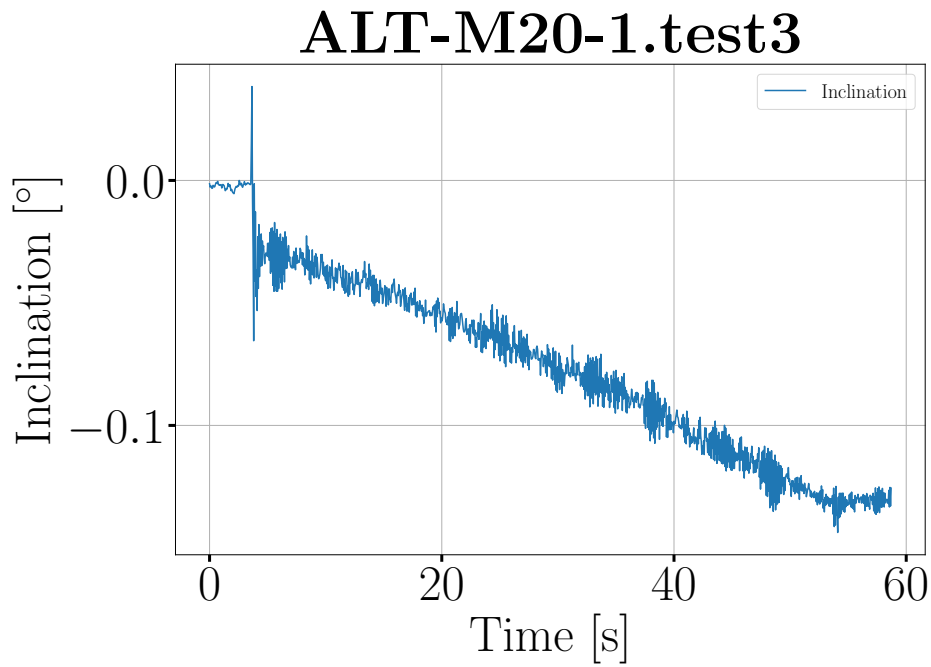


Figure 10.19: Inclination plotted against time.

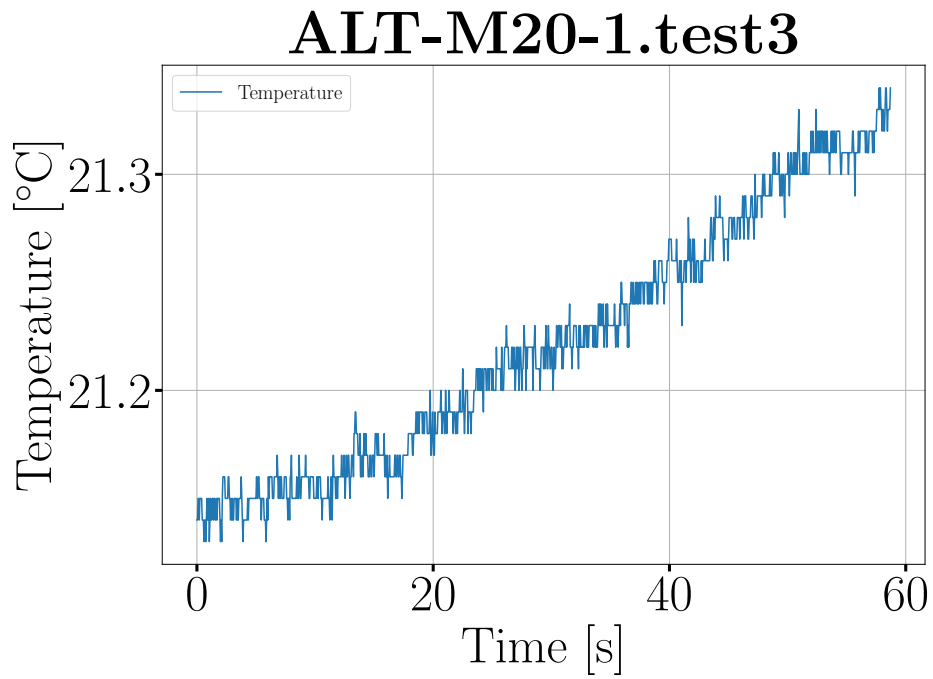


Figure 10.20: Temperature plotted against time.

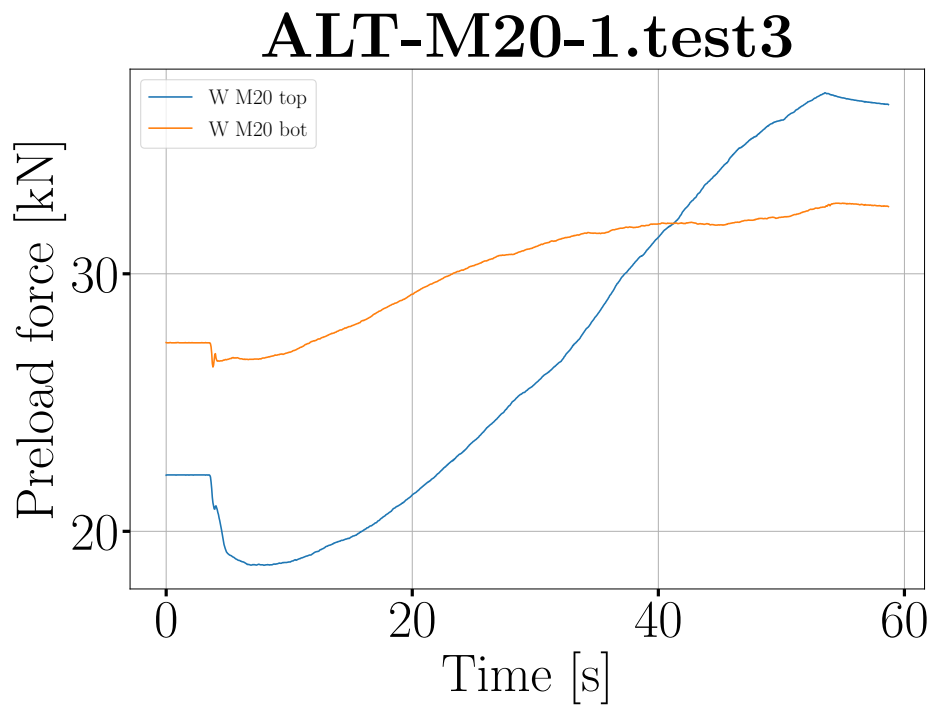


Figure 10.21: Preload in bolts.

10.3 Test 10.4

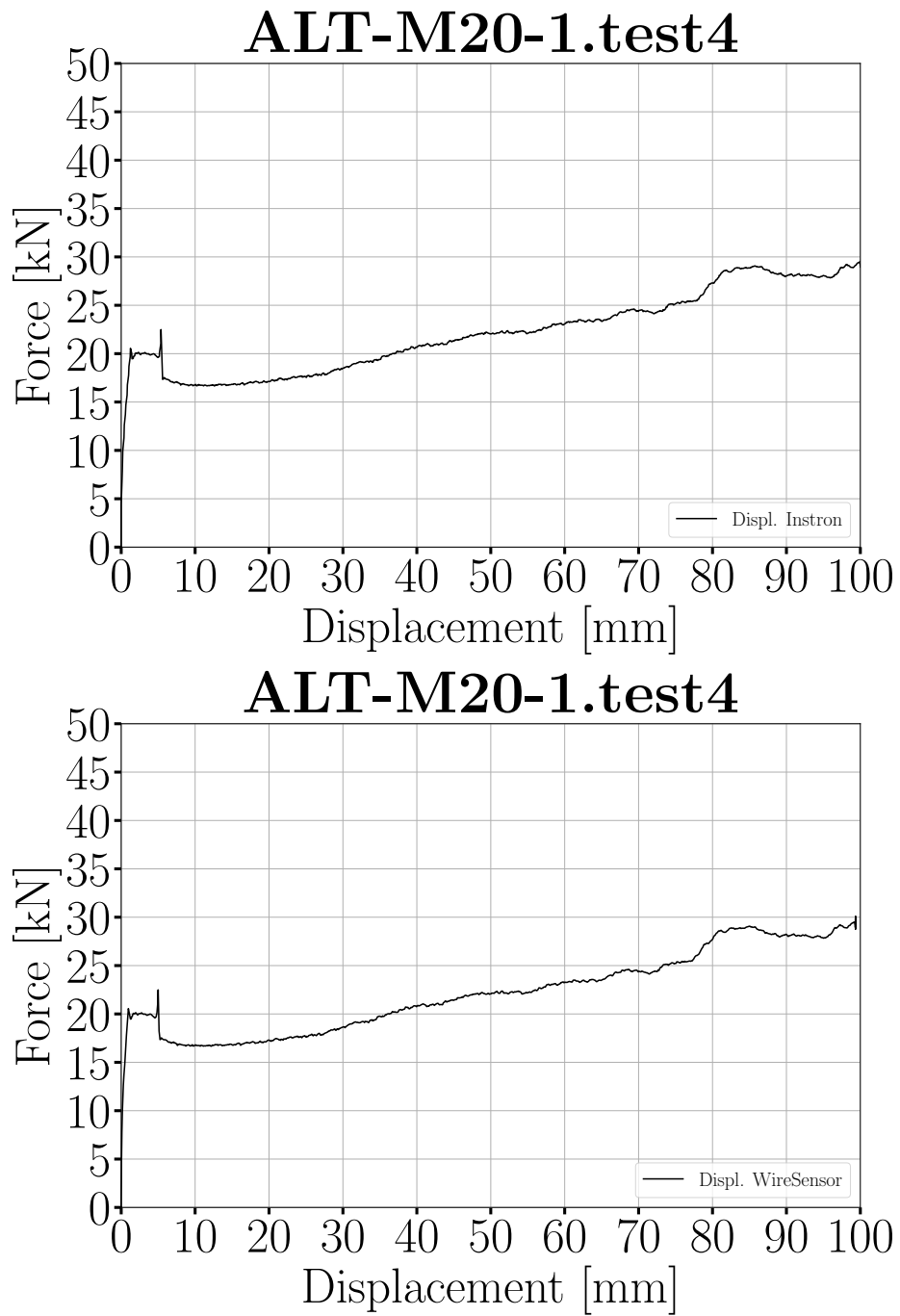


Figure 10.22: Load displacement graph.

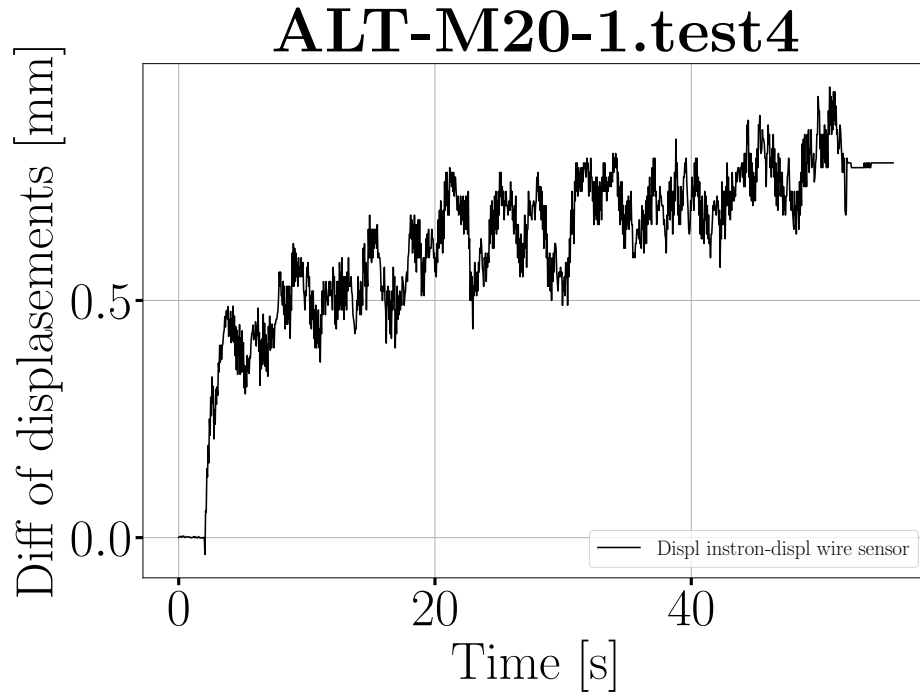


Figure 10.23: Difference of displacement between instron press and wire sensor.

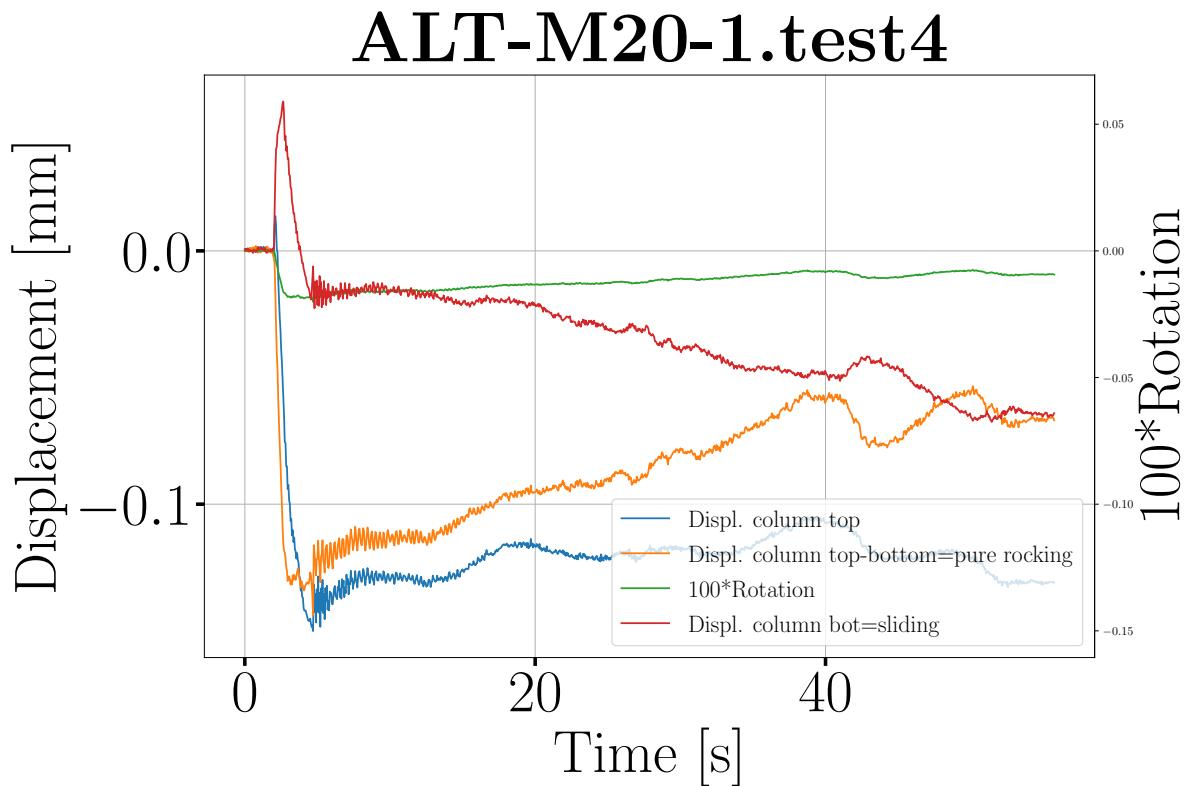


Figure 10.24: Movements of the column.

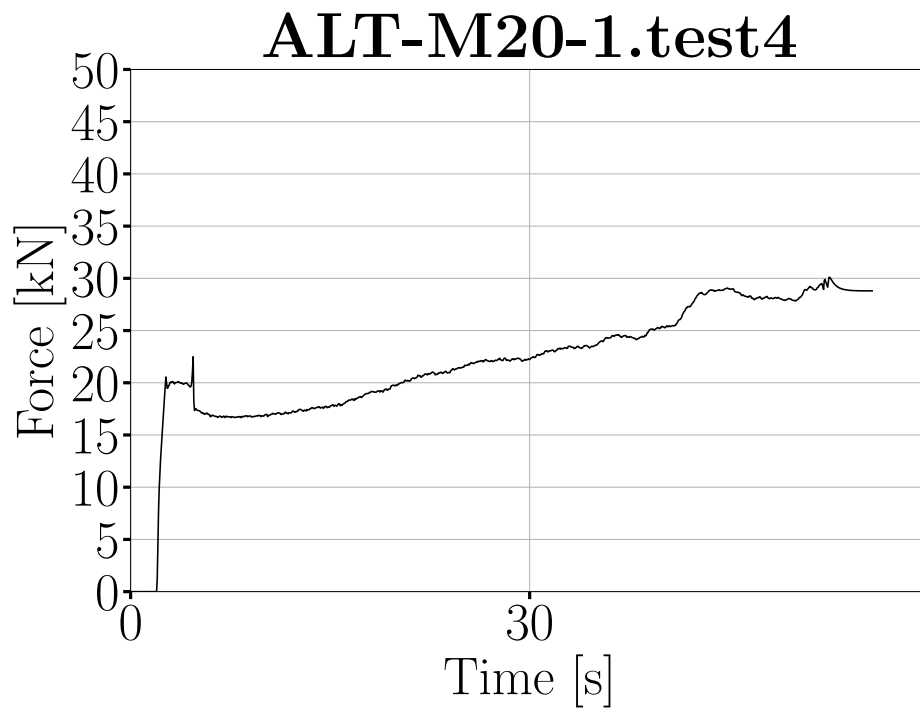


Figure 10.25: Force plotted against time.

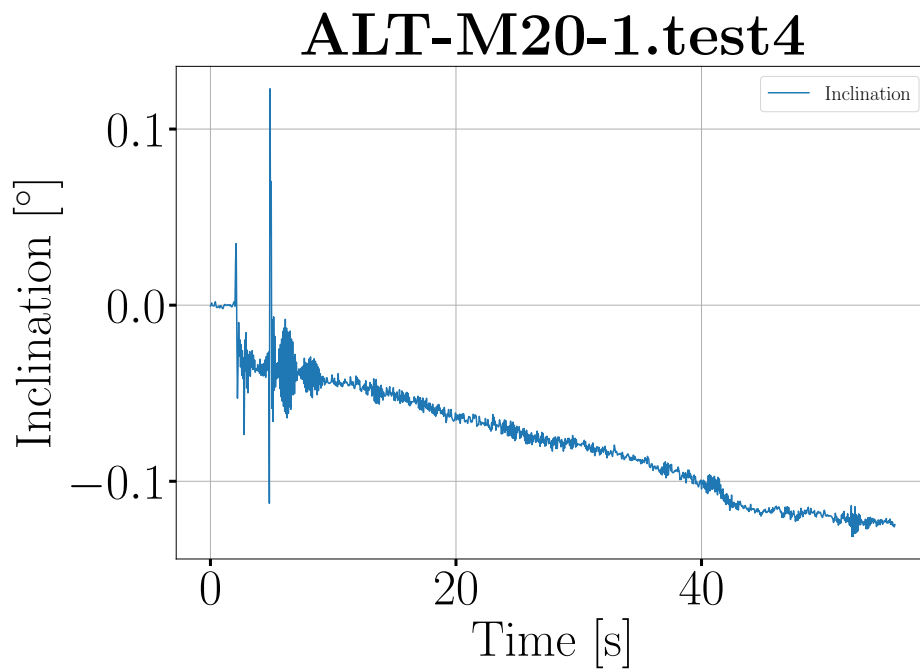


Figure 10.26: Inclination plotted against time.

ALT-M20-1.test4

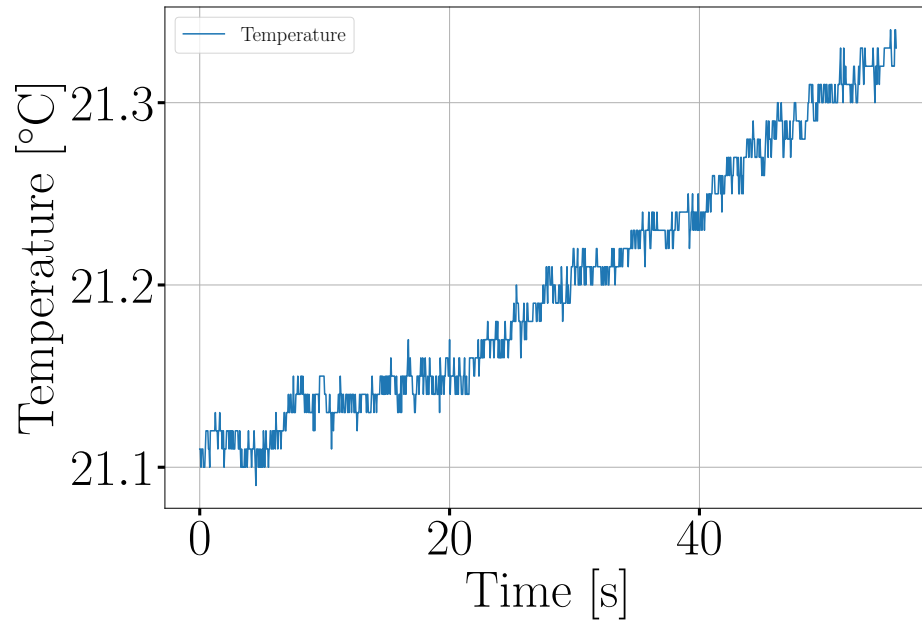


Figure 10.27: Temperature plotted against time.

10.4 Test 10.5

$$F_{\text{slip}} = 34.3kN \quad F_{SD} = 10.8kN \quad COV = 0.3 \quad \lambda = 3.2 \quad (10.1)$$

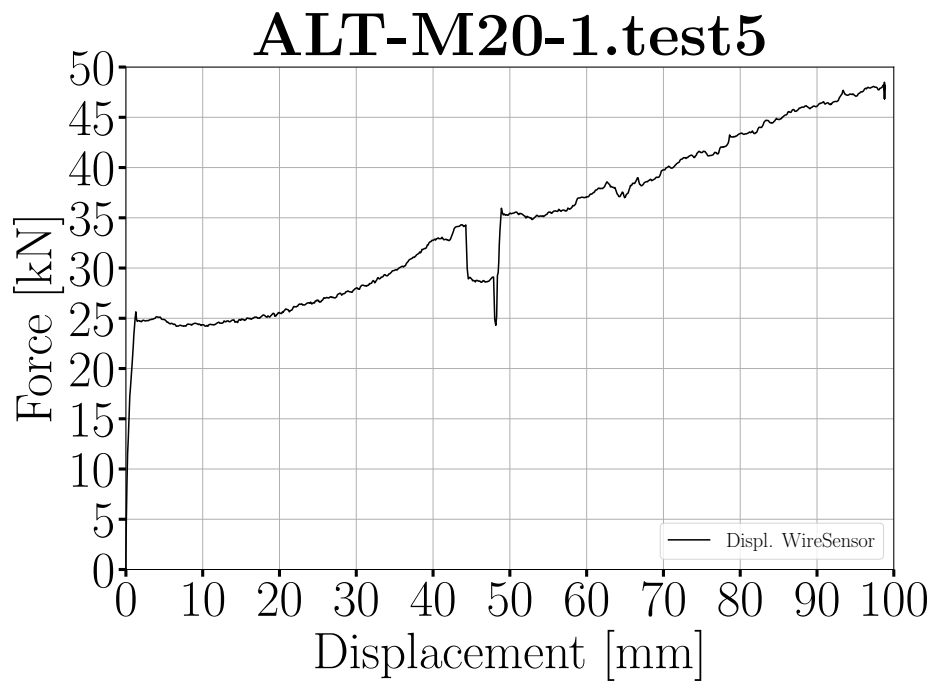
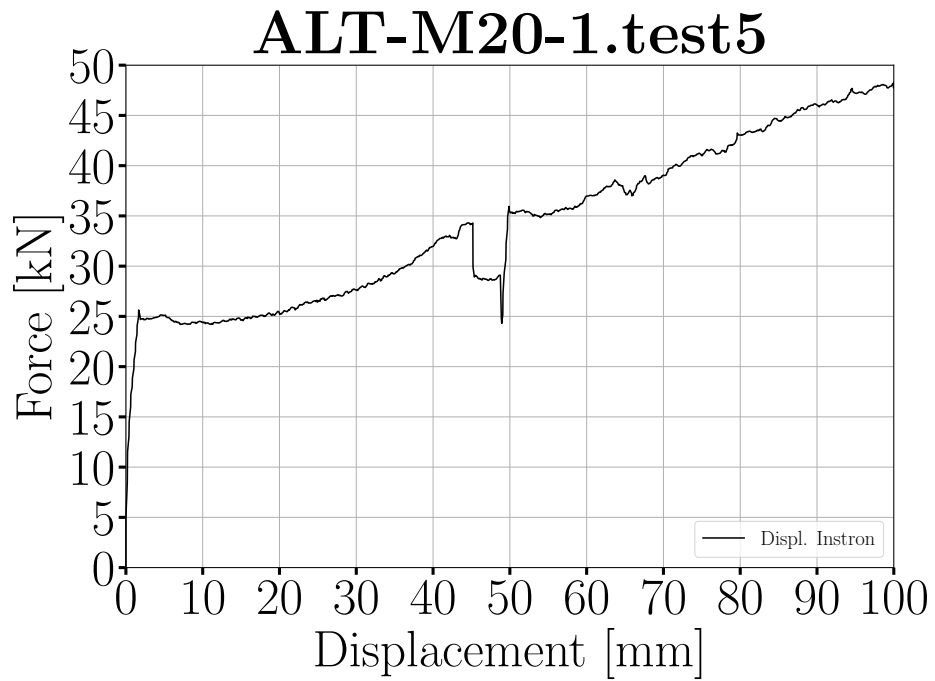


Figure 10.28: Load displacement graph.

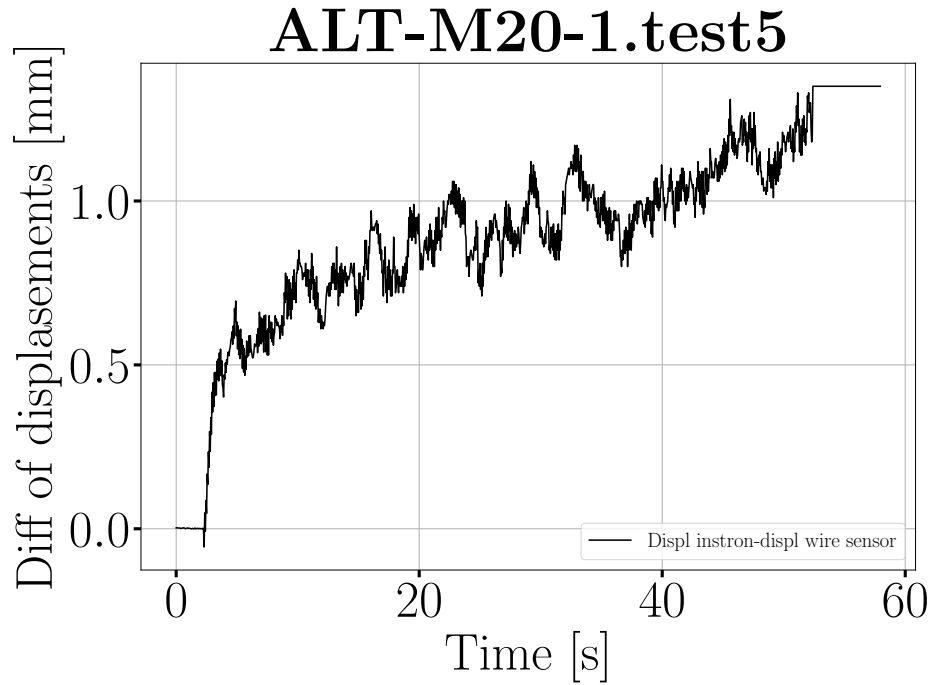


Figure 10.29: Difference of displacement between instron press and wire sensor.

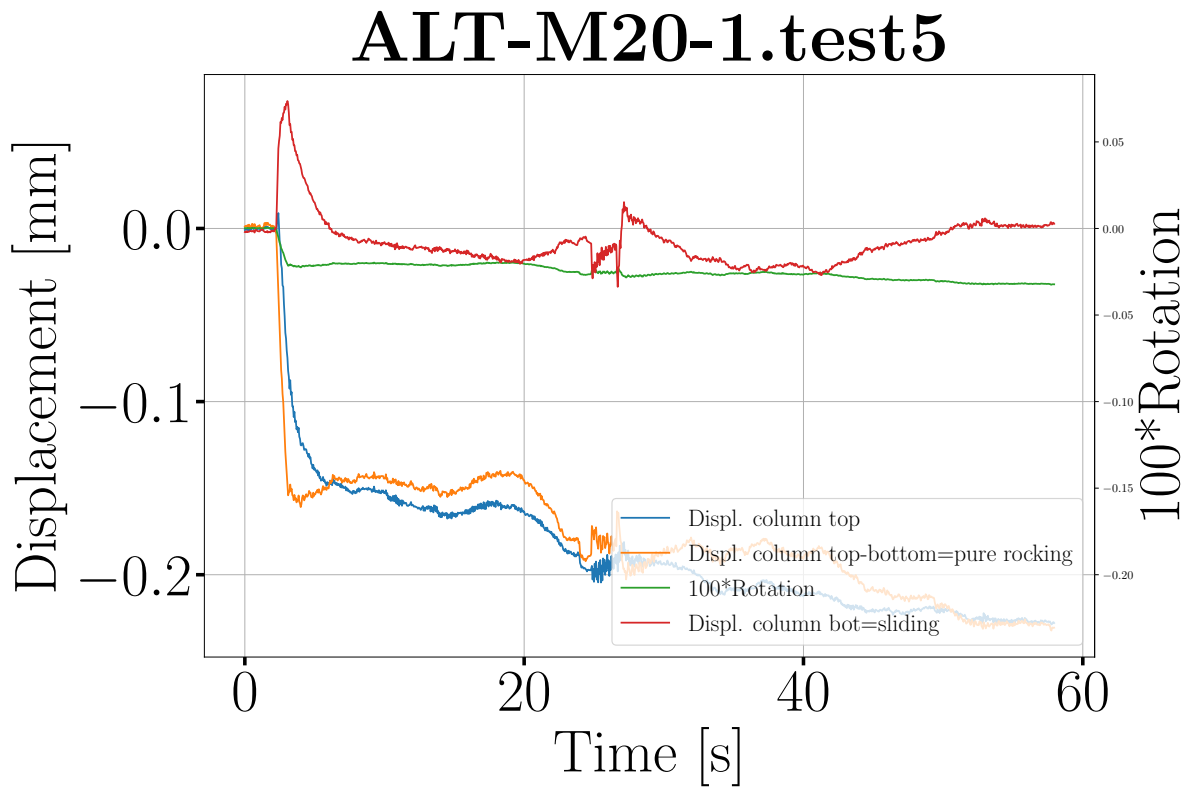


Figure 10.30: Movements of the column.

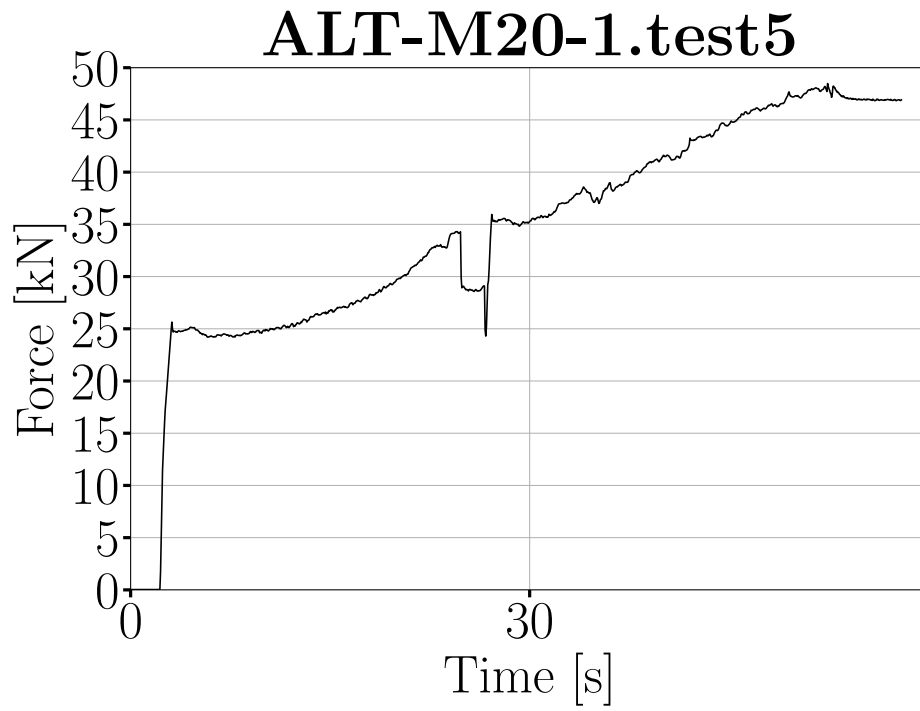


Figure 10.31: Force plotted against time.

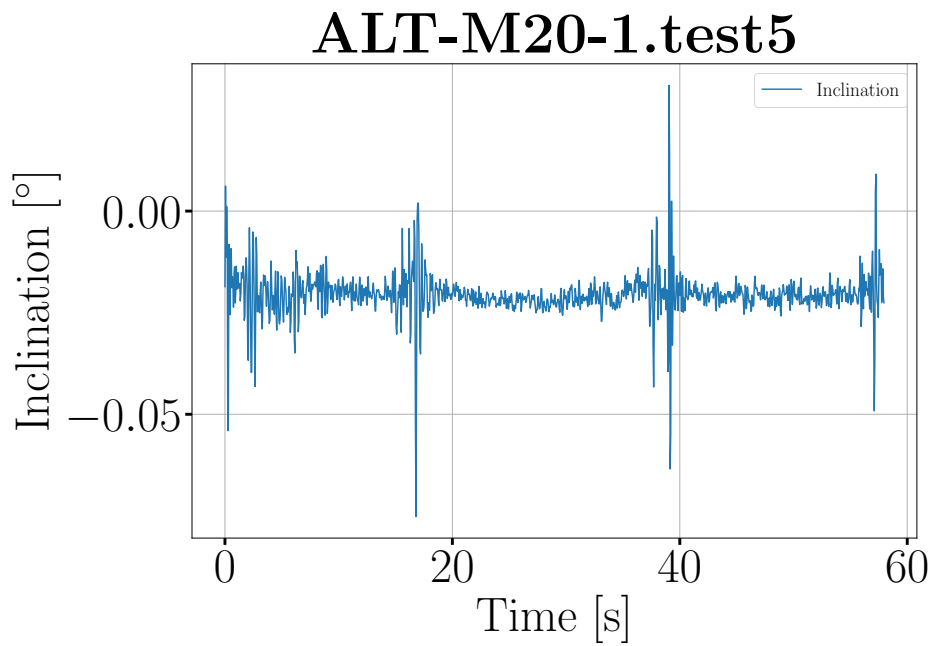


Figure 10.32: Inclination plotted against time.

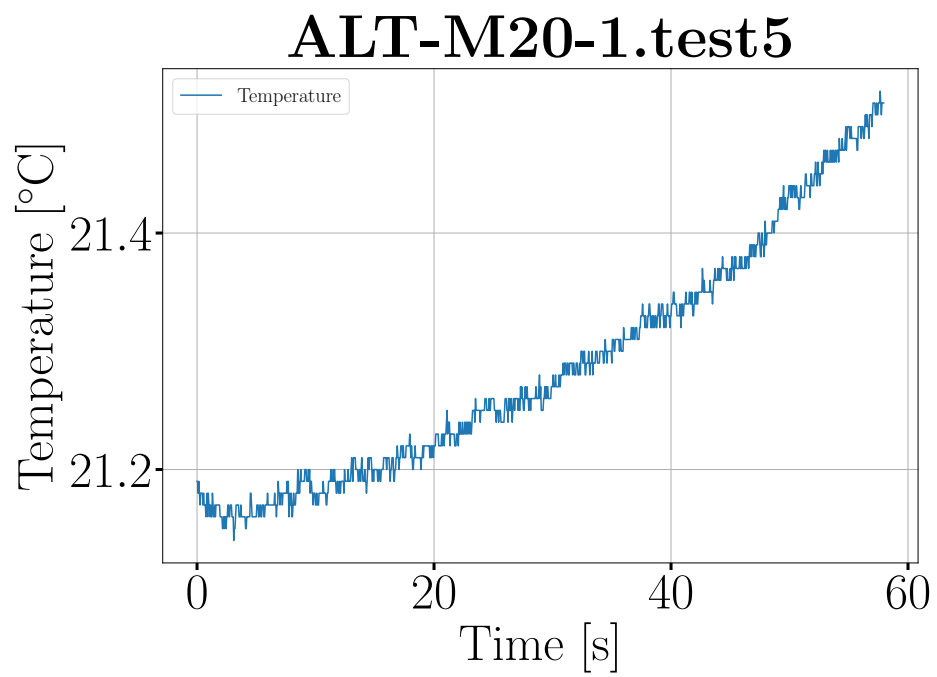


Figure 10.33: Temperature plotted against time.

Chapter 11

Test 11 - ALT-M20_1 - 14.05.21

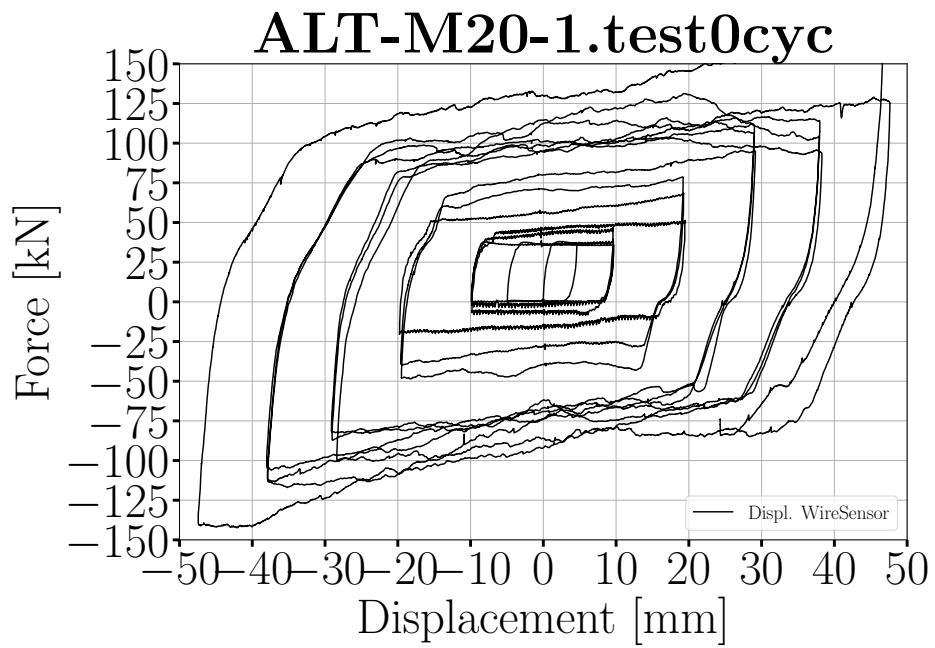
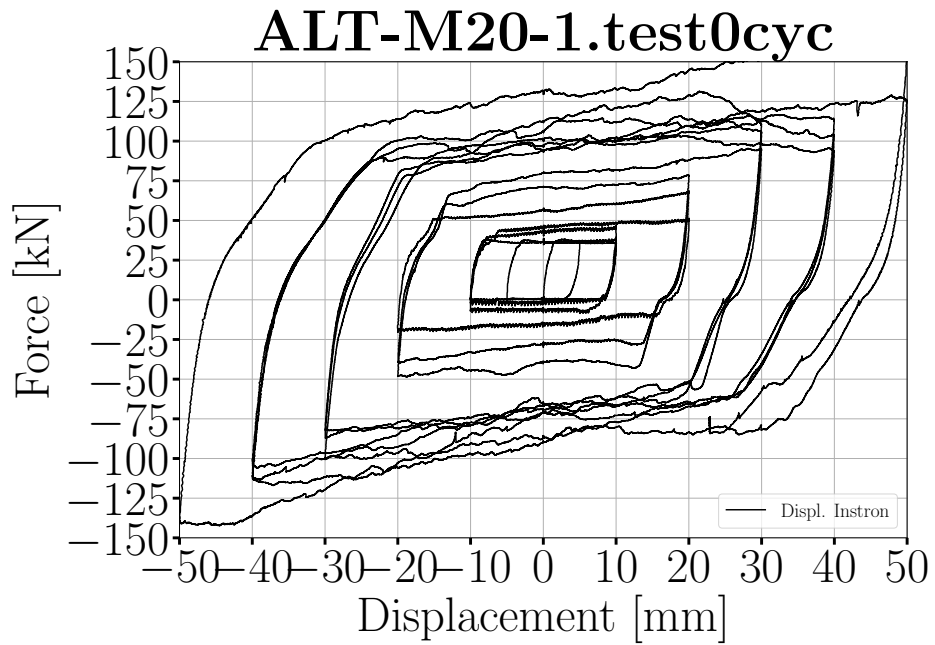


Figure 11.1: Load displacement graph.

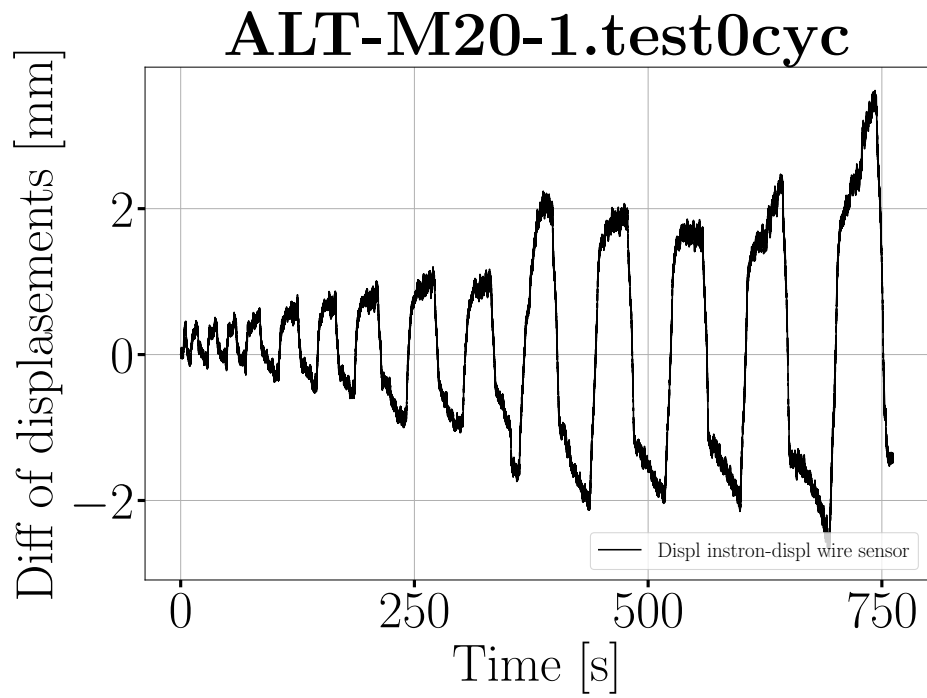


Figure 11.2: Difference of displacement between instron press and wire sensor.

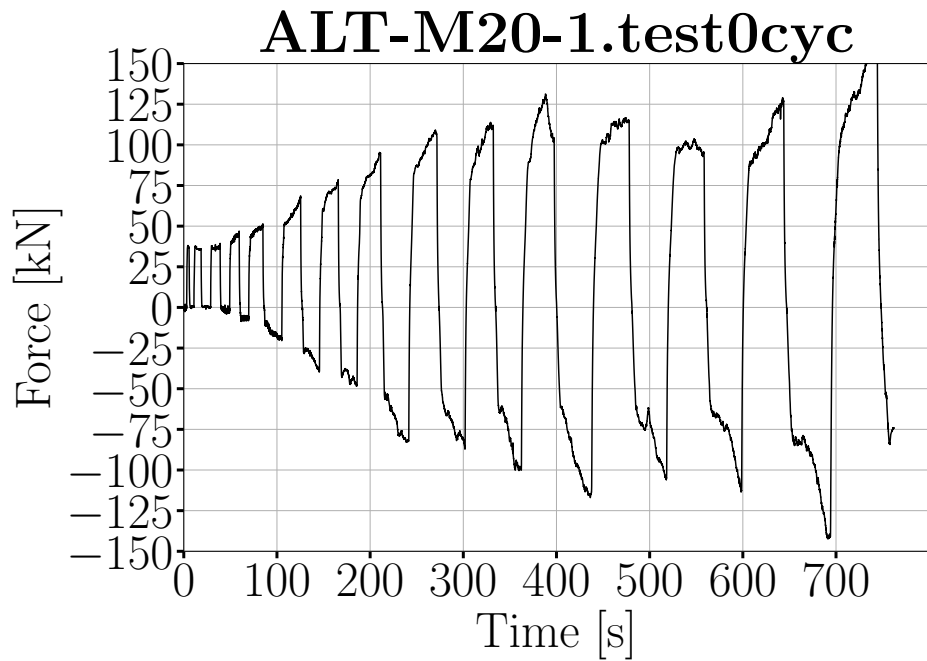


Figure 11.3: Force plotted against time.

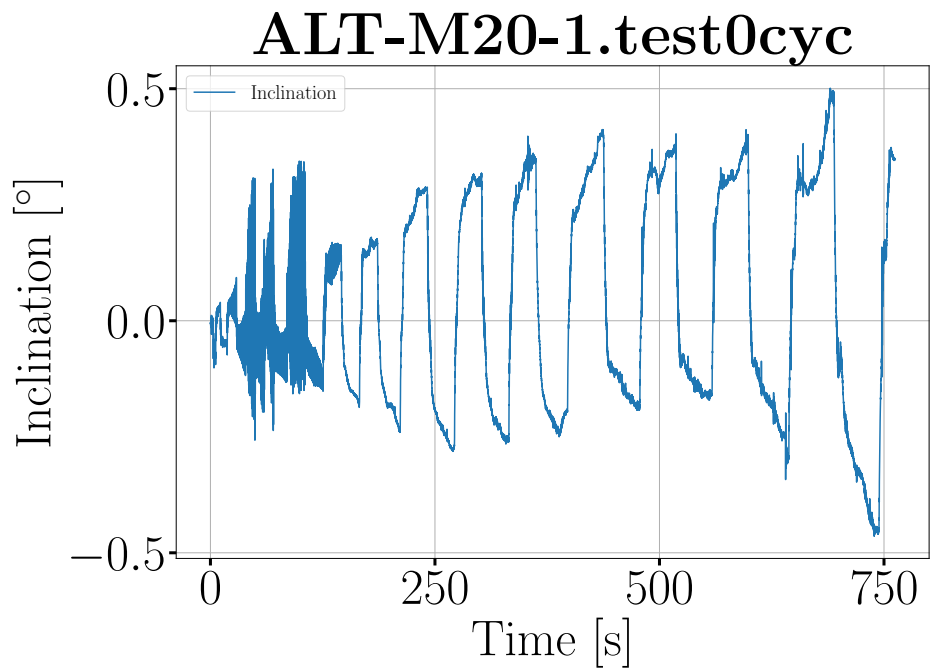


Figure 11.4: Inclination plotted against time.

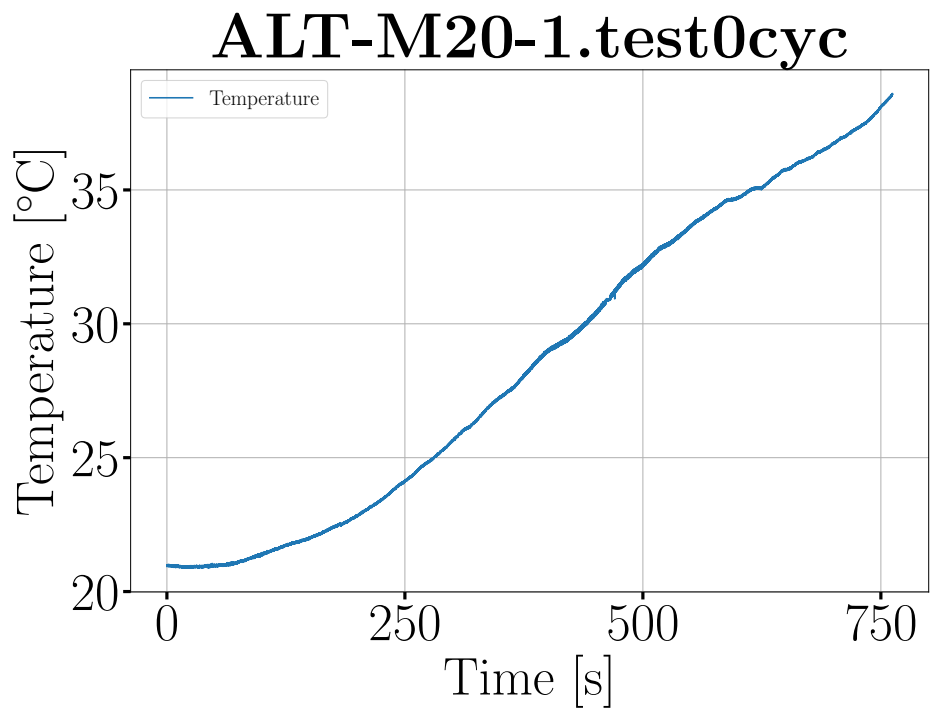


Figure 11.5: Temperature plotted against time.

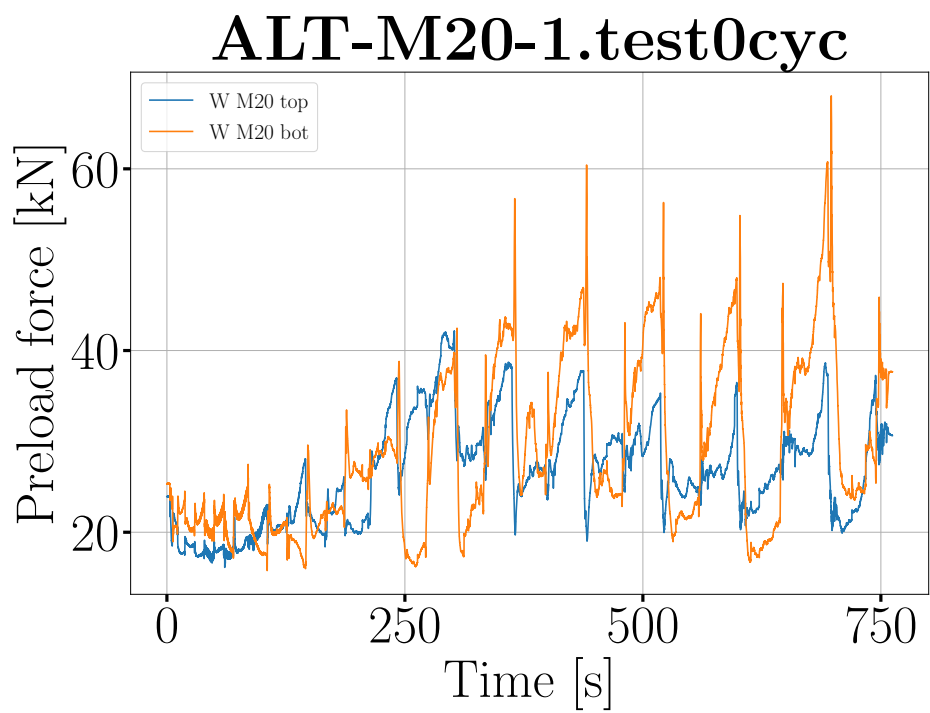


Figure 11.6: Preload in bolts.

Chapter 12

Test 12 - ALT-M20_2 - 15.05.21

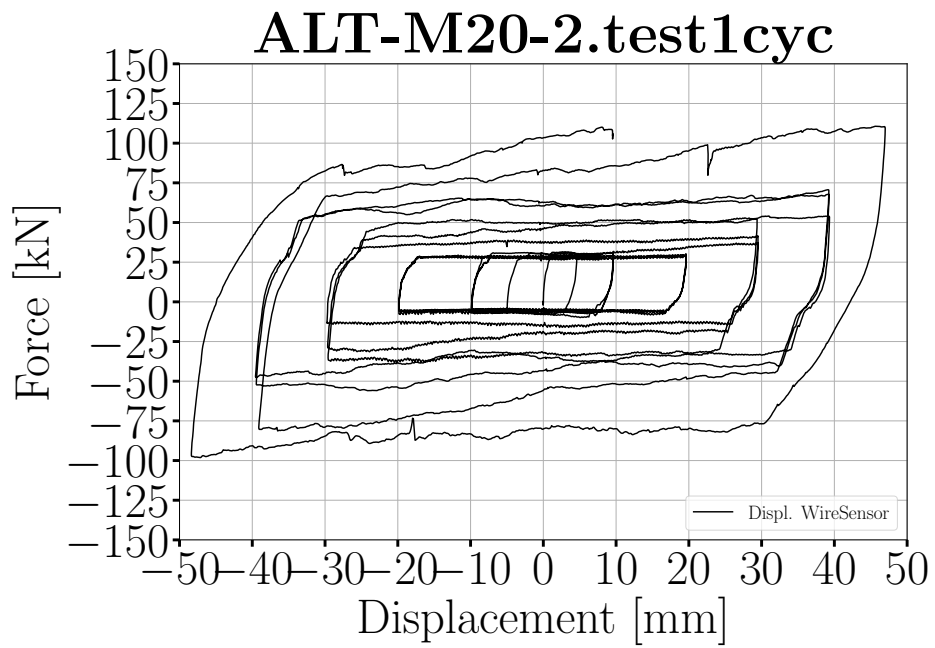
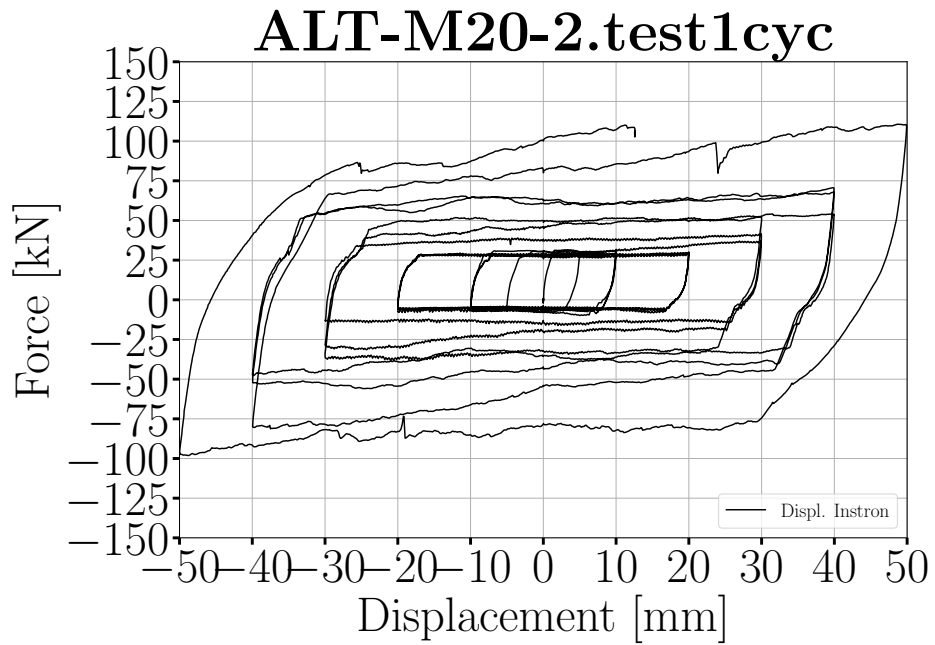


Figure 12.1: Load displacement graph.

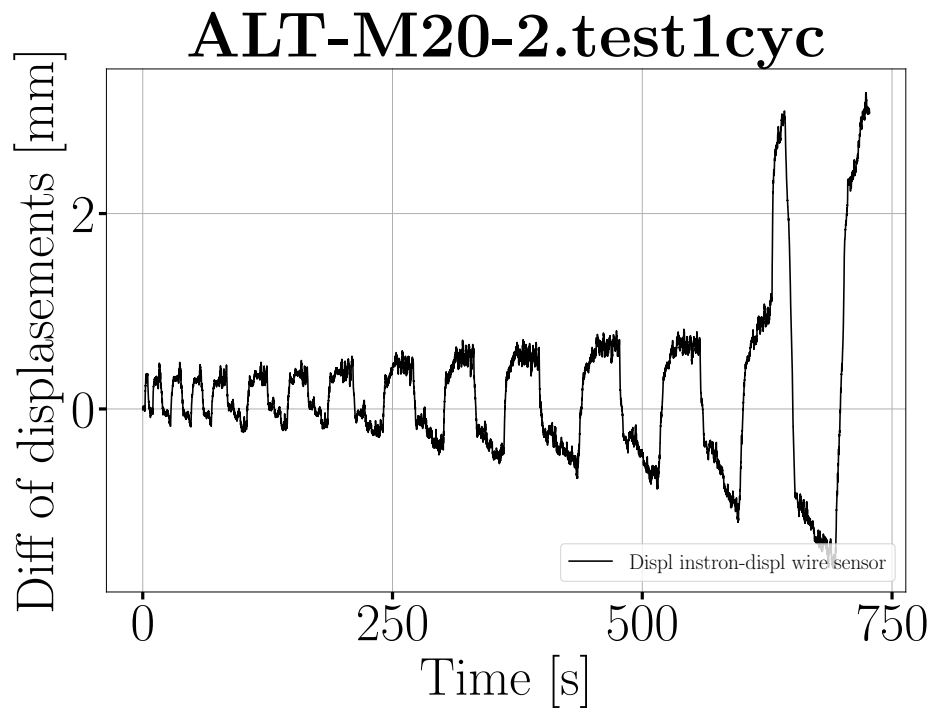


Figure 12.2: Difference of displacement between instron press and wire sensor.

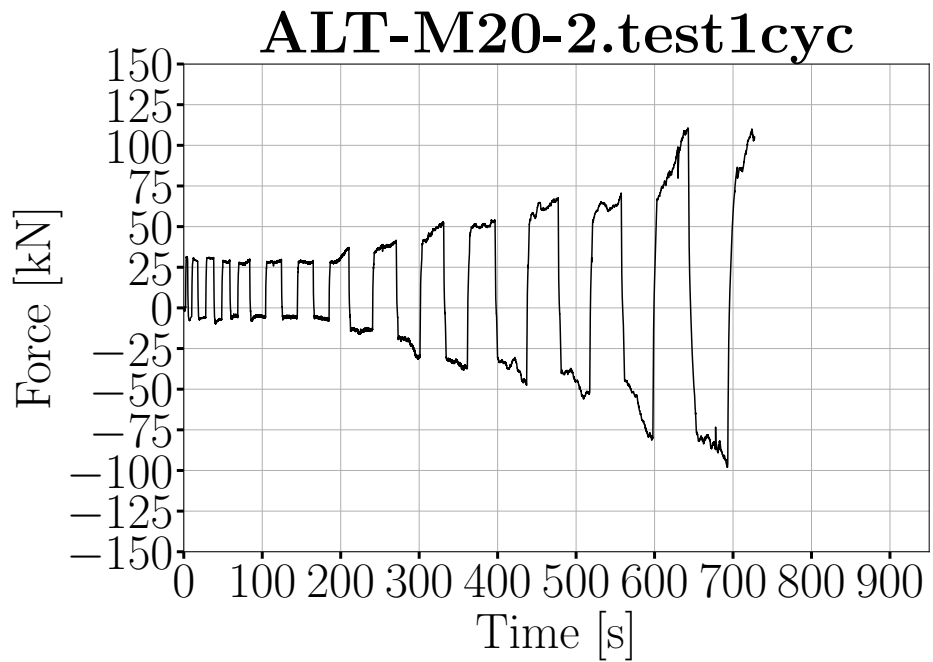


Figure 12.3: Force plotted against time.

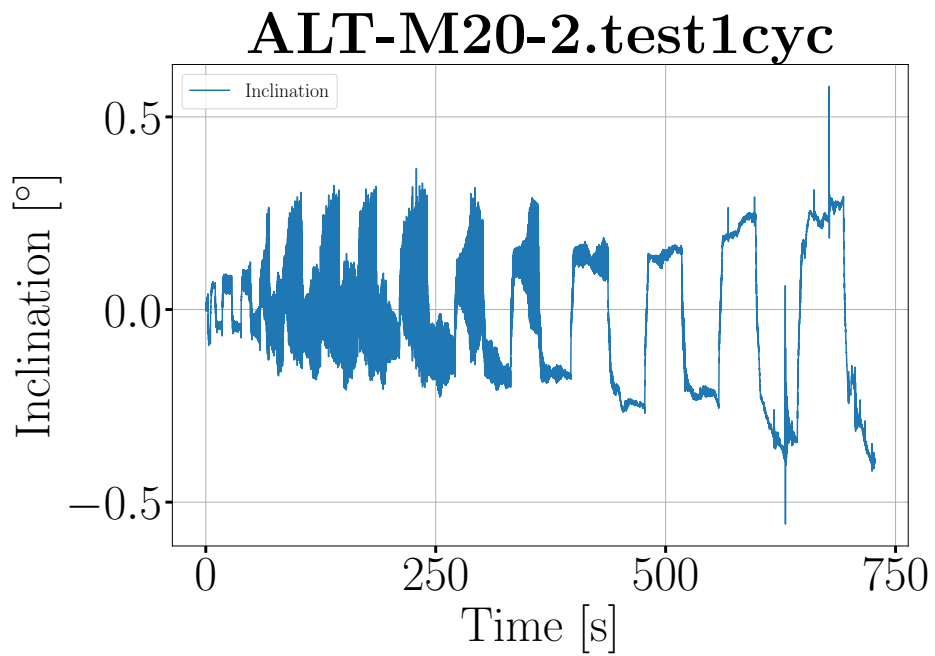


Figure 12.4: Inclination plotted against time.

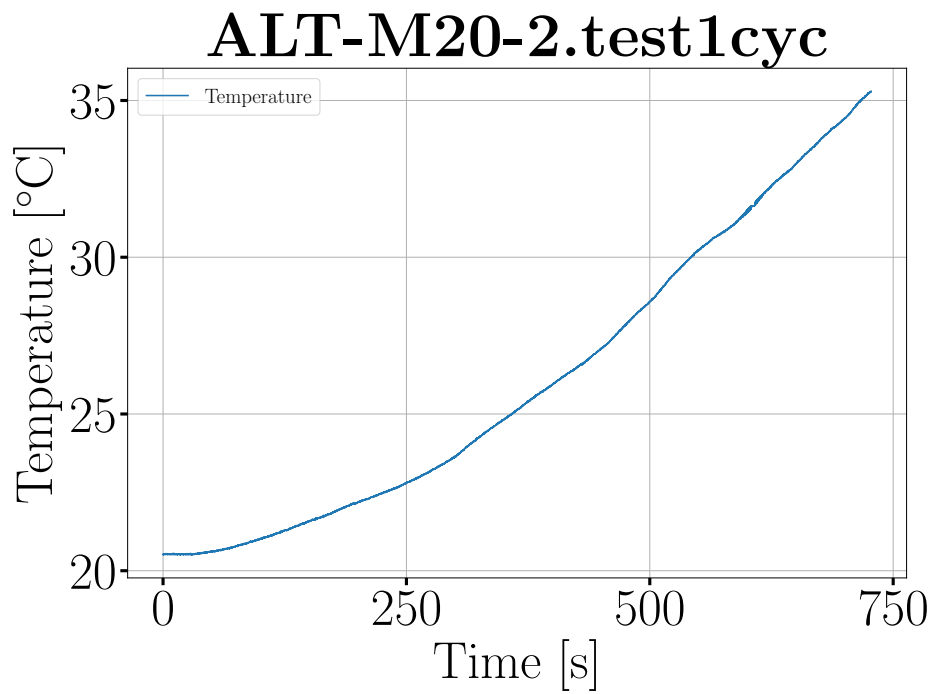


Figure 12.5: Temperature plotted against time.

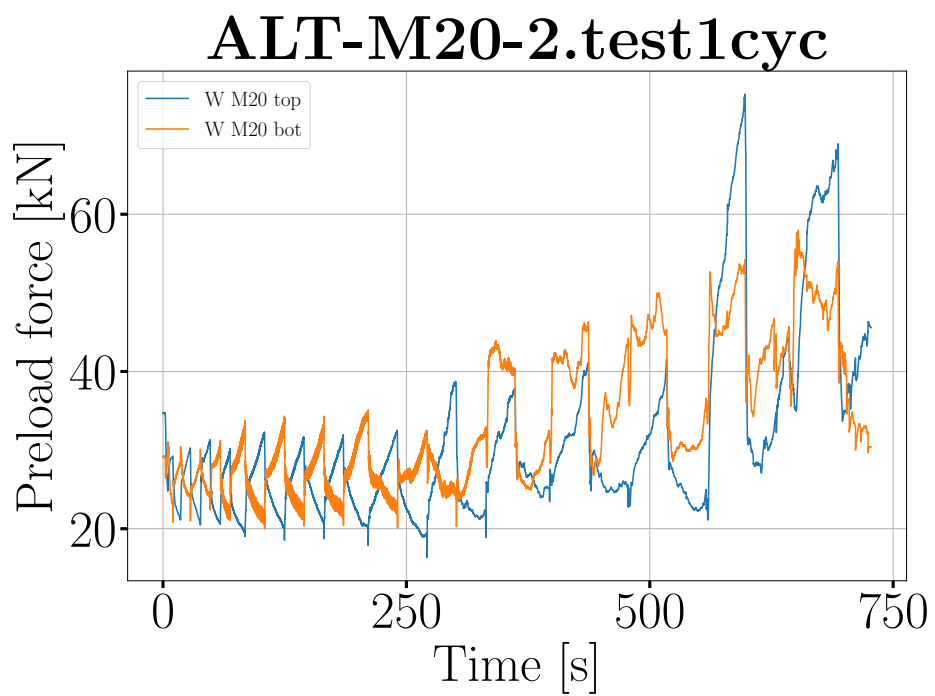


Figure 12.6: Preload in bolts.

Chapter 13

Test 13 - ALT-M10_1 - 15.05.21

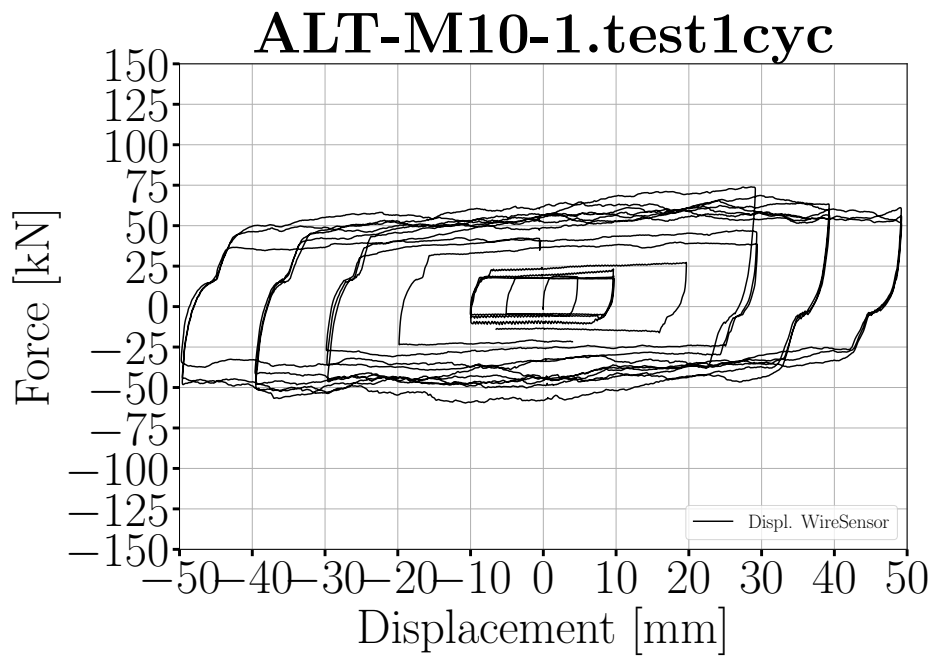
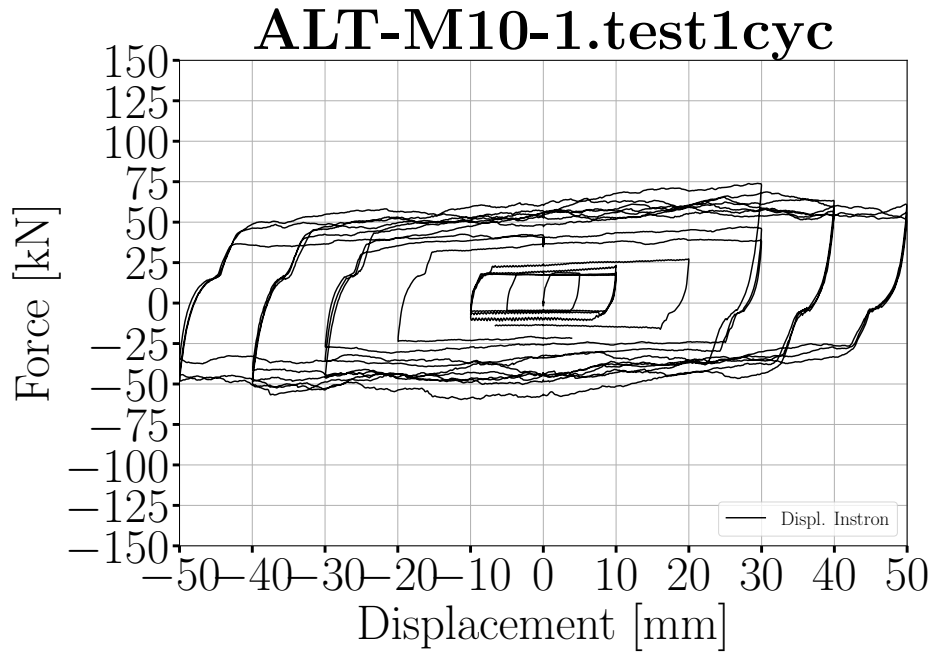


Figure 13.1: Load displacement graph.

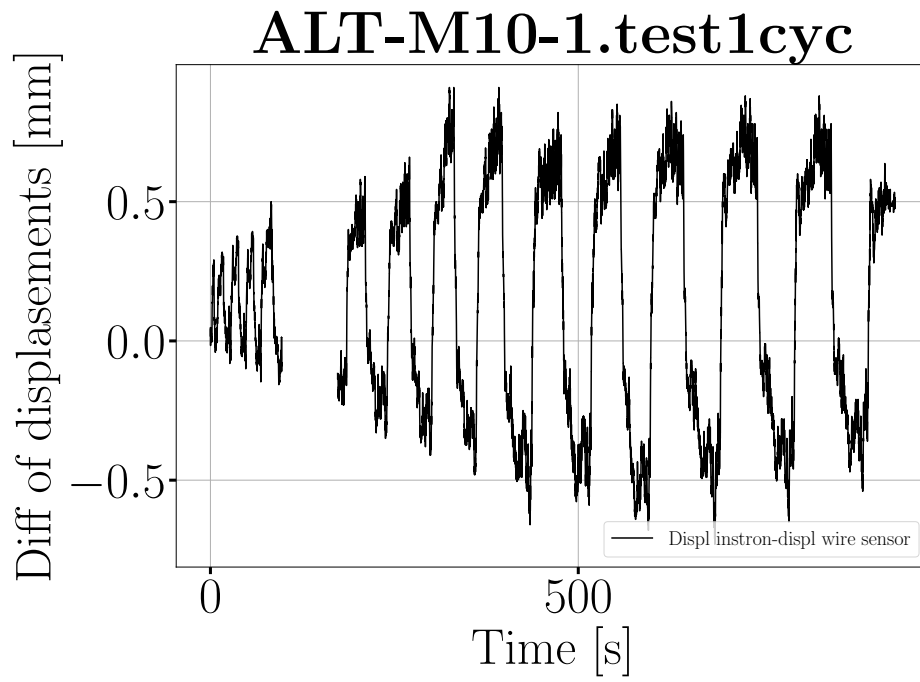


Figure 13.2: Difference of displacement between instron press and wire sensor.

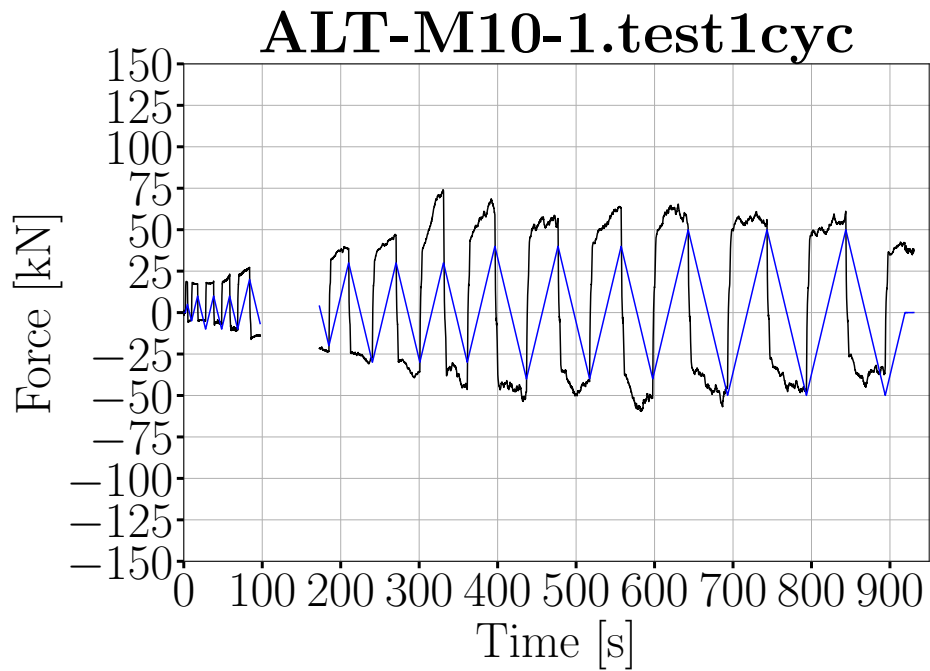


Figure 13.3: Force plotted against time.

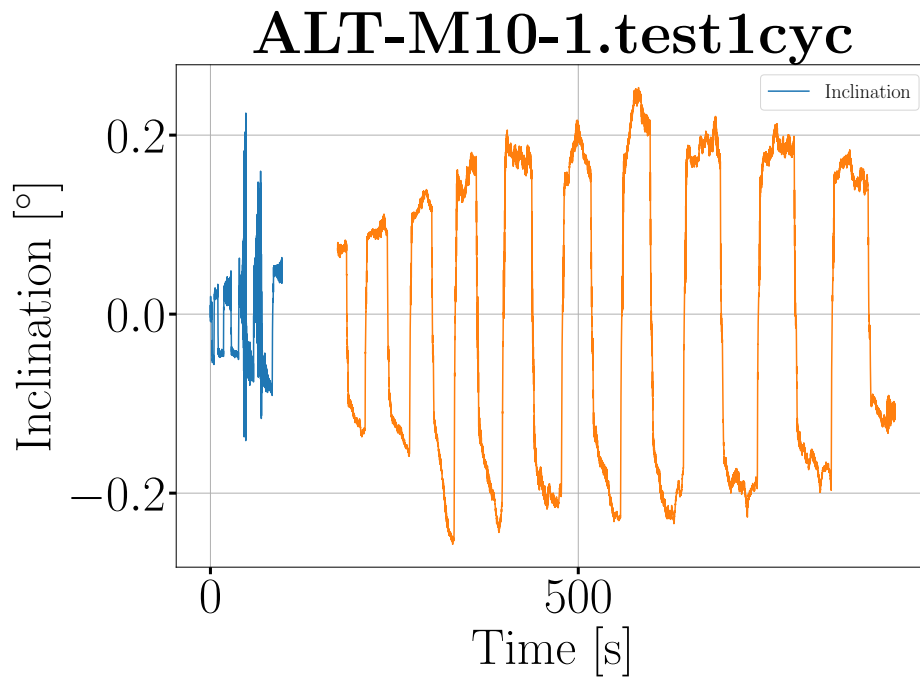


Figure 13.4: Inclination plotted against time.

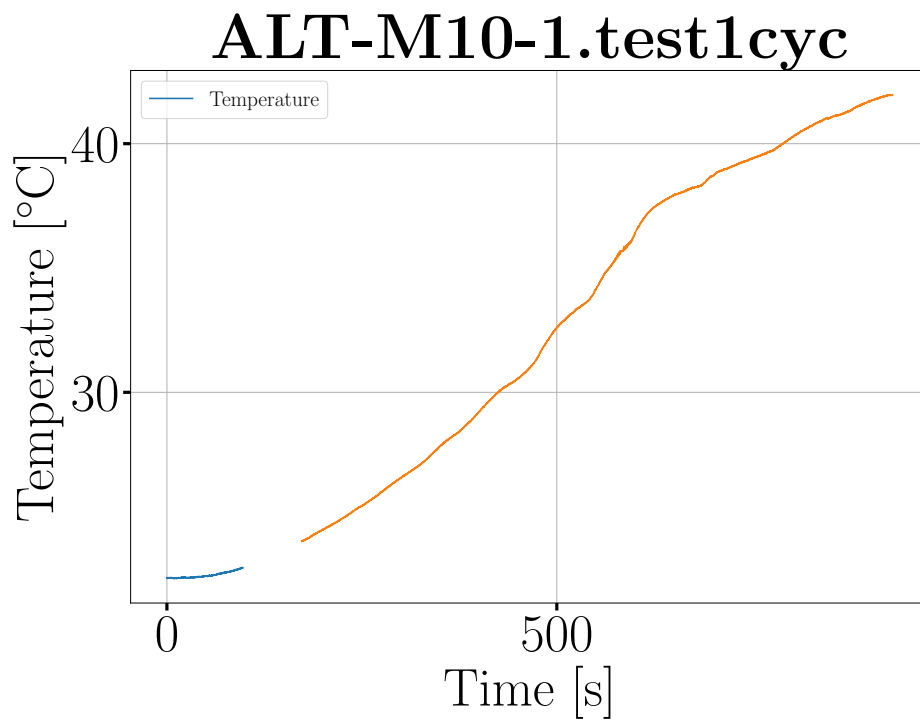


Figure 13.5: Temperature plotted against time.

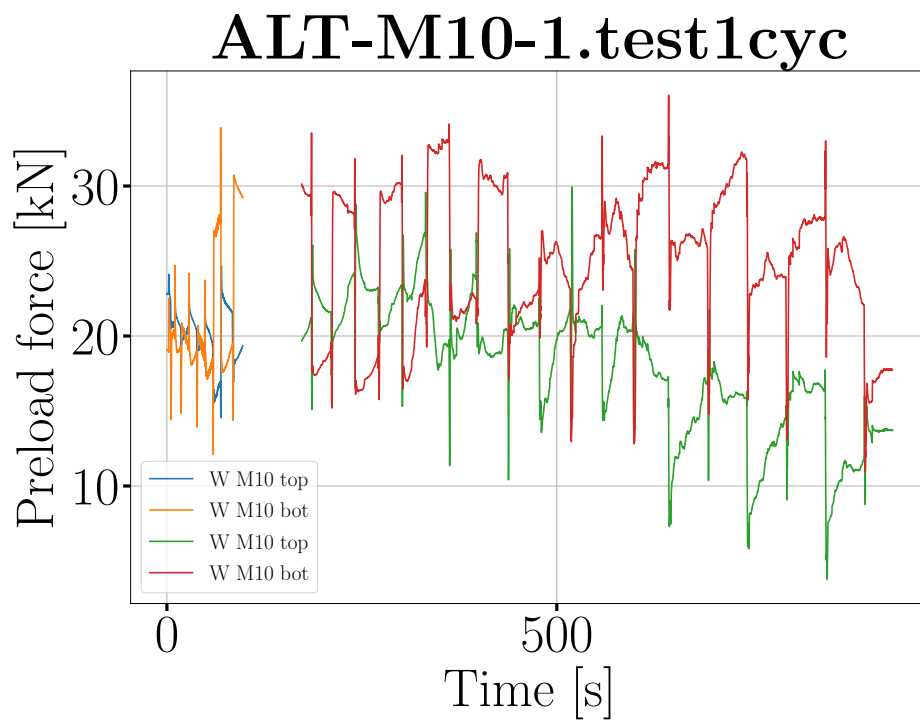


Figure 13.6: Preload in bolts.

Chapter 14

Test 14 - ALT-M10_1 - 16.05.21

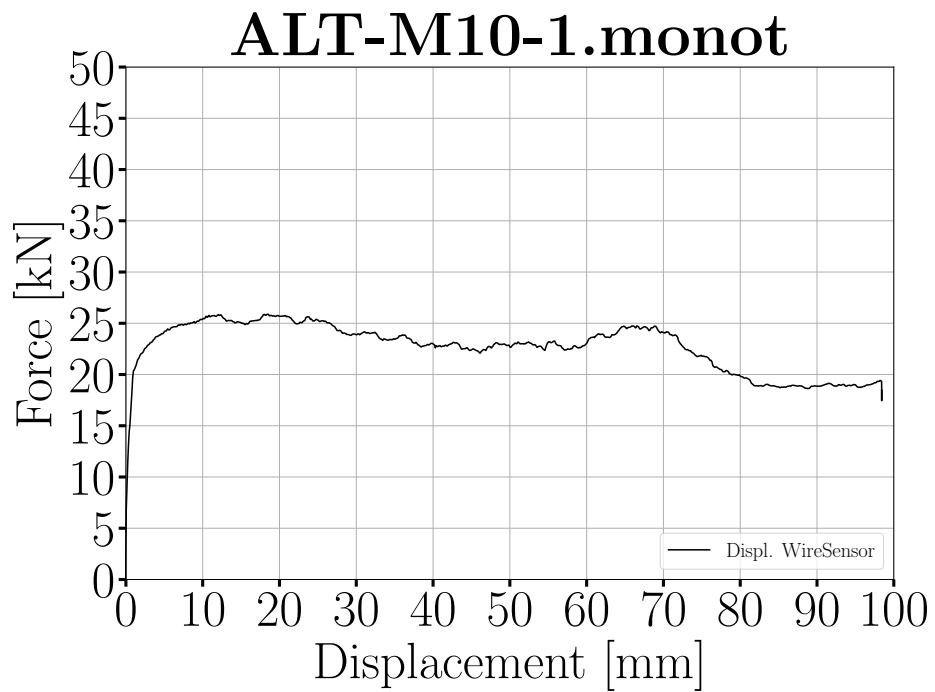
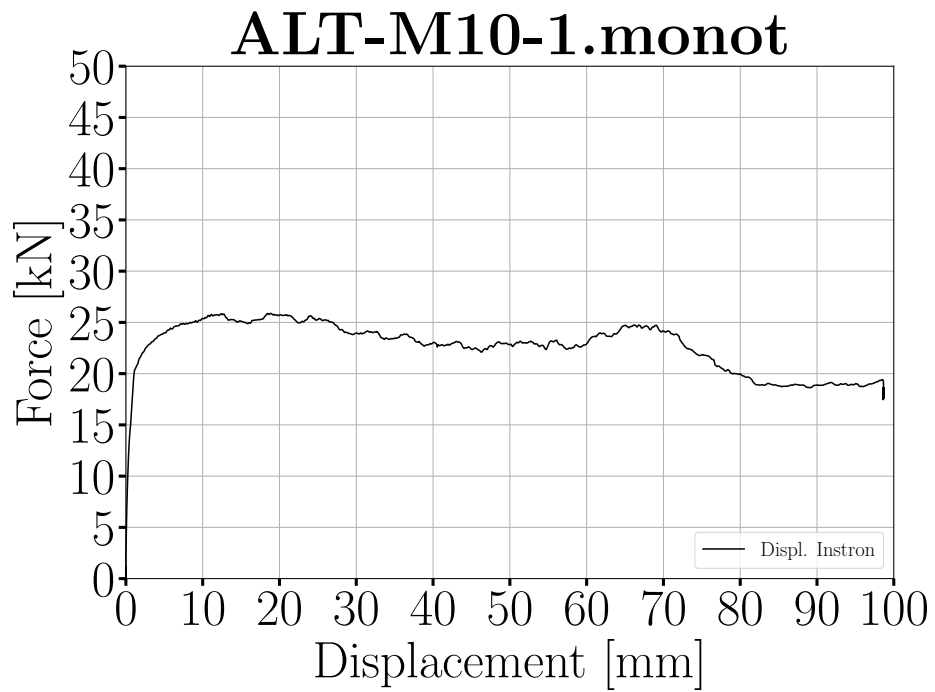


Figure 14.1: Load displacement graph.

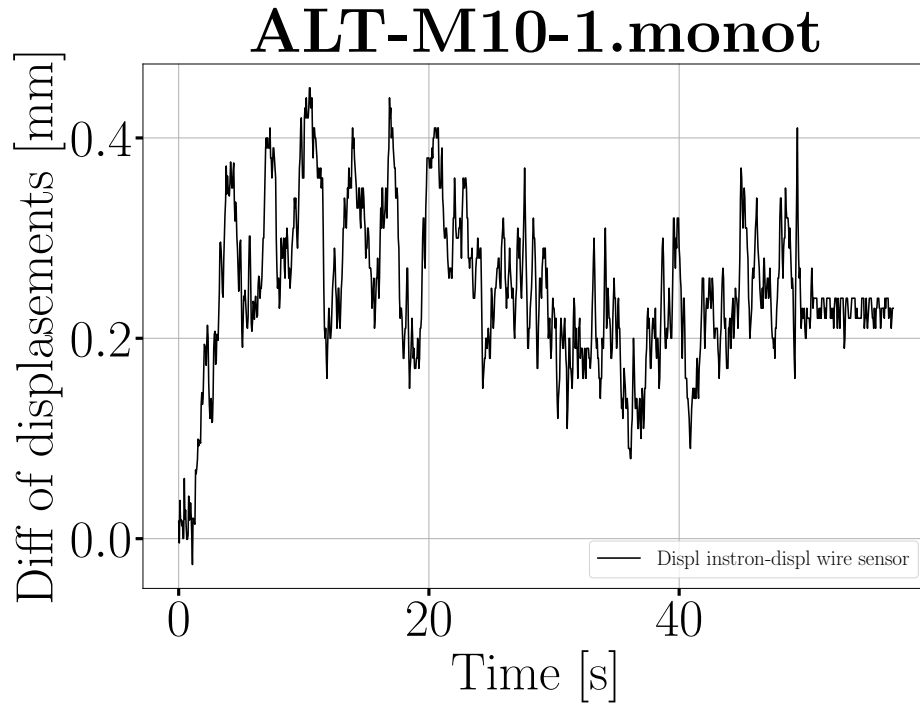


Figure 14.2: Difference of displacement between instron press and wire sensor.

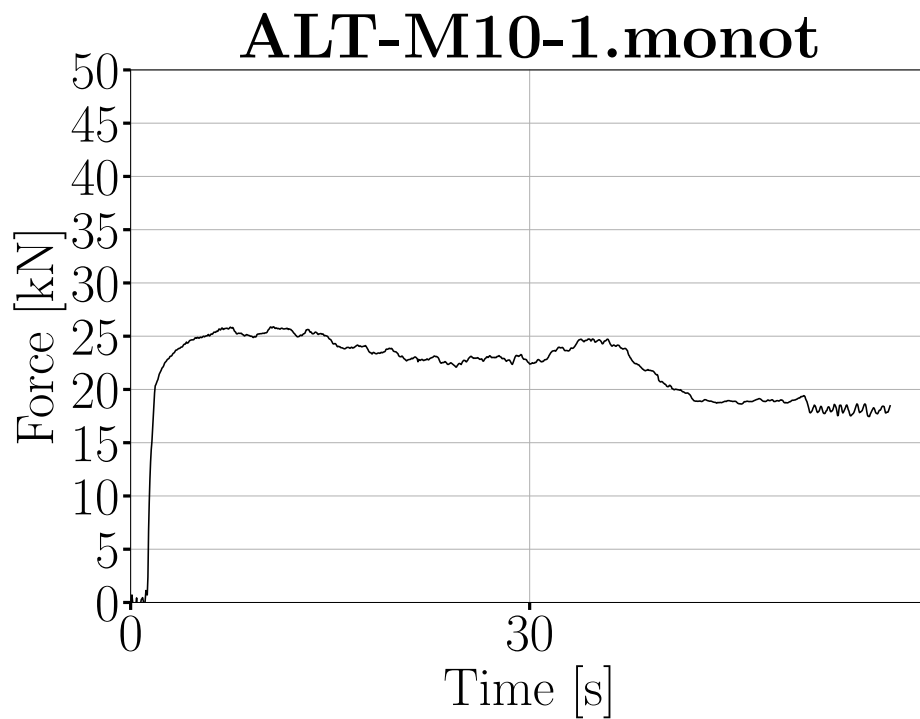


Figure 14.3: Force plotted against time.

ALT-M10-1.monot

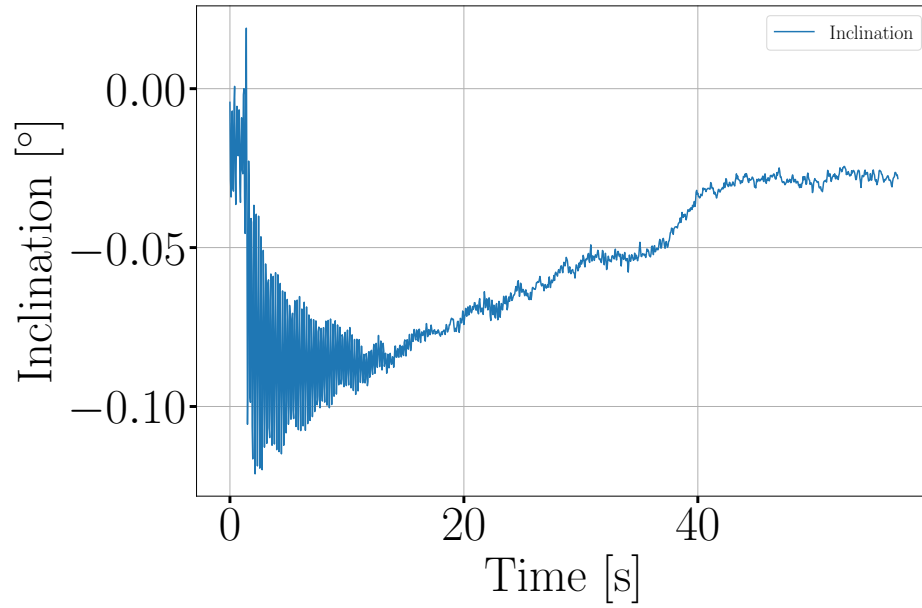


Figure 14.4: Inclination plotted against time.

ALT-M10-1.monot

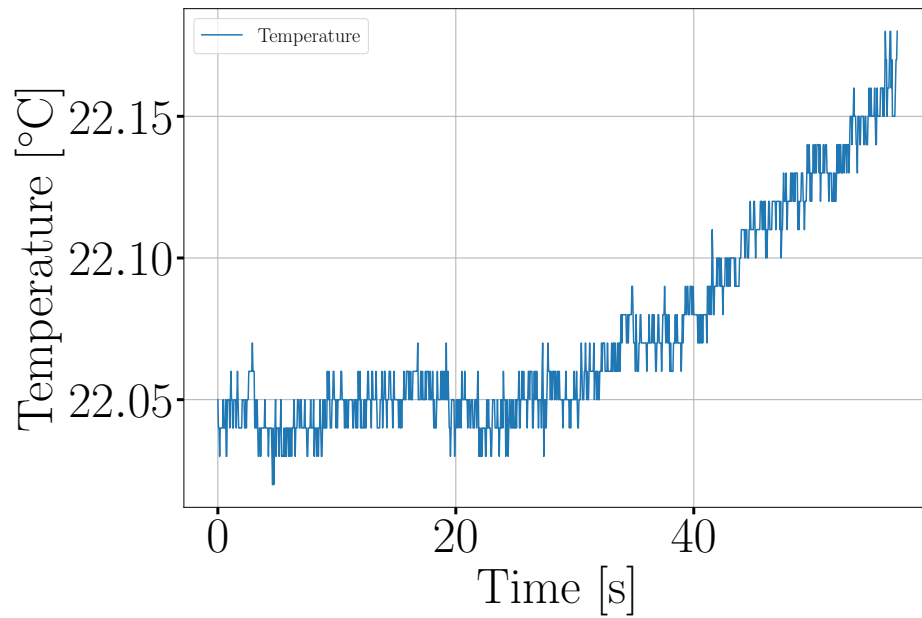


Figure 14.5: Temperature plotted against time.

ALT-M10-1.monot

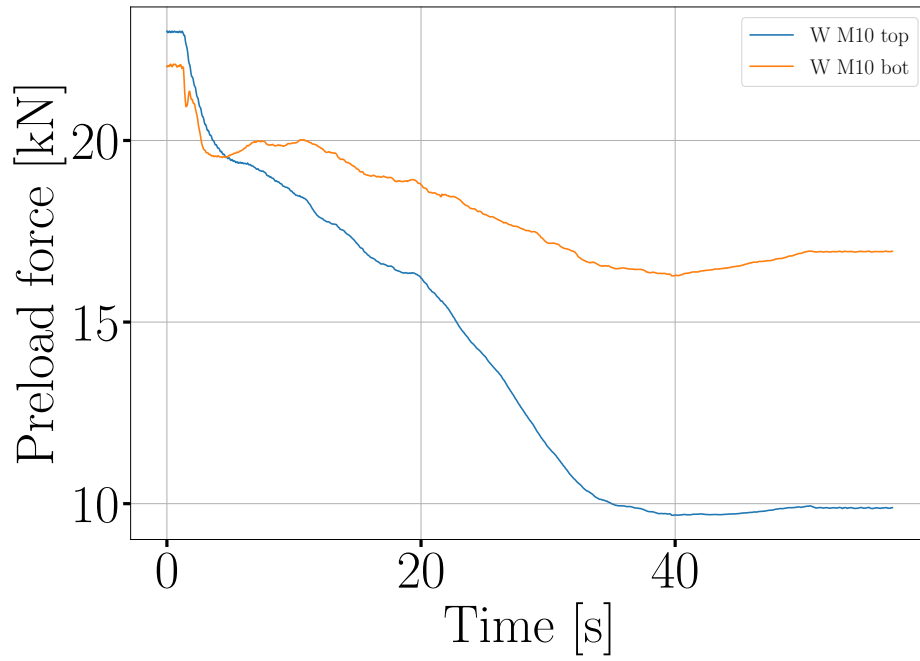


Figure 14.6: Preload in bolts.

Chapter 15

Test 15 - ALT-AS-M10_1 - 16.05.21

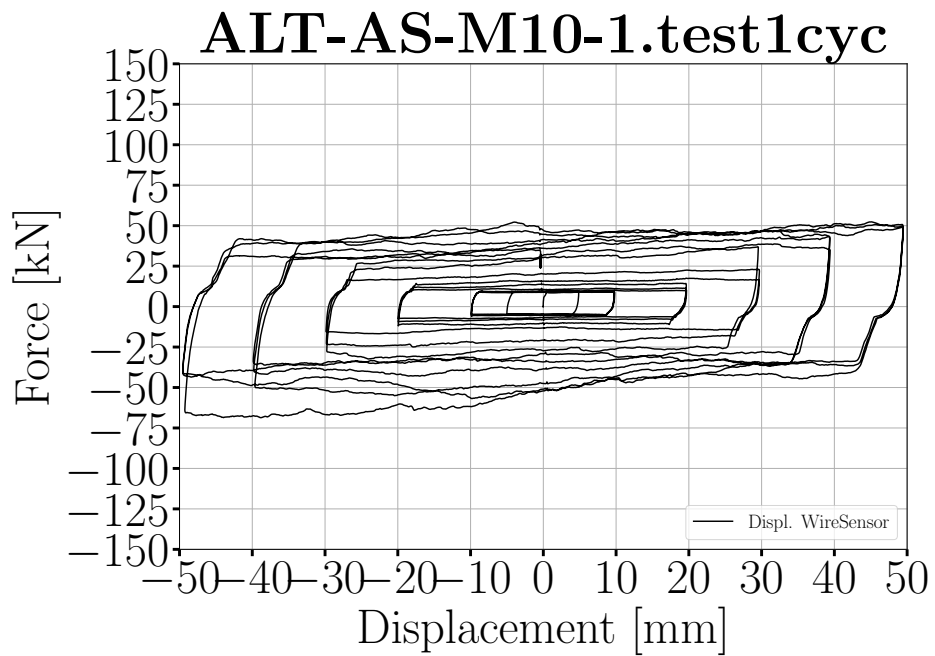
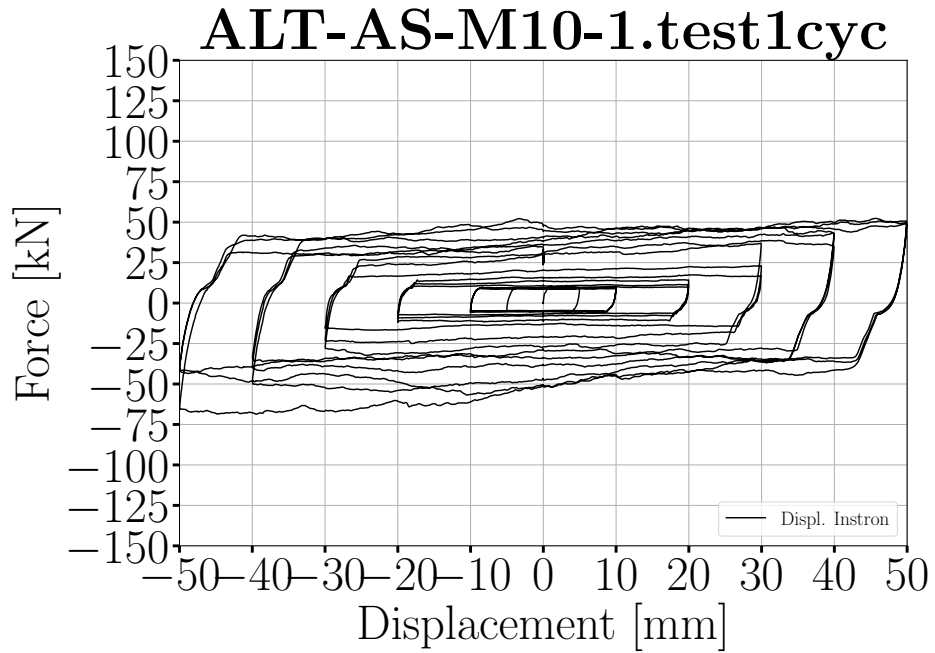


Figure 15.1: Load displacement graph.

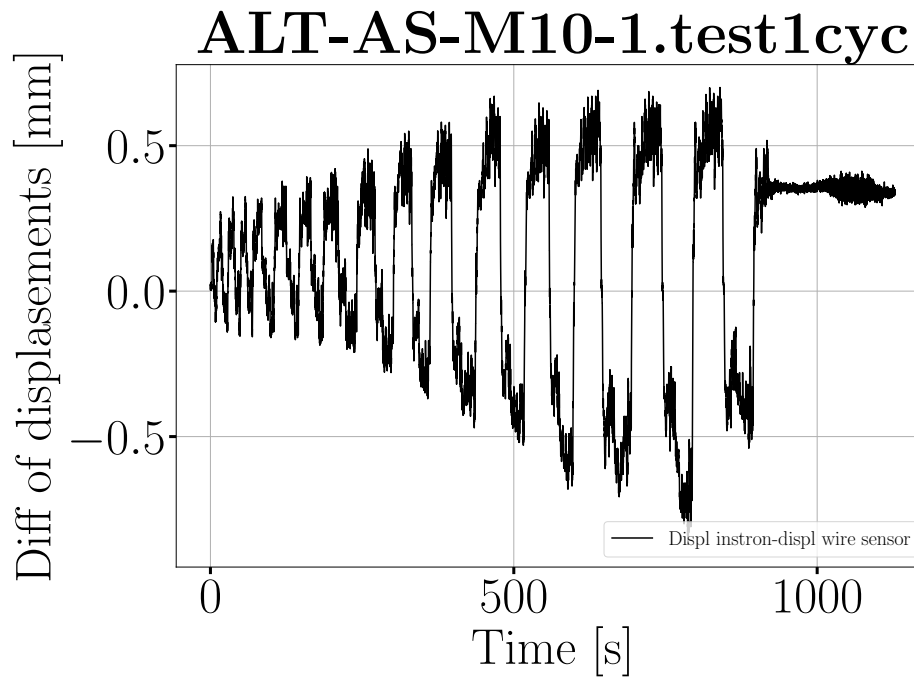


Figure 15.2: Difference of displacement between instron press and wire sensor.

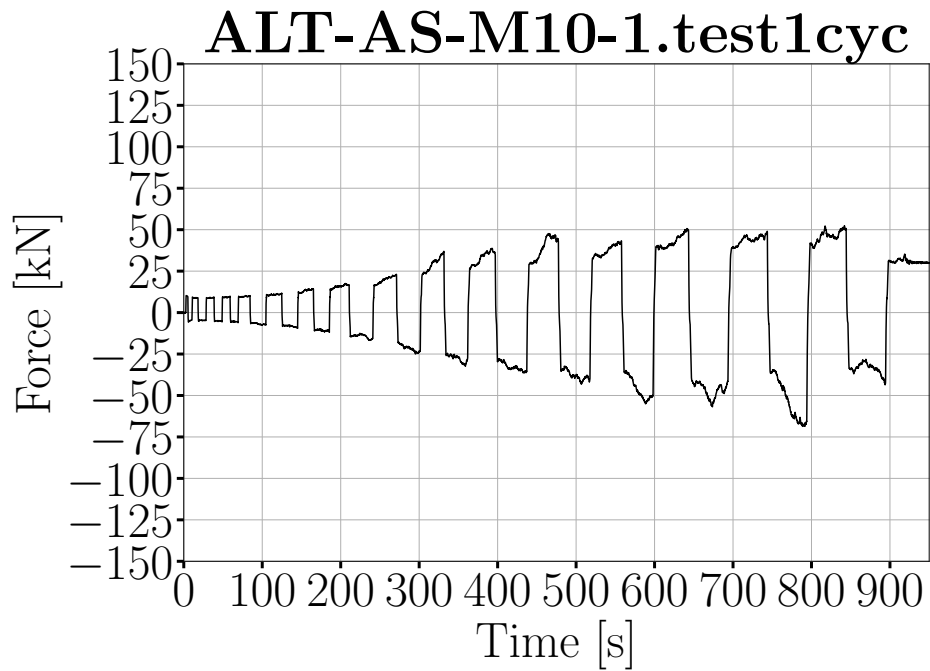


Figure 15.3: Force plotted against time.

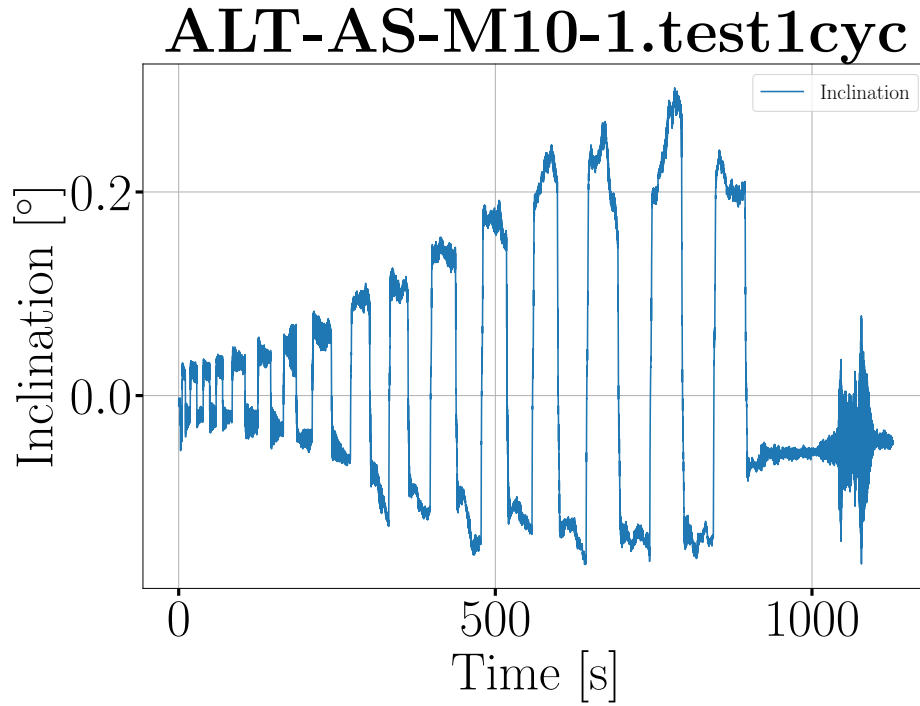


Figure 15.4: Inclination plotted against time.

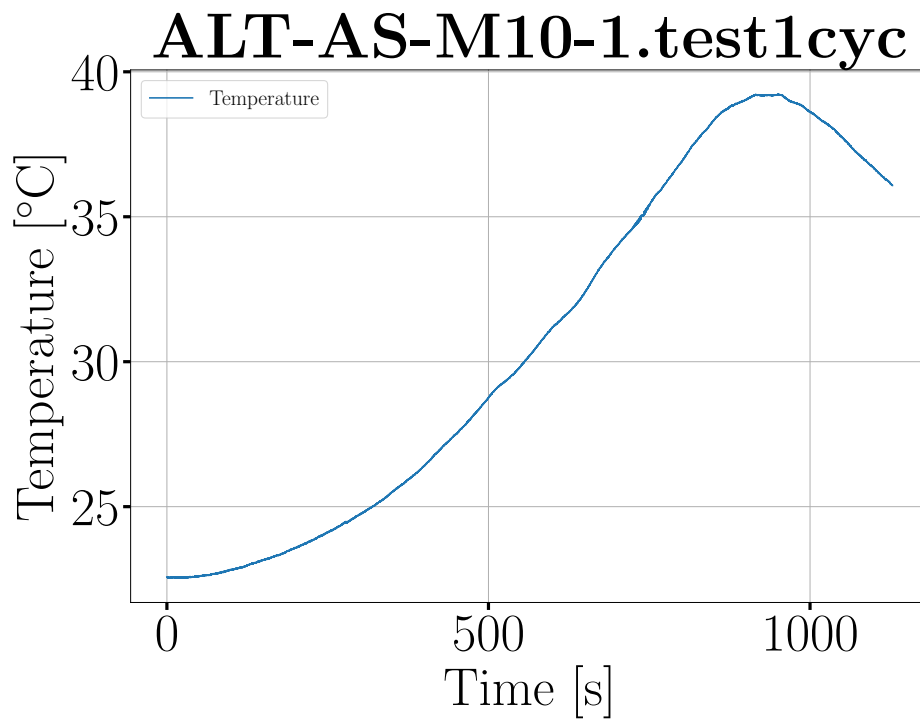


Figure 15.5: Temperature plotted against time.

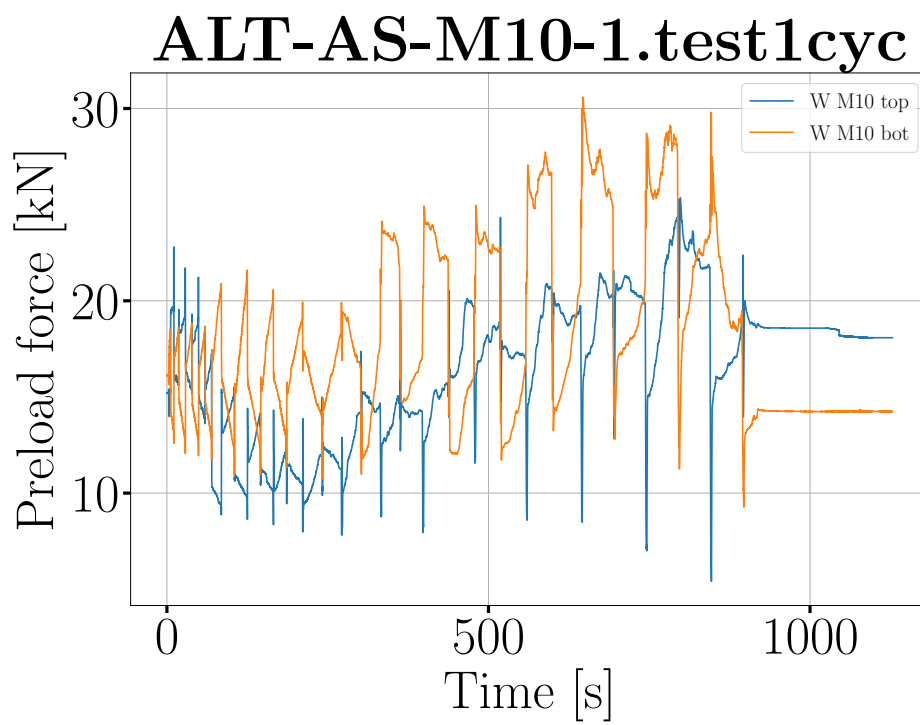


Figure 15.6: Preload in bolts.

Chapter 16

Test 16 - ALT-AS-M20_1 - 16.05.21

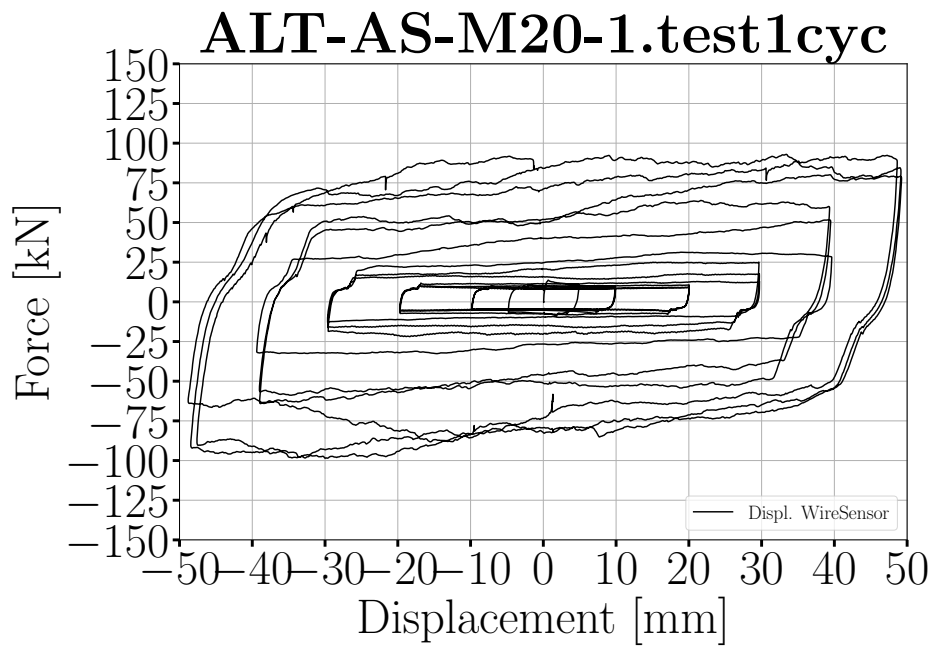
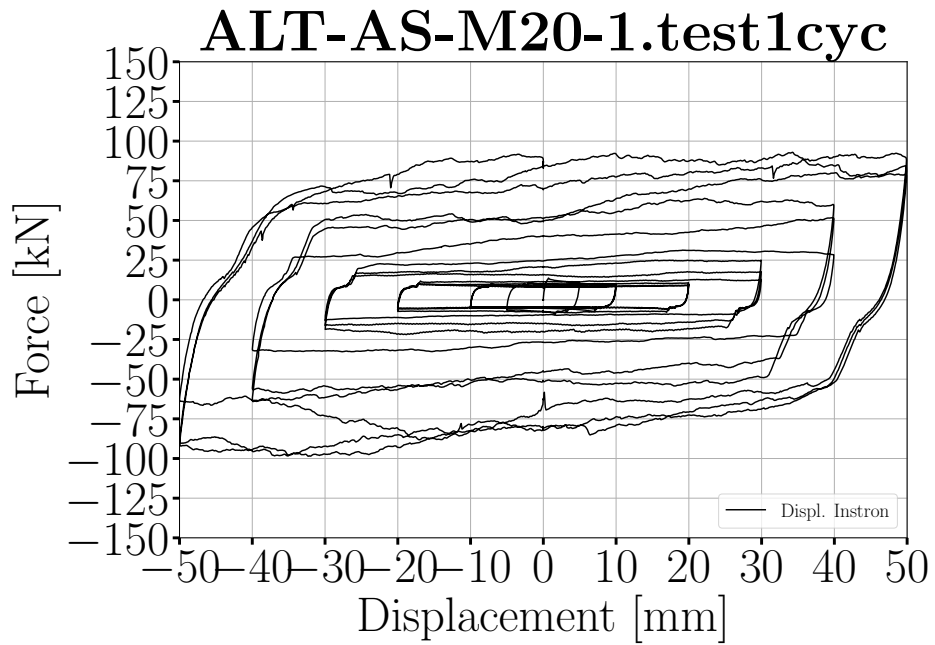


Figure 16.1: Load displacement graph.

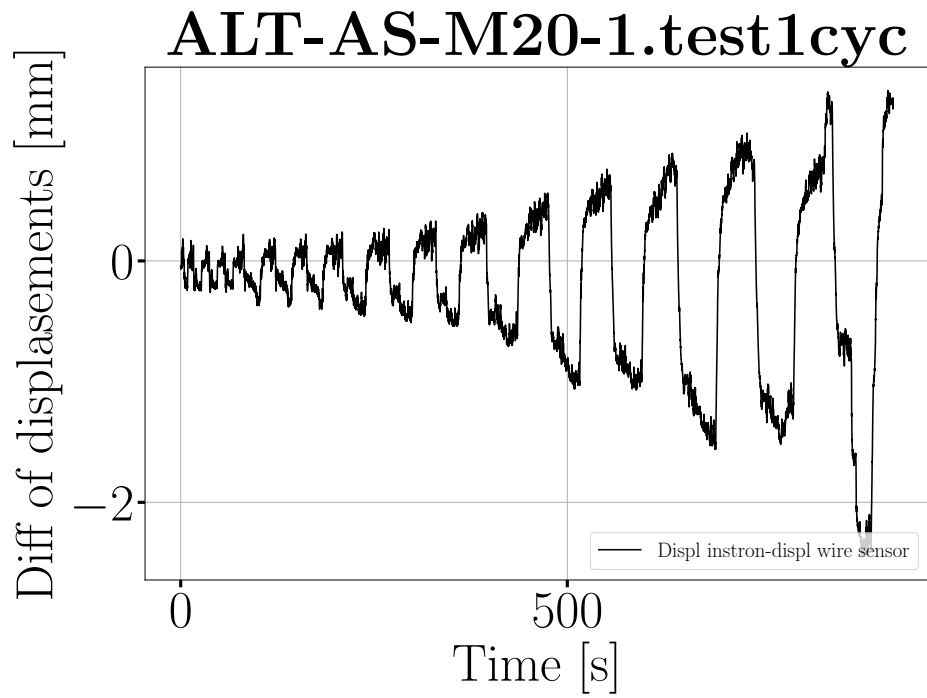


Figure 16.2: Difference of displacement between instron press and wire sensor.

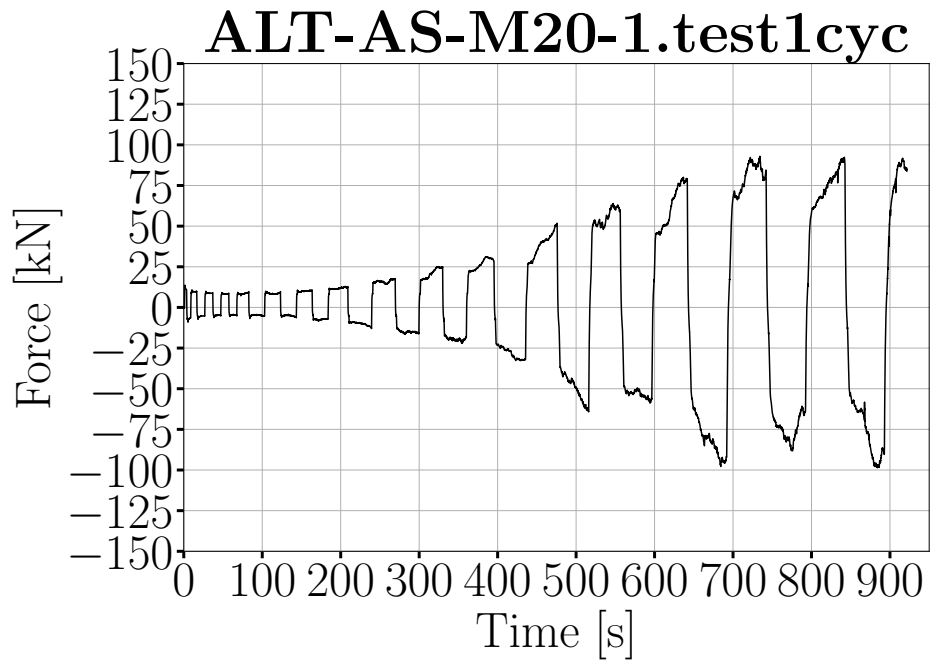


Figure 16.3: Force plotted against time.

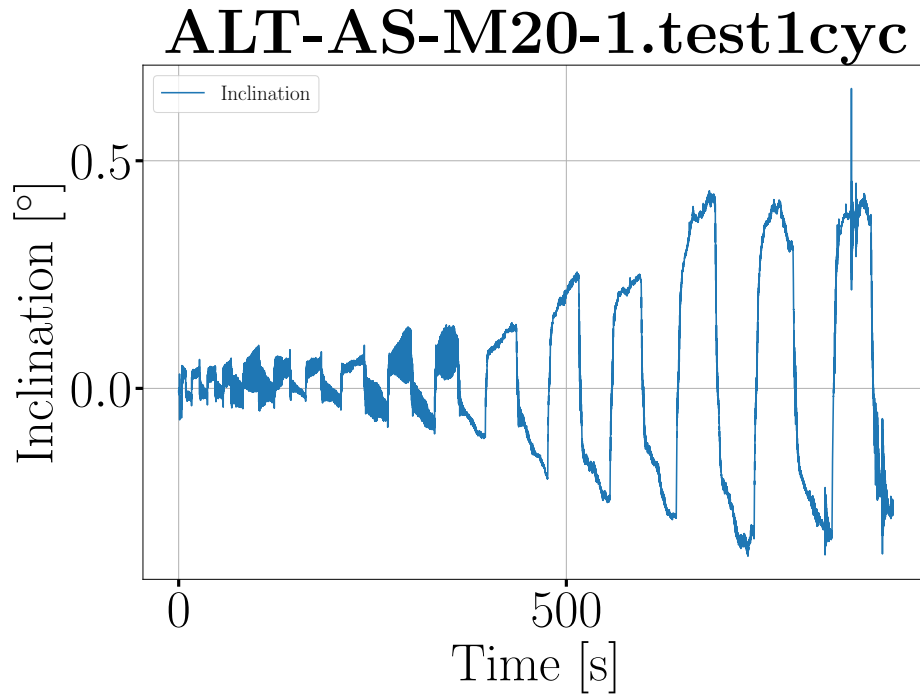


Figure 16.4: Inclination plotted against time.

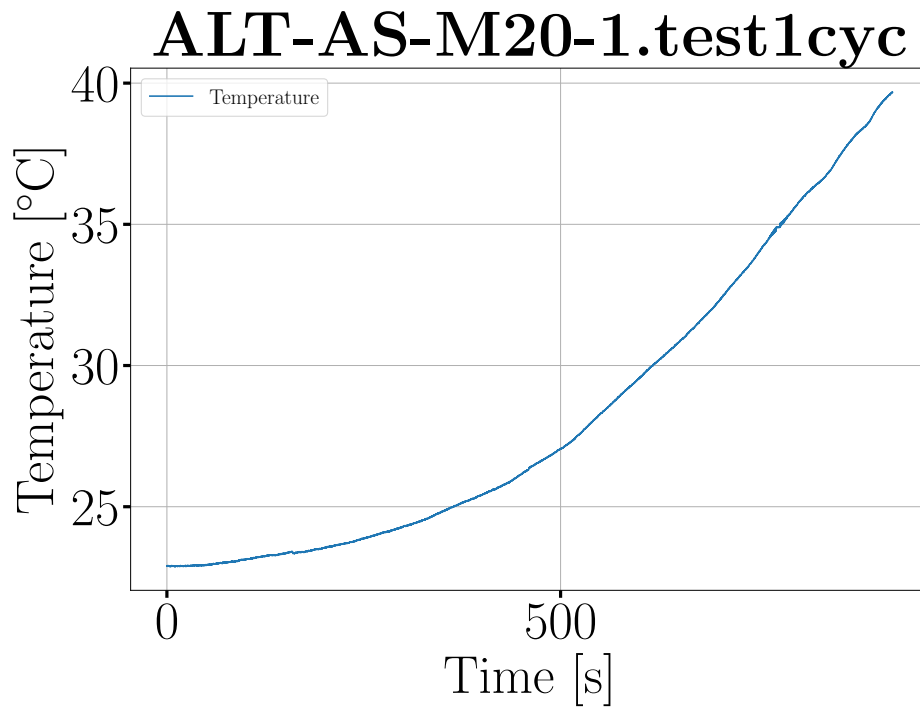


Figure 16.5: Temperature plotted against time.

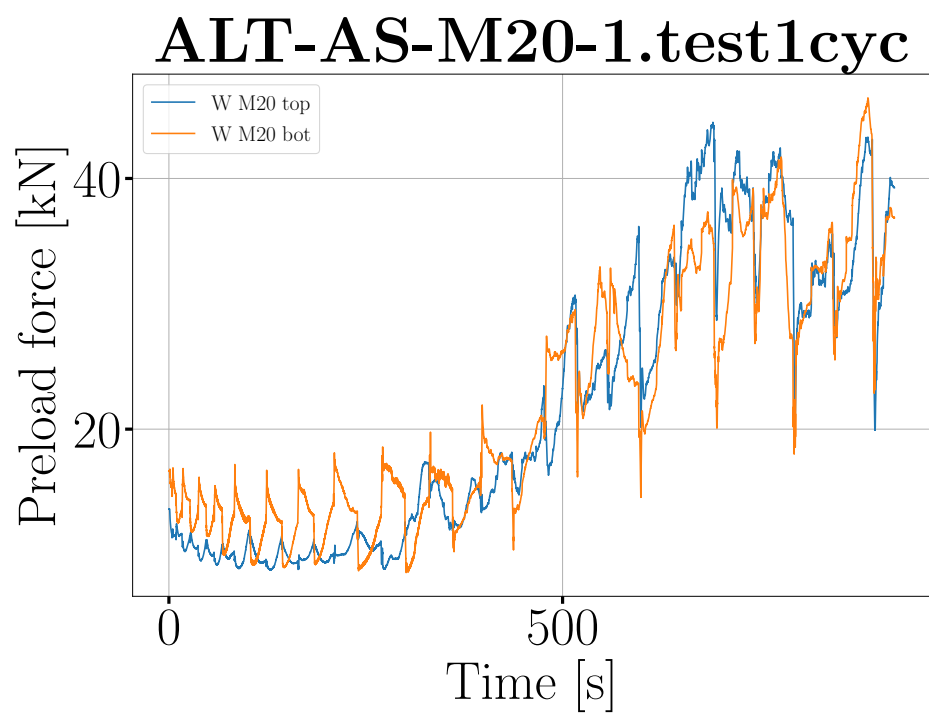


Figure 16.6: Preload in bolts.

Chapter 17

Test 17 - STD-1H-M10_1 - 16.05.21

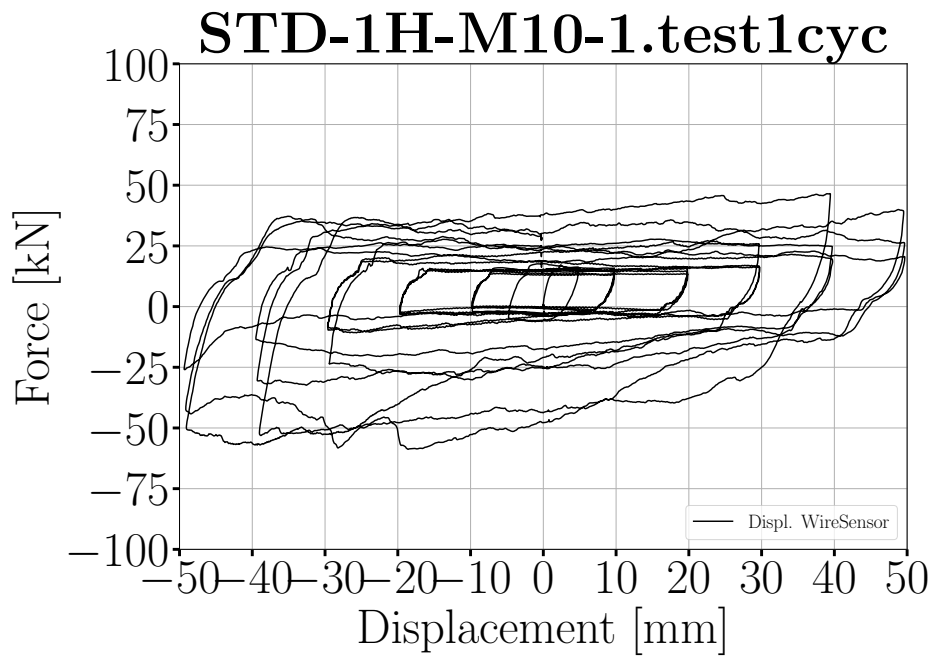
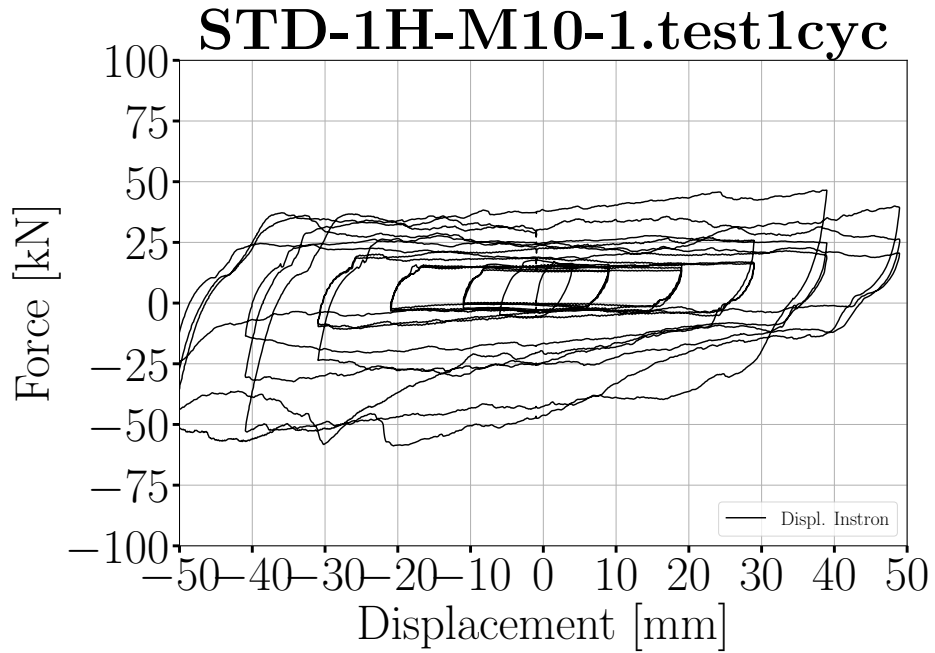


Figure 17.1: Load displacement graph.

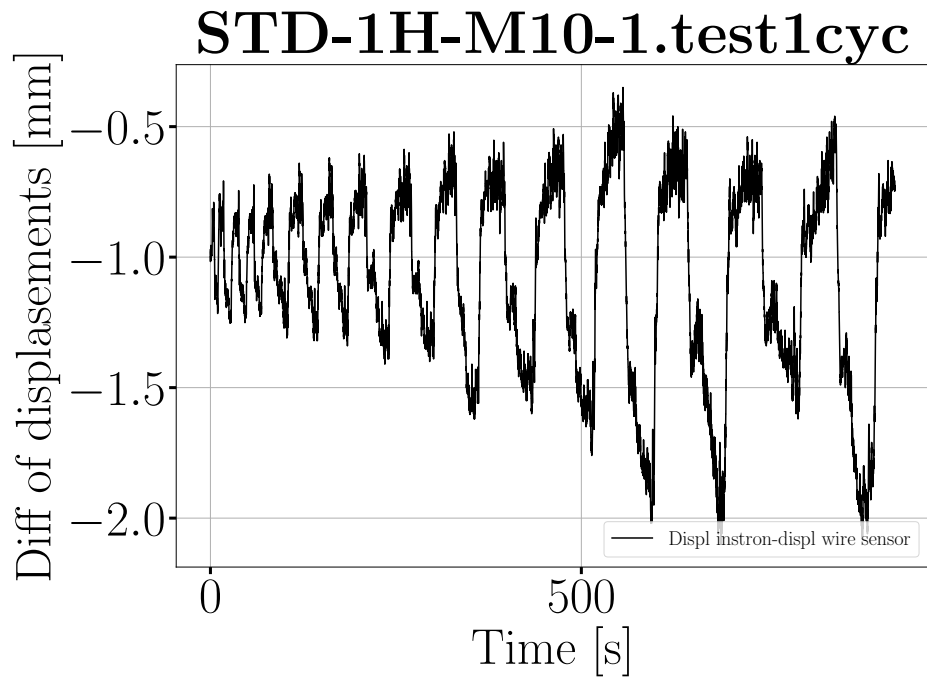


Figure 17.2: Difference of displacement between instron press and wire sensor.

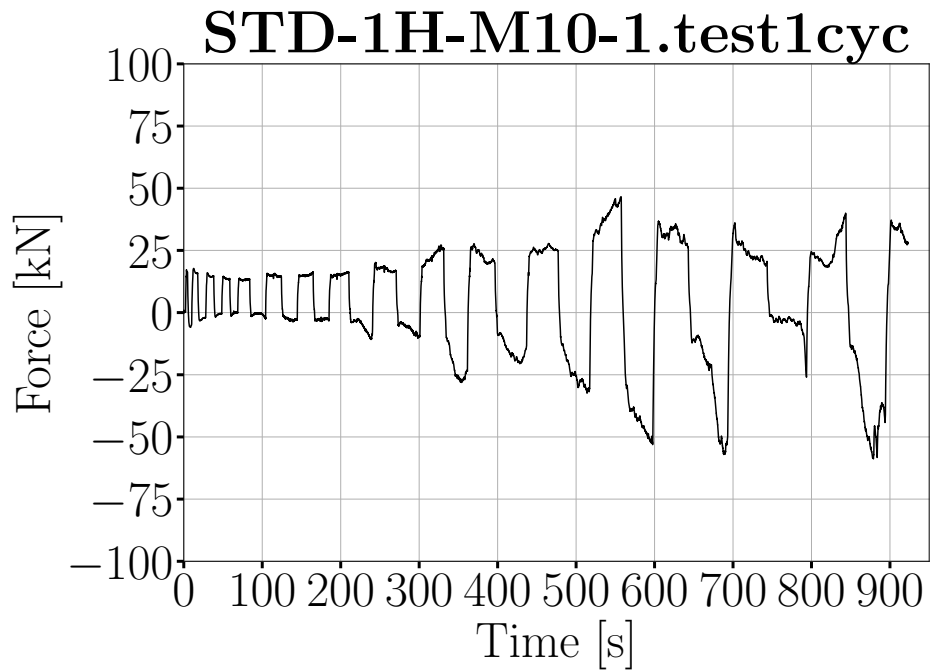


Figure 17.3: Force plotted against time.

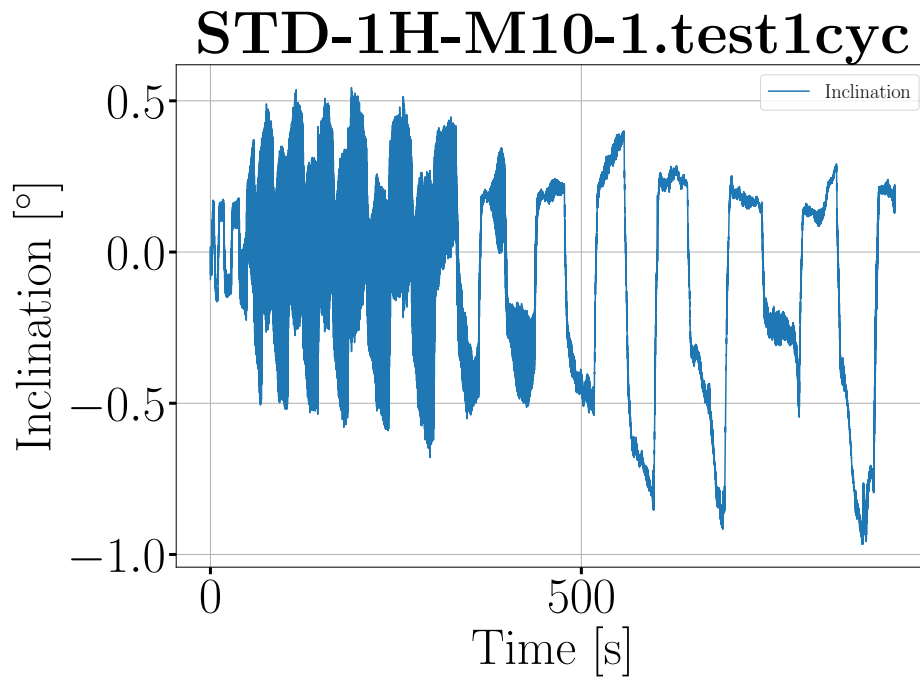


Figure 17.4: Inclination plotted against time.

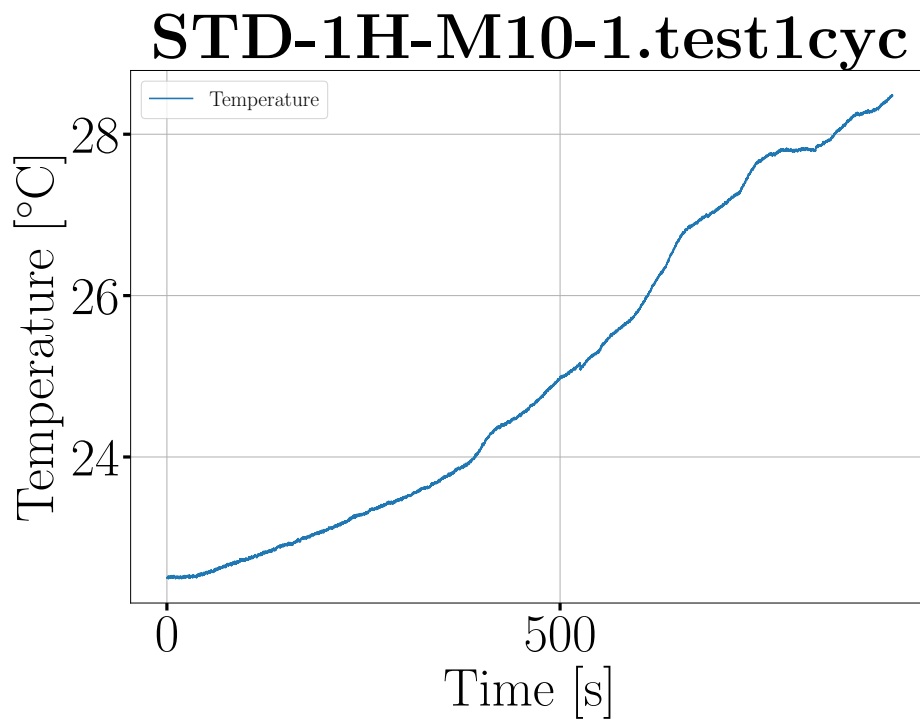


Figure 17.5: Temperature plotted against time.

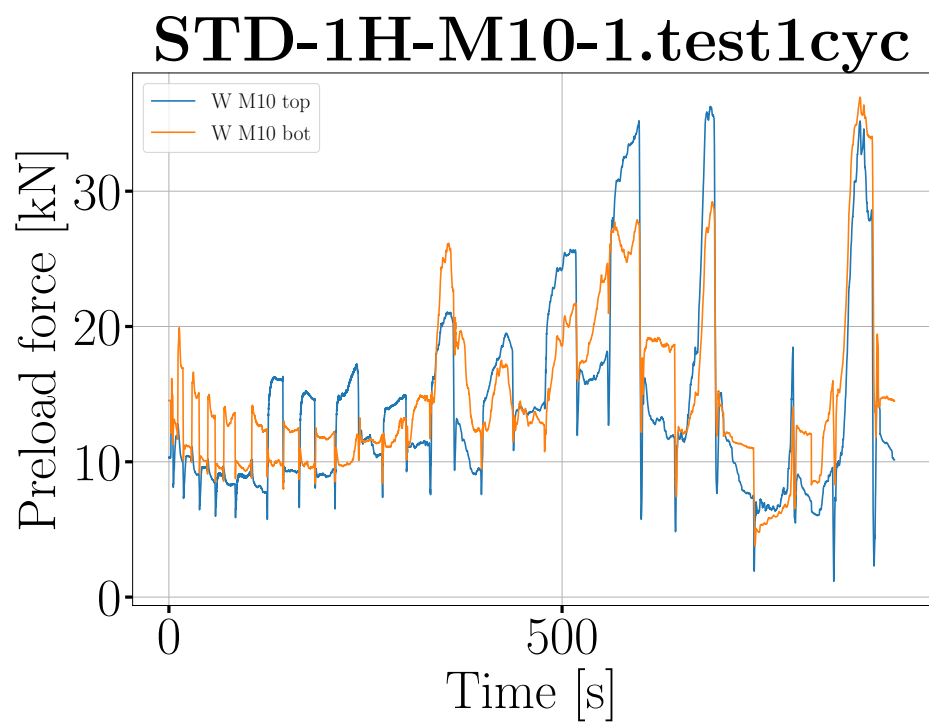


Figure 17.6: Preload in bolts.

Chapter 18

Test 18 - STD-1H-M20_1 - 16.05.21

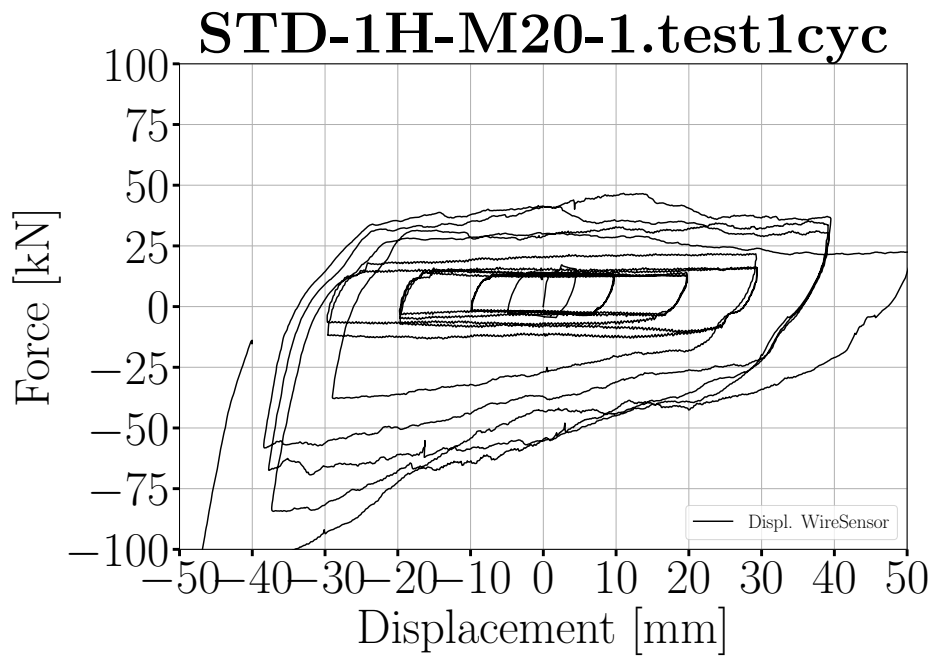
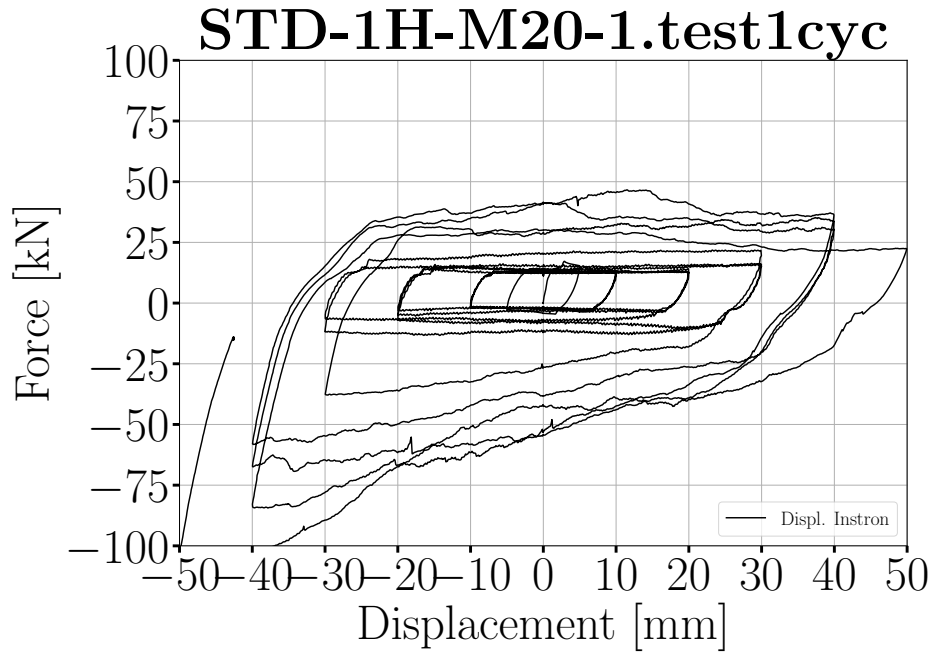


Figure 18.1: Load displacement graph.

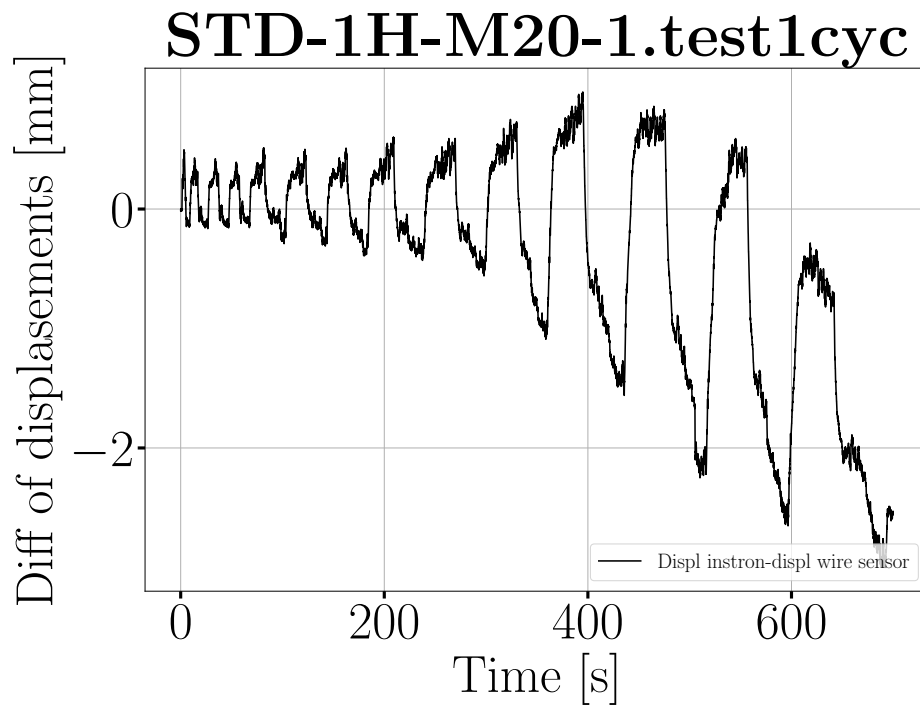


Figure 18.2: Difference of displacement between instron press and wire sensor.

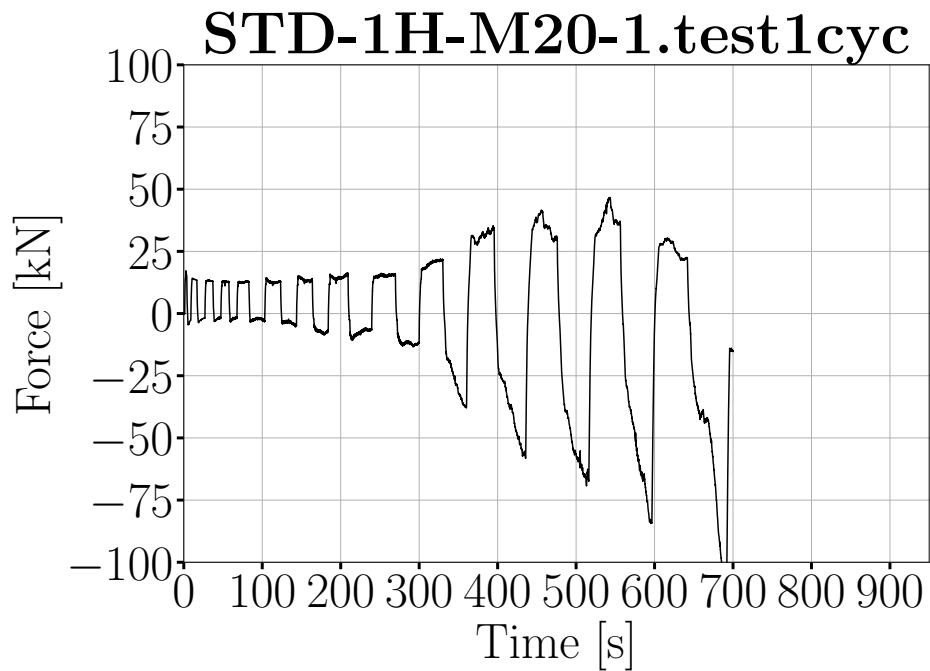


Figure 18.3: Force plotted against time.

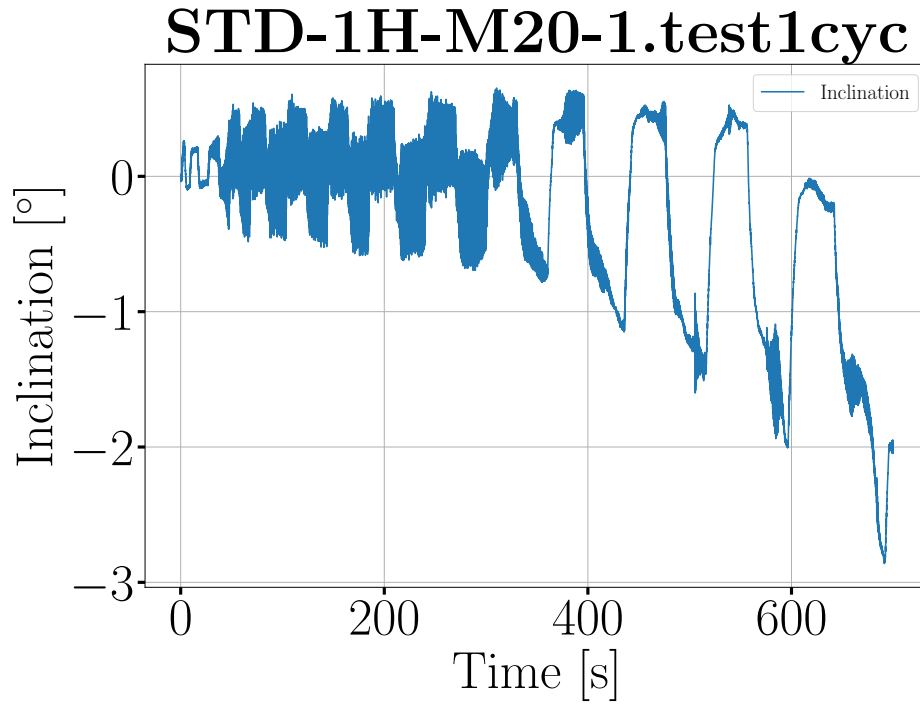


Figure 18.4: Inclination plotted against time.

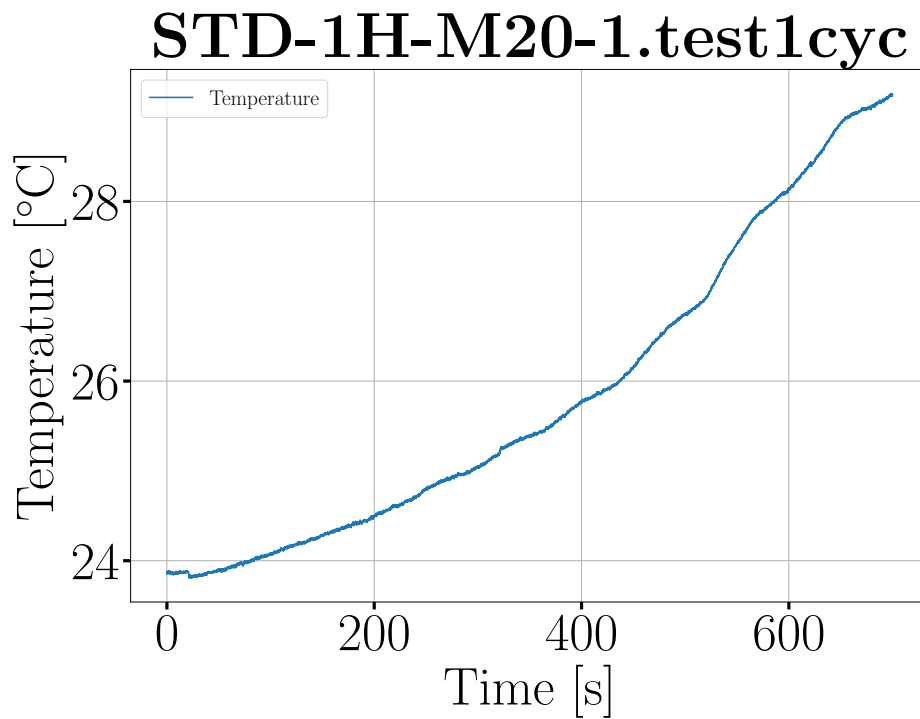


Figure 18.5: Temperature plotted against time.

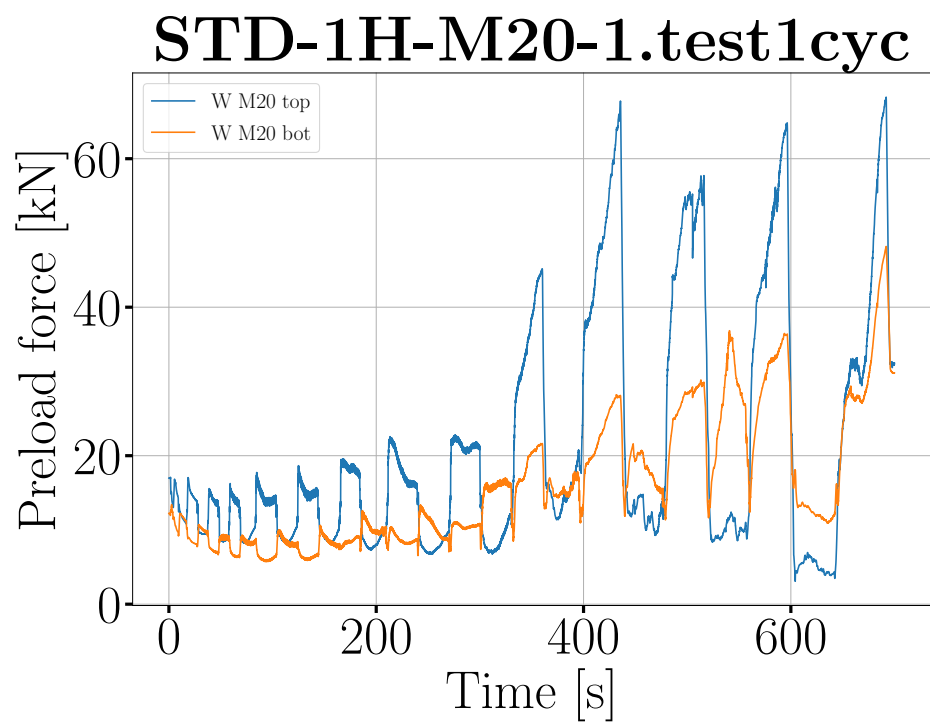


Figure 18.6: Preload in bolts.

Chapter 19

Test 19 - STD-2H-M10_1 - 18.05.21

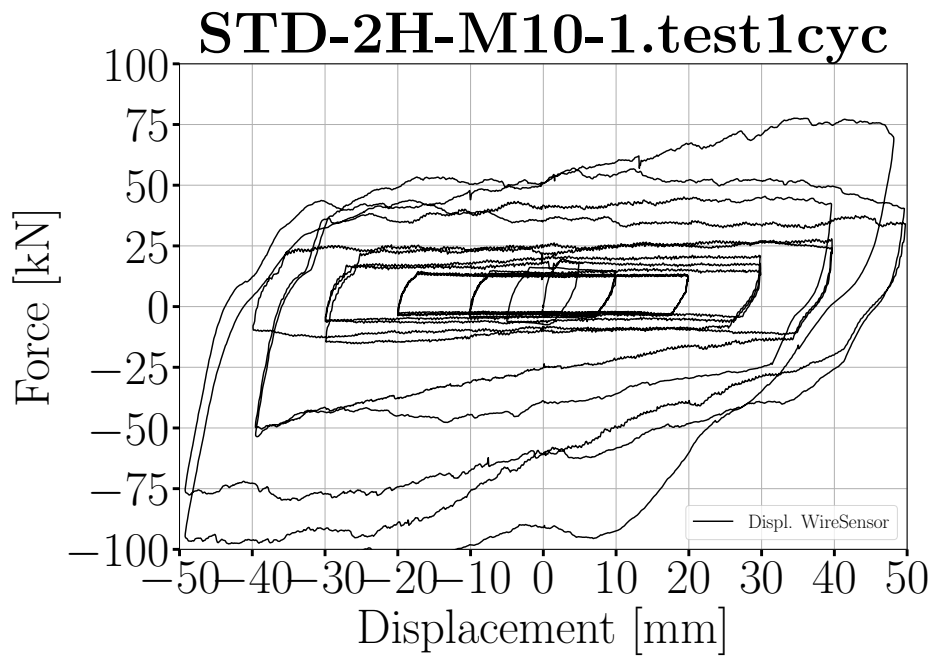
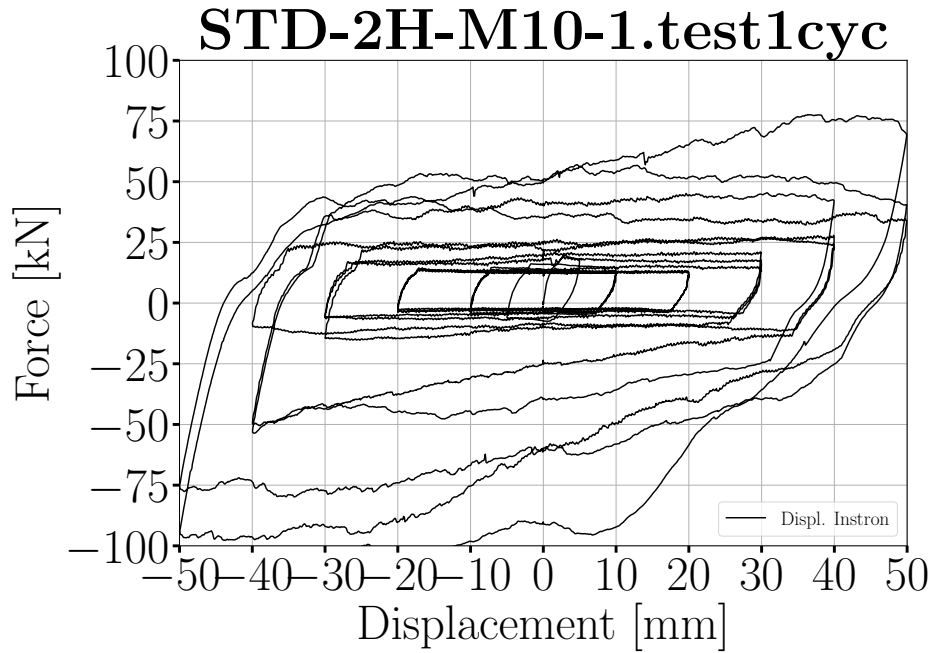


Figure 19.1: Load displacement graph.

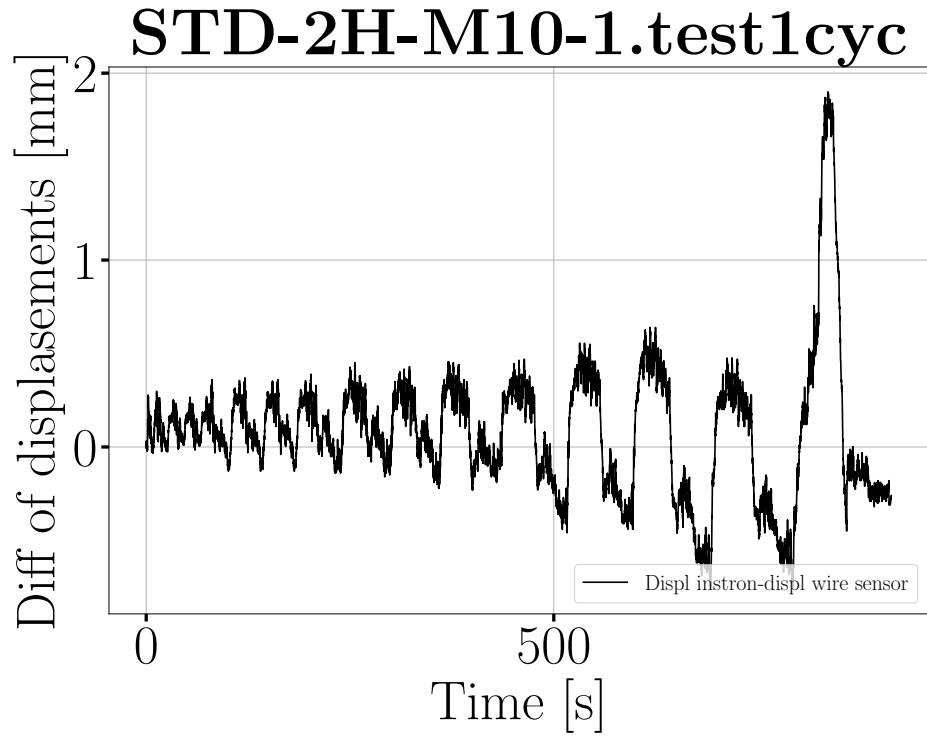


Figure 19.2: Difference of displacement between instron press and wire sensor.

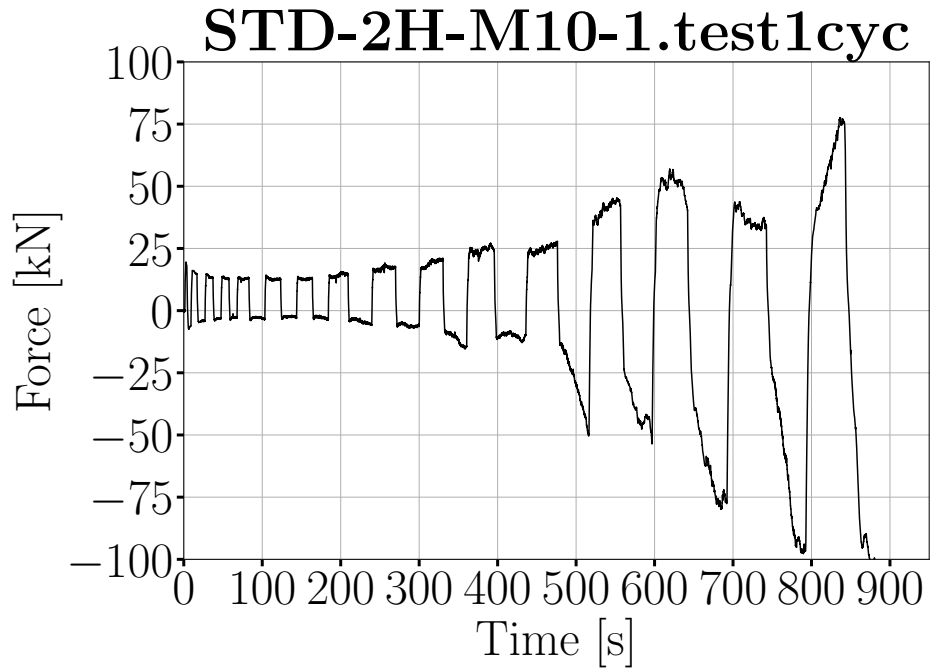


Figure 19.3: Force plotted against time.

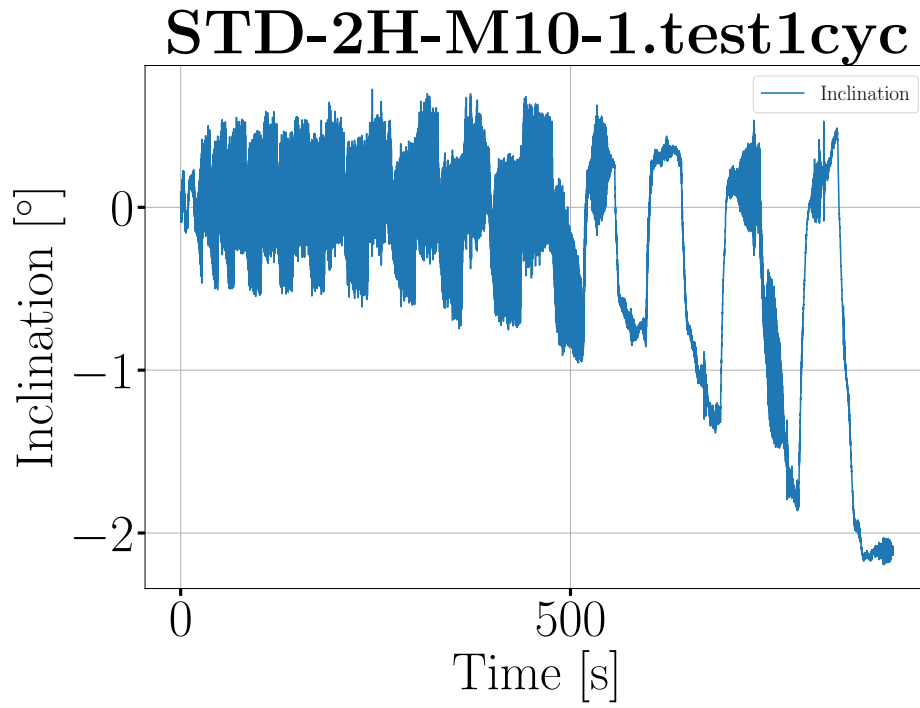


Figure 19.4: Inclination plotted against time.

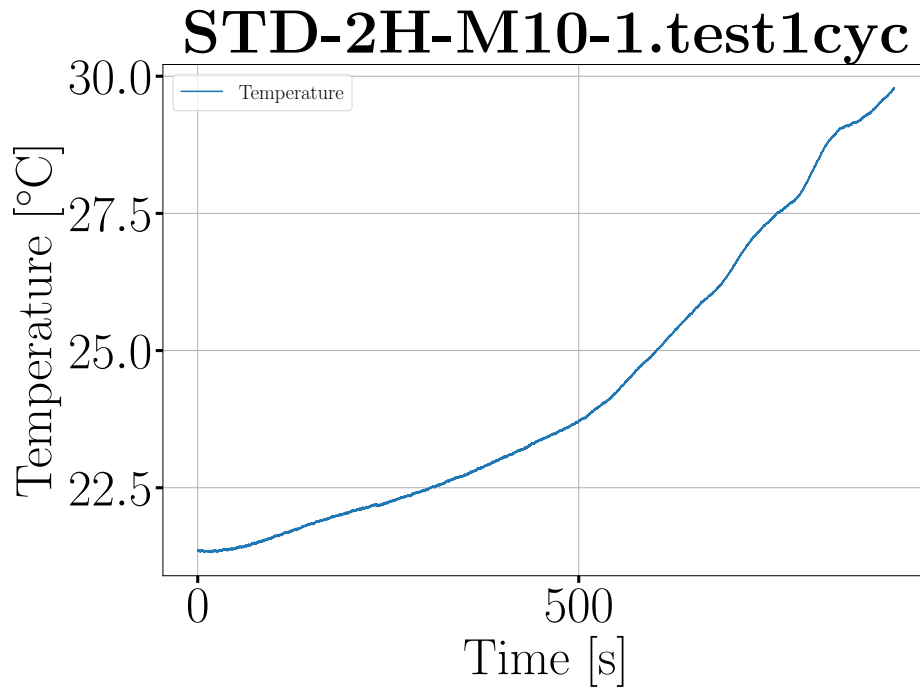


Figure 19.5: Temperature plotted against time.

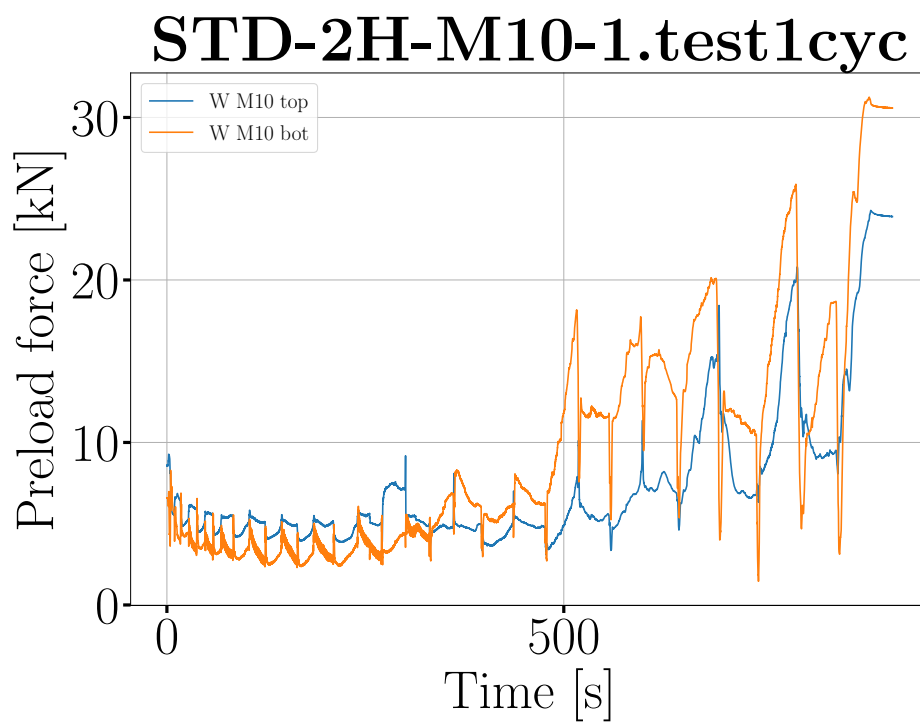


Figure 19.6: Preload in bolts.

Chapter 20

Test 20 - HYBRID-M10_1 - 18.05.21

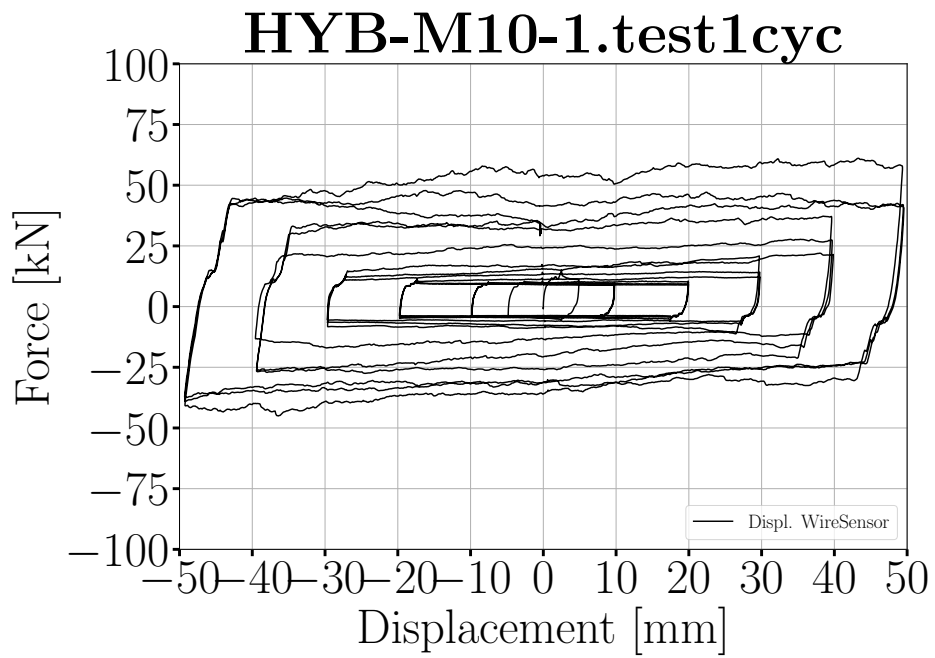
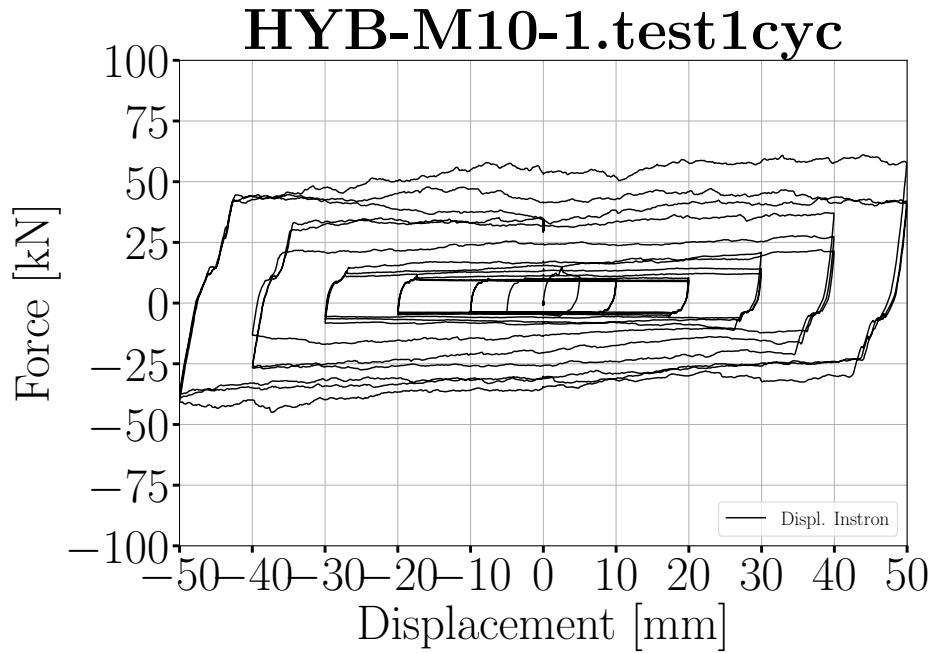


Figure 20.1: Load displacement graph.

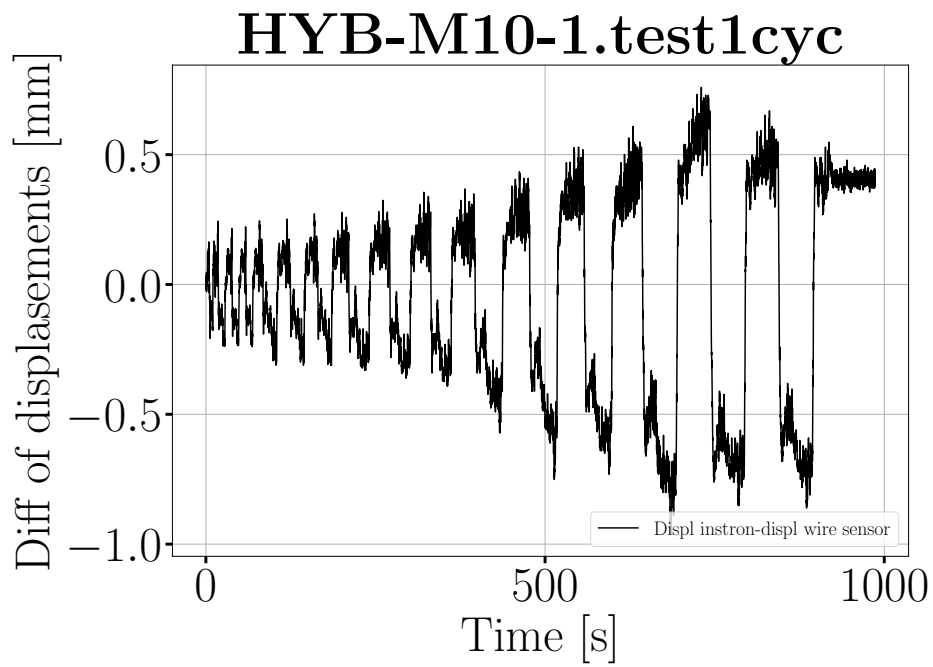


Figure 20.2: Difference of displacement between instron press and wire sensor.

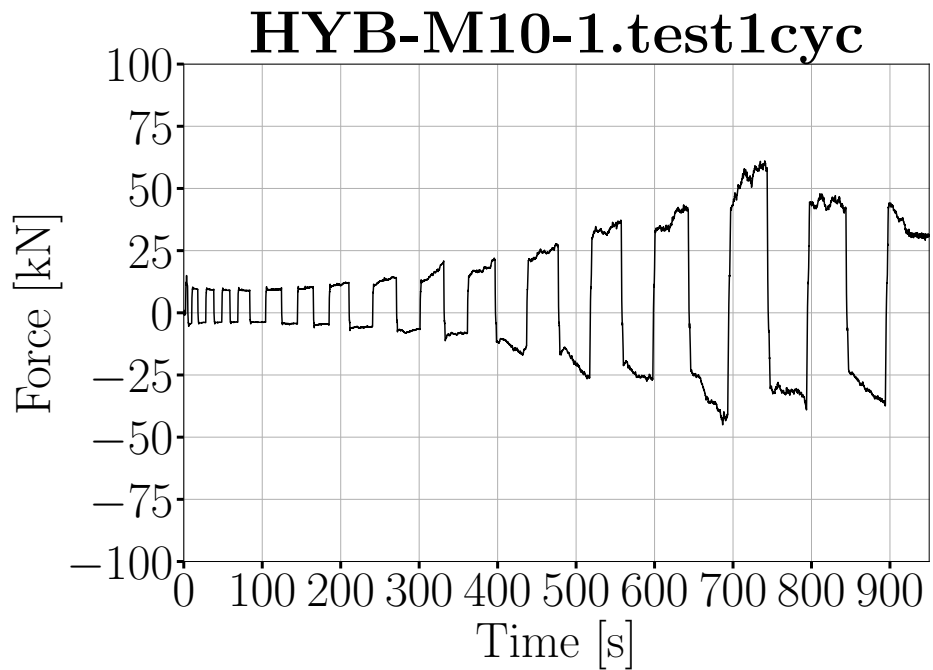


Figure 20.3: Force plotted against time.

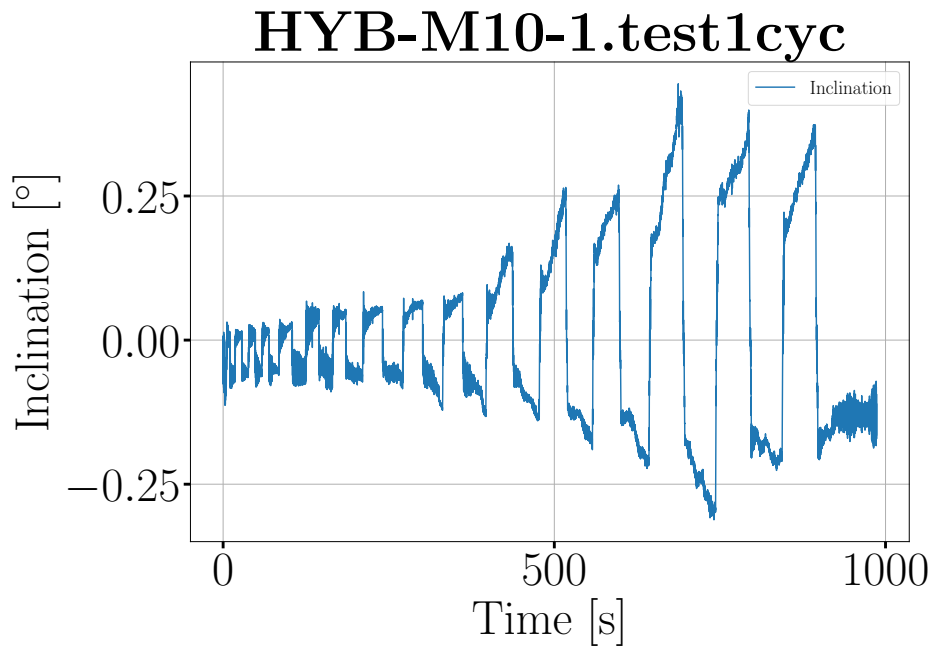


Figure 20.4: Inclination plotted against time.

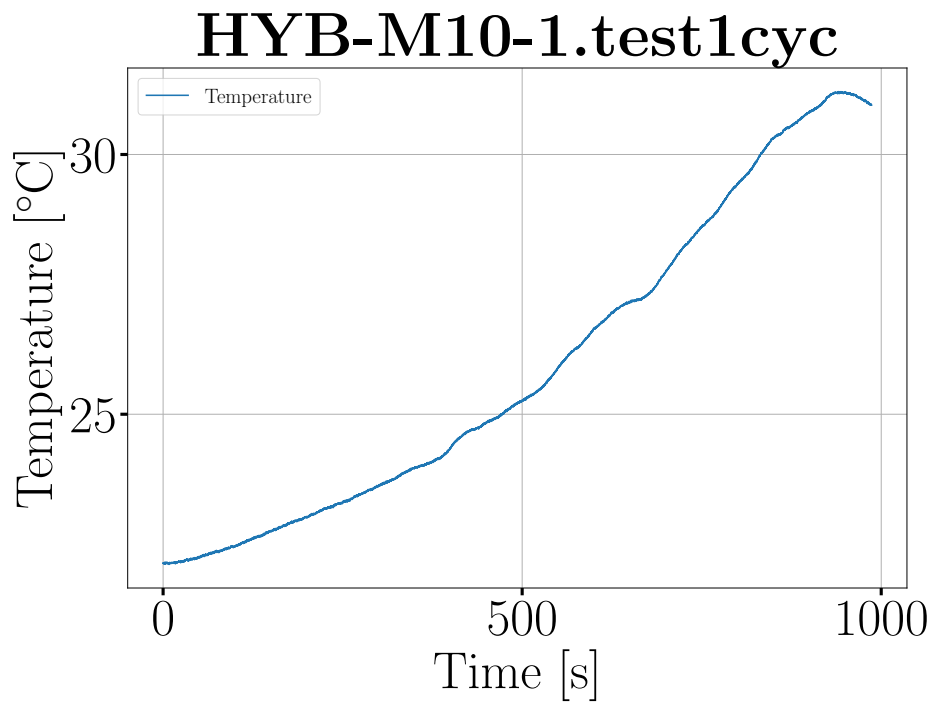


Figure 20.5: Temperature plotted against time.

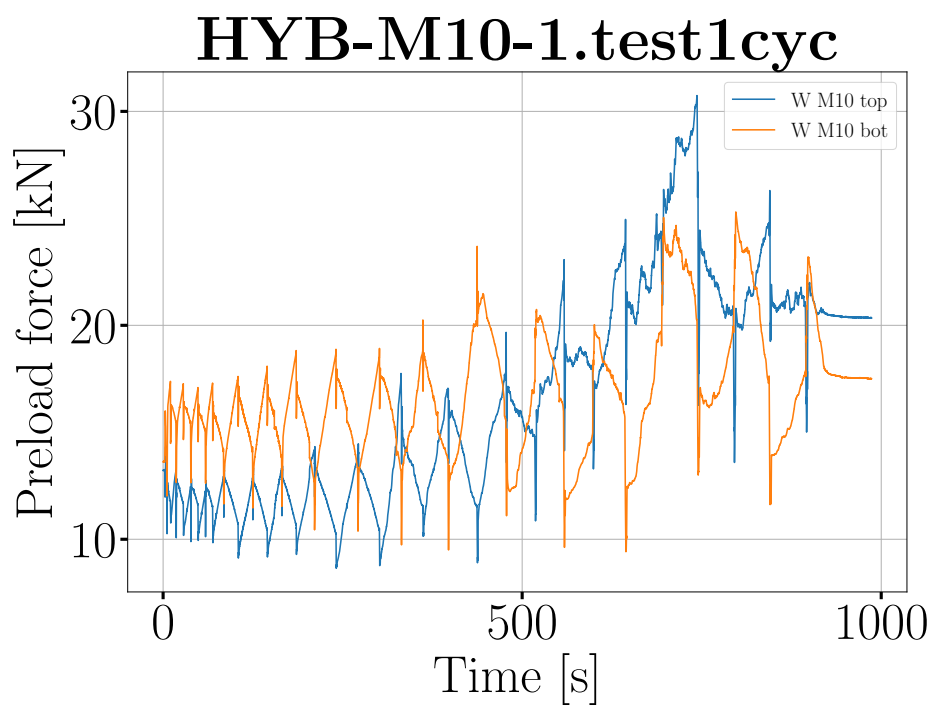


Figure 20.6: Preload in bolts.

Chapter 21

Test 21 - HYBRID-M20_1 - 18.05.21

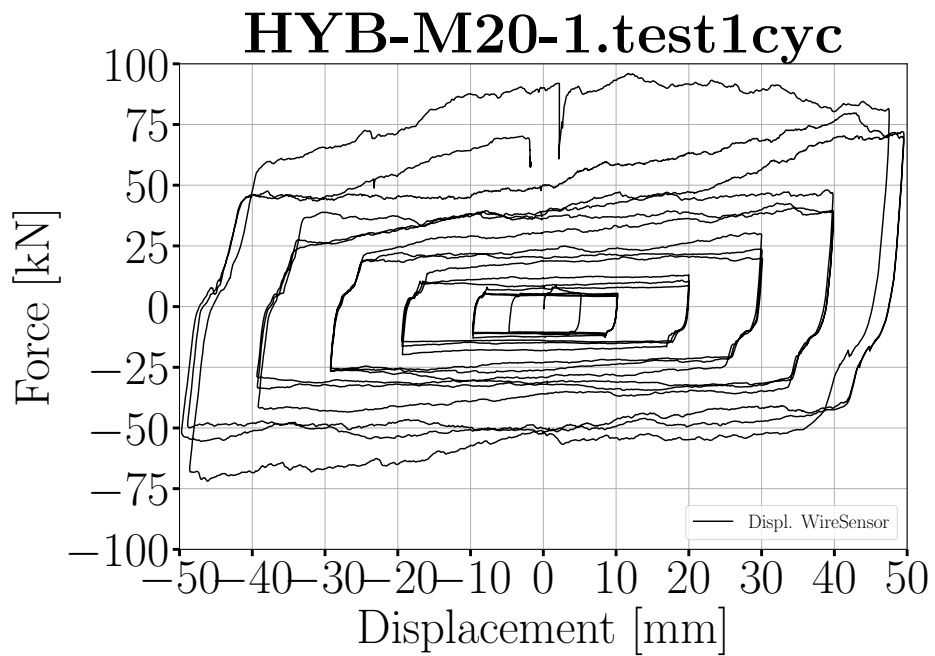
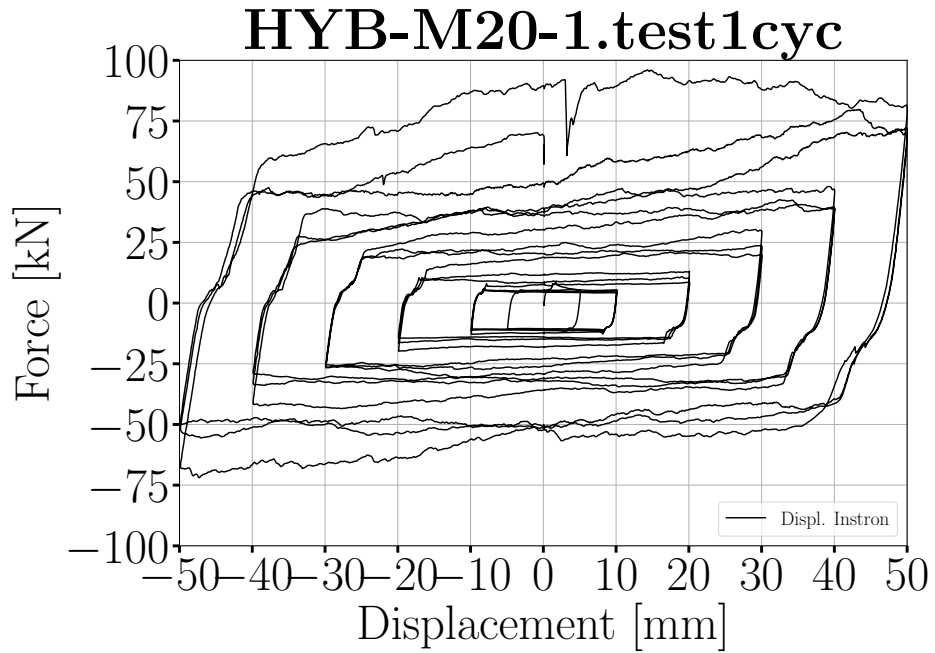


Figure 21.1: Load displacement graph.

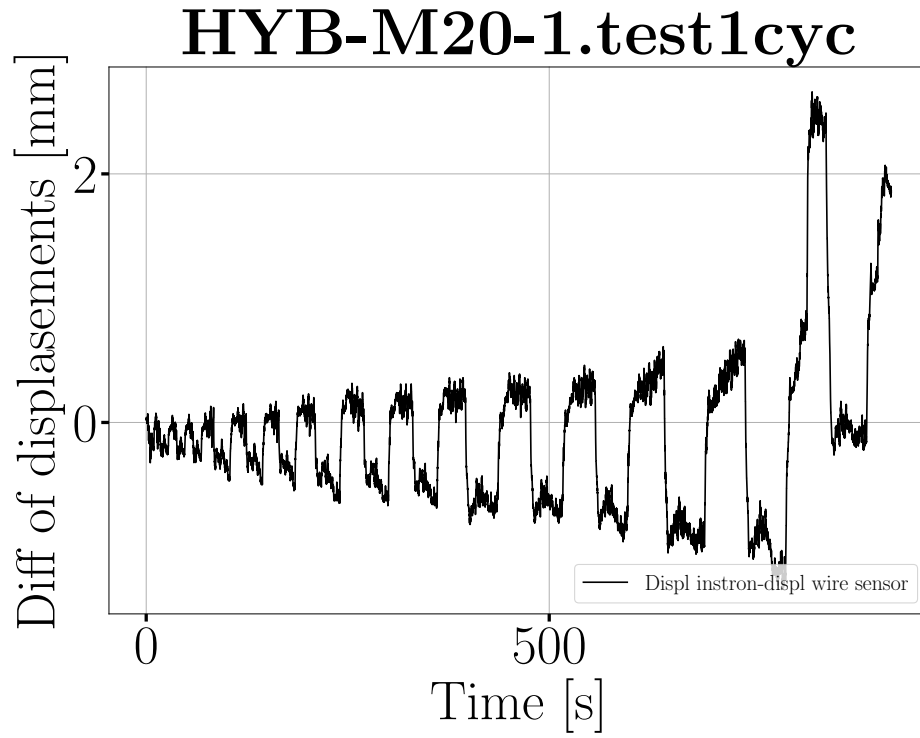


Figure 21.2: Difference of displacement between instron press and wire sensor.

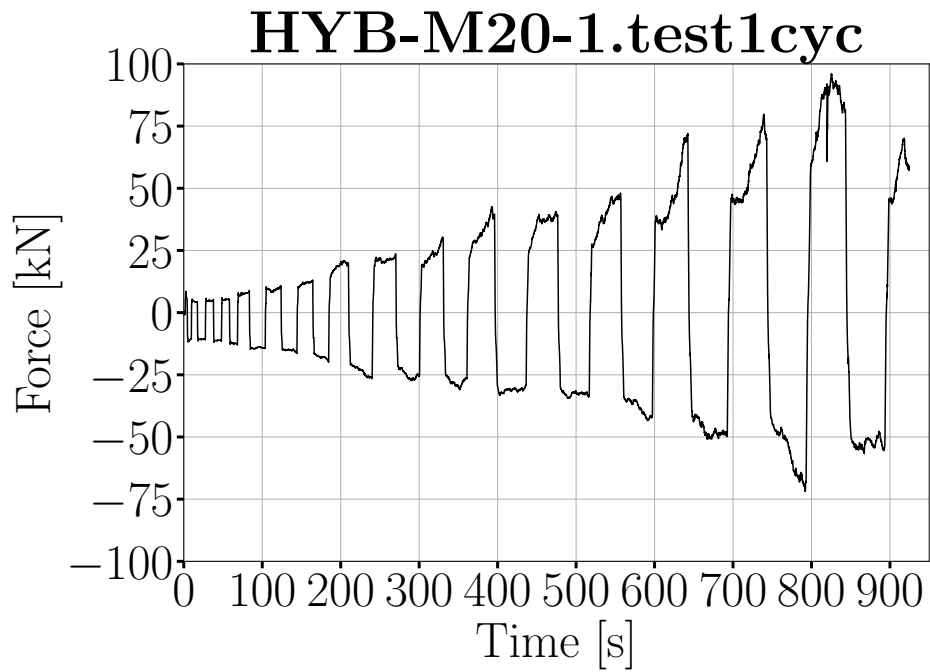


Figure 21.3: Force plotted against time.

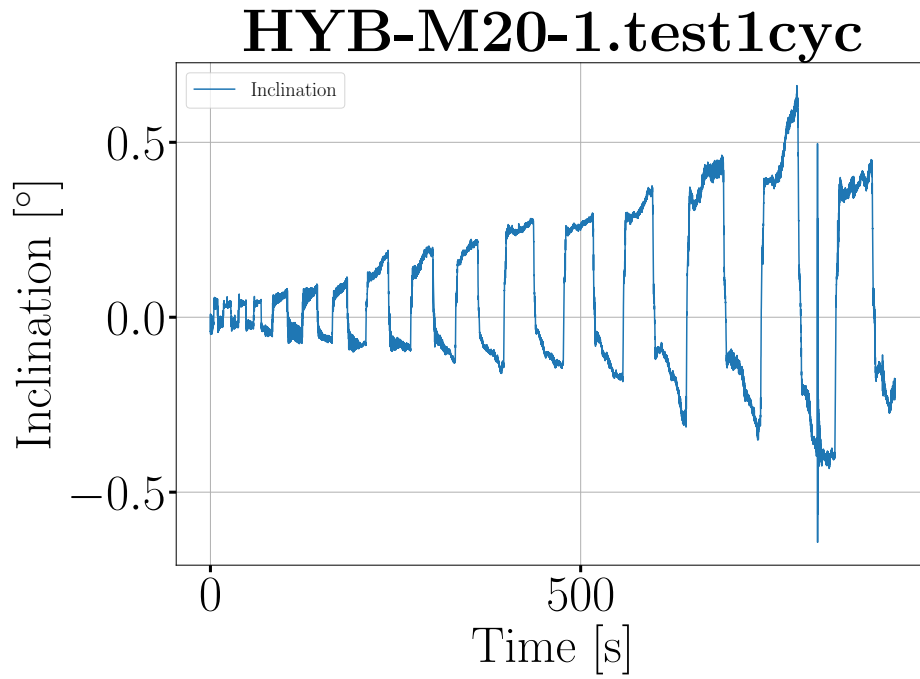


Figure 21.4: Inclination plotted against time.

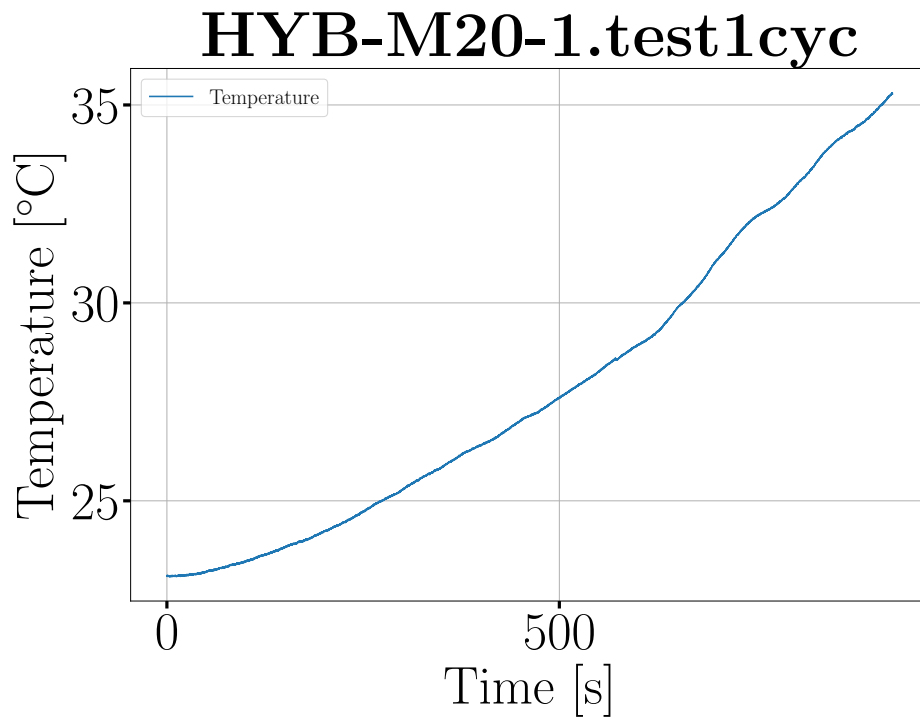


Figure 21.5: Temperature plotted against time.

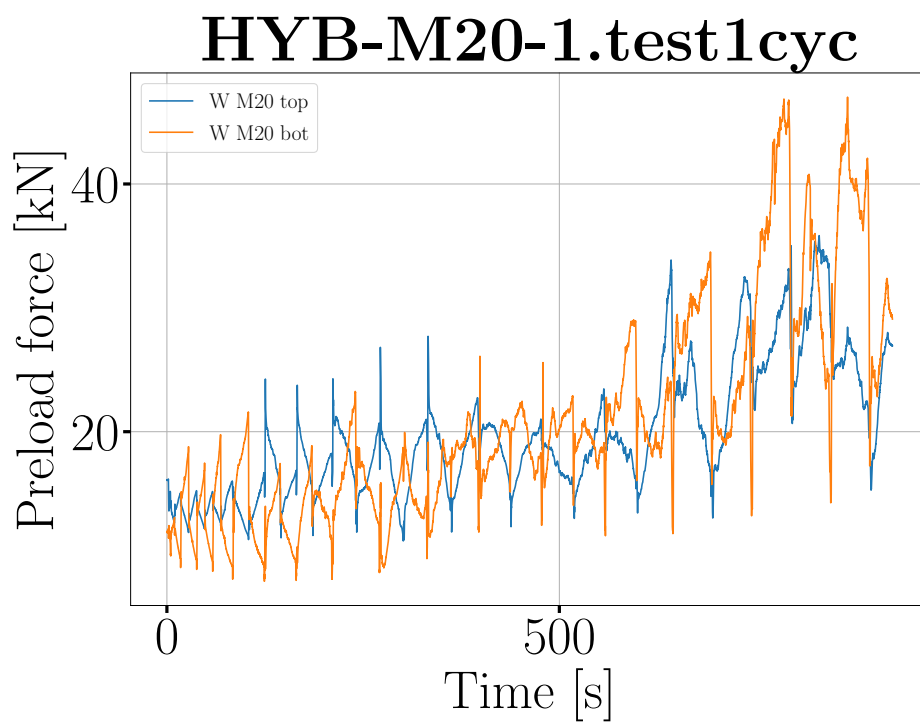


Figure 21.6: Preload in bolts.

Appendix D:
Sensor characteristics

Contents

- Contents..... 1
- 1. Load from the press..... 2
- 2. Frame position from the press 3
- 3. LDT sensor..... 4
- 4. Displacement wire..... 5
- 5. Inclinator..... 6
- 6. Thermocouple..... 7
- 7. Washer sensor M10..... 8
- 8. Washer sensor M20..... 9

1. Load from the press

Adapt sensor ×

Channel: Load [Help](#)

Voltage ▼

Input characteristic Sensor parameter

2-point Table

Set 1st point of input characteristics

Electrical	<input type="text" value="0,000000"/>	V	Measure
Physical	<input type="text" value="0,000000"/>	kN	▼

Set 2nd point of input characteristics

Electrical	<input type="text" value="10,000000"/>	V	Measure
Physical	<input type="text" value="300,000000"/>	kN	

Correct for cable resistance (4-wire)

mV/V Cal mV/V

R-Bridge Ohm [Details...](#)

Physical measuring range


Maximum	<input type="text" value="300"/>	kN	Details...
Minimum	<input type="text" value="-300"/>	kN	

Type of measurement

▼ s duration

Update in sensor database

2. Frame position from the press

 Adapt sensor ×


Channel: Position Frame [Help](#)

Voltage ▼


Input characteristic Sensor parameter

2-point Table

Set 1st point of input characteristics

Electrical	<input type="text" value="0,000000"/>	V	 Measure
Physical	<input type="text" value="0,000000"/>	mm ▼	

Set 2nd point of input characteristics

Electrical	<input type="text" value="10,000000"/>	V	 Measure
Physical	<input type="text" value="350,000000"/>	mm	

Correct for cable resistance (4-wire)

mV/V Cal	<input type="text" value="2"/>	mV/V	
R-Bridge	<input type="text" value="350"/>	Ohm	Details...

Physical measuring range


Maximum	<input type="text" value="100"/>	mm	Details...
Minimum	<input type="text" value="-100"/>	mm	

Type of measurement

<input type="text" value="Current value"/>	▼	<input type="text" value="2"/>	s duration
--------------------------------------------	---	--------------------------------	------------

Update in sensor database

3. LDT sensor

 Configure hardware ×


Channel: Displacement frame bottom [Help](#)

Voltage ▼


Input characteristic Sensor parameter

2-point Table

Set 1st point of input characteristics

Electrical	<input type="text" value="0,000000"/>	V	 Measure
Physical	<input type="text" value="0,000000"/>	mm ▼	

Set 2nd point of input characteristics

Electrical	<input type="text" value="0,020000"/>	V	 Measure
Physical	<input type="text" value="50,000000"/>	mm	

Correct for cable resistance (4-wire)

mV/V Cal	<input type="text" value="2"/>	mV/V	
R-Bridge	<input type="text" value="350"/>	Ohm	Details...

Physical measuring range

Maximum	<input type="text" value="250"/>	mm	Details...
Minimum	<input type="text" value="-250"/>	mm	

Type of measurement

<input type="text" value="Current value"/> ▼	<input type="text" value="2"/>	s duration	
----------------------------------------------	--------------------------------	------------	--

4. Displacement wire

Configure hardware ×


Channel: Displacement wire [Help](#)

Voltage ▾


Input characteristic Sensor parameter

2-point Table

Set 1st point of input characteristics

Electrical	<input type="text" value="0,000000"/>	V	 Measure
Physical	<input type="text" value="0,000000"/>	mm ▾	

Set 2nd point of input characteristics

Electrical	<input type="text" value="9,992500"/>	V	 Measure
Physical	<input type="text" value="500,000000"/>	mm	

Correct for cable resistance (4-wire)

mV/V Cal	<input type="text" value="2"/>	mV/V	
R-Bridge	<input type="text" value="350"/>	Ohm	Details...

Physical measuring range

Maximum	<input type="text" value="500,3753"/>	mm	Details...
Minimum	<input type="text" value="-500,3753"/>	mm	

Type of measurement

<input type="text" value="Current value"/>	▾	<input type="text" value="2"/>	s duration
--------------------------------------------	---	--------------------------------	------------

5. Inclinometer

Configure hardware ×

Channel: Inclinometer [Help](#)

Voltage ▾

Input characteristic Sensor parameter

2-point Table

Set 1st point of input characteristics

Electrical	<input type="text" value="2,500770"/>	V	Measure
Physical	<input type="text" value="0,000000"/>	°	▾

Set 2nd point of input characteristics

Electrical	<input type="text" value="4,500650"/>	V	Measure
Physical	<input type="text" value="10,000000"/>	°	

Correct for cable resistance (4-wire)

mV/V Cal	<input type="text" value="2"/>	mV/V	
R-Bridge	<input type="text" value="350"/>	Ohm	Details...

Physical measuring range

Maximum	<input type="text" value="37,4984"/>	°	Details...
Minimum	<input type="text" value="-37,4984"/>	°	

Type of measurement

Current value	▾	<input type="text" value="2"/>	s duration
---------------	---	--------------------------------	------------

6. Thermocouple

Configure hardware ×

Channel: SCM-TCK [Help](#)


Thermocouple K ▼

Sensor parameter

Parameter	
Unit	°C

Create new sensor OK Cancel

7. Washer sensor M10

 Configure hardware ×


Channel: Washer M10 top [Help](#)

SG full bridge ▼


Input characteristic Sensor parameter

2-point Table

Set 1st point of input characteristics

Electrical	<input type="text" value="0,000000"/>	mV/V	 Measure
Physical	<input type="text" value="0,000000"/>	kN ▼	

Set 2nd point of input characteristics

Electrical	<input type="text" value="2,000000"/>	mV/V	 Measure
Physical	<input type="text" value="60,000000"/>	kN	

Correct for cable resistance (4-wire)

mV/V Cal	<input type="text" value="2,000000"/>	mV/V	
R-Bridge	<input type="text" value="350,00"/>	Ohm	Details...


Physical measuring range

Maximum	<input type="text" value="150"/>	kN	Details...
Minimum	<input type="text" value="-150"/>	kN	

Type of measurement

<input type="text" value="Current value"/> ▼	<input type="text" value="2"/>	s duration	
----------------------------------------------	--------------------------------	------------	--

8. Washer sensor M20

 Configure hardware ×


Channel: Washer M20 top [Help](#)

SG full bridge ▼


Input characteristic Sensor parameter

2-point Table

Set 1st point of input characteristics

Electrical	<input type="text" value="0,000000"/>	mV/V	 Measure
Physical	<input type="text" value="0,000000"/>	kN ▼	

Set 2nd point of input characteristics

Electrical	<input type="text" value="2,000000"/>	mV/V	 Measure
Physical	<input type="text" value="300,000000"/>	kN	

Correct for cable resistance (4-wire)

mV/V Cal	<input type="text" value="2,000000"/>	mV/V	
R-Bridge	<input type="text" value="350,00"/>	Ohm	Details...

Physical measuring range

Maximum	<input type="text" value="750"/>	kN	Details...
Minimum	<input type="text" value="-750"/>	kN	

Type of measurement

<input type="text" value="Current value"/> ▼	<input type="text" value="2"/>	s duration
----------------------------------------------	--------------------------------	------------



Norges miljø- og biovitenskapelige universitet
Noregs miljø- og biovitenskapelige universitet
Norwegian University of Life Sciences

Postboks 5003
NO-1432 Ås
Norway